Ionic Transition Metal Complexes Containing Iridium(III) for Lighting Applications

Inauguraldissertation

zur

Erlangung der Würde eines Doktors der Philosophie

vorgelegt der

Philosophisch-Naturwissenschaftlichen Fakultät

der Universität Basel

von

Gabriel Elias Schneider

von Basel (BS), St. Gallen (SG) und Quarten-Murg (SG), Schweiz

Basel, 2013

Genehmigt von der Philosophisch-Naturwissenschaftlichen Fakultät der Universität Basel auf Antrag von

Prof. Dr. Edwin C. Constable und Prof. Dr. Oliver S. Wenger

Basel, den 21. Mai 2013

Prof. Dr. Jörg Schibler

Dekan

creative commons

Namensnennung-Keine kommerzielle Nutzung-Keine Bearbeitung 2.5 Schweiz

---

Sie dürfen:

das Werk vervielfältigen, verbreiten und öffentlich zugänglich machen

Zu den folgenden Bedingungen:

Namensnennung. Sie müssen den Namen des Autors/Rechteinhabers in der von ihm festgelegten Weise nennen (wodurch aber nicht der Eindruck entstehen darf, Sie oder die Nutzung des Werkes durch Sie würden entlohnt).

Keine kommerzielle Nutzung. Dieses Werk darf nicht für kommerzielle Zwecke verwendet werden.

Keine Bearbeitung. Dieses Werk darf nicht bearbeitet oder in anderer Weise verändert werden.

- Im Falle einer Verbreitung müssen Sie anderen die Lizenzbedingungen, unter welche dieses Werk fällt, mitteilen. Am Einfachsten ist es, einen Link auf diese Seite einzubinden.
- Jede der vorgenannten Bedingungen kann aufgehoben werden, sofern Sie die Einwilligung des Rechteinhabers dazu erhalten.
- Diese Lizenz lässt die Urheberpersönlichkeitsrechte unberührt.

Die gesetzlichen Schranken des Urheberrechts bleiben hiervon unberührt.

Die Commons Deed ist eine Zusammenfassung des Lizenzvertrags in allgemeinverständlicher Sprache: http://creativecommons.org/licenses/by-nc-nd/2.5/ch/legalcode.de

Haftungsausschluss:
Die Commons Deed ist kein Lizenzvertrag. Sie ist lediglich ein Referenztext, der den zugrundeliegenden Lizenzvertrag übersichtlich und in allgemeinverständlicher Sprache wiedergibt. Die Deed selbst entfaltet keine juristische Wirkung und erscheint im eigentlichen Lizenzvertrag nicht. Creative Commons ist keine Rechtsanwaltsgesellschaft und leistet keine Rechtsberatung. Die Weitergabe und Verlinkung des Commons Deeds führt zu keinem Mandatsverhältnis.

Quelle: http://creativecommons.org/licenses/by-nc-nd/2.5/ch/ Datum: 3.4.2009

Acknowledgements

First of all, I would like to thank my supervisors Prof. Dr. Edwin C. Constable and Prof. Dr. Catherine E. Housecroft for giving me the opportunity to do my PhD project in their group. During the last three and a half years, they did a great job in helping, advising and supporting me.

I would like to thank Prof. Dr. Oliver S. Wenger for being my co-examiner.

I would like to thank all the supporting staff of the Department of Chemistry: Dr. Jennifer A. Zampese and Dr. Markus Neuburger for solving the crystal structures, Werner Kirsch and Sylvie Mittelheisser for providing the elemental analyses, Markus Hauri for the supply of materials and Beatrice Erismann for managing all administrative issues.

I would like to thank the current and former members of the Constable-Housecroft group for the good and productive working atmosphere. Specially, I want to thank Andreas Bünzli, Cathrin Ertl and Jonas Schönle for fruitful discussions about the chemistry. Furthermore, I would like to thank Andreas Bünzli, Cathrin Ertl, Heiko Gsellinger, Dr. Daniel Häussinger, Nik Hostettler, Dr. Peter Kopecky, Jonas Schönle, Roche M. Walliser and Kaspar Zimmermann for their help and support concerning NMR spectroscopy and Nik Hostettler for the supply of some of the ligands.

I would really like to thank Andreas Bünzli, Dr. Colin J. Martin, Dr. Niamh S. Murray, Dr. Jennifer A. Rudd, Dr. Jennifer A. Zampese and last but not least Prof. Dr. Catherine E. Housecroft for their big help in proof reading this script.

For the financial support, I acknowledge the University of Basel, the Swiss National Science Foundation, The Swiss Nanoscience Institute, the National Centre of Competence in Research *Nanoscale Science* and the European Union for supporting the collaboration with the group of Dr. Henk J. Bolink (CELLO; STRP 248043).

I would like to thank Dr. Henk J. Bolink, Daniel Tordera, Antonio Pertegas and Prof. Dr. Enrique Ortí for their work on LEC devices and theoretical studies of the complexes.

And last but not least, I want to thank my wife, my family and my friends for their constant support.

Abstract

This PhD thesis concerns the synthesis of new ionic transition metal complexes based on iridium(III) complexes for applications in light-emitting electrochemical cells (LECs).

Chapter 1 gives a short introduction to the historical and chemical backgrounds of the element iridium and of LECs.

Chapter 2 shows the importance of the purity of the anion in the iridium(III) complexes on the performance of LEC devices.

Chapter 3 shows the influence of changing the size of the anion on the LEC performance and its direct influence on the mobility of the ions in thin films.

Chapter 4 describes the synthesis and characterization of iridium(III)-based blue emitters with high quantum efficiency.

Chapter 5 details the introduction of 2,2':6',2''-terpyridine (tpy) ligands in the field of iridium(III) complexes. The pendant pyridine ring undergoes intramolecular face-to-face π-stacking interactions, similar to pendant phenyl rings of 2,2'-bipyridine (bpy) ligands. The NMR spectroscopic assignments of these iridium(III) complexes are shown. Through the extension of the π-conjugation of the ancillary ligand, the emission maximum of the complexes is shifted towards the red region of the visible spectrum.

Chapter 6 reports further tpy-based iridium(III) complexes and their performances in LEC devices.

Chapter 7 discusses the stereochemistry of the octahedral iridium(III) atom and shows trials towards multinuclear iridium compounds.

Chapter 8 concludes this PhD thesis and gives an outlook for further research efforts.

Parts of this work have been published:

E. Baranoff, H. J. Bolink, E. C. Constable, M. Delgado, D. Häussinger, C. E. Housecroft, M. K. Nazeeruddin, M. Neuburger, E. Ortí, G. E. Schneider, D. Tordera, R. M. Walliser, J. A. Zampese, *Dalton Trans*., 2013, **42**, 1073. My contribution was the synthesis and analysis of the complexes, as well as the solution properties.

E. C. Constable, C. E. Housecroft, G. E. Schneider, J. A. Zampese, *Polyhedron*, 2013, **52**, 530. My contribution was the synthesis and characterization of the described complexes.

List of abbreviations:

Å	Ångström
BARF	$[B[3,5\text{-}(CF_3)_2C_6H_3]_4]^-$ anion
$[BMIM]^+$	1-butyl-3-methylimidazolium
bpy	2,2'-bipyridine
2,4'-bpy	2,4'-bipyridine
4,4'-bpy	4,4'-bipyridine
calc.	calculated
CH_2Cl_2	dichloromethane
COSY	correlation spectroscopy
C^N ligand	cyclometallating ligand (e.g. 2-phenylpyridine)
CV	cyclic voltammetry
δ	chemical shift [ppm]
DFT	density functional theory
DMSO	dimethyl sulfoxide
E	standard half-cell potential
EA	elemental analysis
EL	electroluminescence
ESI	electron spray ionisation
Et_2O	diethyl ether
EQE	external quantum efficiency
eV	electron volt
Hdfppy	2,4-difluorophenylpyridine
Hdfppz	2,4-difluorophenylpyrazole
Hdmppz	3,5-dimethylphenylpyrazole
HMBC	heteronuclear multiple bond correlation
HMQC	heteronuclear multiple quantum coherence
HOMO	highest occupied molecular orbital
Hppy	2-phenylpyridine

IL	ionic liquid
iTMC	ionic transition metal complex
λ_{abs}	absorption wavelength
λ_{em}	emission wavelength
λ_{ex}	excitation wavelength
LC	ligand centred transition
LCD	liquid crystal display
LEC	light-emitting electrochemical cell
LED	light-emitting diode
LFSE	ligand-field stabilization energy
LMCT	ligand to metal charge transfer
LUMO	lowest unoccupied molecular orbital
MC	metal centred transition
MeCN	acetonitrile
MeOH	methanol
MLCT	metal to ligand charge transfer
MS	mass spectrometry
NMe_2	dimethylamino
NMR	nuclear magnetic resonance, with the signals being identified as singlet (s), doublet (d), triplet (t), quartet (q) and broad (br)
N^N ligand	polypyridine ligand (e.g. 2,2'-bipyridine)
NOESY	nuclear overhauser enhancement spectroscopy
OLED	organic light-emitting diode
pbpy	6-phenyl-2,2'-bipyridine
PEDOT	poly(3,4-ethylenedioxythiophene)
phen	1,10-phenanthroline
PJ	petajoule
PMMA	1-(4-methoxyphenyl)-*N*-methyl-propan-2-amine/ polymethylmethacrylate
ppm	parts per million

PSS	poly(styrene sulfonic acid)
S	total spin quantum number
sh	shoulder
SSL	solid-state lighting
TBA	tetra-n-butyl ammonium
TBACl	tetra-n-butyl ammonium chloride
TBAOTf	tetra-n-butyl ammonium trifluoromethanesulfonate
$TBAPF_6$	tetra-n-butyl ammonium hexafluoridophosphate
^{t}Bu	*tert*-butyl
TMS	tetramethylsilane
tpy	2,2':6',2''-terpyridine
vs.	versus

Table of contents

Materials and Methods

General Experimental

^{1}H, ^{11}B, ^{13}C, ^{19}F and ^{31}P NMR spectra were recorded on Bruker DRX-400, DRX-500, DRX-600 or Bruker Avance III-400, Avance III-500, or Avance III-600 NMR spectrometers. The chemical shifts were referenced as follows: for ^{1}H and ^{13}C NMR spectra, chemical shifts were referenced to residual solvent peaks with respect to δ(TMS) = 0 ppm, for ^{11}B with respect to $Et_2O.BF_3$ = δ_B 0 ppm, for ^{19}F an external reference of $CFCl_3$ with respect to δ = 0 ppm, and for ^{31}P with respect to 85% H_3PO_4 = δ_P 0 ppm. Solution absorption spectra were recorded on an Agilent 8453 spectrophotometer. Solution emission spectra were recorded on a Shimadzu RF-5301 PC spectrofluorometer. Solution and solid state quantum yield measurements were recorded on a Hamamatsu 11347-11 (Standard type) Absolute PL Quantum Yield Measurement System. The quantum yield measurements were performed using HPLC MeCN or CH_2Cl_2 solutions of the complexes. Prior to measurement, the solutions were bubbled with argon for 15 minutes. The concentration of the solution was adjusted to correspond to give absorption = 0.1 a.u. FT-IR spectra were recorded using a Shimadzu 8400S instrument with Golden Gate accessory for solid samples. Electrospray ionization (ESI) mass spectra were measured using a Bruker esquire 3000^{plus} mass spectrometer. Elemental analyses were measured on a Leco CHN-900 microanalyser. Electrochemical measurements were carried out using cyclic voltammetry and were recorded using a VersaSTAT 3 potentiostat from Princeton Applied Research with glassy carbon working and platinum auxiliary electrodes; a silver wire was used as a pseudo-reference electrode. Solvent was dry, purified MeCN or CH_2Cl_2 and 0.1 M [$^{n}Bu_4N$][PF_6] was used as supporting electrolyte. Cp_2Fe was used as internal reference. A Biotage Initiator 8 reactor was used for the syntheses under microwave conditions. Fluka silica 60 and Merck alumina 90 were used for column chromatography. NH_4PF_6 was purchased from Alfa Aesar and used without further purification. $KB(CN)_4$ was purchased from SelectLab and used without further purification.

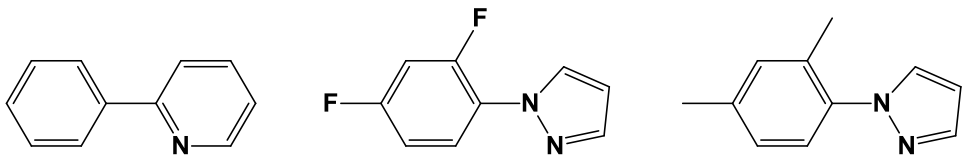

Hppy Hdfppz Hdmppz

Scheme 1 C^N ligand structures and abbreviations.

Tetrakis[3,5-bis(trifluoromethyl)phenyl]borate was prepared using a literature procedure[1] $[Ir_2(ppy)_4(\mu\text{-}Cl)_2]$ and $[Ir_2(dmppz)_4(\mu\text{-}Cl)_2]$ were prepared using a literature procedure,[2] $[Ir_2(dfppz)_4(\mu\text{-}Cl)_2]$ was prepared by the method reported by Nonoyama.[3] Scheme 1 depicts the structures of the C^N ligands. The ligands bpy, 2,4'-bpy, 4,4'-bpy and tbpy were purchased from Acros Organics and were used without further purification (see Scheme 2). The ligands pbpy,[4] **1**,[5] **2**,[6] **3**,[7] tpy,[8] **4**,[9] **5** [PF_6],[10] **6**,[11] **7**,[12,] 9 **8**,[13] and **9**[12, 9] were prepared by literature procedures (see Scheme 2 for structures).

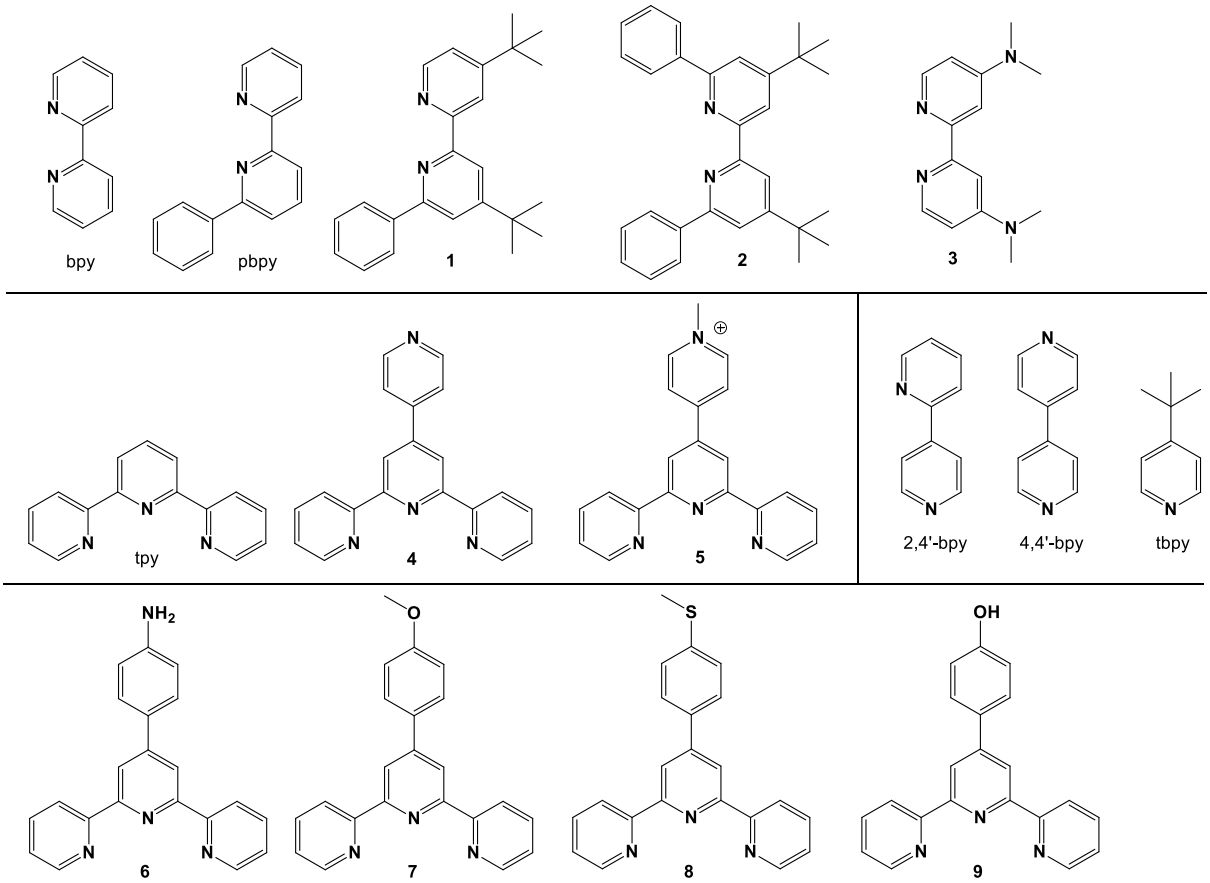

Scheme 2 N^N ligand structures and abbreviations.

Crystallography

Data were collected on either a Bruker-Nonius KappaAPEX diffractometer with data reduction, solution and refinement using the programs APEX2,[14] SIR92,[15] and CRYSTALS,[16] or on a Stoe IPDS diffractometer using Stoe IPDS software[17] and SHELXL97.[18] Structures were analysed using Mercury v. 3.0.[19, 20]

LEC devices

The research groups of Profs. E. C. Constable and C. E. Housecroft and Dr. H. J. Bolink have collaborated for several years on ionic transition metal complexes for lighting applications. For this thesis the collaboration was continued. The preparations and measurements of the complexes in LEC devices were carried out in the laboratory of Dr. Henk. J. Bolink in Valencia, Spain. Measurements were performed with different set-ups: 5% iTMC in PMMA, the iTMC together with an ionic liquid [BMIM][PF_6], or in a LEC configuration (ITO/PEDOT:PSS/iTMC/Al).

[1] H. Nishida, N. Takada, M. Yoshimura, T. Sonods, H. Kobayshi, *Bull. Chem. Soc. Jpn.,* 1984, **57** (9): 2600.
[2] S. Sprouse, K. A. King, P. J. Spellane, R. J. Watts, *J. Am. Chem. Soc*., 1984, **106**, 6647.
[3] M. Nonoyama, *Bull. Chem. Soc. Jpn*., 1974, **47**, 767.
[4] E. C. Constable, R. P. G. Henney, T. A. Leese, D. A. Tocher, *J. Chem. Soc., Dalton Trans*., 1990, 443.
[5] W. Lu, B.-X. Mi, M. C. W. Chan, Z. Hui, C.-M. Che, N. Zu, S.-T. Lee, *J. Am. Chem. Soc*., 2004, **126**, 4958.
[6] M. Lepeltier, T. K.-M. Lee, K. K.-W. Lo, L. Toupet, H. Le Bozec, V. Guerchais, *Eur. J. Inorg. Chem*., 2005, 110.
[7] D. Zhang, J. P. Telo, C. Liao, S. E. Hightower, E. L. Clennan, *J. Phys. Chem. A*, 2007, **111**, 13567.
[8] K. T. Potts, P. Ralli, G. Theodoridis and P. Winslow, *Org. Synth*., 1986, **64**, 189.
[9] J. Wang, G. S. Hanan, *Synlett*, 2005, 1251.
[10] E. C. Constable, C. E. Housecroft, M. Neuburger, D. Phillips, P. R. Raithby, E. Schofield, E. Sparr, D. A. Tocher, M. Zehnder, Y. Zimmermann, *J. Chem. Soc., Dalton Trans*, 2000, **13**, 2219.
[11] G. D. Storrier, S. B. Colbran, D. C. Craig, *J. Chem. Soc., Dalton Trans.*, 1997, **17**, 3011.
[12] F. Kröhnke, *Synthesis*, 1976, 1.
[13] E. C. Constable, C. E. Housecroft, E. Medleycott, M. Neuburger, F. Reinders, S. Reymann, S. Schaffner, *Inorg. Chem. Comm.*, 2008, **11**, 518.
[14] *APEX2, version 2 User Manual, M86-E01078*, Bruker Analytical X-ray Systems, Inc., Madison, WI, 2006.
[15] A. Altomare, G. Cascarano, G. Giacovazzo, A. Guagliardi, M. C. Burla, G. Polidori, M. Camalli, *J. Appl. Crystallogr.*, 1994, **27**, 435.
[16] P. W. Betteridge, J. R. Carruthers, R. I. Cooper, K. Prout and D. J. Watkin, *J. Appl. Crystallogr*., 2003, **36**, 1487.
[17] Stoe & Cie, IPDS software v 1.26, Stoe & Cie, Darmstadt, Germany, 1996.
[18] G. M. Sheldrick, *Acta Crystallogr*., *Sect. A*, 2008, **64**, 112.
[19] I. J. Bruno, J. C. Cole, P. R. Edgington, M. K. Kessler, C. F. Macrae, P. McCabe, J. Pearson, R. Taylor, *Acta Crystallogr., Sect. B: Struct. Sci*., 2002, **58**, 389.
[20] C. F. Macrae, I. J. Bruno, J. A. Chisholm, P. R. Edgington, P. McCabe, E. Pidcock, L. Rodriguez-Monge, R. Taylor, J. Van de Streek, P. A. Wood, *J. Appl. Crystallogr*., 2008, **41**, 466.

Chapter 1

1. Introduction

1.1. Iridium

Over two hundred years ago, many elements were still missing from today's periodic table of the elements. In London in 1803 Smithson Tennant, who also discovered osmium, was working with crude *platina, aqua regia* and several other chemicals. After heating, fusing and cooling, he finally obtained a white powder which he described as follows:

"...appeared of a white colour, and was not capable of being melted, by any degree of heat I could apply... I should incline to call this metal Iridium, from the striking variety of colours which it gives, while dissolving in marine acid...".[1, 2, 3]

The element iridium, together with ruthenium, osmium, rhodium, palladium and platinum, is a member of the platinum-family and belongs to the third row of the transition metals. In today's periodic table of the elements, iridium has atomic number 77 and belongs to group 9. It naturally occurs with osmium in osmiridium. This native alloy has variable compositions with 15-40% osmium and 50-80% iridium.[4] The natural abundance of iridium is very low, with only 6 x 10^{-6} ppm Earth's crust. Even for heavier transition metals, this abundance is very low. Compared to gold, iridium is five times less abundant in the Earth's crust.4, [5] The element iridium is very hard, brittle, lustrous, silver-coloured and is, after osmium, the second densest element (22.56 g cm^{-3}).4 Iridium is very unreactive and the most corrosion-resistant metal known, even at high temperatures around 2000 °C.[6] In 1889 the *Bureau International des Poids et Mesures* near Paris made the international prototype meter and kilogram mass out of an alloy of 10% iridium and 90% platinum.6

Iridium, although rare, has a number of very important applications. Today, iridium-compounds are used for many purposes. In the catalysis field, in the Cativa™ process iridium catalysts are used for the large scale production of acetic acid;[7] Pfaltz and co-workers showed how efficient asymmetric iridium catalysts could be for asymmetric hydrogenation;[8] the dehydrogenation of alkanes (i.e. the reverse of hydrogenation) is also possible with iridium catalysts.[9] Another field of iridium complexes is their use as therapeutic agents. Only recently, it was discovered, that bioactive complexes based on iridium (and rhodium) are potential alternatives to the existing platinum and ruthenium metallodrugs.[10] Another application is the use of iridium compounds for water splitting,[11, 12, 13] for pH sensing,[14] or for photovoltaic applications.[15]

1.2. Oxidation states and geometries of the complexes

Iridium has the ability to form compounds in many different oxidation states, starting with -3 (very rare) and all the states between -1 to +6. The most stable ones are +3 and +4.[16] Iridium(III) has a [Xe] $5d^6$ electron configuration. The geometrical arrangement of donor atoms around an iridium(III) metal centre is normally octahedral.[17] A tris-chelate iridium complex in an octahedral environment is always chiral, yielding two enantiomers. To

distinguish the two forms, the octahedron is viewed down a 3-fold axis. The enantiomer with left-handedness is labelled Λ, and that with right-handedness is Δ (Scheme 1.1).

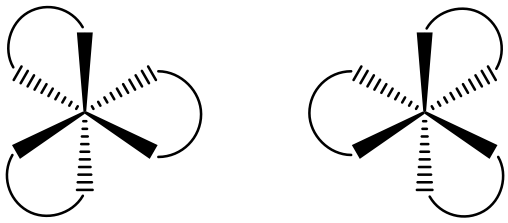

Scheme 1.1 Λ- (left-handed) and Δ-handedness (right-handed) of enantiomers of octahedral complexes.

In the free Ir^{3+} ion, the *d* orbitals are degenerate, i.e. in the gas phase ion with no ligand field. They split in an octahedral ligand field by the amount of Δ_{oct} (Figure 1.).[18, 19] In an O_h-symmetric complex, a d^6 electronic configuration can be low or high-spin, with a configuration of $t_{2g}^6 e_g^0$ or $t_{2g}^4 e_g^2$ respectively. Heavier metals have a larger splitting of the t_{2g} and e_g levels (i.e. large Δ_{oct} value) than 1st row metals. This leads to heavier metal ions invariably being low spin.

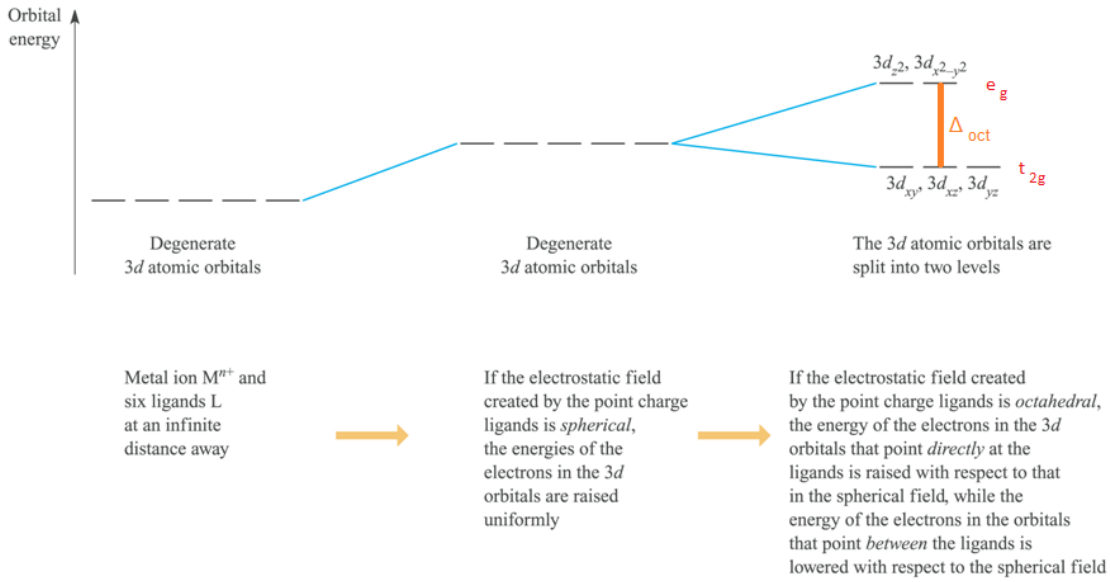

Figure 1.1 The changes in the energies of the electrons occupying the 3*d* orbitals of a first row M^{n+} ion when the latter is in an octahedral crystal field. The energy changes are shown in terms of the orbital energies. Similar diagrams can be drawn for second (4*d*) and third (5*d*) row metal ions.[19]

Thus the electrons in d^6 iridium(III) are paired, leading to kinetically inert compounds with diamagnetic properties.[20] The amount of the splitting is dependent on the field strength exerted by the ligands.

1.3. Photophysical properties

Upon light absorption, the possible electronic transitions from the ground state (GS) are metal-centred (MC), ligand-centred (LC) or metal-to-ligand charge transfer (MLCT). These

transitions are normally between singlet states, e.g. from the singlet GS to ^{1}LC, ^{1}MC or ^{1}MLCT. For ease of presentation, in Figure 1.2 the metal and ligand orbitals are depicted separately. Additional to the drawn pathways in Figure 1.2, in principle ligand-to-metal charge transfers (LMCT) can be involved too. Depending on the influence of the ligands substituents (S in Figure 1.2), the energy level of the ligand orbitals will be altered.

According to the spin selection rule, *d-d* transitions are Laporte forbidden (e.g. MC transitions in Figure 1.2). Due to the high spin-orbit coupling in iridium, a singlet state mixes to some extent with a triplet state and thus, these spin-forbidden transitions become "allowed", although they are still very weak.[21]

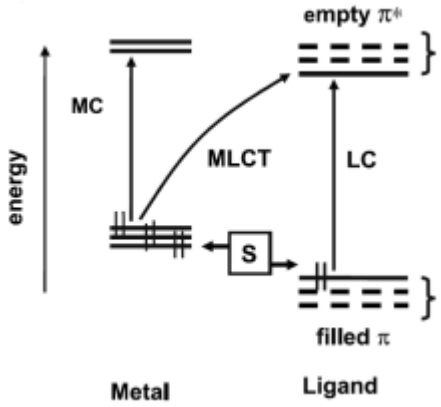

Figure 1.2 Orbital description of MC, MLCT and LC transitions; S is a substituent group capable of exerting electron withdrawing or donating effects (resulting in stabilization or destabilization, respectively, of the energy level of the filled d and π orbitals).[18]

Finally, the emission is normally from triplet states back to the ground state (Figure 1.3). This is due to the high spin-orbit coupling constant of iridium (ζ = 3909 cm^{-1}), which leads to an efficient intersystem crossing (ISC) from the singlet to the triplet excited state and inhibits non-luminescent pathways of electron-hole recombinations.[22, 23, 24]

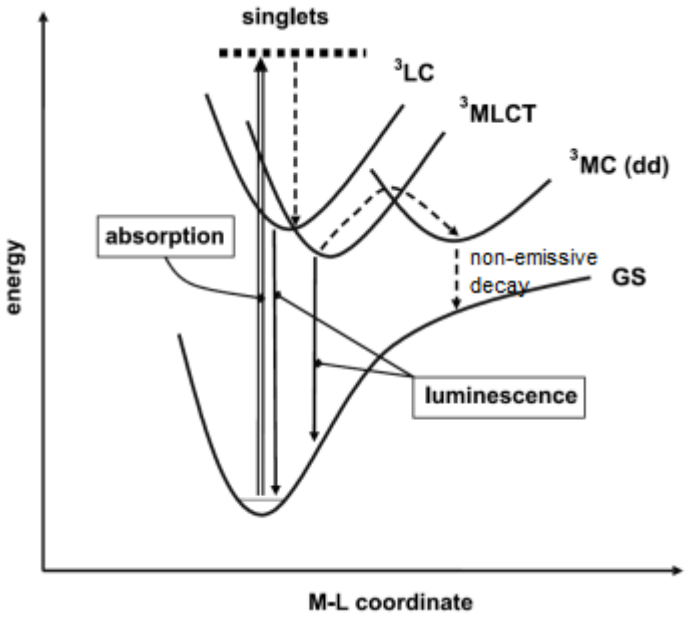

Figure 1.3 Electronic transitions involving MC, MLCT and LC excited states; the MC levels are non-emissive (dashed arrows).[18]

As the emission maximum of an iridium compound strongly depends on the energy of the triplet excited MLCT state (^{3}MLCT), this level may easily be modified by changing the ligands of the iridium compound (S in Figure 1.2). Therefore, in recent years, these properties of iridium compounds opened the field for using them in electroluminescence applications like organic light-emitting diodes (OLEDs) and light-emitting electrochemical cells (LECs).[25, 26] The emission maxima can be altered from the blue region (λ_{em} = 452 nm),[27] through the visible spectrum to the red region (λ_{em} = 687 nm)[28] and they offer high quantum efficiency.[26]

1.4. General synthetic strategies

The synthesis of $[Ir(C\hat{}N)_2(N\hat{}N)]^+$ complexes is relatively facile. Starting with iridium trihalide (e.g. $IrCl_3.xH_2O$) and a cyclometallating ligand (e.g. 2-phenylpyridine), initial studies by Watts and co-workers[29, 30] established the chlorido-bridged iridium dimer (e.g. $[Ir_2(ppy)_4(\mu\text{-}Cl)_2]$) as the key intermediate for the preparation of the cationic iridium(III) complexes.[31] Upon reacting the dimer with a suitable N^N ligand (e.g. 2,2'-bipyridine), followed by the exchange of the anion (e.g. using NH_4PF_6), the complexes presented in this work were prepared (e.g. $[Ir(ppy)_2(bpy)][PF_6]$, see Chapter 2).

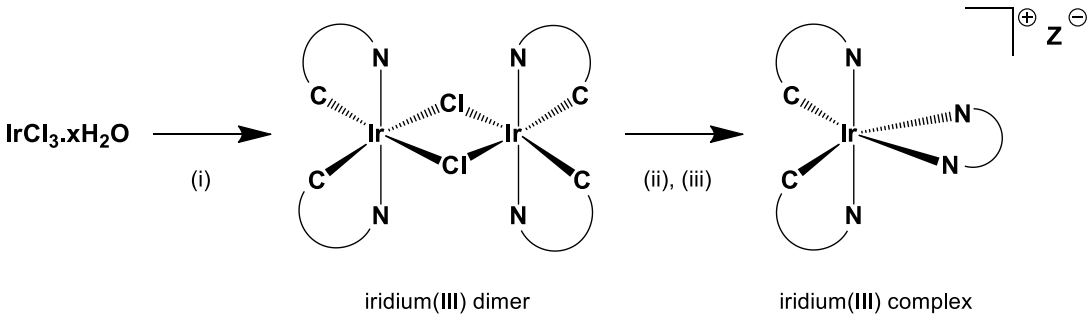

Scheme 1.2 Reaction scheme of the complexation reaction. (i): C^N ligand, 2-ethoxyethanol and water, 12 hr, reflux under nitrogen; (ii): N^N ligand, methanol, 2 hrs, 120 °C, in microwave reactor; (iii): precipitation via anion exchange.

There is a wide variety of iridium(III) complexes known, with, for example 2-phenylpyridine, 2-(2,4'-difluorophenyl)pyridine, 1-phenylpyrazole, 7,8-benzoquinoline, 3,5-dimethyl-1-phenylpyrazole as C^N ligands, and 2,2'-bipyridine, 6-phenyl-2,2'-bipyridine, 1,10-phenanthroline, 4,4'-di-*tert*-butyl-2,2'-bipyridine as N^N ligands.6' [24, 25]

1.5. Motivation

In the last decade the worldwide energy consumption drastically increased. After the Second World War, one solution was the construction of nuclear power plants. They seemed ideal for all needs of energy for future decades. In 1969 in Lucens (VD) a nuclear research reactor had a partial nuclear meltdown. Luckily, nobody was hurt, as this nuclear reactor was built underground and nobody was present during the accident.[32] In 1979 this image was shattered with the incident at the *Three Mile Island* power plant. In 1986 the accident in Chernobyl clearly showed the possible dangers of nuclear power. But it took 25 years and another accident, in Fukushima in 2011, to help the Swiss Government to think about a future without nuclear power stations.

One possibility to prohibit future nuclear accidents is to replace them by wind turbines, geothermal energy and solar cells. But independent of any new energy generators, a good plan is to reduce the energy consumption. Therefore, the change to renewable energies can be done more easily. In 2009, the research about energy in Switzerland was supported by 213'500'000 CHF.[33]

In Switzerland in 2011 13% of the total electric power consumption was used for lighting.[34] From 2000 to 2011 the energy consumption for illumination increased about 7% to total 26.7 PJ (1 PJ = 10^{15} J). In order to reduce this huge power consumption, conventional light sources like light bulbs and fluorescent tubes, which lose up to 95% of the electrical power via non-emissive heat radiation,[35] have to be replaced with more efficient technologies, which will result in environmental and economic savings.[36] These more efficient technologies involve solid-state lighting (SSL) using organic or inorganic materials. The working principle of SSL is based on the phenomena of electroluminescence (EL). EL is the conversion of electrical energy into light (Figure 1.4). When an external circuit is applied to a light-emitting material, at the cathode electrons are injected into the lowest unoccupied

molecular orbital (LUMO), whereas at the anode electrons are extracted from the highest occupied molecular orbital (HOMO). Upon charge migration, eventually they meet and recombine radiatively, producing light.[37]

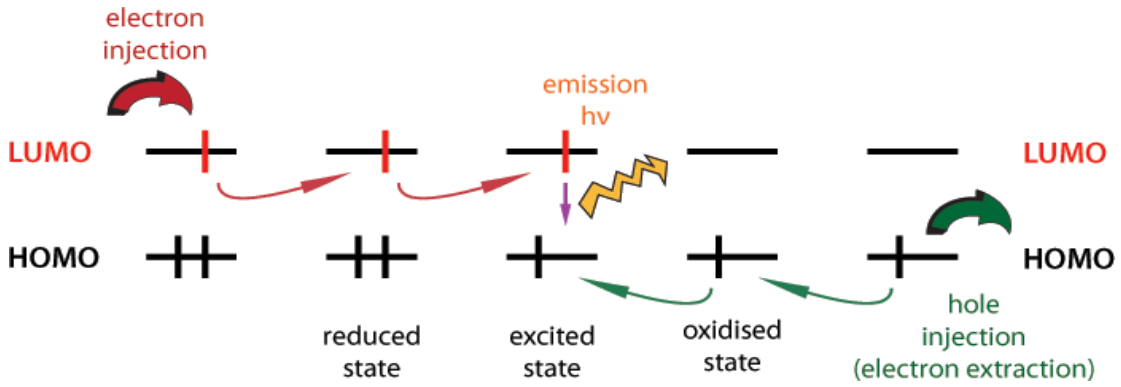

Figure 1.4 The principle of electroluminescence (EL). At the cathode (left hand side), electrons are injected into the luminophore. At the anode (right hand side), electrons are extracted, and thus, holes are generated. Both electrons and holes migrate through the film, eventually meeting each other at a particular luminophore, thus generating an excited state ("exciton"). Upon the return of the electron to the ground state, a photon is released.6

The difference of photoluminescence (PL) compared to EL is, that the excitation occurs upon an optical excitation, followed by the relaxation and emission of a photon.[37]

1.6. The history of light sources

Starting from the first light bulb fabricated in the 19th century, there has been a significant development in their design. Initially, the working principle stayed the same with a filament, and has developed to use a tungsten filament, leading to a warm and bright white light. Most people connect the invention of the light bulb with the name Thomas Edison but historians acknowledge many other contributors to this discovery, starting with the discovery of an electric arc by Humphry Davy in 1803.[38] 120 years later, Oleg Losev, a Russian technician working in radio laboratories, discovered the luminescence of silicon carbide. His results were published 1927 by the journal *Telegrafiya i Telefoniya bez Provodov* (*Wireless Telegraphy and Telephony)* in Nizhniy Novgorod, Russia.[39] This has evolved into today's well known light-emitting diode (LED). The research effort in the field of LEDs has yielded many applications used in our daily lives, e.g. in computers, displays, lighting devices and mobile phones. Some advantages of a LED compared to a light bulb are its higher robustness, lower energy consumption and a longer lifetime. But the production is still very energy-consuming, e.g. as they need high-vacuum conditions to grow the doped single crystals which are the cores of the LEDs.

Possible successors of LEDs fabricated from solid state materials, at least in some of its applications, are LEDs based on organic molecules. Today there are many commercial products available using organic light-emitting diodes (OLEDs). The first report of electroluminescent organic molecules was in 1953.[40] The potential of their applications for display technology has led to a big effort in researching the field of OLEDs. Today OLED

displays offer better contrast, lower energy consumption and wider angles of vision in applications like mobile phones, digital cameras and computer screens, replacing liquid-crystal displays (LCD). The production of OLEDs needs less energy, compared to a LED, due to the absence of single crystals. The development of OLEDs allows depositing the material with inkjet printers.[41] This may ease the production of lighting applications towards low-cost roll-to-roll coating methods for large-area emissive devices.[42] The big research effort led to higher efficiencies, enhanced brightness and improved lifetimes of the devices.[43] Today, OLEDs are already used in flat-panels, e.g. computer and TV screens or in mobile phones, and they are suitable for flexible applications.[43]

But there are also some disadvantages of OLEDs. As they contain neutral emissive organic molecules, they need a multilayer structure (see Figure 1.5). The different layers are used for efficient electron injection, as the injection barrier is too high, and for charge transport. Due to the need for a low work function in the cathode, air-reactive materials are used. Overall, the multilayer structure requires multiple evaporation-sublimation processes under vacuum and finally the OLED device needs a rigorous encapsulation to prevent degradation processes and to protect the air-reactive electrodes.[24, 25]

1.7. The discovery of the LEC

The first solid-state light-emitting electrochemical cell (LEC) was reported in 1995.[44] This LEC was based on polymers: a semiconducting polymer, an ion-conducting polymer and an inorganic salt, sandwiched between two electrodes. Besides the polymer-based LECs, there is another family of LECs which employ small cationic complexes. To this family belong the LECs based on ionic transition metal complexes (iTMCs).[45, 46] In 2004, the first iTMC LEC based on ionic iridium(III) complexes was reported.[24] The iTMC LEC offers a simplified device structure compared to polymer LECs, as no additional inorganic salts or ion conducting polymers are required, but the iTMC supports all the required processes for driving the LEC device: charge injection, charge transport and finally emissive recombination. The simplest LECs containing ionic species may consist of only a single active layer of the iTMC sandwiched by two electrodes (Figure 1.5).

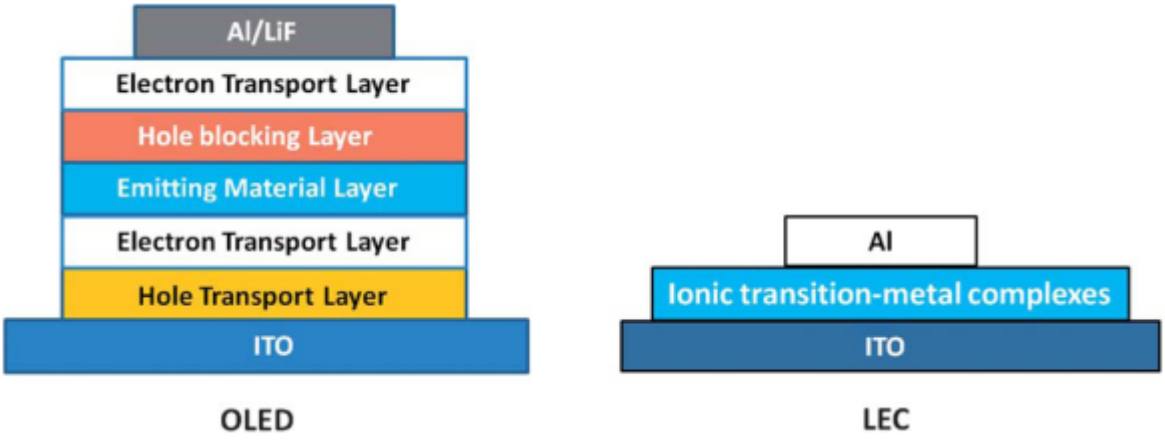

Figure 1.5 Comparison of the device architecture of an OLED and an iTMC LEC.[25]

In a LEC, the anode consists of indium-tin-oxide (ITO) and injects positive charges, or holes, into the highest occupied molecular orbital (HOMO) of the iTMC. The cathode consists of aluminium or other conducting metal (e.g. gold, silver) and negative charges, or electrons, are injected into the lowest unoccupied molecular orbital (LUMO) of the iTMC. When applying a bias, the holes and electrons migrate towards the cathode and anode respectively. When they meet in the emissive layer, they may form an exciton, which may lead to a radiative recombination and therefore emission of light.[59]

There are many benefits in using LECs for lighting applications. In addition to the points mentioned above, LECs operate at very low driving voltages, yielding high power efficient devices.[43] The device architecture type is simple, iTMCs allow solution processing and spin-coating techniques and the air-stable electrodes do not require rigid encapsulation. [25, 58]

The iTMCs are intrinsic molecular semiconductors. Assuming an octahedral (O_h) metal centre (e.g. iridium(III)), the HOMO is the t_{2g} of the metal centre, whereas the LUMO is a π* orbital of the ligands.[47] The calculated HOMO and the LUMO of the complex $[Ir(dfppz)_2(pbpy)][PF_6]$ is given in Figure 1.6 (also see Chapter 4).[67]

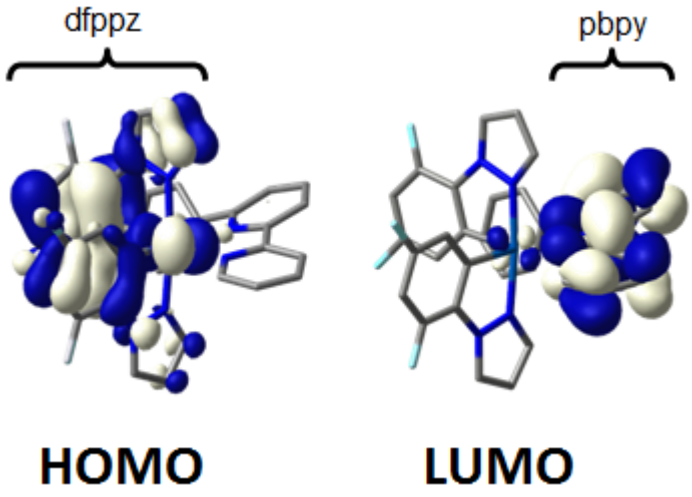

Figure 1.6 Locations of the calculated HOMO on the dfppz and LUMO on the pbpy ligand of the complex $[Ir(dfppz)_2(pbpy)][PF_6]$.[67]

When a bias is applied in a LEC, electrons are injected from the cathode and holes from the anode into the iTMC. Via hopping, these carriers are transported towards the opposite electrode. They may recombine under emission of light at a characteristic colour, corresponding to the energy gap of the iTMC. Very important for the operation of these LECs are the counter ions, e.g. $[PF_6]^-$ which are mobile in the film at room temperature. Under bias, they redistribute and thus assist the injection of electronic carriers,[47] e.g. $[Ir(ppy)_2(bpy)][PF_6]$[48] is ionically conducting. Under an applied current, the $[PF_6]^-$ anion moves towards the anode, whereas the cation $[Ir(ppy)_2(bpy)]^+$ moves towards the cathode. This rearrangement eases the electronic charge injection, makes the device independent of the work function of the electrodes and therefore, unlike in OLEDs, air-stable electrodes can be used, e.g. gold, silver or aluminium.

Even with the extensive research efforts in the field of iTMC-based LECs in the last few years, the detailed working principles are still being debated. There are principally two different models about the role of the ions and the spatial distribution of the electric field in an operating LEC device.[44, 46, 47]

Additionally, the synthesis and purification of the complexes is relatively facile (see Scheme 1.2)[23] and as they have a phosphorescent nature, they potentially emit with high efficiencies.[49, 50]

The phosphorescent emission comes from triplet states (S=1, spin-forbidden transition), whereas the fluorescent emission originates from singlet state (S=0, spin-allowed transition). In an electrically driven device (EL), statistics of the number of states (1 singlet state, 3 triplet states) leads to the following total-excited state populations: 25% of the injected charges are in a singlet state, whereas 75% are in triplet states.[51] A direct consequence is the higher efficiency of compounds which are not exclusively fluorescent, but also phosphorescent. Iridium(III) complexes containing cyclometallating 2-phenylpyridine (Hppy) ligands or their derivatives offer high triplet quantum yields which leads to high phosphorescent efficiencies.[22, 49, 50, 52] As the high spin-orbit coupling leads to a mixing of the singlet and the triplet excited states, the population of the triplet state is enhanced through inter-system crossing and thus the high quantum yield. Additionally, a relatively short phosphorescence lifetime further increases the performance of a phosphorescent material.

1.8. From ruthenium(II) and osmium(II) to iridium(III)

The first LECs based on iTMCs consisted mainly of ruthenium(II) and osmium(II) complexes[23, 53] However, emission maxima were limited to the region of red to orange because of the low ligand-field stabilization energies (LFSEs). Additionally their luminescent efficiencies are low and therefore limit their applications in lighting devices.[40] In 2002, the highest reported external quantum efficiency (EQE) of a ruthenium based LEC was 0.055.[54] To achieve this high efficiency multi-layered devices were needed. The first iTMC LEC based on an iridium(III) complex exhibited a four times higher quantum efficiency with 0.235.[24]

Additionally, there was a significant shift in the emission maximum towards the blue region with λ_{em} = 558 nm, being a bright yellow. This emission maximum was achievable in acetonitrile solutions as well as in spin-coated films.

Since 2004, most of the breakthroughs in the research field of LECs, such as colour tuning, efficiency, turn-on time and stability, have been done incorporating iridium(III) complexes.[6, 24, 25, 43] As mentioned before, the advantages of iridium(III) LECs over ruthenium(II) LECs are the better colour tunability, the higher quantum yields and the higher stability of the complexes.

1.9. Tuning the emission maximum

Starting with the yellow emission of the first iridium(III) LEC,[25] DFT calculations helped in understanding the localization of the HOMO and LUMO in these compounds.[55] As seen in Figure 1.6, the HOMO is usually centred over the cyclometallating C^N ligands and the iridium atom, while the LUMO is localized on the ancillary N^N ligand (see Figure 1.6 and Figure 1.7). These are the two main points to change the environment of the iridium atom and therefore to alter the emission maximum of an iridium(III) complex.

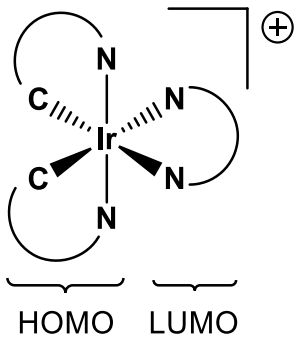

Figure 1.7 Locations of the HOMO and LUMO on an ionic iridium(III) complex.

To increase the band gap between the HOMO and LUMO, the HOMO needs to be stabilized, thus lowering its energy level, and/or the LUMO needs to be destabilized, i.e. increasing its energy level.

To stabilize the HOMO, electron-withdrawing substituents such as -F or -CF_3 are widely used. To destabilize the LUMO, electron-donating substituents such as -$N(CH_3)_2$ are attached to the ancillary ligand. [6, 24, 55, 56, 57, 58]

With the reverse approach, compounds can be designed with emission maxima in the red region of the visible spectrum. A smaller band gap, and therefore a red shift, will be achieved by destabilizing the HOMO and/or stabilizing the LUMO. This can be achieved by attaching electron-withdrawing groups to the ancillary ligand or by increasing the conjugation length of the ligands.[50, 57, 59] Combining red and blue emitting iridium(III) compounds may lead to a white emitting LEC device.[60] This has been achieved by doping a small amount of a red

emitting complex (λ_{em} = 656 nm, QY = 0.20, 0.2-0.4% of weight), into a layer of a blue-green emitting complex (λ_{em} = 497 nm, QY = 0.66).

1.10. Lifetime, turn-on time and efficiency

The lifetime of a LEC is a measure of the stability of the device and is still a difficult problem. The turn-on time and finally the efficiency of the emission are also properties of a LEC that must be improved.

A major breakthrough in device lifetime was the discovery of intramolecular face-to-face π-π stacking interaction[61] within the iridium(III) complex $[Ir(ppy)_2(pbpy)][PF_6]$.6′ [62] The intramolecular stacking interaction is between the free phenyl ring of the ancillary bpy ligand and one of the phenyl rings of the cyclometallating ligands. This leads to a cage effect, which protects the complex from degradation reactions, even in the excited state of the molecule. The result was an enhancement of the lifetime from 60 hours to more than 3000 hours. Additionally the increase of the lifetime did not affect the turn-on time, compared with a non-supramolecularly caged complex.

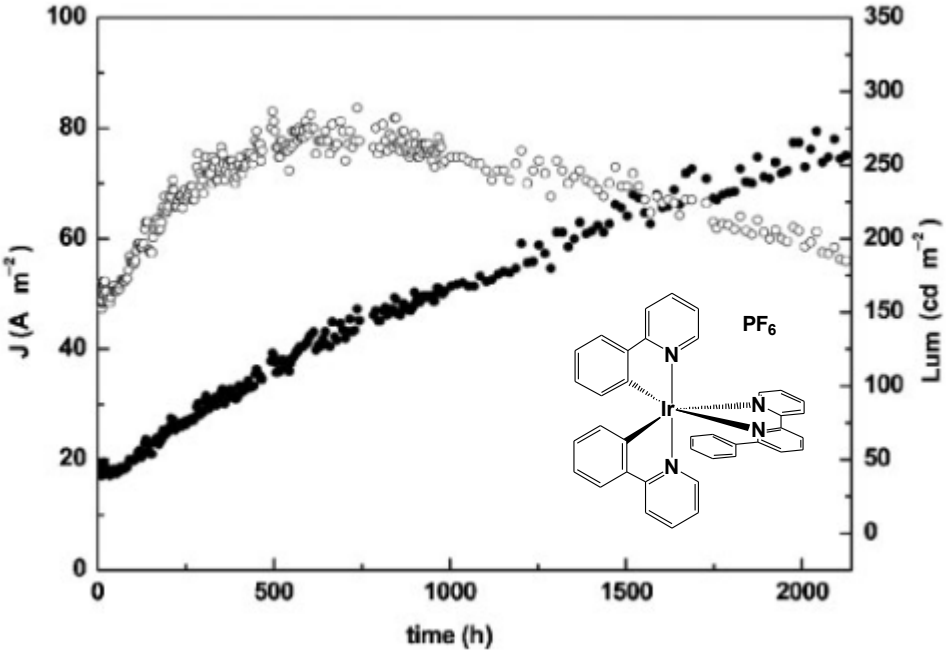

Figure 1.8 Current density (●) and luminance (○) versus time for the complex $[Ir(ppy)_2(pbpy)][PF_6]$.[62]

A second pendant phenyl ring on the N^N ligand leads to a second intramolecular face-to-face π-stacking with the other C^N ligand in the complex.[63] Interestingly, this second intramolecular π-stacking interaction did not improve the lifetime further. A possible explanation is the distortion of the planarity of the bipyridine ligand due to the two stacking interactions. Quantum chemical calculations show that this distortion of planarity leads to decreased energy difference between the emitting triplet and the MC triplet state, therefore yielding a complex more susceptible to emission losses and degradation reactions.

The discovery of this intramolecular stacking interaction restarted the research for a wider range of emitted colours with enhanced lifetimes. The second possibility to protect the complex from degradation is the introduction of bulky side-groups. These lower the possibility of a degradation reaction of the complex as well.[25, 64] The approach was similar to the colour tuning after the first reported iridium based LEC and is still under investigation.[65, 66]

Besides the lifetime of an LEC, the turn-on time is also very important. The turn-on time is the time required under constant bias to reach maximum brightness. The range of turn-on times for LEC devices is between several seconds and hundreds of hours.[24, 67] For commercial products, the turn-on time has generally to be shortened to seconds. There are several starting points to shorten the turn-on time of a LEC device, such as the applied bias, the mobility of the ions and the addition of ionic liquids or polymers. Unfortunately, a gain in the turn-on time often yields a lower stability and therefore a shorter lifetime of the LEC device.[24, 25]

The third important issue is efficiency of a LEC device. To compare different LEC devices, often the external quantum efficiency (EQE) is measured. The EQE is the ratio of photons emerging from the device per electron injected.[24] As already shown in the first publication concerning iridium LECs, high EQEs can be achieved with a single layer of an iTMC sandwiched between two electrodes.[23, 24]

In LEC devices, if the complexes are spatially very close, they likely undergo non-radiative self-quenching processes. There are two possibilities, to reduce the close proximity of the complexes. The addition of an inert polymer such as poly(methyl methacrylate) (PMMA) or poly(carbonate) (PC), or by introduction of steric hindrance on the ancillary ligand, via bulky groups, in order to improve the device efficiency.[24, 56]

[1] W. P. Griffith, *Platinum Metals Rev.*, 2004, **48**, 4, 182.
[2] Smithson Tennant, *Phil. Trans*., 1804, **94**, 411.
[3] *J. Nat. Philos., Chem. Arts*, 1805, **10**, 24; *ibid*., 1804, **8**, 220.
[4] C. E. Housecroft, A. G. Sharpe, *Inorganic Chemistry*, *3rd Edition*, Prentice Hall, 2007.
[5] J. Emsley, Nature's building blocks: An a-z guide to the elements, Oxford University Press, Oxford, **2001**.
[6] S. Graber, *From STM to LEECs,* PhD Thesis, Cuvillier Verlag Göttingen, 2009.
[7] G. J. Sunley, D. J. Watson, *Catalysis Today*, 2000, **58**, 293.
[8] D. Rageot, A. Pfaltz, *Helv. Chim. Acta,* 2012, **95**, 2176.
[9] R. H. Crabtree, *Organomet. Chem*., 2011, **34**, 1.
[10] C.-H. Leung, H.-J. Zhong, D. S.-H. Chan, D.-L. Ma, *Coord. Chem. Rev.*, 2013, **257**, 1764.
[11] J. D. Blakemore, N. D. Schley, M. N. Kushner-Lenhoff, A. M. Winter, F. D'Souza, R. H. Crabtree, G. W. Brudvig, *Inorg. Chem.*, 2012, **51**, 7749.
[12] E. Garand, J. A. Fournier, M. Z. Kamrath, N. D. Schley, R. H. Crabtree, M. A. Johnson, *Phys. Chem. Chem. Phys.*, 2012, **14**, 10109.
[13] M. S. Lowry, S. Bernhard, *Chem. Eur. J.*, 2006, **12**, 7970.
[14] K. J. Arm, W. Leslie, J. A. G. Williams, *Inorg. Chim. Act.*, 2006, **359**, 1222.
[15] L. Flamigni, J.-P. Collin, J.-P. Sauvage, *Acc. Chem. Res.,* 2008, **41**, 7, 857.
[16] N. N. Greenwood, A. Earnshaw, *Chemistry of the Elements*, Butterworth-Heinemann, Oxford, 1995.
[17] A. F. Holleman, E. Wiberg, N. Wiberg, *Lehrbuch der Anorganischen Chemie*, Walter de Gruyter, Berlin, 2007.
[18] L. Flamigni, A. Barbieri, C. Sabatini, B. Ventura, F. Barigelletti, *Top. Curr. Chem.*, 2007, **281**, 143.
[19] C. E. Housecroft, A. G. Sharpe, *Inorganic Chemistry*, *3rd Edition*, Prentice Hall, 2007, 640.
[20] G. Schneider, New inorganic iridium(III) complexes for lighting applications, *Master Thesis,* 2009.
[21] C. E. Housecroft, A. G. Sharpe, *Inorganic Chemistry*, *3rd Edition*, Prentice Hall, 2007, 662.
[22] M. Montalti, A. Credi, L. Prodi, M. T. Gandolfi, *Handbook of Photochemistry*, 2006, Taylor and Francis, Boca Raton, Fl.
[23] S. Bernhard, X. C. Gao, G. G. Malliaras, H. D. Abruña, *Adv. Mater.,* 2002, **14***,* 433.
[24] J. D. Slinker, A. A. Gorodetsky, M. S. Lowry, J. J. Wang, S. Parker, R. Rohl, S. Bernhard, G. G. Malliaras, *J. Am. Chem. Soc.*, 2004, **126**, 2763.
[25] T. Hu, L. He, L. Duan, Y. Qiu, *J. Mat. Chem*., 2012, **22**, 4206.
[26] J. D. Slinker, J. Rivnay, J. S. Moskowitz, J. B. Parker, S. Bernhard, H. D. Abruña, G. G. Malliaras, *J. Mater. Chem.*, 2007, **17**, 2976.
[27] M. Mydlak, C. Bizzarri, D. Hartmann, W. Sarfert, G. Schmid, L. De Cola, *Adv. Funct. Mater.*, 2010, **20**, 1812.
[28] J. L. Rodríguez-Redondo, R. D. Costa, E. Ortí, A. Sastre-Santos, H. J. Bolink, F. Fernández-Lázaro, *Dalton Trans.*, 2009, 9787.
[29] S. Sprouse, K. A. King, P. J. Spellane, R. J. Watts, *J. Am. Chem. Soc*., 1984, **106**, 6647.
[30] F. O. Garces, K. A. King, R. J. Watts, *Inorg. Chem.*, 1988, **27**, 3464.
[31] M. Nonoyama, *Bull. Chem. Soc. Jpn.*, 1974, **47**, 767.
[32] Bundesamt für Gesundheit, 04.2012, http://www.news.admin.ch/message/index.html?lang=de&msg-id=44057.
[33] Projektliste der Energieforschung des Bundes 2008/2009, *Bundesamt for Energie*, 2011.
[34] A. Kemmler, A. Piégsa, A. Ley, Analyse des schweizerischen Energieverbrauchs 200-2011 nach Verwendungszwecken, *Bundesamt für Energie*, 2012.
[35] Osram, Technik und Anwendung: Halogen-Niedervoltlampen.
[36] C. J. Humphreys, *MRS Bulletin*, 2008, **33**, 459.
[37] U. Mitschke and P. Bäuerle, *J. Mater. Chem*., 2000, **10**, 1471.
[38] R. Friedel, Edison's electric light: the art of invention*, Johns Hopkins University Press*, Baltimore, 2010.
[39] N. Zheludev, The life and times of the LED – a 100-year history, *Nature Photonics*, 1, 2007.
[40] A. Bernanose, M. Comte, P. Vouaux, *J. Chim. Phys*., 1953, **50**, 64.
[41] B. J. Gans, U. S. Schubert, *Macromol. Rapid Commun.,* 2003, **24***,* 659.
[42] A. Sandström, H. F. Dam, F. C. Krebs, L. Edman, *Nature Commun.*, 2012, **3**, 1.
[43] E. Holder, B. M. W. Langeveld, U. S. Schubert, *Adv. Mater*., 2005, **17**, 1109.
[44] Q. Pei, G. Yu, C. Zhang, Y. Yang, A. Heeger, *Science*, 1995, **269**, 1086.
[45] J. K. Lee, D. S. Yoo, E. S. Handy, M. F: Rubner, *Appl. Phys. Lett.*, 1996, **69**, 1686.
[46] F. G. Gao, A. J. Bard, *J. Am. Chem. Soc.*, 2000, **122**, 7426.
[47] J. D. Slinker, J. A. DeFranco, M. J. Jaquith, W. R. Silveira, Y.-W. Zhong, J. M. Moran-Mirabal, H. G. Craighead, H. D. Abruña, J. A. Marohn, G. G. Malliaras, *Nature Mater.*, 2007, **6**, 894.

[48] R. D. Costa, E. Ortí, H. J. Bolink, S. Graber, S. Schaffner, M. Neuburger, C. E. Housecroft, E. C. Constable, *Adv. Funct. Mater.*, 2009, **19**, 3456.
[49] L. He, L. Duan, J. Qiao, R. J. Wang, P. Wei, L. D. Wang, Y. Qiu, *Adv. Funct. Mater.,* 2008, **18***,* 2123.
[50] L. He, J. Qiao, L. Duan, G. F. Dong, D. Q. Zhang, L. D. Wang, Y. Qiu, *Adv. Funct. Mater.,* 2009, **19***,* 2950.
[51] M. A. Baldo, D. F. O'Brien, Y. You, A. Shoustikov, S. Sibley, M.E. Thompson, S. R. Forrest, *Nature,* 1998**, 395***,* 151.
[52] X. Gong, J. C. Ostrowski, G. C: Bazan, D. Moses, A. J. Heeger, M. S. Liu, A. K. Y. Jen, *Adv. Mater.*, 2003, **15**, 45.
[53] A. R. Hosseini, C. Y. Koh, J. D. Slinker, S. Flores-Torres, H. D. Abruña, G. G. Malliaras, *Chem. Mater.,* 2005, **17***,* 6114.
[54] H. Rudmann, S. Shimada, M. F. Rubner, *J. Am. Chem. Soc.,* 2002, **124**, 4918.
[55] M. S. Lowry, J. I. Goldsmith, J. D. Slinker, R. Rohl, R. A. Pascal, G. G. Malliaras, S. Bernhard, *Chem. Mater.,* 2007, **17**, 5712.
[56] Md. K. Nazzeruddin, R. T. Weigh, Z. Zhou, C. Klein, Q. Wang, F. De Angelis, S. Fantacci, M. Graetzel, *Inorg. Chem.,* 2006*,* **45**, 9245.
[57] E. C. Constable, C. E. Housecroft, G. E. Schneider, unpublished results, 2013.
[58] C.-H. Hsieh, F.-I. Wu, C.-H. Fan, M. J. Huang, K.-Y. Lu, P.-Y. Chou, Y.-H. Ou Yang, S.-H. Wu, I.-C. Chen, S.-H. Chou, K.-T. Wong, C.-H. Cheng, *Chem. Eur. J.*, 2011, **17**, 33, 9180.
[59] R. D. Costa, F. J. Cespedes-Guirao, E. Ortí, H. J. Bolink, J. Gierschner, F. Fernandez-Lazaro, A. Sastre-Santos, *Chem. Commun.,* 2009, 3886.
[60] H.-C. Su, H.-F. Chen, F.-C. Fang, C.-C. Liu, C.-C. Wu, K.-T. Wong, Y.-H. Liu, S.-M. Peng, *J. Am. Chem. Soc.,* 2008*,* **130**, 3413.
[61] C. Janiak, *J. Chem. Soc., Dalton Trans.*, 2000, 3885.
[62] H. J. Bolink, E. Coronado, R. D. Costa, E. Ortí, M. Sessolo, S. Graber. K. Doyle, M. Neuburger, C. E. Housecroft, E. C. Constable, *Adv. Mater.,* 2008*,* **20***,* 3910.
[63] R. D. Costa, E. Ortí, H. J. Bolink, S. Graber, C. E. Housecroft, M. Neuburger, S. Schaffner, E. C. Constable, *Chem. Commun.,* 2009, 2029.
[64] R. D. Costa, E. Ortí, H. J. Bolink, S. Graber, C. E. Housecroft, E. C. Constable, *J. Am. Chem. Soc.*, 2010, **132**, 5978.
[65] R. D. Costa, E. Ortí, H. J. Bolink, S. Graber, C. E. Housecroft, E. C. Constable, *Chem. Commun.,* 2011, **47***,* 3207.
[66] D. Tordera, S. Meier, M. Lenes, R. D. Costa, E. Orti, W. Sarfert, H. J. Bolink, *Adv. Mater.,* 2012, **24***,* 897.
[67] E. Baranoff, H. J. Bolink, E. C. Constable, M. Delgado, D. Häussinger, C. E. Housecroft, M. K. Nazeeruddin, M. Neuburger, E. Ortí, G. E. Schneider, D. Tordera, R. M. Walliser, J. A. Zampese, *Dalton Trans*., 2013, **42**, 1073.

Chapter 2

2. The influence of trace amounts of chloride counterions on the performance of an iridium(III) complex in LEC devices

2.1. Introduction

The established collaboration between the research group of Profs. E. C. Constable and C. E. Housecroft with the group of Dr. H. J. Bolink in Valencia (Spain) has generated many results towards the understanding of LEC devices consisting of ionic transition metal complexes (iTMCs). Compounds, such as $[Ir(ppy)_2(pbpy)][PF_6]$,[1,2] $[Ir(ppy)_2(bpy)][PF_6]$[3] and $[Ir(ppy)_2(phen)][PF_6]3$ have previously been used to investigate enhancements of the architecture and the working principles of the LEC devices.

The group of H. J. Bolink needed approximately 1 g of the complex $[Ir(ppy)_2(bpy)][PF_6]$ to continue studies on this compound. The synthesis was done using the same experimental methodology as the previously synthesized batches.3 For convenience, this established synthetic route is labelled batch 1 in the experimental section (see section 2.7.1). The newly synthesised 1 g is labelled batch 2. After purification, NMR spectroscopic analysis and ESI-MS, batch 2 (see section 2.7.2) was sent to Valencia, but the LEC devices using batch 2 did not perform as well as the previously measured devices. The luminance was approximately half that of batch 1, although the devices made with the two different batches appeared to have similar lifetimes (Figure 2.1).

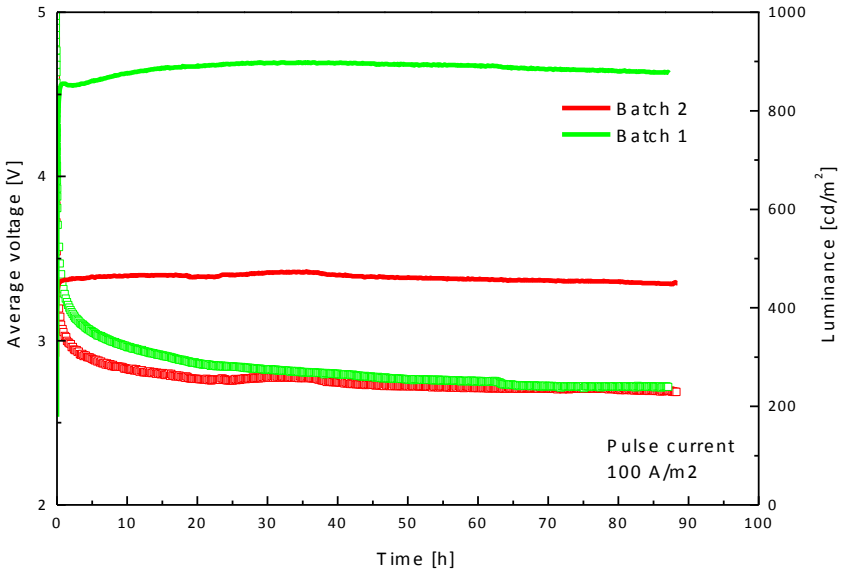

Figure 2.1 Device performance using the two batches of $[Ir(ppy)_2(bpy)][PF_6]$ in LEC configuration (ITO/PEDOT:PSS/$[Ir(ppy)_2(bpy)][PF_6]$ + $[BMIM][PF_6]$(4:1)/Al).

Batch 2 of the complex was sent back to Basel from Valencia for more detailed analytics, i.e. further NMR spectroscopic measurements, elemental analysis, ESI-MS, and further purification. X-ray crystal structure determination, ^{1}H, ^{19}F and ^{31}P NMR spectroscopic titrations were carried out to establish the reason for the lower performances.

2.2. Results and discussion

The syntheses of $[Ir(ppy)_2(bpy)][PF_6]$ were all performed in a microwave reactor, followed by precipitation of the complex with an excess (10 eq.) of ammonium hexafluoridophosphate. The purification of the complex was done twice via column chromatography. In general, the reaction works well even on large scales (up to 1 g) with quantitative yields (up to 95%, batch 1, see section 2.7.1).

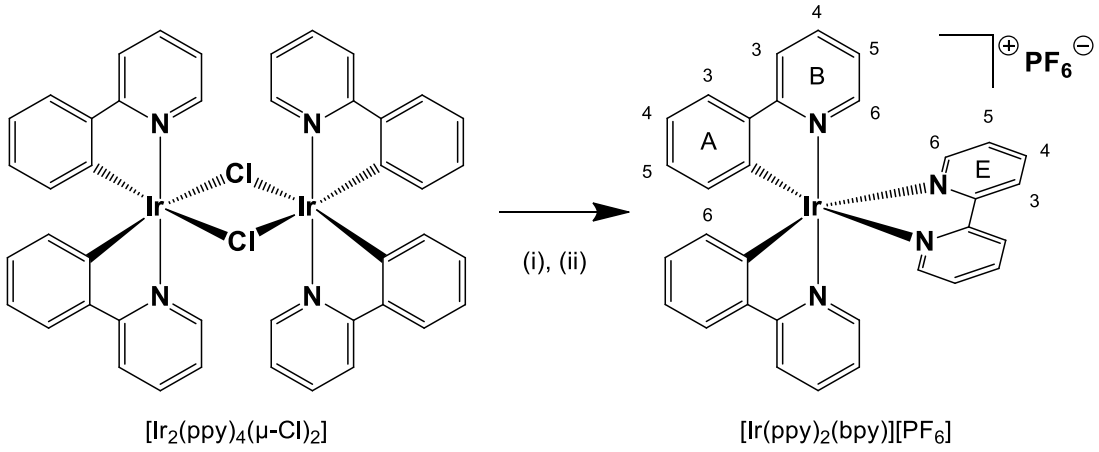

Scheme 2.1 Synthesis of $[Ir(ppy)_2(bpy)][PF_6]$ with ring labelling and atom numbering for NMR spectroscopic assignments. Conditions: (i) bpy, MeOH, microwave, 2 h, 120 °C; (ii) $[NH_4][PF_6]$.

For batch 2, the reaction was repeated using the same experimental conditions as batch 1. As the ^{1}H NMR spectra looked essentially identical to that of the original compound (Figure 2.2), it was used to prepare the LEC devices.

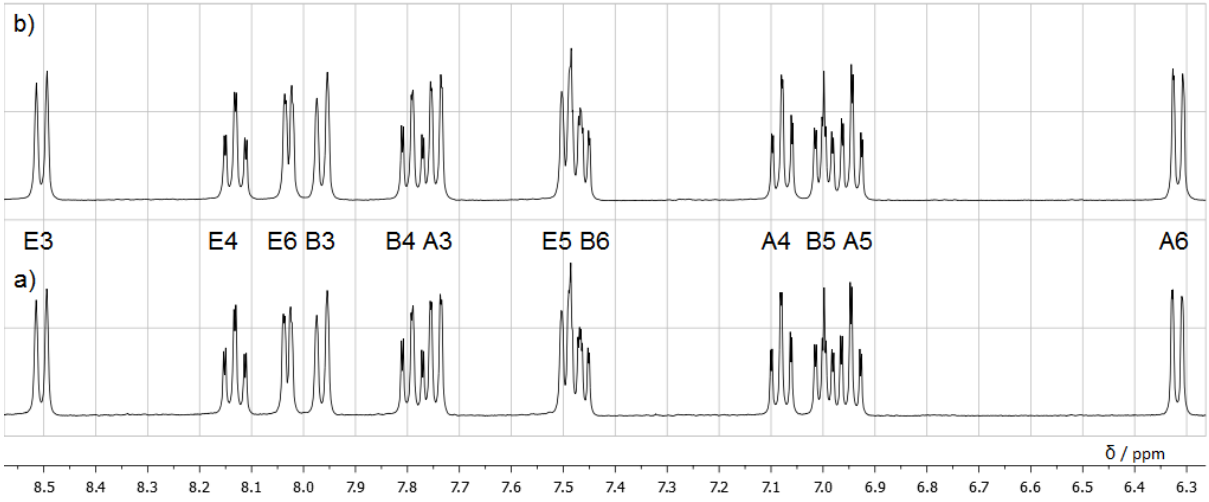

Figure 2.2 ^{1}H NMR spectra comparison of a) batch 2 of $[Ir(ppy)_2(bpy)][PF_6]$ and b) batch 1 (500 MHz, CD_2Cl_2, 298K).

However the complex formed as batch 2 performed significantly worse in the LEC devices than the previous batche had done (see Figure 2.1). As such, it was decided to repurify the sample. Careful comparison of the ^{1}H NMR spectra of batch 2 with batch 1 indicated very minor shifts in the protons of ring E; proton E3 is shifted about δ 0.001 ppm (Scheme 2.1 and Figure 2.3).

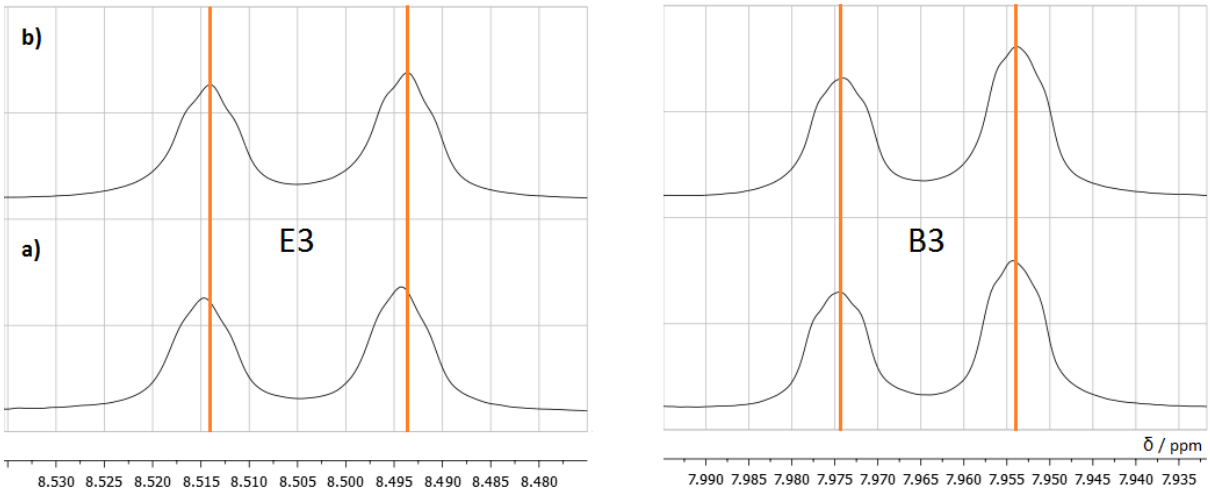

Figure 2.3 ^{1}H NMR spectra comparison of a) batch 2 of $[Ir(ppy)_2(bpy)][PF_6]$ and b) batch 1 (500 MHz, CD_2Cl_2, 298K).

Elemental analysis of batch 2 showed that the compound did not analyse as $[Ir(ppy)_2(bpy)][PF_6]$ but suggested that the complex contained a mixture of counterions: 99% $[PF_6]^-$ and 1% Cl^- (found: C = 44.52%, H = 2.94%, N = 6.80%. Calcd. for $[Ir(ppy)_2(bpy)][0.99\ PF_6][0.01\ Cl]+1CH_2Cl_2$: C = 44.76%, H = 2.96%, N = 6.33%). Subsequent structural analysis of $[Ir(ppy)_2(bpy)][Cl]$ showed that the Cl^- ion is closely associated with the cation in the solid state and we wondered whether the slight differences in the ^{1}H NMR spectra between batches 1 and 2 could be associated with the presence of chloride ion. Thus, the NMR data appeared to be consistent with the elemental analysis.

The repurification of batch 2 was done by repeating the precipitation with ammonium hexafluoridophosphate and additionally with silver hexafluoridophosphate to ensure removal of Cl^-. The column chromatography (Fluka Silica 60) was followed by a recrystallization (DCM with Et_2O) carried out on this sample. Afterwards the ^{1}H NMR spectrum was identical to that of the original complex and the elemental analysis fitted for $[Ir(ppy)_2(bpy)][PF_6]$ (found: C = 47.82%, H = 3.12%, N = 7.32%. Calcd. for $[Ir(ppy)_2(bpy)][PF_6]$: C = 47.94%, H = 3.02%, N = 7.32%). Upon retesting, the new devices performed as expected, consistent with measurements using batch 1.

Fortuitously, during the synthesis of batch 2, a small sample of the crude reaction mixture (i.e. before addition of NH_4PF_6) was set on one side for crystal growth.

2.3. Solid state structure of $[Ir(ppy)_2(bpy)][Cl]$

From a MeOH solution of the crude reaction mixture of batch 2 layered with Et_2O, X-ray quality crystals of $2\{[Ir(ppy)_2(bpy)][Cl]\}.2CH_2Cl_2.[H_3O].[Cl]$ were grown by diffusion over several days at room temperature. The complex crystallizes in the monoclinic, centrosymmetric C_2/c space group and both Δ- and Λ-cations are present in the unit cell. The structure of the Δ-cation is depicted in Figure 2.4. The asymmetric unit contains one cation, one anion, one CH_2Cl_2 solvent molecule, half a Cl^- ion and half a H_3O^+ cation.

The atom Ir1 is in a slightly distorted octahedral environment and the N-donors of the two cyclometallating ligands are in a *trans*-arrangement, as expected and previously seen in similar compounds.[1, 2, 3] The two C^N ligands are almost planar with deviation angles between the least squares planes of the phenyl and pyridine rings of 4.8 and 5.0°. The bpy ligand is slightly more twisted, the angle between the least squares planes of the two pyridine rings being 8.7°. The chloride anion is close to the protons E3, consistent with NMR spectroscopy, and forms hydrogen bonds[4] to the two CH units (H4A and H7A) with Cl...H distances of 2.79 and 2.87 Å (Figure 2.4).

Comparison with the solid state structure of $[Ir(ppy)_2(bpy)][PF_6]$ shows that the fluorines of the $[PF_6]^-$ anion are at H...F distances in the range between 2.87 to 3.10 Å around proton E3.3

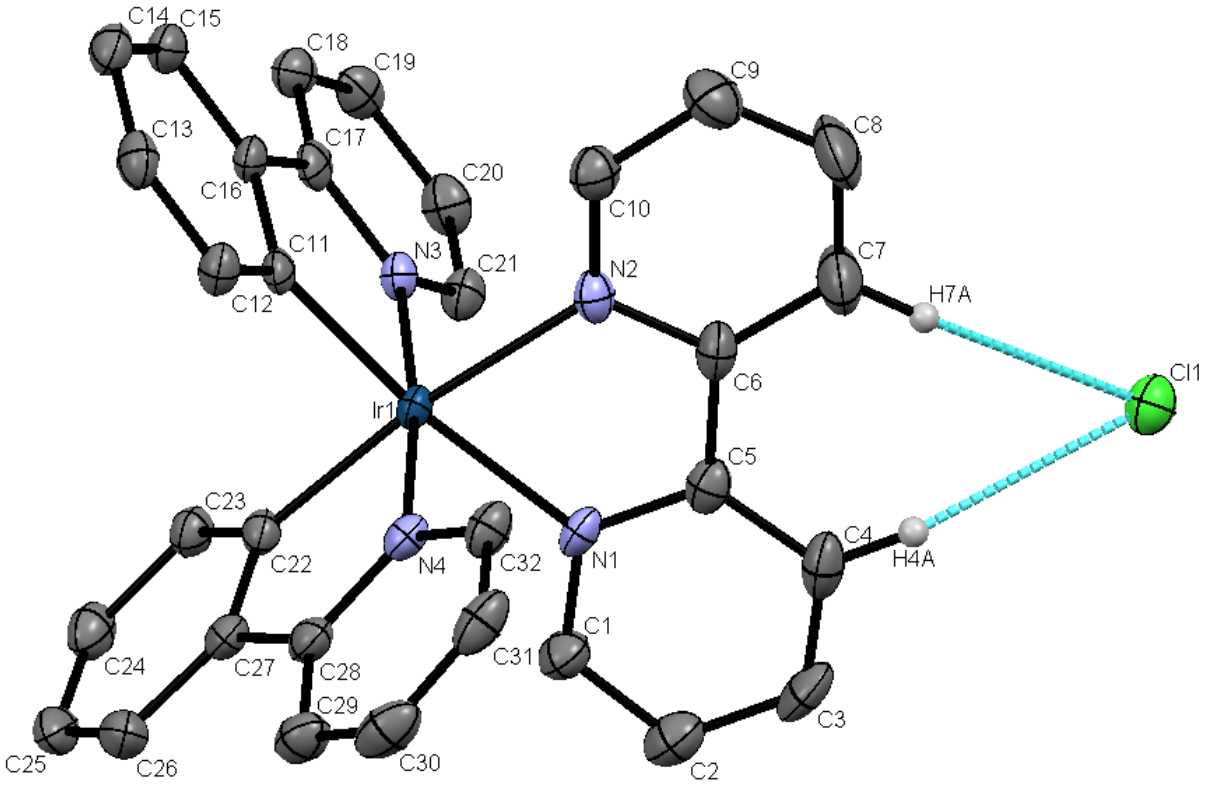

Figure 2.4 Structure of the Δ-cation of $2\{[Ir(ppy)_2(bpy)][Cl]\}.2CH_2Cl_2.[H_3O].[Cl]$ with ellipsoids plotted at 50% probability level, H atoms omitted except for protons E3 (see NMR ring labelling). Selected bond lengths (in Å) and bond angles (in °); Ir1–C11: 2.011(3), Ir1–C22: 2.012(3), Ir1–N4: 2.042(3), Ir1–N3: 2.050(3), Ir1–N2: 2.135(3), Ir1–N1: 2.142(3); N1–Ir1–N2: 76.5(1), N3–Ir1–C11: 80.2(1), N4–Ir1–C22: 80.4(1).

The crystal packing consists of multiple edge-to-face π-stacking interactions. There are interactions between cations with the same handedness and between the two different enantiomers. Two molecules with the same handedness exhibit two π-contacts between atom H20A and pyridine ring containing atom $N4^i$ (symmetry code i = x, y – 1, z) with distance of 3.25 Å between the atom H20A and the centroid of the pyridine ring, and atom $H30A^i$ and pyridine ring containing atom N1 with a distance of 3.05 Å between atom $H30A^i$ and the centroid of the pyridine ring. This embrace is depicted in Figure 2.5. A further π-contact is between atom H18A and phenyl ring containing atom $C22^{ii}$ (symmetry code ii = ½

– x, y – ½, ½ – z) with a distance of 2.69 Å between atom H18A and the centroid of the phenyl ring. The contacts between different enantiomers are between atom H9A and phenyl ring containing atom C22^{iii} (symmetry code iii = x, 1 – y, z + ½) with a distance of 3.00 Å between atom H9A and the centroid of the phenyl ring.

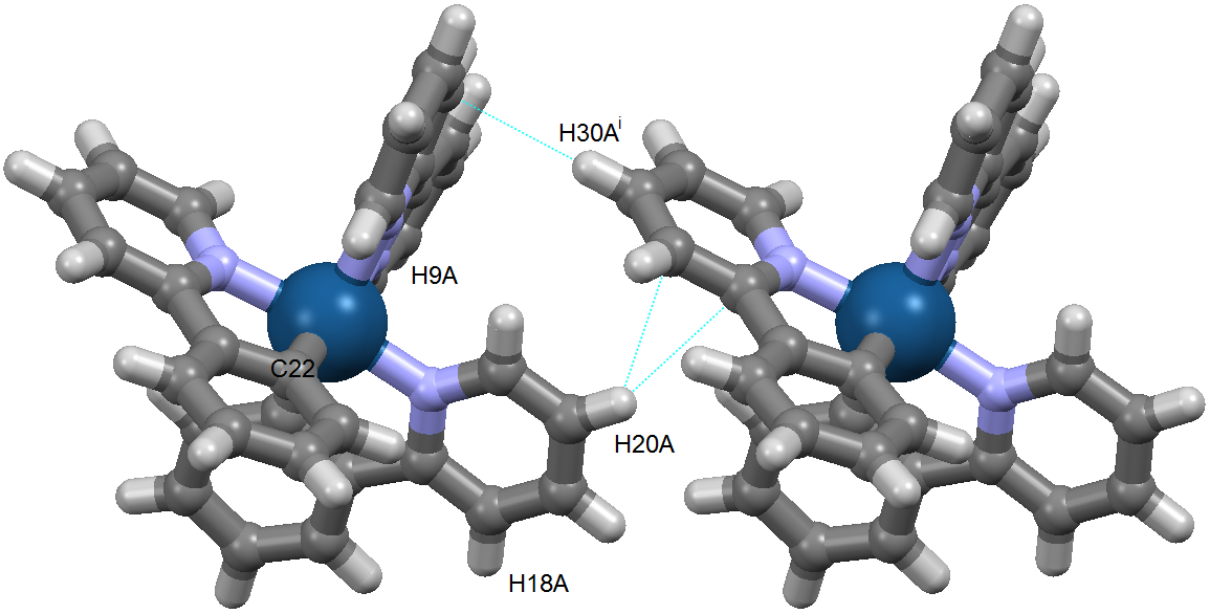

Figure 2.5 Edge-to-face π-interactions between two Δ-cations of $[Ir(ppy)_2(bpy)]^+$ seen along the c-axis.

Each chloride anion interacts with 4 cations with Cl...H contacts at a range between 2.68 and 3.17 Å. According to the definition of Emsley, all these contacts are strong hydrogen bonds.4 Additionally there are contacts between both ions with the solvent molecules. All the interactions together lead to alternating rows of cations with alternating handedness separated by anions and the solvent molecules (see Figure 2.6).

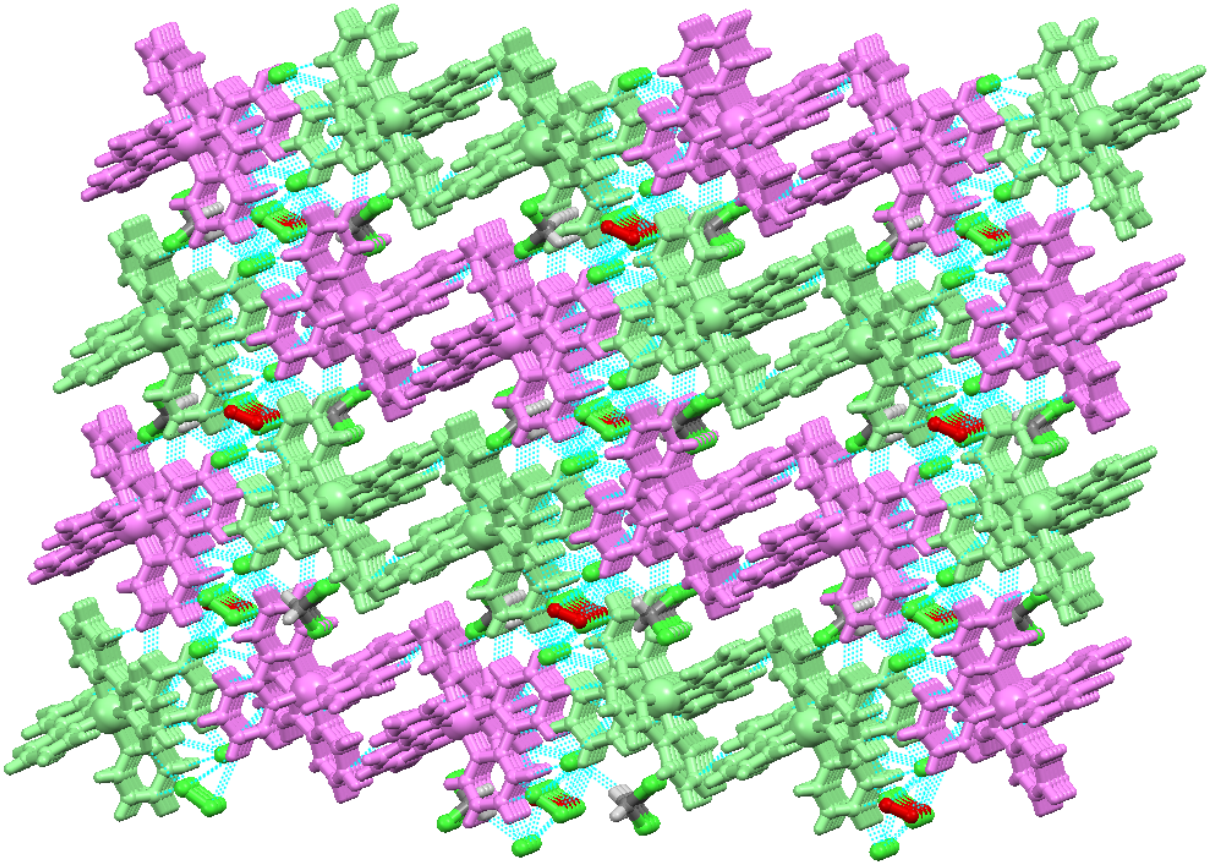

Figure 2.6 Packing in $2\{[Ir(ppy)_2(bpy)][Cl]\}.2CH_2Cl_2.[H_3O].[Cl]$, rows of alternating Δ- (purple), Λ-cations (light green), with interstitial $[Cl]^-$ anions (green) and $[H_3O]^+$ cations (red).

All the cations, anions and solvent molecules in $2\{[Ir(ppy)_2(bpy)][Cl]\}.2CH_2Cl_2.[H_3O].[Cl]$ are ordered.

2.4. NMR spectroscopic investigations

In the solid state structure of $[Ir(ppy)_2(bpy)][Cl]$ (see section 2.3), the chloride ion has a close ion-pairing to the cation, in particular to ring E of the complex (see Scheme 2.1). In order to examine the chloride interactions with the cation of $[Ir(ppy)_2(bpy)][PF_6]$ in solution, a series of ^1H, ^{19}F and ^{31}P NMR spectroscopic measurements were recorded. For this series, samples were titrated, starting with the pure complex $[Ir(ppy)_2(bpy)][PF_6]$ in increments of 0.1 equivalents of tetra-n-butyl ammonium chloride (TBACl) added, up to 1.1 equivalents (Figure 2.7).

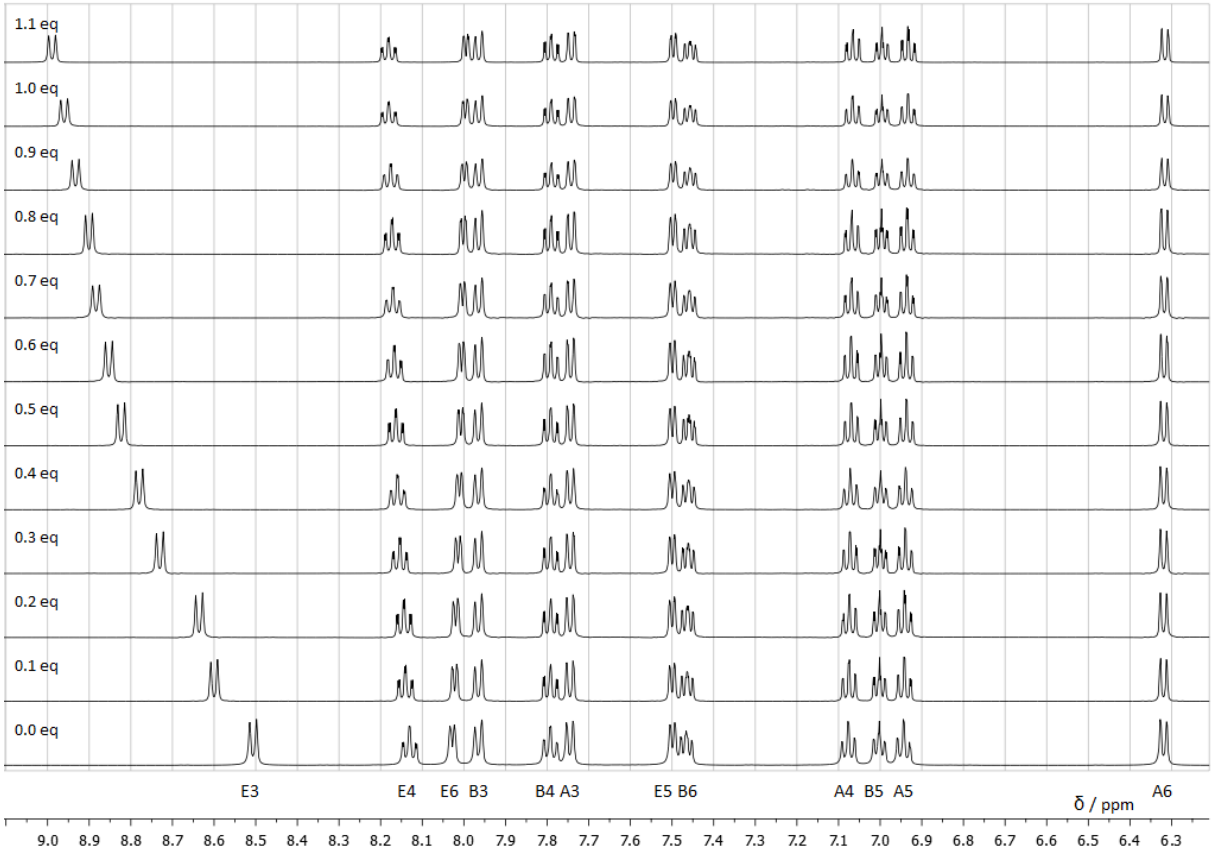

Figure 2.7 ^{1}H NMR spectra of $[Ir(ppy)_2(bpy)][PF_6]$ (0.02 mmol in 0.75 ml of CD_2Cl_2) by stepwise addition of 0.1 eq. TBACl to 1.1 eq. (500 MHz, CD_2Cl_2, 298K) with labels of the proton signals for the cation.

The proton signals affected the most upon addition of TBACl arose from ring E (see Scheme 2.1). The ^{1}H signal exhibiting the most significant shift (from δ 8.505 to 8.989 ppm) was that of proton E3. Upon addition of a large excess of TBACl (> 10 eq.) the signal for proton E3 shifted to δ 9.326 ppm.

As the exchange equilibrium involving the anions is faster than the NMR timescale, only 1 set of signals is seen in the NMR spectra and not a mixture of the spectra from the two salts. The set observed represents the average of the complex with two different anions in solution.

The ion exchange in this complex was evaluated from non-linear least squares fitting of the chemical shift of proton E3 to appropriate equations by using WinEQNMR2 (version 2.00 by Michael J. Hynes[5]). The equilibrium constant was calculated according to K. Hirose[6] for a logarithmic fitting process. The output of this fit was then used as input for a linear fit to determine the equilibrium constant of the ion exchange reaction (residuals squares = 0.00274 and R-factor = 0.001789; 0 for perfect fit).

$$[Ir(ppy)_2(bpy)][PF_6] + [Cl]^- \rightleftharpoons [Ir(ppy)_2(bpy)][Cl] + [PF_6]^- \qquad \log K = 2.24$$

This log*K* value indicates that the chloride is the more favourable counterion, if both ions, chloride and hexafluoridophosphate, are available. The regression of the linear fit is depicted in Figure 2.8. As expected, the deviation is larger for the small equivalents of TBACl, as the error on the balance is bigger, the smaller the amount weighed.

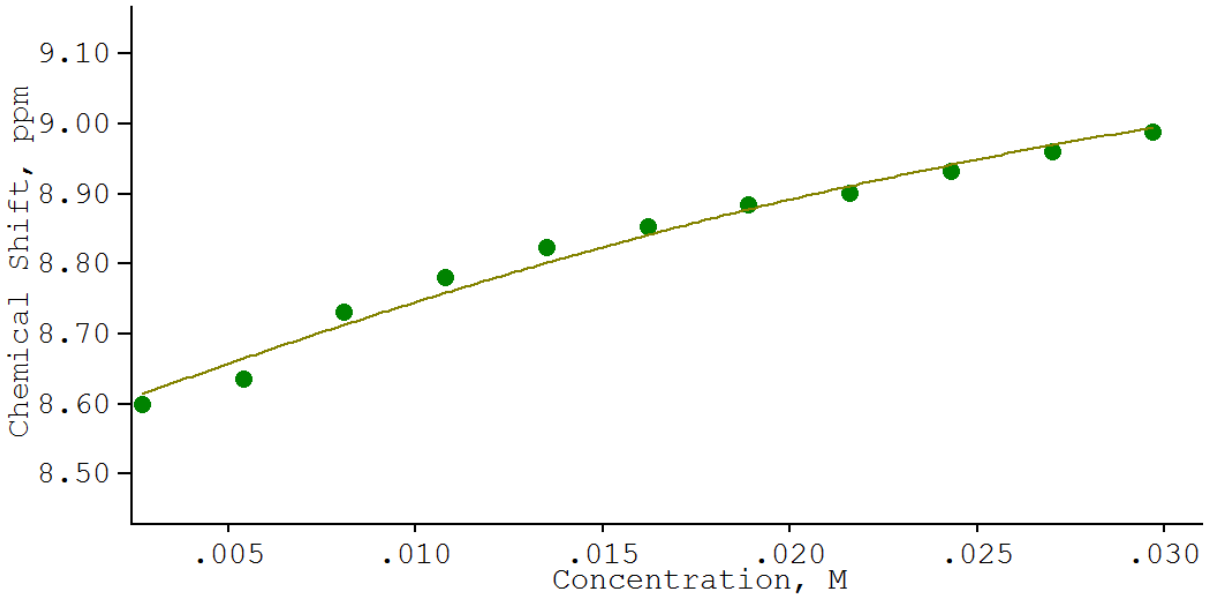

Figure 2.8 Plot showing the measured values of the chemical shift of proton E3 upon addition of TBACl (0 to 1.1 eq.) along with the statistical best fit (green line).

As with the ^{1}H NMR spectra, in the ^{19}F NMR spectroscopic measurements, the doublet signal (arising from phosphorus-fluorine splitting J_{FP} = 710.7 Hz) of the $[PF_6]^-$ anion moves upon addition of TBACl. The doublet from the pure complex is shifted by δ 0.73 ppm by addition of an excess of TBACl (Figure 2.9); the ^{19}F NMR signal with an excess of TBACl is in the region of $TBAPF_6$ in CD_2Cl_2. It has to be mentioned, that the change in the shift of this signal is relatively small, compared to the proton shift. While the ^{1}H NMR signals are normally in the region between 0 to 10 ppm, the ^{19}F NMR signals are typically in a range of -200 to +200 ppm.[7]

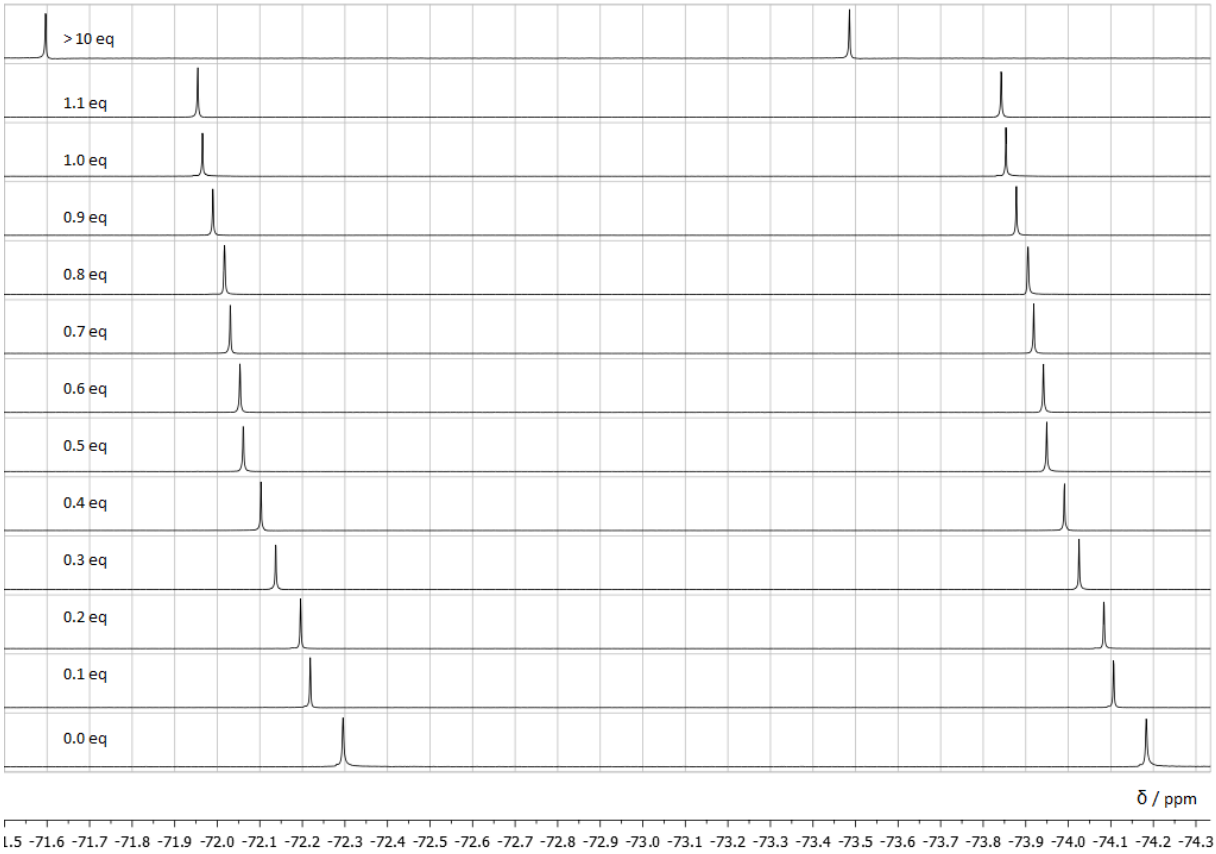

Figure 2.9 ^{19}F NMR spectroscopic measurements of $[Ir(ppy)_2(bpy)][PF_6]$ by stepwise addition of 0.1 eq. TBACl to 1.1eq and with an excess of TBACl (last line, 376 MHz, CD_2Cl_2, 298K). The two apparent signals in each spectrum in each spectrum are in fact a doublet (J_{FP} = 710.7 Hz).

In the ^{31}P NMR spectroscopic measurements the signals are not shifted upon addition of TBACl. This indicates that the fluorine atoms of the $[PF_6]^-$ anion protect the phosphorus so that the NMR environment is not changed by the addition of chloride atoms.

Comparison of the behaviour of similar iridium(III) complexes (e.g. $[Ir(ppy)_2(pbpy)][PF_6]$ or $[Ir(ppy)_2(phen)][PF_6]$) in the presence of chloride ions yielded the same result in shifting the protons which correspond to the E3 protons on the bpy ligand (Scheme 2.2, Figure 2.10).

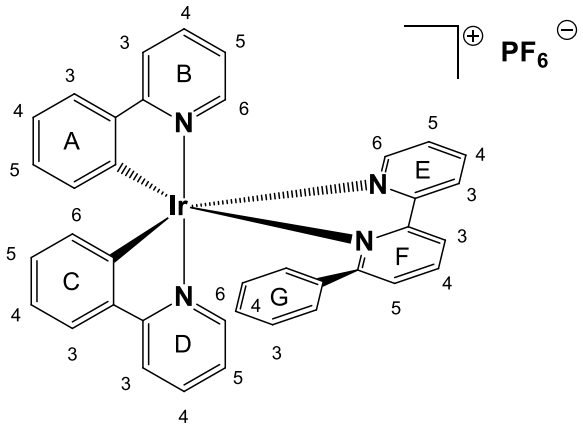

Scheme 2.2 Structure of $[Ir(ppy)_2(pbpy)][PF_6]$ with labels for NMR spectroscopic assignments.

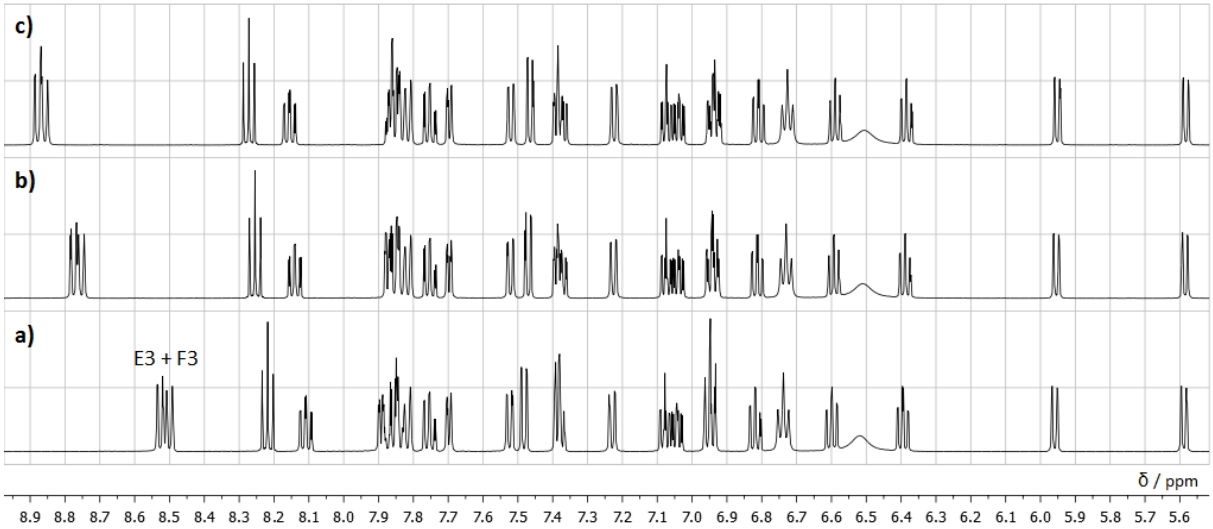

Figure 2.10 ^{1}H NMR spectra of a) the asymmetric complex $[Ir(ppy)_2(pbpy)][PF_6]$, b) by addition of 0.5 eq. TBACl and c) by addition of 1.0 eq. TBACl (500 MHz, CD_2Cl_2, 298K).

Obviously, the ratio of counterions present has an influence on the NMR spectroscopic environment of the complex, as can be seen in the ^{1}H and ^{19}F NMR spectra. As the shift of the NMR signals for these atoms is dependent on the ratio of the counterions, by addition of $TBAPF_6$ to the NMR sample, the shift in peaks can be moved to higher field (test reaction in Figure 2.11). This leads to a simple test method to prove the absence of Cl^- anions. A ^{1}H NMR spectrum of a purified complex should be recorded, $TBAPF_6$ added to the NMR sample and a second ^{1}H NMR spectrum recorded. If the two recorded spectra are exactly the same, the original complex does not contain any Cl^- anions.

This procedure eliminates one possible cause for low performances in LEC devices.

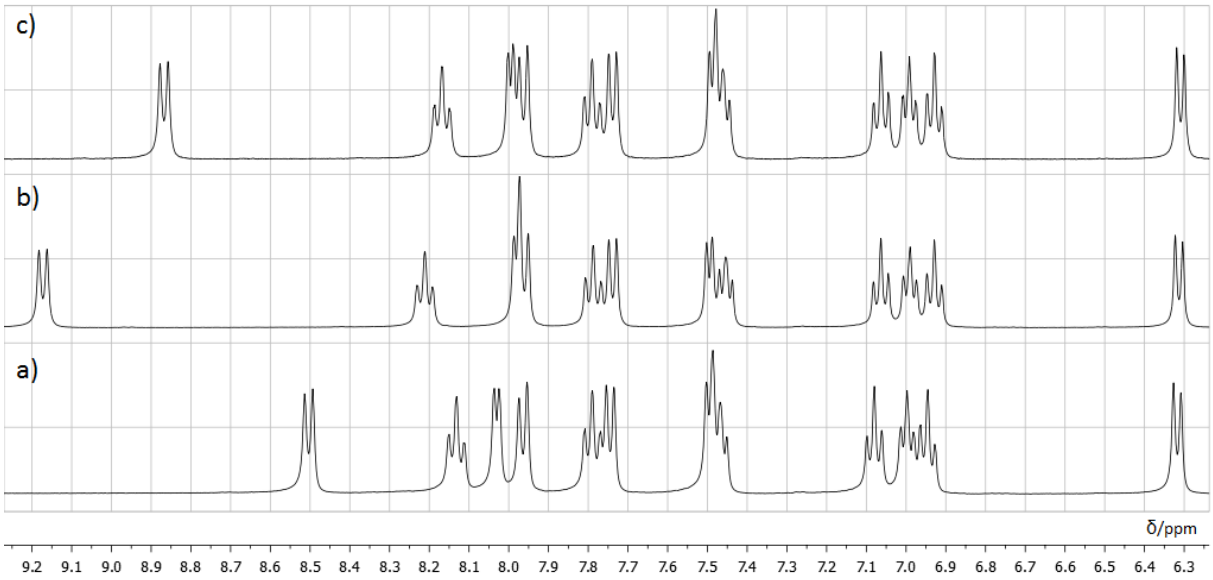

Figure 2.11 The shifts of the signals can be moved in both directions: a) pure $[Ir(ppy)_2(bpy)][PF_6]$, b) $[Ir(ppy)_2(bpy)][PF_6]$ with TBACl (spatula tip), c) addition of $TBAPF_6$ (spatula tip) to spectrum b) (400 MHz, CD_2Cl_2, 298K).

2.5. Photophysical studies

Photophysical studies of $[Ir(ppy)_2(bpy)][PF_6]$ and $[Ir(ppy)_2(bpy)][Cl]$, isolated from reaction mixture of batch two before addition of NH_4PF_6, were performed on the solid samples and in MeCN solutions; CH_2Cl_2 was avoided to ensure the solvent could not be implicated as a source of Cl^-. In solution, all complexes with different ratios of counterions exhibited the same properties (emission maxima λ_{em} = 600 nm, quantum yield = 0.13). In the solid state, the two measured samples, $[Ir(ppy)_2(bpy)][PF_6]$ and $[Ir(ppy)_2(bpy)][Cl]$ yielded different emission maxima (λ_{em} = 510 nm and 540 nm, Figure 2.12) but the quantum yields were similar for both with values (QY = 0.16).

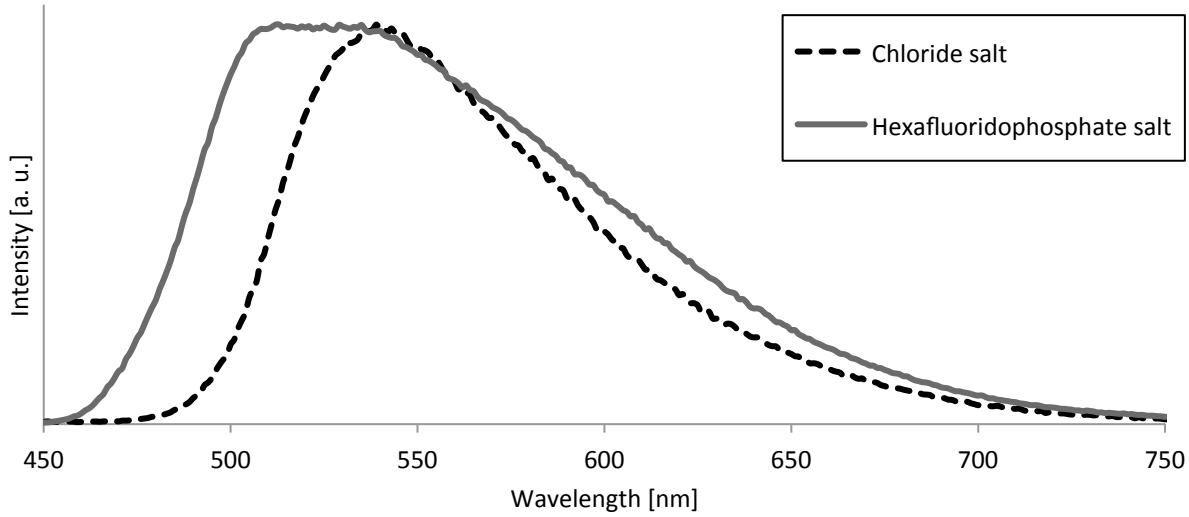

Figure 2.12 Solid state emission spectra of $[Ir(ppy)_2(bpy)][Cl]$ and $[Ir(ppy)_2(bpy][PF_6]$.

2.6. Conclusion and Outlook

The dependence of the device performance upon the presence of trace-amounts of chloride atoms is obviously very strong. One possible explanation could be, that in LEC devices under bias, the high mobility of the chloride ions, which are smaller and more mobile than $[PF_6]^-$, leads to a short circuit and therefore significantly lowers the device performance. To increase the efficiency of LEC devices (e.g. the luminance), the purity of the complex, especially the exclusivity of the anion is crucial. An easy proof for absence of chloride counterions, and therefore the purity of the complex, can be achieved with the help of ^1H NMR spectroscopy. After recording a spectrum, a second spectrum has to be recorded after the addition of $TBAPF_6$ to the NMR sample. If all proton signals are exactly the same, the compound is pure.

It is suspected that the 1% of chloride ions as found by elemental analysis, caused the deviation in LEC performance as seen initially in batch 2 by the Bolink group (see Figure 2.1), as after the purification, the device performed as seen before.

2.7. Experimental

2.7.1. Batch 1: $[Ir(ppy)_2(bpy)][PF_6]$

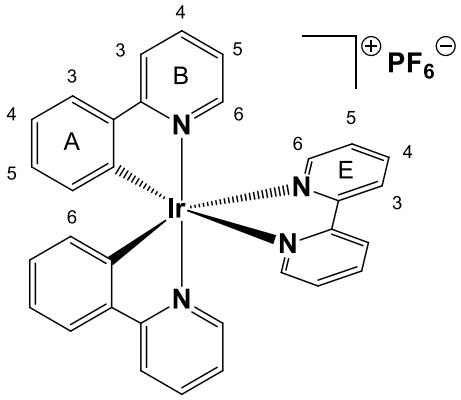

This synthesis yielded a pure complex with good device performances in LECs. A yellow suspension of $[Ir_2(ppy)_4(\mu\text{-}Cl)_2]$ (700 mg, 0.653 mmol) and 2,2'-bipyridine (205 mg, 1.31 mmol) in methanol (20 mL) was heated in a microwave reactor for 2 hours at 120°C (P = 15 bar). The yellow solution was then cooled to room temperature, and an excess of NH_4PF_6 (1064 mg, 6.53 mmol, 10.0 eq.) was added. The mixture was stirred for 30 min at room temperature and then evaporated to dryness. The crude yellow material was purified twice by column chromatography (Merck aluminium oxide 90 and Fluka Silica 60; CH_2Cl_2 changing to CH_2Cl_2:MeOH = 100:5). $[Ir(ppy)_2(bpy)][PF_6]$ was isolated as a yellow solid (993 mg, 1.24 mmol, 94.8%).

2.7.2. Batch 2: $[Ir(ppy)_2(bpy)][PF_6]$ and $[Ir(ppy)_2(bpy)]Cl$

Batch 2 was synthesized on the same scale as batch 1.

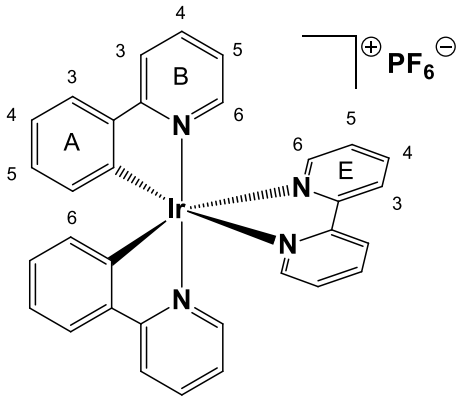

A yellow suspension of $[Ir_2(ppy)_2(\mu\text{-}Cl)_2]$ (700 mg, 0.653 mmol) and 2,2'-bipyridine (205 mg, 1.31 mmol) in methanol (20 mL) was heated in a microwave reactor for 2 hours at 120°C (P = 14 bar). The yellow solution was then cooled to room temperature and a few millilitres of the yellow solution were put away for crystal growth (methanol solution layered with diethyl ether, crystals grew over several days at room temperature). To the rest of the solution, an excess of NH_4PF_6 (1064 mg, 6.53 mmol) was added, the mixture was stirred for 30 min at

room temperature and then evaporated to dryness. The crude yellow material was purified by column chromatography (Merck aluminium oxide 90; CH_2Cl_2 changing to CH_2Cl_2:MeOH = 100:5). The proton NMR looked the same like the original $[Ir(ppy)_2(bpy)][PF_6]$ and the ESI-MS exhibited the mass peaks of both ions, the cations (m/z +657) and $[PF_6]^-$ (m/z -145), therefore 910 mg of the compound was sent to Valencia. As the LEC devices did not perform well, the batch was sent back for further analyses and purifications. The elemental analysis of batch 3, found: C = 44.52%, H = 2.94%, N = 6.80%. Calcd. for $[Ir(ppy)_2(bpy)][0.99\ PF_6][0.01\ Cl]+1CH_2Cl_2$: C = 44.76%, H = 2.96%, N = 6.33%.

Repurification:

The yellow solid was redissolved in a mixture of DCM and MeOH, an excess of NH_4PF_6 and $AgPF_6$ were added and the mixture was stirred for 1 hr at room temperature. The solution was slightly orange at the beginning, and after evaporation of the DCM it turned yellow. The solid was filtered. The volume of the mother liquor was reduced and filtered again. The yellow solid was washed with MeOH (2x 10 ml) and diethyl ether (3x 20 ml) and dried under vacuum.

The yellow solid was purified by column chromatography (Fluka Silica 60; CH_2Cl_2 changing to CH_2Cl_2:MeOH = 100:3), redissolved in DCM, filtered and the mother liquor was precipitated by the addition of diethyl ether, the solid was filtered and dried under vacuum. Elemental analysis found: C = 47.82%, H = 3.12%, N = 7.32%. Calcd. for $[Ir(ppy)_2(bpy)][PF_6]$: C = 47.94%, H = 3.02%, N = 7.32%.

Overall yield: $[Ir(ppy)_2(bpy)][PF_6]$ was isolated as a yellow solid (825 mg, 1.03 mmol, 78.8%).

[1] H. J. Bolink, E. Coronado, R. D. Costa, E. Ortí, M. Sessolo, S. Graber, K. Doyle, M. Neuburger, C. E. Housecroft, E. C. Constable, *Adv. Mater.*, 2008, **20**, 3910.
[2] S. Graber, K. Doyle, M. Neuburger, C. E. Housecroft, E. C. Constable, R. D. Costa, E. Ortí, D. Repetto, H. J. Bolink, *J. Am. Chem. Soc.*, 2008, **130**, 14944.
[3] R. D. Costa, E. Ortí, H. J. Bolink, S. Graber, S. Schaffner, M. Neuburger, C. E. Housecroft, E. C. Constable, *Adv. Funct. Mater.*, 2009, **19**, 3456.
[4] J. Emsley, *Chem. Soc. Rev.*, 1980, **9**, 91.
[5] M. J. Hynes, *J. Chem. Soc., Dalton Trans.*, 1993, 311.
[6] K. Hirose, *J. of Incl. Phen. and Macr. Chem.*, 2001, **39**, 193.
[7] M. Hesse, H. Meier, B. Zeeh, *Spektroskopische Methoden in der organischen Chemie,* Thieme, 2005.

Chapter 3

3. Changing the counterion in iridium(III) complexes in order to alter their ionic mobility in a LEC device

3.1. Introduction

As seen in the previous chapter, the influence of the counter ion in an iridium(III) complex is essential for the performance in LEC device (see Chapter 2). The size and the molecular mass of the anion have a direct influence on its mobility when biased. The mobility of the anions shows a direct influence on the turn-on time of the device.[1] The lower the mobility, the expectations are for longer turn-on times and the longer the lifetimes of the devices. Studies with ruthenium(II) based LECs showed a significant decrease in the turn-on time, upon a change from $[PF_6]^-$ to smaller anions such as $[BF_4]^-$ or $[ClO_4]^-$.[2, 3] But unfortunately, this change also reduces the device lifetime. Interestingly, upon addition of the ionic liquid (IL) tetrabutylammonium trifluoromethanesulfonate (TBAOTf) to different iridium complexes, this has not been seen.[4, 5] Comparison of the $[PF_6]^-$ and $[BF_4]^-$ salts of different iridium cations yielded a shorter turn-on time for the bigger anion. But consistent with the observation without an IL, the shorter turn-on time of a LEC device leads to a shorter lifetime.

In this chapter, starting from the known $[PF_6]^-$ complexes of $[Ir(ppy)_2(pbpy)]^+$ and $[Ir(ppy)_2(bpy)]^+$,[6] the anion was changed to the smaller and lighter $[B(CN)_4]^-$ ion and to the larger and much heavier $[BARF]^-$ anion in order to investigate the effect upon the LEC device performances.

3.2. Results and discussion

The complexation reactions were performed according to the established methodology, by treating a dichlorido bridged iridium(III) dimer with two equivalents of an N^N ligand (Scheme 3.1).[7] After the reaction in the microwave reactor, the complexes were precipitated with potassium tetracyanidoborate or sodium tetrakis[3,5-bis(trifluoromethyl)phenyl]borate (Na[BARF]), followed by purification by column chromatography.

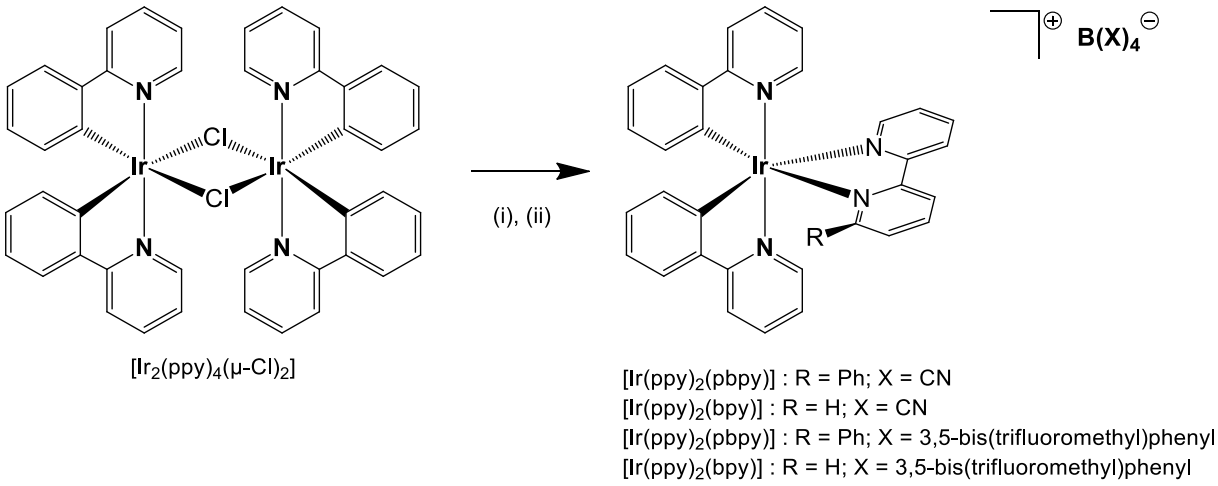

$[Ir_2(ppy)_4(\mu\text{-}Cl)_2]$

$[Ir(ppy)_2(pbpy)]$: R = Ph; X = CN
$[Ir(ppy)_2(bpy)]$: R = H; X = CN
$[Ir(ppy)_2(pbpy)]$: R = Ph; X = 3,5-bis(trifluoromethyl)phenyl
$[Ir(ppy)_2(bpy)]$: R = H; X = 3,5-bis(trifluoromethyl)phenyl

Scheme 3.1 Syntheses of the complexes. Conditions: (i) pbpy or bpy, MeOH, microwave, 2hr; (ii) $KB(CN)_4$ or NaB(3,5-bis(trifluoromethyl)phenyl)$_4$

The reactions all performed well with yields around 90%. The ESI mass spectra of each of the complexes showed the peaks of both ions in positive and negative mode, respectively, and the observed isotope patterns were in accord with those simulated. By the addition of a half to two solvent molecules, the elemental analyses could be resolved.

The NMR spectroscopic assignments were done with the routine 1D and 2D techniques (COSY, NOESY, HMQC, HMBC). In addition to the ^{1}H and ^{13}C NMR spectra, ^{11}B NMR spectra were recorded of all the complexes to confirm the presence of the anion. In the two complexes with 2,2'-bpy as the N^N ligand, there is a C_2 axis in the complex yielding the cyclometallating $[ppy]^-$ ligands to be equivalent. This leads to relatively simple proton NMR spectra. The introduction of the pendant phenyl ring leads to a doubling of the signals. Comparison of the symmetric compound with $[B(CN)_4]^-$ counterion with the asymmetric compound with $[BARF]^-$ anions are shown in Figure 3.1 (see Scheme 3.2 for ring labelling). Ring H originates from the $[BARF]^-$ anion.

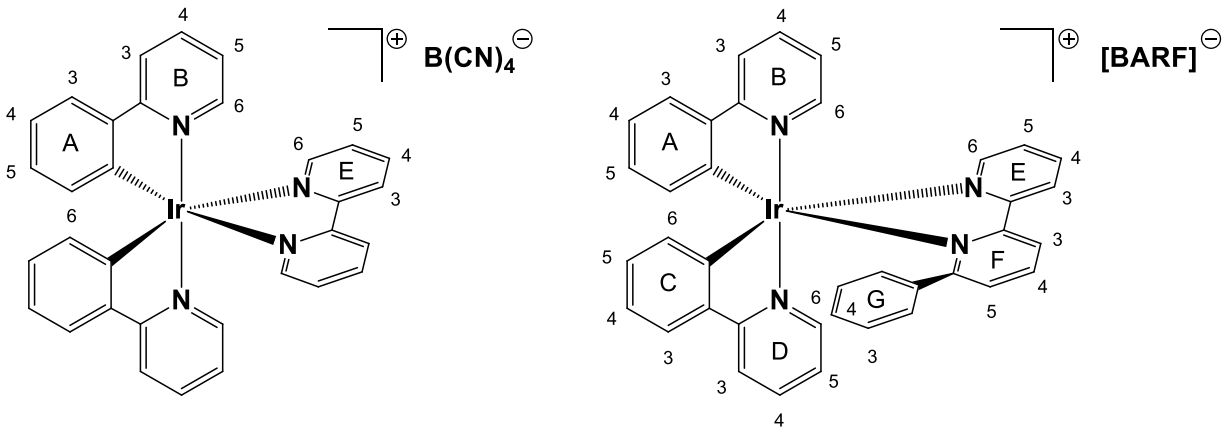

Scheme 3.2 Structures of the complexes and ring labelling for NMR spectroscopic assignments.

The additional broadened signals originate from ring G. The broad peaks are an indication of the ability of ring G to undergo hindered rotation at room temperature on the NMR timescale, and are also seen in similar compounds (see Section 4.2).

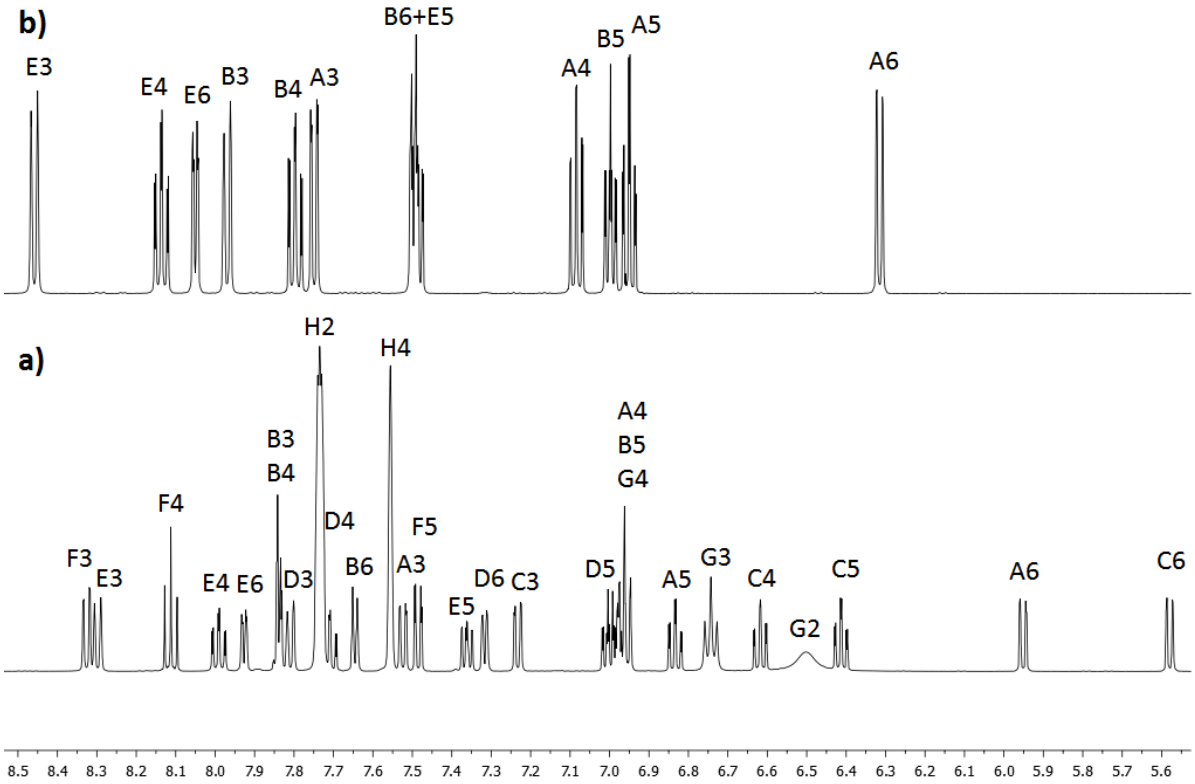

Figure 3.1 Comparison of the ^{1}H NMR spectra of a) [Ir(ppy)$_2$(pbpy)][BARF] and b) [Ir(ppy)$_2$(bpy)][B(CN)$_4$] in CD_2Cl_2 (500 MHz, 298 K, TMS).

Besides the additional proton signals from the phenyl ring of the anion, changing the anion has little effect on the ^{1}H signals. Similar to the other complexes discussed in this work, the ^{13}C NMR spectroscopic signals are weakly affected by the change of the N^N ligand and also are not influenced by the change of the anion.

3.3. Solid state structures

X-ray quality crystals of three of the complexes were grown. Table 3.1 shows a summary of the crystallographic data of the compounds.

Table 3.1 Crystallographic data of the four complexes.

Compound	$[Ir(ppy)_2(pbpy)][B(CN)_4]$. $0.5C_4H_{10}O$	$[Ir(ppy)_2(bpy)][B(CN)_4]$	$[Ir(ppy)_2(pbpy)][BARF]$	8{$[Ir(ppy)_2(bpy)][BARF]$}. $3CH_2Cl_2$
Formula	$C_{42}H_{28}BIrN_8O_{0.5}$	$C_{36}H_{24}BIrN_8$	$C_{70}H_{40}BF_{24}Ir_2N_4$	$C_{515}H_{294}B_8Cl_6F_{192}Ir_8N_8$
Formula weight / g mol^{-1}	863.73	771.66	1596.09	12414.77
Crystal colour and habit	yellow needle	yellow block	yellow block	yellow block
Crystal system	triclinic	monoclinic	orthorhombic	monoclinic
Space group	*P*-1	$P2_1/n$	*Pbca*	$P2_1/n$
a, b, c / Å	12.5005(4)	8.7019(7)	18.6490(8)	13.4211(15)
	18.5328(6)	27.448(2)	25.0203(11)	53.159(6)
	18.7871(6)	13.9732(11)	26.7417(11)	17.941(2)
α, β, γ/ °	61.549(2)	90	90	90
	84.998(2)	91.137(5)	90	108.3520(10)
	88.485(2)	90	90	90
U / $Å^3$	3811.6(2)	3122.0(4)	12477.8(9)	12149(2)
*D*c / Mg m^{-3}	1.505	1.642	1.699	1.697
Z	4	4	8	1
μ(Mo-Kα) / mm^{-1}	3.547	4.317	2.260	2.350
T/ K	123	123	123	123
Refln. collected (R_{int})	105137 (0.0383)	41784 (0.0614)	331781 (0.0613)	130556 (0.0707)
Unique refln.	20158	6128	20319	30721
Refln. for refinement	16505	5042	14564	21221
Parameters	982	415	957	1775
Threshold	$I > 2.0\sigma$	$I > 2.0\sigma$	$I > 2.0\sigma$	$I > 2.0\sigma$
*R*1 (*R*1 all data)	0.0378 (0.0523)	0.0457 (0.0661)	0.0270 (0.0487)	0.0658 (0.1034)
*wR*2 (*wR*2 all data)	0.0875 (0.0967)	0.1189 (0.1515)	0.0662 (0.0904)	0.1732 (0.2047)
Goodness of fit	1.108	1.228	1.091	1.099

3.3.1. $[Ir(ppy)_2(pbpy)][B(CN)_4]$

From a CH_2Cl_2 solution of the complex layered with Et_2O, crystals of poor X-ray quality were grown. Ambiguous residual electron density between two independent cations probably related to twinning was observed, and could not be resolved and therefore this structure is not publishable. However, the data show that the complex crystallizes in space group *P*-1, with two independent cations, two anions and one Et_2O in the asymmetric unit. The iridium atom is in an octahedral environment, the N-donors are mutually *trans* and the boron atom is in a tetrahedral environment. The phenyl ring displays face-to-face intramolecular π-stacking with the phenyl ring of one $[ppy]^-$ ligand (Figure 3.2).

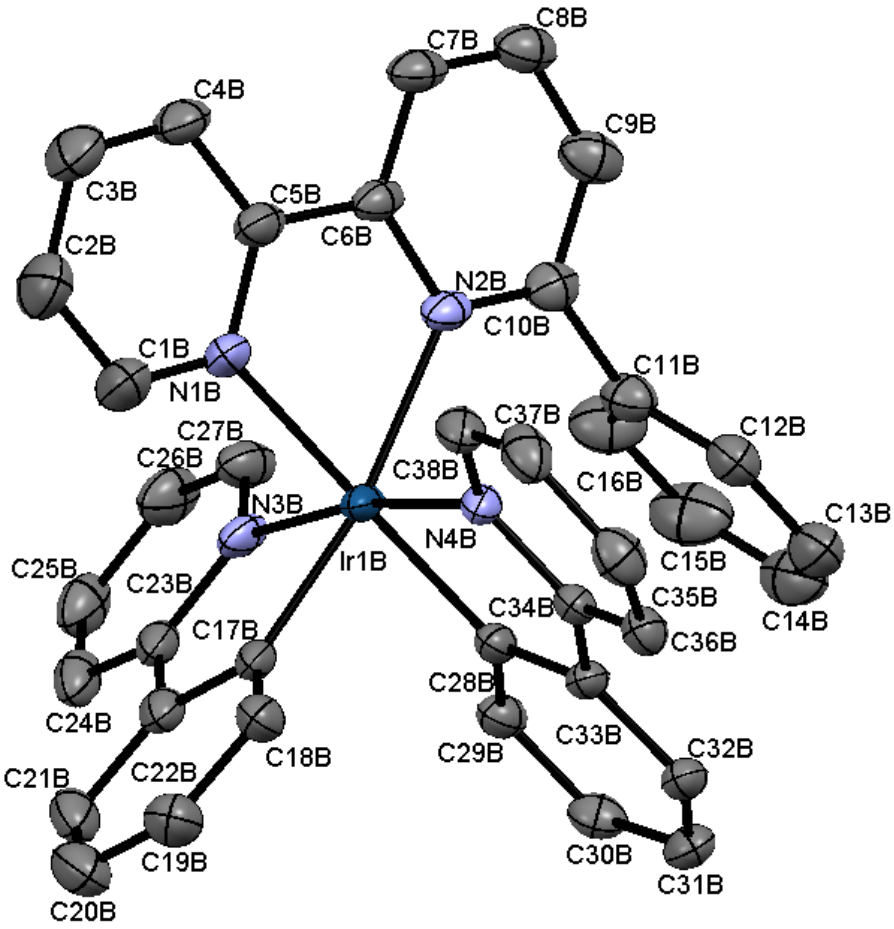

Figure 3.2 Preliminary structure of the Δ-form of cation B $[Ir(ppy)_2(pbpy)]^+$ with ellipsoids plotted at 50% probability level; H atoms and anion omitted.

3.3.2. $[Ir(ppy)_2(bpy)][B(CN)_4]$

From a CH_2Cl_2 and MeOH solution of the complex, X-ray quality crystals of $[Ir(ppy)_2(bpy)][B(CN)_4]$ were grown by slow evaporation of CH_2Cl_2. The complex crystallizes in the monoclinic $P2_1/n$ space group with both enantiomers of the cation present in the unit cell. The structure of the Λ-cation along with the anion is depicted in Figure 3.3. The atom Ir1 is in an octahedral environment and the N-donors of the two cyclometalled $[ppy]^-$ ligands are in a *trans*-arrangement, as expected and already seen before.1 Both cyclometalled C^N ligands are almost planar with angles between the least squares planes of 5.9 and 7.6°. The bpy ligand is also almost planar with an angle between the least squares planes of 3.7°. The absence of a pendant aromatic ring on the N^N ligands allows this small twisting angle, as there is no intramolecular π-stacking. The atom B1 of the anion is in the expected tetrahedral environment with tetrahedral angles around the boron atom between 106.9(9) and 113.8(9)°.

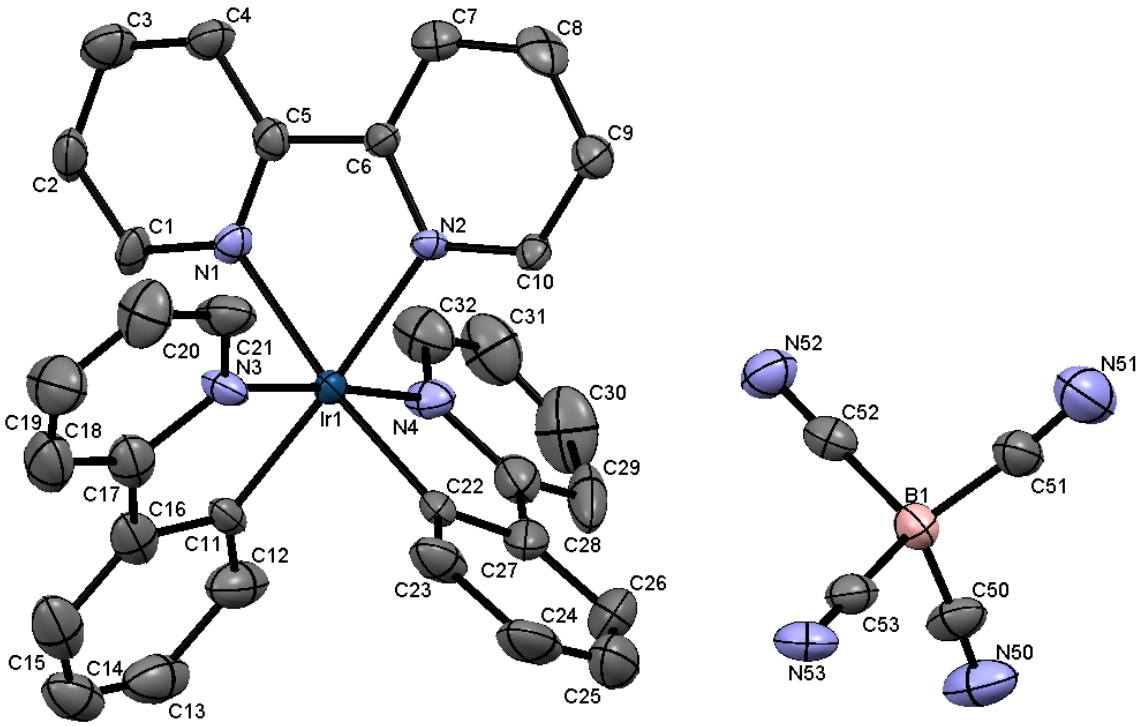

Figure 3.3 Structure of Λ-[Ir(ppy)$_2$(bpy)][B(CN)$_4$] with ellipsoids plotted at 50% probability level; H atoms omitted. Selected bond lengths (in Å) and bond angles (in °): Ir1–C22: 2.011(9), Ir1–C11: 2.017(9), Ir1–N4: 2.033(8), Ir1–N3: 2.044(8), Ir1–N2: 2.127(7), Ir1–N1: 2.130(7); N1–Ir1–N2: 76.8(3), N3–Ir1–C11: 82.7(3), N4–Ir1–C22: 82.6(4).

The packing interactions are dominated by cation – cation and cation – anion interactions. The cation – cation interactions lead to rows of cations with alternating Λ- and Δ-handedness (see Figure 3.4). The edge-to-face π-contacts between the phenyl rings of the [ppy]$^-$ ligands are drawn. The atoms involved are H24A, H25A and C14^i, C15^i (symmetry code i = x - ½, ½ - y, z – ½). The angle between the least squares planes of the two rings is 84.7°, the C...H separation is 2.85 Å and the C-H...phenyl ring centroid distance is 3.19 Å. These values are well within the range for π-stacking interactions discussed by Janiak.[8] Sandwich-type transition metal complexes with ruthenium and osmium show edge-to-face C...H π-contacts up to 3.04 Å.[9]

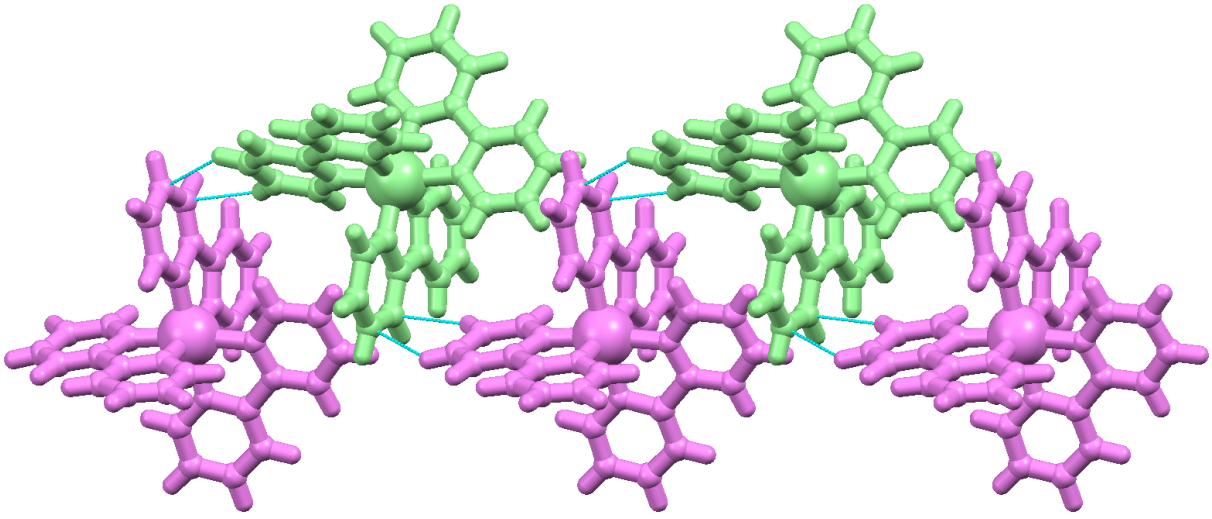

Figure 3.4 Rows of cations of alternating Δ- (purple) and Λ-handedness (green) in [Ir(ppy)$_2$(bpy)][B(CN)$_4$].

Each anion undergoes N...H contacts with six cations at distances between 2.45 – 2.73 Å. The anions build pairs with boron...boron separations of 4.80 Å. A view along the a-axis of the crystal packing is depicted in Figure 3.5. The rows of the cations from Figure 3.3 are on an almost vertical line in this picture.

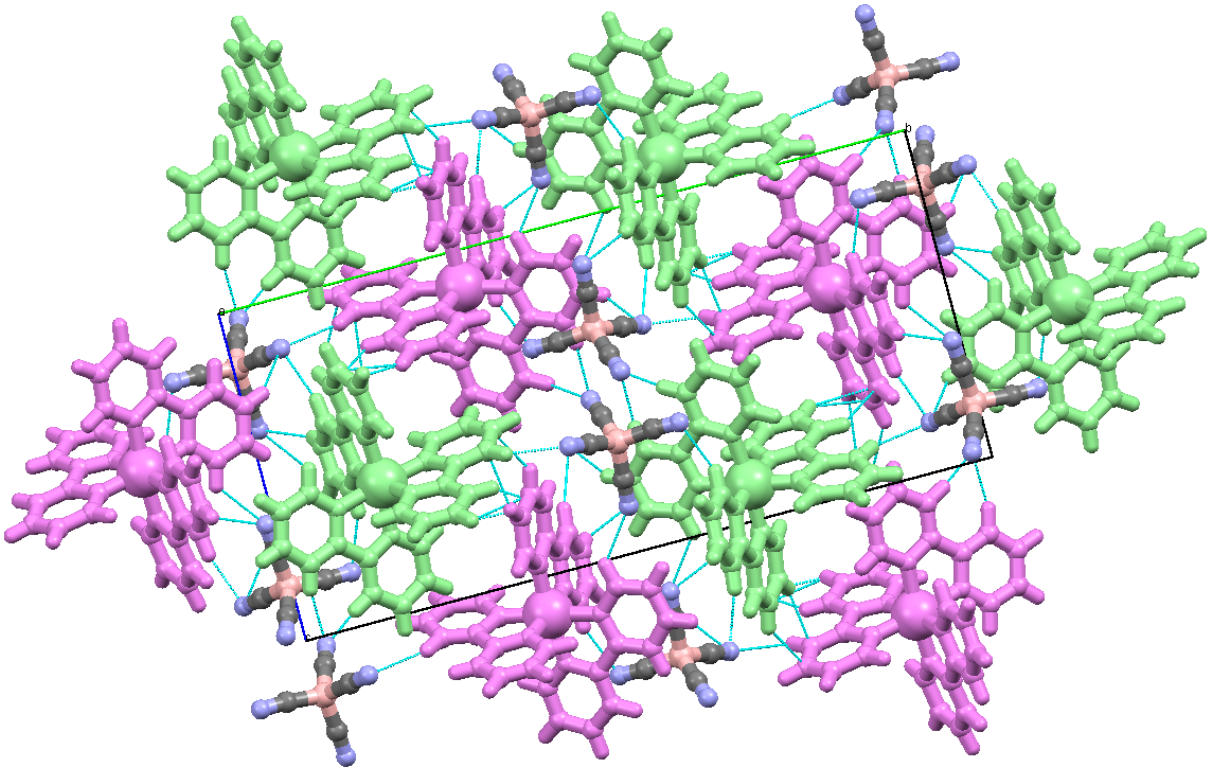

Figure 3.5 Cation-anion interactions withing $[Ir(ppy)_2(bpy)][B(CN)_4]$. Δ-form in purple and Λ-form in green.

All molecules are ordered and there are no solvent molecules in the crystal.

3.3.3. $[Ir(ppy)_2(pbpy)][BARF]$

The complex $[Ir(ppy)_2(pbpy)][BARF]$ was dissolved in MeCN, and Et_2O was allowed to diffused into the solution. After several days, X-ray quality crystals of $[Ir(ppy)_2(pbpy)][BARF]$ were grown. The complex crystallizes in the orthorhombic *Pbca* space group with both enantiomers of $[Ir(ppy)_2(pbpy)]^+$ in the unit cell. The structure of the Λ-cation with one anion is depicted in Figure 3.6. The atom Ir1 is in an octahedral environment and the N-donors of the cyclometalled $[ppy]^-$ ligands are in a *trans*-arrangement. Both cyclometallating ligands are almost planar with twisting angles between the least squares planes below 7.9°. This is in contrast to the bpy ligand with an angle between the least squares planes of the two pyridine rings of 23.8°. The pendant phenyl ring of the bpy ligand is twisted through 58.9° with respect to the bonded pyridine ring. This non-planarity allows the free phenyl ring to undergo intramolecular face-to-face π-stacking with one of the phenyl rings of one of the C^N ligands. The inter-centroid separation is 3.49 Å and the angle between the least squares planes is 12.8°. These values are well within the range discussed by Janiak8 making it an

efficient interaction. The atom B1 is in a tetrahedral environment with tetrahedral angles around the boron atom between 109.0(2) and 111.8(2)°.

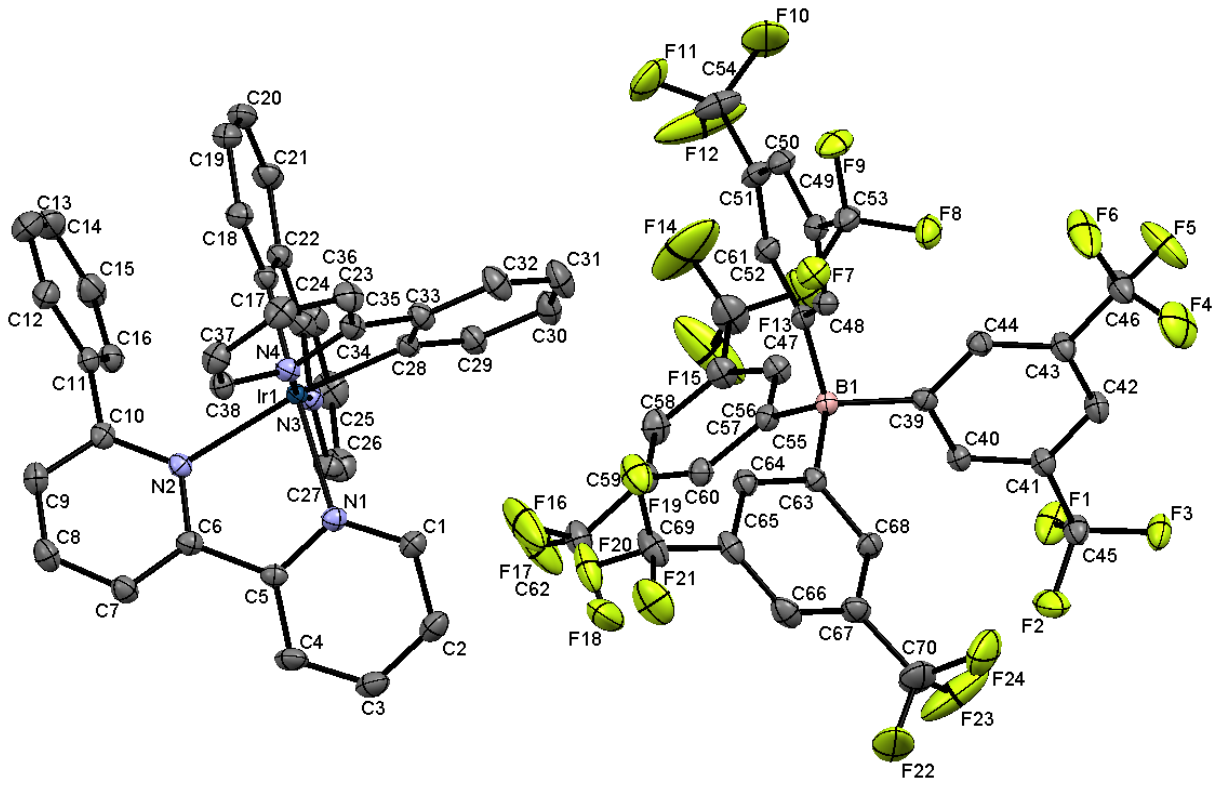

Figure 3.6 Structure of Λ-cation and the tetrahedral anion of [Ir(ppy)$_2$(pbpy)][BARF] with ellipsoids plotted at 50% probability level; H atoms omitted. Selected bond distances (in Å) and bond angles (in °): Ir1–C28: 2.003(3), Ir1–C17: 2.014(3), Ir1–N3: 2.042(2), Ir1–N4: 2.058(2), Ir1–N1: 2.148(2), Ir1–N2: 2.226(2); N1–Ir1–N2: 75.8(1), N3–Ir1–C17: 80.5(1), N4–Ir1–C28: 80.5(1).

The size of both ions is comparable, the packing interactions are mainly cation-anion interactions and each cation undergoes contacts with five anions. The H...F distances are between 2.54 and 2.83 Å. The packing interactions lead to alternating sheets of cations and anions. Within each sheet of cations there are alternating rows of Δ- and Λ-handedness (see Figure 3.7). The different enantiomers of the cations within one sheet are close with distances between atoms C29...H4A^{i} of 2.96 Å and H24A...C3^{i} of 3.09 Å (symmetry code i = x – ½, y, ½ - z).

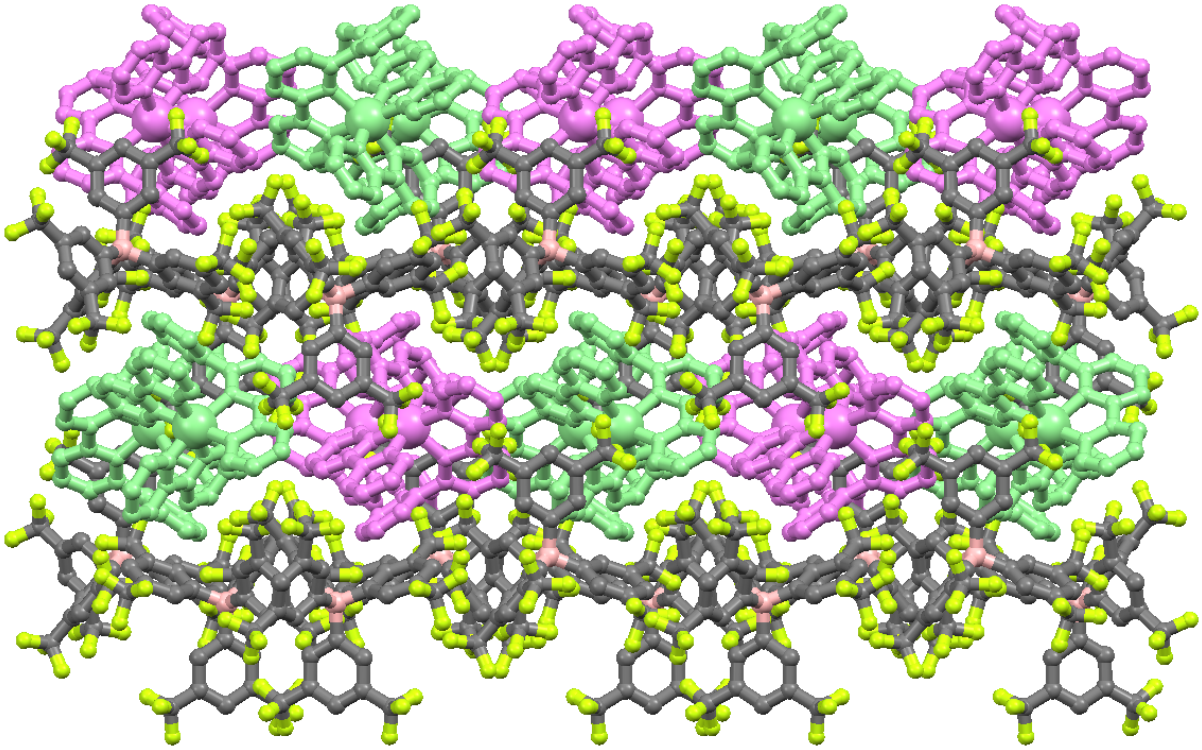

Figure 3.7 Packing of [Ir(ppy)$_2$(pbpy)][BARF] leads to alternating layers of cations and anions. Within the layers of cations there are alternating rows of Δ- (purple) and Λ-handedness (green).

The cations are ordered. In the anions there are two -CF_3 groups with rotational disorder, 0.89:0.11 for fluorines F16, F17 and F17 and 0.62:0.38 for the fluorines F22, F23 and F24.

3.3.4. [Ir(ppy)$_2$(bpy)][BARF]

The complex [Ir(ppy)$_2$(bpy)][BARF] was dissolved in a mixture of CH_2Cl_2 and MeCN, and Et_2O was allowed to diffuse into the solution. After several days, X-ray quality crystals of 8{[Ir(ppy)$_2$(bpy)][BARF]}.3CH_2Cl_2 were grown. The complex crystallizes in the monoclinic $P2_1/n$ space group with both enantiomers in the unit cell. In the asymmetric unit there are two cations, two anions and 0.75 CH_2Cl_2 present. There are two independent cations, both being very similar, and two independent anions, again both similar. The structure of cation A in the Λ-form and anion A are depicted in Figure 3.8. Both atoms Ir1A and Ir1B are in an octahedral environment with the N-donors in *trans*-arrangement. All the cyclometallating $[ppy]^-$ ligands are almost planar with angles between the least squares planes below 5.2°. Also the bpy ligands are almost planar with even smaller angles between the least squares planes (cation A: 0.1° and cation B: 4.9°). As there is no pendant ring which can undergo intramolecular interactions, the bpy ligand is not distorted. The atoms B1A and B1B are in tetrahedral environments with tetrahedral angles around the atom B1A between 102.5(4) and 114.7(4)° and around atom B1B between 102.0(4) and 113.5(4)°.

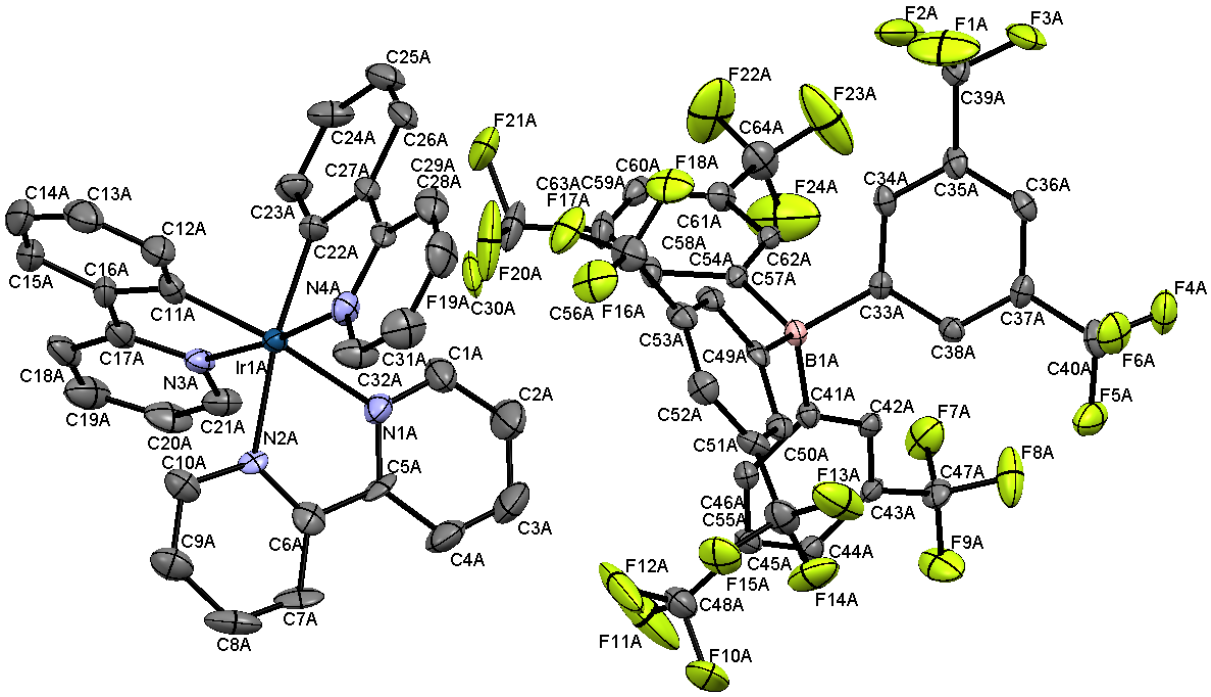

Figure 3.8 Structure of Λ-cation A and the tetrahedral anion A of 8{[Ir(ppy)$_2$(bpy)][BARF]}.3CH$_2$Cl$_2$ with ellipsoids plotted at 50% probability level; H atoms omitted. Selected bond lengths (in Å) and bond angles (in °): Ir1A–C11A: 2.023(6), Ir1A–C22A: 2.040(5), Ir1A–N3A: 2.049(4), Ir1A–N4A: 2.065(4), Ir1A–N2A: 2.111(4), Ir1A–N1A: 2.157(5); N1A–Ir1A–N2A: 75.0(2), N3A–Ir1A–C11A: 80.1(2), N4A–Ir1A–C22A: 80.0(2). Selected bond lengths (in Å) and bond angles (in °): Ir1B–N4B: 2.027(4), Ir1B–C22B: 2.040(5), Ir1B–N1B: 2.065(4), Ir1B–C11B: 2.071(4), Ir1B–N3B: 2.084(4), Ir1B–N2B: 2.095(4); N1B–Ir1B–N2B: 78.7(2), N3B–Ir1B–C11B: 78.8(2), N4B–Ir1B–C22B: 80.0(2).

The crystal packing is dominated by cation-anion interactions. The H...F distances are between 2.47 and 2.64 Å. Additionally, there are interactions between cations with different handedness of cations A and B, respectively. These interactions consist of edge-to-face C-H...π-contacts.

For cations A the C-H...phenyl ring centroid distance is 3.58 Å, between atom H7AA^{i} and centroid of the ring containing atom C11A (symmetry code i = x + ½, ½ - y, z + ½). This interaction leads to pseudo-π-stacking between the cyclometallating [ppy]$^-$ ligand containing atom C22A and the bpy ligand atom N1A^{i} with a twisting angle between the least squares planes of 13.0° but the inter-centroid distance of 4.24 Å is way out of the range for π-stacking interactions discussed by Janiak.8

Similarly, between cations B there is an edge-to-face C-H...phenyl ring centroid contact at a distance of 3.52 Å, between atom H15B and phenyl ring containing atom C22B^{ii} (symmetry code ii = -x, -y, 1 – z). These cations show also a pseudo face-to-face π-stacking interaction between the [ppy]$^-$ ligands of adjacent cations containing atoms C11B and C11B^{i} (symmetry code i = -x, -y, 1 – z) with a distance between the parallel planes (symmetry imposed by an inversion centre) of 3.44 Å (see Figure 3.9). But the centroid distances are out of the range discussed by Janiak.8

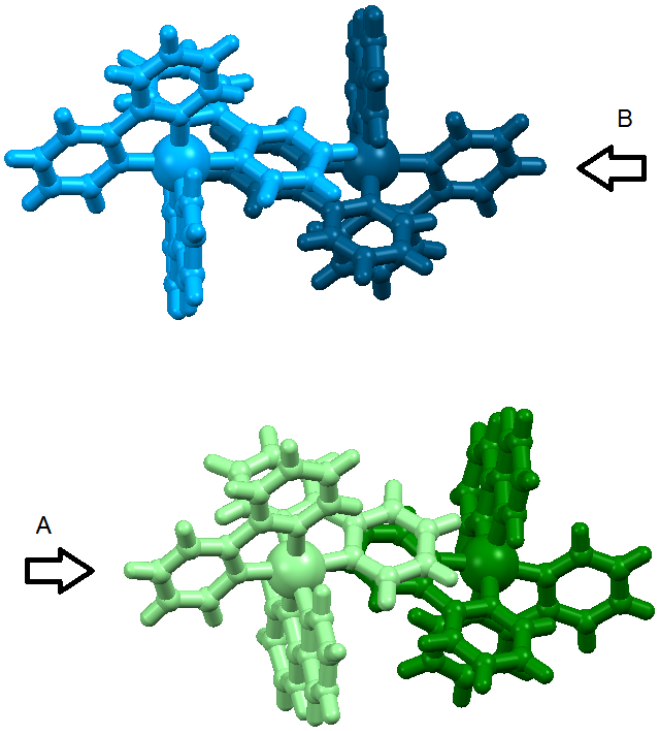

Figure 3.9 Intermolecular stacking interactions in $[Ir(ppy)_2(bpy)][BARF]$ between cations of molecules A (green) and B (blue) with Δ- (dark) and Λ- form (light). Anions and solvent molecules are omitted in this presentation.

The crystal packing with the anions together with the cations is depicted in Figure 3.10. The anions separate the layers of cations A and B. Within each layer of cations, there are columns of alternating Δ- and Λ-enantiomers. Within each layer of anions, there are columns of alternating anions A and anions B.

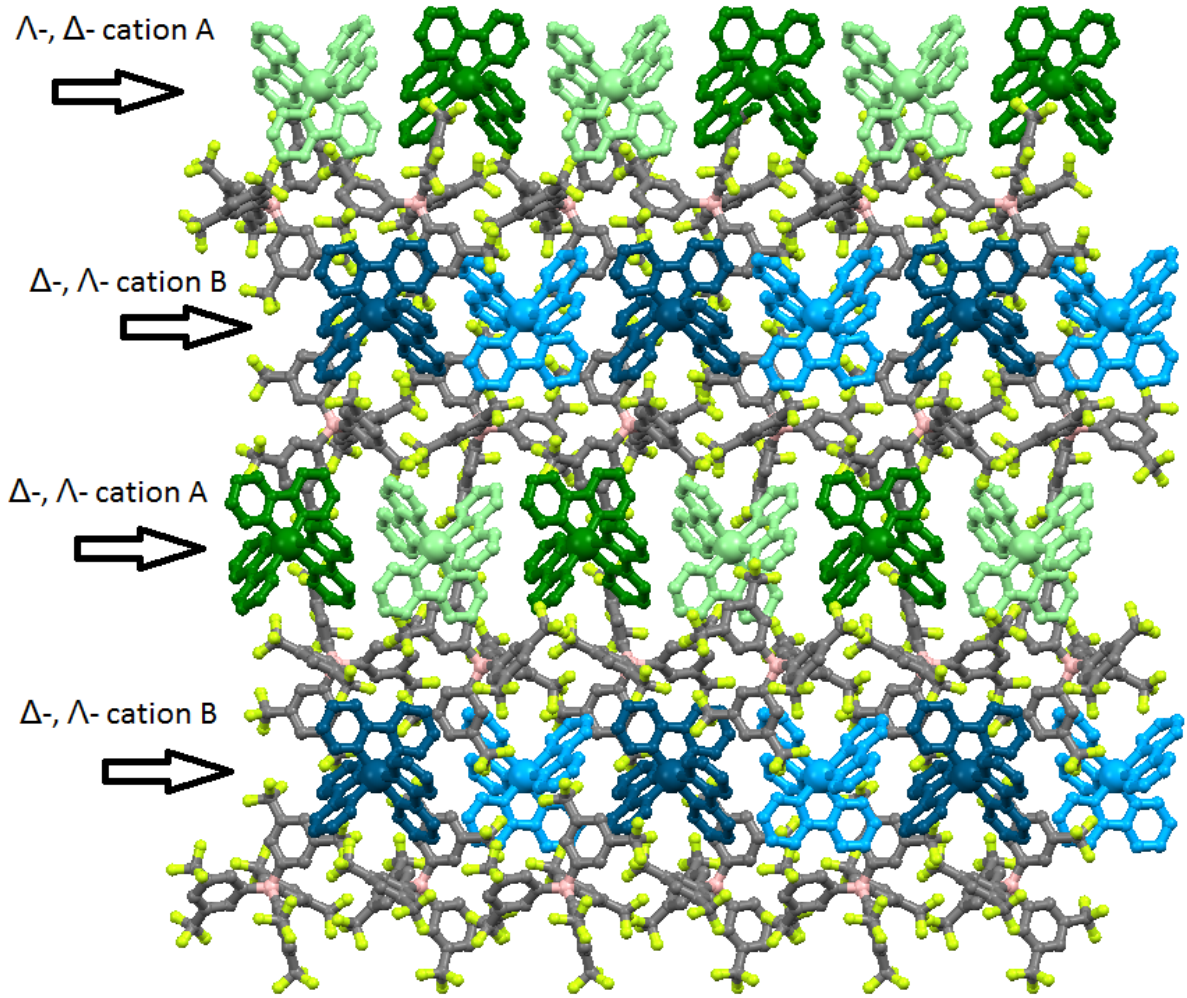

Figure 3.10 Alternating sheets of cations A (green), anions (alternating A and B in each sheet) and cations B (blue). Within the sheets of cations there are alternating Δ- (dark) and Λ-forms (light).

The solvent molecule is disordered as 0.5 + 0.25 occupancy. Additionally the -CF_3 group containing atom F19 has rotational disorder of 0.558:0.442.

3.4. Photophysical properties

The photophysical properties of the four complexes have been measured in aerated MeCN solutions at concentrations of c = 1.00 x 10^{-5} M. The absorption and the emission spectra of the four complexes are very similar (see Figure 3.11). In the absorption spectra, each complex shows a relatively strong band around 265 nm with a shoulder around 320 nm. These bands were assigned to ligand based π* ← π transitions with extinction coefficients around 48'000 and 25'000 dm^3 mol^{-1} cm^{-1}. Around 370 nm, there are spin-allowed MLCT transitions with extinction coefficients around 6'000 dm^3 mol^{-1} cm^{-1}.

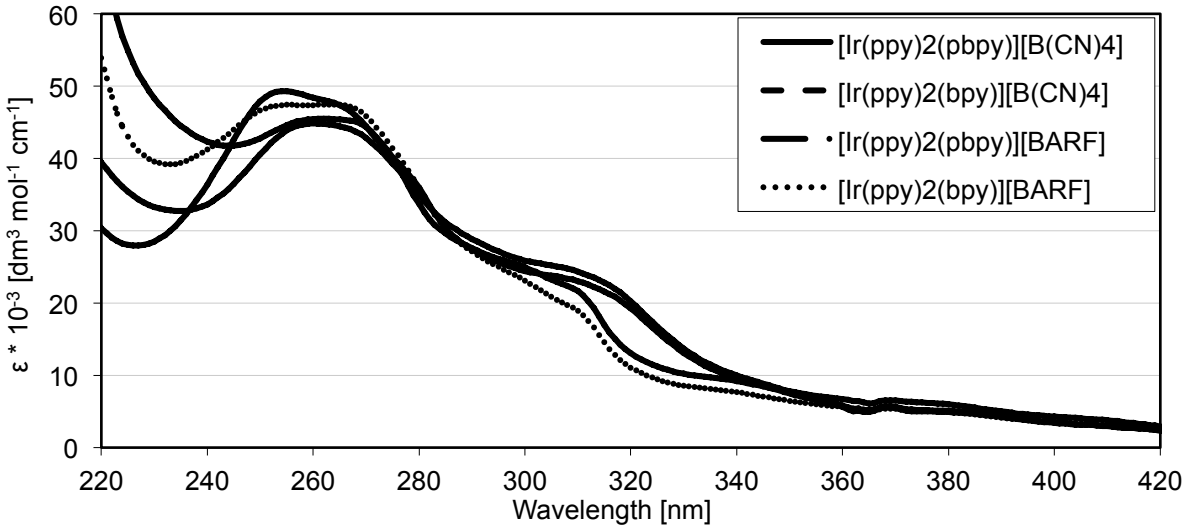

Figure 3.11 Absorption spectra of the four complexes in MeCN solutions (c = 10^{-5} M).

Excitation at 265 nm leads to an orange emission in solution for all four complexes. The counterion seems not to influence the emission maximum of the complexes. The emission maxima are 605 nm for the two asymmetric compounds and 590 nm for the two symmetric compounds. These emission maxima are comparable to the asymmetric $[Ir(ppy)_2(pbpy)][PF_6]$ (λ_{em} = 595 nm) and the symmetric $[Ir(ppy)_2(bpy)][PF_6]$ compound (λ_{em} = 590 nm).[6, 10] The emission spectra show the well known, broad and unstructured shape which is characteristic of complexes containing a combination of neutral diimine and cyclometallating ligands.

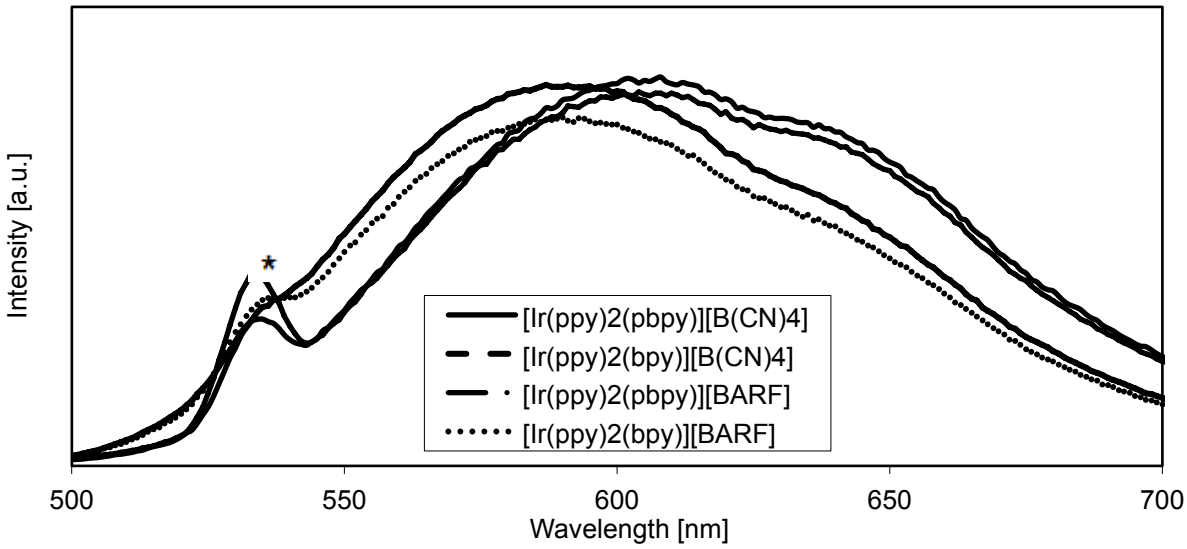

Figure 3.12 Emission spectra of the four complexes in MeCN solutions (c = 10^{-5} M, λ_{ex} = 265 nm).

The quantum yield measurements were performed in MeCN solutions of the complexes. The solutions were degassed with argon for 15 minutes prior to the measurements. The quantum yields for the asymmetric complexes are much lower than for the complexes without the intramolecular stacking interaction (3.4 and 2.7 versus 11.0 and 8.3%). This behaviour is also seen in the similar $[PF_6]^-$ salts of the complexes with similar quantum yields (3 and 14%).6

3.5. Electrochemical properties

All four compounds are electrochemically active. The electrochemical properties have been measured in deaerated MeCN solutions with 0.1 M [^{n}Bu$_4$N][PF$_6$] supporting electrolyte at a scan rate of 0.1 V s^{-1}. Table 3.2 presents the cyclic voltammetric data with respect Fc/Fc$^+$. Unless otherwise stated, the electrochemical processes are reversible or near-reversible. In general, the four complexes show very similar oxidations and reductions. For all four complexes, the reversible or quasi-reversible oxidation between +0.78 and +0.88 V was assigned to an iridium-centred process. All four complexes show bpy-centred reduction processes. The $\Delta E_{1/2}$ values of the complexes are directly comparable with the [PF$_6$]$^-$ analogues of the two complexes, with a difference of only 0.01 V.6

Table 3.2 Cyclic voltammetric data with respect to Fc/Fc$^+$; MeCN solutions with [^{n}Bu$_4$N][PF$_6$] supporting electrolyte, and scan rate of 0.1 V s^{-1} (ir = irreversible; qr = quasi-reversible).

Compound	$E_{1/2}^{ox}$ / V	$E_{1/2}^{red}$ / V	$\Delta E_{1/2}$ / V
[Ir(ppy)$_2$(pbpy)][B(CN)$_4$]	+0.81^{qr}	–1.78, –2.43^{ir}	2.59
[Ir(ppy)$_2$(bpy)][B(CN)$_4$]	+0.87	–1.78, –2.47^{ir}	2.65
[Ir(ppy)$_2$(pbpy)][BARF]	+0.78^{qr}	–1.81, –2.47^{ir}	2.59
[Ir(ppy)$_2$(bpy)][BARF]	+0.88	–1.78, –2.47^{ir}	2.66

3.6. Device performances

The luminescent properties of the four complexes in LEC devices (PEDOT:PSS/iTMC/Al, without IL) have been investigated.

Comparison of the two [B(CN)$_4$]$^-$ complexes with their [PF$_6$]$^-$ analogues shows that changing the anion to the lower mass [B(CN)$_4$]$^-$ leads to an increase of the device performance in terms of efficiency and external quantum efficiency, but the maximum luminance is lowered (Table 3.3).

Table 3.3 Device performances of the tetracyanidoborate complexes compared with the [PF$_6$]$^-$ analogues.

iTMC	turn-on time t_{on} hr	Lum_{max} cd/m^2	Efficacy cd/A	EQE	Power Efficiency lm/W
[Ir(ppy)$_2$(pbpy)][B(CN)$_4$]	27	76	≈5.5	≈1.8%	≈3.5
[Ir(ppy)$_2$(pbpy)][PF$_6$]	14	88	2.5	0.9%	1.9
[Ir(ppy)$_2$(bpy)][B(CN)$_4$]	1.5	580	11.1	2.5%	6.5
[Ir(ppy)$_2$(bpy)][PF$_6$]	4.5	2000	5.2	1.8%	4.1

Interestingly, there is no general trend for the turn-on times of the LEC devices. While in [Ir(ppy)$_2$(pbpy)]$^+$ the turn-on time is considerably shorter with the lighter anion, in [Ir(ppy)$_2$(bpy)]$^+$ the observation is the opposite.

Preliminary tests of mixing the salts with different cations yielded an overall decrease of the LEC device performance. This phenomenon needs further experiments to fully understand the observations.

In the two $[BARF]^-$ complexes, the mobility of the anions is extremely low. Thus, the devices do not show any luminance at temperatures below 60 °C. Upon heating a LEC device to 60 °C or higher, the ionic conductivity is strongly increased and produces a sudden light emission at 60 °C. Unfortunately, the lifetime of the LEC devices is very short.

3.7. Conclusion and outlook

The synthesis and characterization of the four complexes was successful. Unfortunately, trials towards the two cations with the non-fluorinated tetraphenylborate anion $[B(Ph)_4]^-$ were not successful.

Changing the $[PF_6]^-$ to the large $[BARF]^-$ anion, yielded in the desired reduction of the ionic mobility. Reducing the weight of the anion, from $[PF_6]^-$ to $[B(CN)_4]^-$ leads to an enhancement in the efficiency and EQE of the LEC device. But the luminance decreased and the effect on the turn-on time is not yet understood.

Currently, there are ongoing investigations for a better understanding of the behaviour of the LEC devices based on the four complexes and their $[PF_6]^-$ analogues.

For the $[BARF]^-$ complexes, currently different cooling methods with different cooling rates are being used, to decrease the ionic mobility after the onset of the luminance. Furthermore, an ionic liquid will be used to avoid crystal formation during the cooling process, which has already been detected in preliminary studies.

3.8. Experimental

3.8.1. [Ir(ppy)$_2$(pbpy)][B(CN)$_4$]

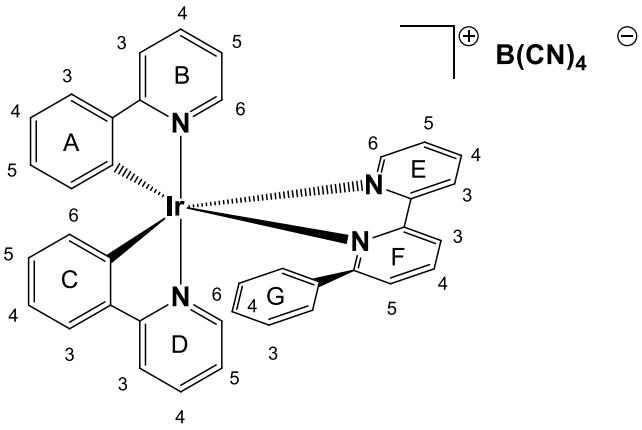

A yellow suspension of [$Ir_2(ppy)_4(\mu\text{-}Cl)_2$] (107.2 mg, 0.100 mmol) and 6-phenyl-2,2'-bipyridine (46.7 mg, 0.201 mmol) in methanol (15 mL) was heated in a microwave reactor for 2 hours at 120°C (P = 14 bar). The orange solution was then cooled to room temperature, and solid $KB(CN)_4$ (254 mg, 1.6 mmol, 16.0 eq) was added. The mixture was stirred for 1 h at room temperature and then evaporated to dryness. The crude material was purified twice by column chromatography (Fluka Silica 60 and Merck aluminium oxide 90; CH_2Cl_2 changing to CH_2Cl_2:MeOH = 100:3). [Ir(ppy)$_2$(pbpy)][$B(CN)_4$] was isolated as a yellow-orange solid (157 mg, 0.185 mmol, 92.1%). *^{1}H NMR* (500 MHz, CD_2Cl_2, 295 K) δ/ppm 8.48 (dd, *J* = 8.2, 1.3 Hz, 1H H^{F3}), 8.46 (m, 1H, H^{E3}), 8.22 (t, *J* = 7.9 Hz, 1H, H^{F4}), 8.11 (ddd, *J* = 8.1, 7.7, 1.6 Hz, 1H, H^{E4}), 7.91 (ddd, *J* = 5.5, 1.6, 0.7 Hz, 1H, H^{E6}), 7.89 – 7.80 (m, 3H, $H^{B3+B4+D3}$), 7.76 (ddd, *J* = 8.2, 7.4, 1.5 Hz, 1H, H^{D4}), 7.70 (m, 1H, H^{B6}), 7.53 (dd, *J* = 7.8, 1.3 Hz, 1H, H^{A3}), 7.50 (dd, *J* = 7.7, 1.2 Hz, 1H, H^{F5}), 7.40 (ddd, *J* = 6.5, 3.9, 1.0 Hz, 2H, H^{E5+D6}), 7.23 (dd, *J* = 7.8, 1.2 Hz, 1H, H^{C3}), 7.07 (ddd, *J* = 7.4, 5.9, 1.6 Hz, 1H, H^{D5}), 7.04 (ddd, *J* = 6.8, 5.9, 2.0 Hz, 1H, H^{B5}), 6.95 (tdd, *J* = 7.6, 2.5, 1.2 Hz, 2H, H^{G4+A4}), 6.85 – 6.79 (m, 1H, H^{A5}), 6.74 (t, *J* = 7.8 Hz, 2H, H^{G3}), 6.60 (ddd, *J* = 7.8, 7.3, 1.2 Hz, 1H, H^{C4}), 6.52 (s, 2H, H^{G2}), 6.42 – 6.36 (m, 1H, H^{C5}), 5.96 (dd, *J* = 7.8, 0.8 Hz, 1H, H^{A6}), 5.58 (dd, *J* = 7.7, 0.7 Hz, 1H, H^{C6}). *^{13}C {^{1}H} NMR* (126 MHz, CD_2Cl_2, 295 K) δ/ppm 169.4 (C^{B2}), 167.7 (C^{D2}), 166.5 (C^{F6}), 157.4 (C^{E2}), 157.2 (C^{F2}), 151.3 (C^{C1}), 151.0 (C^{E6}), 149.4 (C^{B6}), 149.3 (C^{D6}), 146.9 (C^{A1}), 143.5 (C^{A2}), 143.3 (C^{C2}), 140.0 (C^{F4}), 139.7 (C^{E4}), 138.7 (C^{D4}), 138.6 (C^{B4}), 138.1 (C^{G1}), 131.9 (C^{C6}), 131.3 (C^{A5}), 130. 7 (C^{A6}), 130.6 (C^{F5}), 130.1 (C^{C5}), 129.6 (C^{G4}), 128.4 (C^{G3}), 128.3 (C^{E5}), 127.9 (C^{G2}), 125.3 (C^{E3}), 125.2 (C^{A3}), 125.1 (C^{C3}), 123.9 (C^{D5}), 123.8 (C^{F3}), 123.4 (C^{A4}), 123.2 ([$B(CN)_4$]$^-$, non-binomial quartet, $J_{B\text{-}C}$ = 71.1 Hz), 122.8 (C^{B5}), 121.4 (C^{C4}), 120.5 (C^{B3}), 120.4 (C^{D3}). *^{11}B NMR* (128 MHz, CD_2Cl_2, 295 K) δ/ppm -38.3 (s).[11] *IR* (solid, ν/cm^{-1}): 3043 (w), 1701 (w), 1607 (m), 1583 (m), 1560 (m), 1477 (s), 1439 (m), 1421 (m), 1315 (w), 1269 (m), 1227 (m), 1163 (m), 1124 (w), 1063 (m), 1030 (m), 999 (w), 928 (m), 820 (w), 754 (s), 729 (s), 694 (s), 629 (m), 569 (m), 559 (m). *MS* (ESI, m/z): positive mode: 733.2 [M-PF_6]$^+$ (calc. 733.2), negative mode: 115.1 [$B(CN)_4$]$^-$ (calc. 115.0). *UV-Vis* λ/nm (ε/dm^3 mol^{-1} cm^{-1}) (CH_2Cl_2, 1.00 × 10^{-5} mol dm^{-3}): 267 (48'700), 383 (6'300). *UV-Vis* λ/nm (ε/dm^3 mol^{-1} cm^{-1}) (MeCN, 2.50 × 10^{-5} mol dm^{-3}): 260 (45'500), 300 (26'400), 375 (5'400). *Luminescence* (CH_2Cl_2, c = 1.00 x 10^{-5} mol dm^{-3}, λ_{ex} = 310 nm): λ_{em} = 596 nm, lifetime τ = 128

ns (χ^2 = 1.003). *Luminescence* (MeCN, c = 2.50x10^{-5} mol dm^{-3}, λ_{ex} = 265 nm): λ_{em} = 605 nm. *Quantum yield* (MeCN, degassed with argon, λ_{ex} = 250 nm, integration range: 520 – 800 nm): 0.034. *Elem. Anal.* calcd. for $C_{42}H_{28}N_8IrB{\cdot}0.75H_2O$ (861.26) C 58.57, H 3.45, N, 13.01; found C 58.61, H 3.54, N 13.01. *Electrochemistry*: E_1^{ox}: +0.87 V/+0.74^{qr} V, E_1^{red}: -1.81 V/-1.75 V, E_2^{red}: -2.43 V/ir.

3.8.2. [Ir(ppy)$_2$(bpy)][B(CN)$_4$]

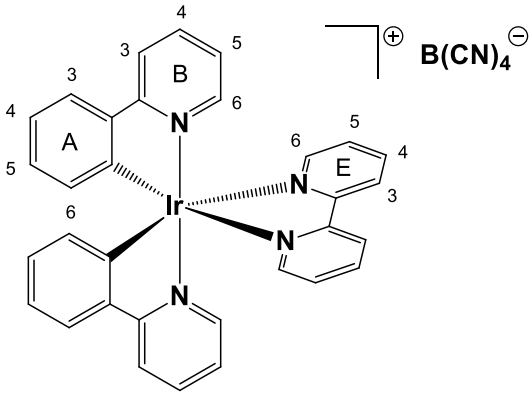

A yellow suspension of [Ir$_2$(ppy)$_4$(μ-Cl)$_2$] (107.2 mg, 0.100 mmol) and 2,2'-bipyridine (31.4 mg, 0.201 mmol) in methanol (15 mL) was heated in a microwave reactor for 2 hours at 120°C (P = 14 bar). The orange solution was then cooled to room temperature, and solid KB(CN)$_4$ (254 mg, 1.6 mmol, 16.0 eq) was added. The mixture was stirred for 3 hrs at room temperature and then evaporated to dryness. The crude material was purified twice by column chromatography (Fluka Silica 60 and Merck aluminium oxide 90; CH_2Cl_2 changing to CH_2Cl_2:MeOH = 100:2). [Ir(ppy)$_2$(bpy)][B(CN)$_4$] was isolated as a yellow-orange solid (134 mg, 0.173 mmol, 86.6%). *^{1}H NMR* (500 MHz, CD_2Cl_2, 295 K) δ/ppm 8.46 (d, *J* = 8.2 Hz, 2H, H^{E3}), 8.14 (td, *J* = 7.9, 1.6 Hz, 2H, H^{E4}), 8.05 (ddd, *J* = 5.5, 1.6, 0.6 Hz, 2H, H^{E6}), 7.97 (d, *J* = 8.0 Hz, 2H, H^{B3}), 7.80 (ddd, *J* = 8.2, 7.5, 1.5 Hz, 2H, H^{B4}), 7.75 (dd, *J* = 7.8, 1.2 Hz, 2H, H^{A3}), 7.52 – 7.47 (m, 4H, H^{B6+E5}), 7.11 – 7.06 (m, 2H, H^{A4}), 7.00 (ddd, *J* = 7.3, 5.9, 1.4 Hz, 2H, H^{B5}), 6.95 (td, *J* = 7.4, 1.3 Hz, 2H, H^{A5}), 6.32 (dd, *J* = 7.6, 0.8 Hz, 2H, H^{A6}). *^{13}C {^{1}H} NMR* (126 MHz, CD_2Cl_2, 295 K) δ/ppm 168.3 (C^{B2}), 156.2 (C^{E2}), 151.5 (C^{E6}), 150.3 (C^{A1}), 149.1 (C^{B6}), 144.2 (C^{A2}), 139.8 (C^{E4}), 138.8 (C^{B4}), 132.2 (C^{A6}), 131.3 (C^{A5}), 129.0 (C^{E5}), 125.5 (C^{A3}), 124.9 (C^{E3}), 123.8 (C^{B5}), 123.3 (C^{A4}), 123.2 ([B(CN)$_4$]$^-$, non-binomial quartet, $J_{B\text{-}C}$ = 71.1 Hz), 120.5 (C^{B3}). *^{11}B NMR* (128 MHzCD_2Cl_2, 295 K,) δ/ppm -38.4 (s).[11] *IR* (solid, ν/cm^{-1}): 3028 (w), 1605 (s), 1583 (m), 1472 (s), 1447 (s), 1418 (s), 1312 (m), 1267 (m), 1163 (m), 1061 (m), 1032 (m), 924 (s), 793 (m), 756 (s), 731 (s), 669 (m), 631 (m) cm^{-1}. *MS* (ESI, m/z): positive mode: 657.1 [M-PF$_6$]$^+$ (calc. 656.8), negative mode: 115.2 [B(CN)$_4$]$^-$ (calc. 115.0). *UV-Vis* λ/nm (ε/dm^3 mol^{-1} cm^{-1}) (MeCN, 2.50 × 10^{-5} mol dm^{-3}): 255 (49'300), 300 (26'300), 375 (6'700). *Luminescence* (MeCN, c = 2.50 x 10^{-5} mol l^{-1}, λ_{ex} = 265 nm): λ_{em} = 590 nm. Quantum yield (MeCN, degassed with argon, λ_{ex} = 250 nm, integration range: 510 – 800 nm): 0.110. *Elem. Anal*. calcd. for $C_{36}H_{24}BIrN_8{\cdot}0.5H_2O$ (780.67) C 55.39, H 3.23, N, 14.35; found C 55.29, H 3.01, N 14.32. *Electrochemistry*: E_1^{ox}: +0.91 V/+0.83 V, E_1^{red}: -1.81 V/-1.75 V, E_2^{red}: -2.47 V/ir.

3.8.3. [Ir(ppy)$_2$(pbpy)][BARF]

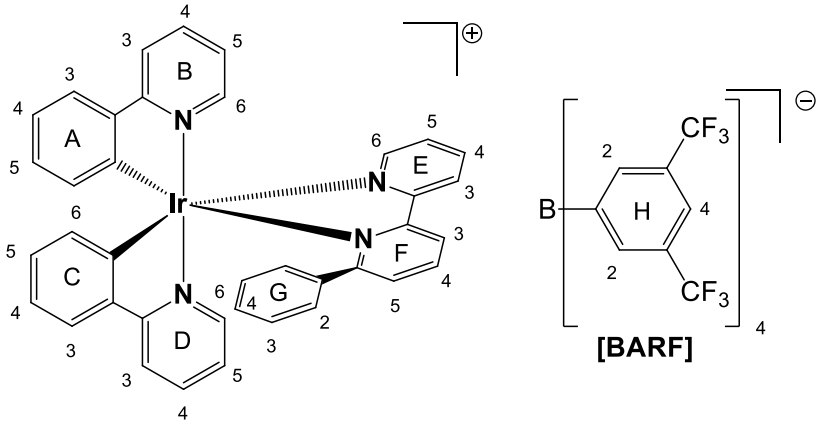

A yellow suspension of [$Ir_2(ppy)_4(\mu\text{-}Cl)_2$] (107.2 mg, 0.100 mmol) and 6-phenyl-2,2'-bipyridine (46.7 mg, 0.201 mmol) in methanol (15 mL) was heated in a microwave reactor for 2 hours at 120°C (P = 11 bar). The orange solution was then cooled to room temperature, and solid sodium tetrakis[3,5-bis(trifluoromethyl)phenyl]borate (709 mg, 0.8 mmol, 8.0 eq) was added. The mixture was stirred for 2 hrs at room temperature and then evaporated to dryness. The crude material was purified twice by column chromatography (Fluka Silica 60 and Merck aluminium oxide 90; CH_2Cl_2). [Ir(ppy)$_2$(pbpy)][BARF] was isolated as a yellow-orange solid (286 mg, 0.179 mmol, 89.7%). *^{1}H NMR* (500 MHz, CD_2Cl_2, 295 K) δ/ppm 8.33 (dd, *J* = 8.1, 1.2 Hz, 1H, H^{F3}), 8.30 (d, *J* = 8.2 Hz, 1H, H^{E3}), 8.11 (t, *J* = 7.9 Hz, 1H, H^{F4}), 8.01 – 7.97 (m, 1H, H^{E4}), 7.93 (ddd, *J* = 5.7, 1.5, 0.7 Hz, 1H, H^{E6}), 7.86 – 7.83 (m, 2H, H^{B4+B3}), 7.81 (d, *J* = 7.9 Hz, 1H, H^{D3}), 7.75 – 7.69 (m, 9H, H^{H2+D4}), 7.65 (dt, *J* = 5.8, 1.1 Hz, 1H, H^{B6}), 7.56 (s, 4H, H^{H4}), 7.52 (dd, *J* = 7.8, 1.2 Hz, 1H, H^{A3}), 7.49 (dd, *J* = 7.7, 1.2 Hz, 1H, H^{F5}), 7.36 (ddd, *J* = 7.6, 5.5, 1.2 Hz, 1H, H^{E5}), 7.32 (ddd, *J* = 5.9, 1.3, 0.7 Hz, 1H, H^{D6}), 7.23 (dd, *J* = 7.8, 1.1 Hz, 1H, H^{C3}), 7.00 (ddd, *J* = 7.3, 5.9, 1.4 Hz, 1H, H^{D5}), 6.99 – 6.93 (m, 3H, $H^{B5+A4+G4}$), 6.83 (td, *J* = 7.5, 1.4 Hz, 1H, H^{A5}), 6.74 (t, *J* = 7.8 Hz, 2H, H^{G3}), 6.62 (td, *J* = 7.8, 1.1 Hz, 1H, H^{C4}), 6.50 (s, 2H, H^{G2}), 6.41 (td, *J* = 7.5, 1.3 Hz, 1H, H^{C5}), 5.95 (dd, *J* = 7.7, 0.9 Hz, 1H, H^{A6}), 5.58 (dd, *J* = 7.6, 0.8 Hz, 1H, H^{C6}). NOESY at room temperature: crosspeak from broad G2 to D6 (7.31 ppm). *^{13}C {^{1}H} NMR* (126 MHz, CD_2Cl_2, 295 K) δ/ppm 169.6 (C^{B2}), 167.9 (C^{D2}), 166.8 (C^{F6}), 162.3 (C^{H1}, non-binomial quartet, $^2J_{B\text{-}C}$ = 49.9 Hz), 157.3 (C^{E2}), 157.2 (C^{F2}), 151.2 (C^{E6}), 151.0 (C^{C1}), 149.1 (C^{B6}), 149.0 (C^{D6}), 146.6 (C^{A1}), 143.4 (C^{A2}), 143.2 (C^{C2}), 139.8 (C^{F4}), 139.5 (C^{E4}), 138.7 (C^{D4}), 138.6 (C^{B4}), 137.9 (C^{G1}), 135.4 (C^{H2}), 131.8 (C^{C6}), 131.5 (C^{A5}), 130.7 (C^{A6}), 130.6 (C^{F5}), 130.2 (C^{C5}), 129.76 (C^{G4}), 129.4 (C^{H3}, qdd, *J* = 31.5, 5.8, 2.9 Hz), 128.5 (C^{G3}), 128.3 (C^{E5}), 127.8 (C^{G2}), 125.2 (2C, C^{A3+C3}), 125.1 (C^{CF_3}, q, $^2J_{C\text{-}F}$ = 272.4 Hz), 124.9 (C^{E3}), 123.8 (C^{D5}), 123.5 (C^{A4}), 123.4 (C^{F3}), 122.7 (C^{B5}), 121.5 (C^{C4}), 120.7 (C^{B3}), 120.5 (C^{D3}), 118.0 (C^{H4}, dt, *J* = 7.8, 3.9 Hz). *^{11}B NMR* (128 MHz, CD_2Cl_2, 295 K) δ/ppm -6.46 – -6.72 (m).[11] *IR* (solid, ν/cm^{-1}): 3045 (w), 2355 (w), 1609 (m), 1479 (m), 1450 (m), 1425 (w), 1354 (s), 1271 (s), 1159 (m), 1115 (s), 1103 (s), 1095 (s), 1067 (s), 935 (m), 887 (s), 841 (m), 756 (s), 735 (s), 712 (s), 681 (s), 669 (s), 615 (m), 581 (w). *MS* (ESI, m/z): positive mode: 733.2 $[M\text{-}PF_6]^+$ (calc. 733.2), negative mode: 863.1 $[BARF]^-$ (calc. 863.1). *UV-Vis* λ/nm (ε/dm^3 mol^{-1} cm^{-1}) (MeCN, 1.00 × 10^{-5} mol dm^{-3}): 259 (46'000), 300 (24'400), 375 (5'000). *Luminescence* (MeCN, c = 2.50 x 10^{-5} mol dm^{-3}, λ_{ex} = 265 nm): λ_{em} = 605

nm. *Quantum yield* (MeCN, degassed with argon, λ_{ex} = 260 nm, integration range: 530 – 800 nm): 0.027. *Elem. Anal.* calcd. for $C_{70}H_{40}BF_{24}IrN_4$ (1596.08) C 52.68, H 2.53, N, 3.51; found C 53.08, H 2.82, N 3.71. *Electrochemistry*: E_1^{ox}: +0.85 V/+0.71^{qr} V, E_1^{red}: -1.83 V/-1.78 V, E_2^{red}: -2.47 V/ir.

3.8.4. [Ir(ppy)$_2$(bpy)][BARF]

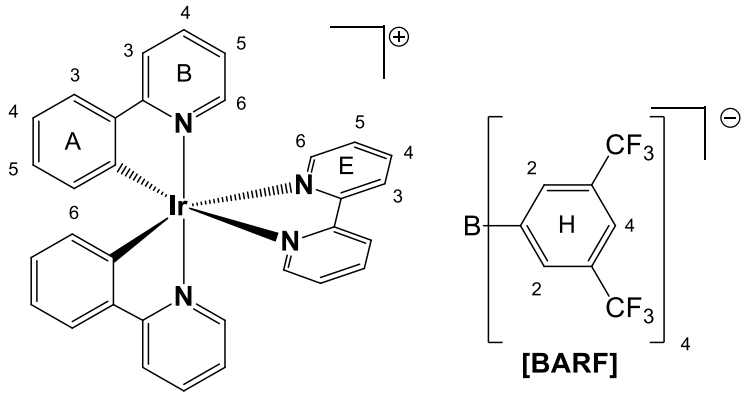

A yellow suspension of $[Ir_2(ppy)_4(\mu\text{-}Cl)_2]$ (107.2 mg, 0.100 mmol) and 2,2'-bipyridine (46.7 mg, 0.201 mmol) in methanol (15 mL) was heated in a microwave reactor for 2 hours at 120°C (P = 14 bar). The orange solution was then cooled to room temperature, and solid sodium tetrakis[3,5-bis(trifluoromethyl)phenyl]borate (709 mg, 0.8 mmol, 8.0 eq) was added. The mixture was stirred for 2 hrs at room temperature and then evaporated to dryness. The crude material was purified twice by column chromatography (Fluka Silica 60 and Merck aluminium oxide 90; CH_2Cl_2). [Ir(ppy)$_2$(bpy)][BARF] was isolated as a yellow-orange solid (276 mg, 0.182 mmol, 90.8%). *^{1}H NMR* (500 MHz, CD_2Cl_2, 295 K) δ/ppm 8.29 (dt, *J* = 8.1, 0.9 Hz, 2H, H^{E3}), 8.06 (ddd, *J* = 5.4, 1.6, 0.7 Hz, 2H, H^{E6}), 8.03 – 7.98 (m, 2H, H^{E4}), 7.97 – 7.95 (m, 2H, H^{B3}), 7.78 – 7.70 (m, 12H, $H^{A3+B4+H2}$), 7.55 (s, 4H, H^{H4}), 7.46 – 7.43 (m, 4H, H^{B6+E5}), 7.11 – 7.07 (m, 2H, H^{A4}), 6.97 – 6.94 (m, 2H, H^{A5}), 6.96 – 6.92 (m, 2H, H^{B5}), 6.32 – 6.29 (m, 2H, H^{A6}). *^{13}C {^{1}H} NMR* (126 MHz, CD_2Cl_2, 295 K) δ/ppm 168.4 (C^{B2}), 162.3 (C^{H1}, non-binomial quartet, $^2J_{B\text{-}C}$ = 49.8 Hz), 156.1 (C^{E2}), 151.7 (C^{E6}), 150.0 (C^{A1}), 148.8 (C^{B6}), 144.1 (C^{B2}), 139.6 (C^{E4}), 138.8 (C^{B4}), 135.3 (C^{H2}), 132.1 (C^{A6}), 131.4 (C^{A5}), 129.4 (C^{H3}, qdd, *J* = 31.5, 5.7, 2.8 Hz), 129.0 (C^{E5}), 125.6 (C^{A3}), 125.1 (C^{CF3}, q, $^2J_{C\text{-}F}$ = 272.4 Hz), 124.4 (C^{E3}), 123.7 (C^{B5}), 123.5 (C^{A4}), 120.6 (C^{B3}), 118.0 (C^{H4}, dt, *J* = 8.0, 3.9 Hz). *^{11}B NMR* (128 MHz, CD_2Cl_2, 295 K) δ/ppm -6.48 – -6.73 (m).[11] *IR* (solid, ν/cm^{-1}): 3069 (w), 2357 (w), 2328 (w), 1609 (m), 1585 (m), 1425 (m), 1354 (s), 1271 (s), 1155 (s), 1113 (s), 1065 (s), 1034 (m), 928 (w), 887 (s), 839 (s), 754 (s), 731 (m), 714 (s), 681 (s), 667 (s), 581 (w). *MS* (ESI, m/z): positive mode: 657.2 $[M\text{-}PF_6]^+$ (calc. 656.8), negative mode: 863.1 $[BARF]^-$ (calc. 863.1). *UV-Vis* λ/nm (ε/dm^3 mol^{-1} cm^{-1}) (MeCN, 1.00 × 10^{-5} mol dm^{-3}): 255 (48'000), 265 (47'400), 300 (23'500), 375 (5'400). *Luminescence* (MeCN, c = 2.50 x 10^{-5} mol l^{-1}, λ_{ex} = 265 nm): λ_{em} = 590 nm. *Quantum yield* (MeCN, degassed with argon, λ_{ex} = 250 nm, integration range: 510 – 800 nm): 0.083. *Elem. Anal*. calcd. For $C_{64}H_{36}BF_{24}IrN_4{\cdot}2CH_3OH$ (1584.07) C 50.04, H 2.80, N, 3.54; found C 50.01, H 2.81, N 3.70. *Electrochemistry*: E_1^{ox}: +0.92 V/+0.83 V, E_1^{red}: -1.81 V/-1.75 V, E_2^{red}: -2.47 V/ir.

[1] J. D. Slinker, J. Rivnay, J. S. Moskowitz, J. B. Parker, S. Berhard, H. D. Abruña, G. G. Malliaras, *J. Mater. Chem.*, 2007, **17**, 2976.
[2] F. G. Gao, A. J. Bard, *J. Am. Chem. Soc.*, 2000, **122**, 7426.
[3] H. Rudmann, S. Shimada, M. F. Rubner, *J. Am. Chem. Soc.*, 2002, **124**, 4918.
[4] M. Mydlak, C. Bizzarri, D. Hartmann, W. Sarfert, G. Schmid, L. De Cola, *Adv. Funct. Mater.*, 2010, **20**, 1812.
[5] C.-H. Yang, J. Beltran, V. Lemaur, J. Cornil, D. Hartmann, W. Sarfert, R. Fröhlich, C. Bizzarri, L. De Cola, *Inorg. Chem.*, 2010, **49**, 9891.
[6] H. J. Bolink, E. Coronado, R. D. Costa, E. Ortí, M. Sessolo, S. Graber, K. Doyle, M. Neuburger, C. E. Housecroft, E. C. Constable, *Adv. Mater.*, 2008, **20**, 3910.
[7] See for example: F. Neve, A. Crispini, S. Campagna and S. Serroni*, Inorg. Chem*., 1999, **38**, 2250 and references cited therein.
[8] C. Janiak, *J. Chem. Soc., Dalton Trans.,* 2000, 3885.
[9] J. C. Gray, A. Pagelot, A. Collins, F. P. A. Fabbianti, S. Parsons, P. J. Sadler, *Eur. J. Inorg. Chem.*, 2009, 2673.
[10] R. D. Costa, E. Ortí, H. J. Bolink, S. Graber, C. E. Housecroft and E. C. Constable, *Adv. Funct. Mater.*, 2010, **20**, 1511.
[11] E. Bernhardt, D. J. Brauer, M. Finze, H. Willner, *Angew. Chem.,* 2006, **118**, 6532.

Chapter 4

4 Shifting the emission maximum towards the blue region of the visible spectrum

4.1 Introduction

Starting from the iridium complex (e.g. $[Ir(ppy)_2(bpy)][PF_6]$, see Chapter 2), the aim was to widen the bandgap between the HOMO and LUMO levels, in order to blue-shift the emission maximum. As mentioned before (see Section 1.9), in a cationic iridium(III) complex this can be achieved by changing either or both the cyclometallating C^N ligand, where the HOMO is localized, and the ancillary N^N ligand, which changes the LUMO of an iridium(III) complex.[1]

To increase the band gap between the HOMO and LUMO, the HOMO needs to be stabilized, thus lowering its energy level, and/or the LUMO needs to be destabilized, i.e. raising its energy level. To stabilize the HOMO, electron-withdrawing substituents such as -F or $-CF_3$ are widely used. To destabilize the LUMO, electron-donating substituents such as $-N(CH_3)_2$ are attached on the ancillary ligand.[1, 2, 3, 4]

In this chapter, electron-donating ^{t}Bu and NMe_2 substituents on the ancillary ligand and electron-withdrawing fluorine atoms on the cyclometallating ligands have been introduced into iridium(III) complexes, in order to shift the emission maximum towards the blue region of the visible spectrum.

4.2 Results and discussion

The four complexes $[Ir(dfppz)_2(N^N)][PF_6]$ (N^N = pbpy, 1, 2, 3) were prepared by the established methodology[5] of treating a dichlorido bridged iridium(III) dimer with two equivalents of an N^N ligand. The reactions were performed in a microwave reactor followed by precipitation with ammonium hexafluoridophosphate, and the purification was done by column chromatography.

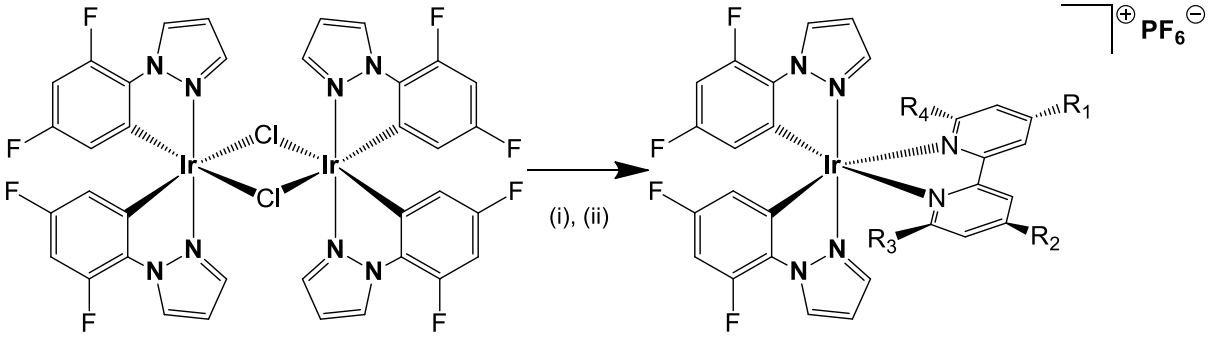

$[Ir_2(dfppz)_4(\mu\text{-}Cl)_2]$

$[Ir(dfppy)_2(pbpy)][PF_6]$: $R_1 = R_2 = H$, $R_3 = Ph$, $R_4 = H$
$[Ir(dfppy)_2(\mathbf{1})][PF_6]$: $R_1 = R_2 = {}^tBu$, $R_3 = Ph$, $R_4 = H$
$[Ir(dfppy)_2(\mathbf{2})][PF_6]$: $R_1 = R_2 = {}^tBu$, $R_3 = R_4 = Ph$
$[Ir(dfppy)_2(\mathbf{3})][PF_6]$: $R_1 = R_2 = NMe_2$, $R_3 = R_4 = H$

Scheme 4.1 Syntheses of the complexes described in this section. Conditions: (i) ligand pbpy, 1, 2 or 3, MeOH, microwave, 2 h, 120 °C; (ii) $[NH_4][PF_6]$.

The yields ranged from 45% for [Ir(dfppz)$_2$(**3**)][PF$_6$] to 71% for [Ir(dfppz)$_2$(N^N)][PF$_6$] (N^N = pbpy and **1**). The ESI mass spectrum of each of the complexes showed a peak that was assigned to the [M – PF$_6$]$^+$ ion and the observed isotope patterns were in accord with those simulated. The elemental analyses could be resolved by the addition of 0.25 to 1 solvent molecules.

Each of the [Ir$_2$(dfppz)$_4$Cl$_2$], [Ir(dfppz)$_2$(**2**)][PF$_6$] and [Ir(dfppz)$_2$(**3**)][PF$_6$] contains a C_2 axis. Therefore the two cyclometallating ligands are equivalent in NMR, whereas in [Ir(dfppz)$_2$(pbpy)][PF$_6$] and [Ir(dfppz)$_2$(**1**)][PF$_6$] the N^N ligand has only one pendant phenyl ring, making it asymmetric and therefore the two cyclometallating ligands are non-equivalent, the ring labelling has been adopted to allow direct comparison of the corresponding atoms (see Scheme 4.2 and Table 4.1).

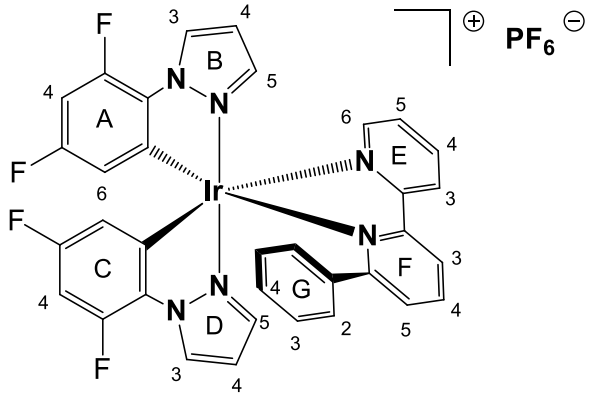

[Ir(dfppz)$_2$(pbpy)][PF$_6$]

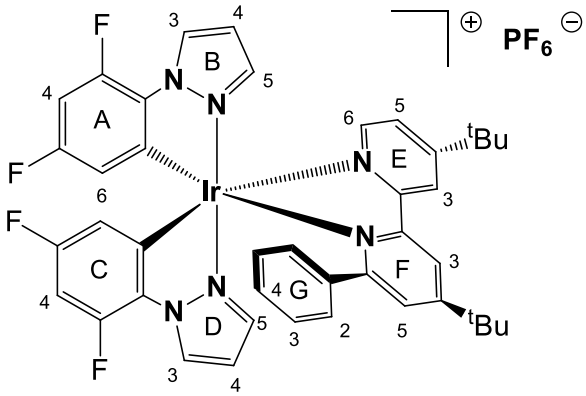

[Ir(dfppz)$_2$(**1**)][PF$_6$]

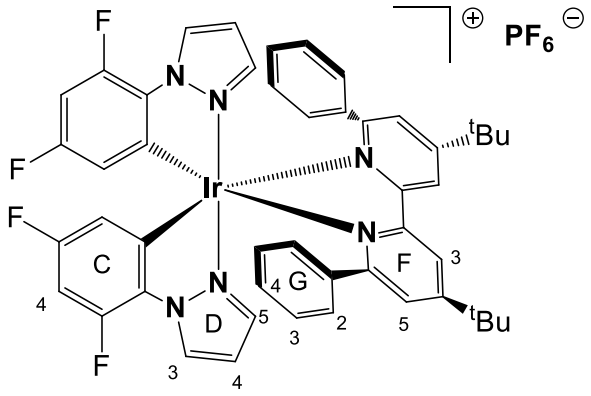

[Ir(dfppz)$_2$(**2**)][PF$_6$]

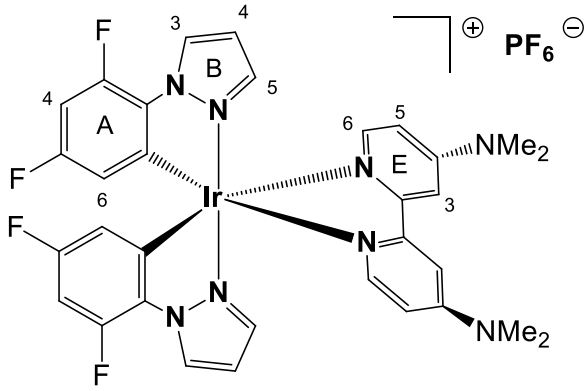

[Ir(dfppz)$_2$(**3**)][PF$_6$]

Scheme 4.2 Structures of the complexes with ring labelling and atom numbering for NMR spectroscopic assignments.

The NMR spectroscopic assignments were done with routine 2D techniques (COSY, NOESY, HMBC and HMQC), in a similar manner to the assignment of the spectrum for the compound [Ir(ppy)$_2$(tpy)][PF$_6$] (see Section 5.3). A good starting point for the NMR assignment of these four new complexes was the dimer. Although this dimer has been used on numerous

occasions[6, 7, 8, 9, 10, 11, 12, 13, 14, 15, 16] full assignment of the ^{13}C NMR spectrum was missing in the literature prior to this work being carried out. Therefore, these data are included in

Table 4.1.

Table 4.1 ^{13}C NMR spectroscopic data (in ppm, 126 MHz, CD_2Cl_2, 298 K, TMS) for the precursor dimer and the four complexes, assigned using low temperature HMQC and HMBC spectra. Coupling constants are in Hz.

Compound	**A1**	**A2**	**A3**	**A4**	**A5**	**A6**	**B3**	**B4**	**B5**	
$[Ir_2(dfppz)_4Cl_2]$	115.0	128.0	149.2 J_{CF} 256	98.8	159.5 J_{CF} 249	115.1	132.3	107.9	140.7	
$[Ir(dfppz)_2(pbpy)][PF_6]$	132.8/ 136.7[a]	126.5	148.3 J_{CF} 256	99.7	160.0 J_{CF} 256	114.1	131.7	108.9	137.4	
$[Ir(dfppz)_2(\mathbf{1})][PF_6]$	134.2/ 138.1[a]	127.4	149.4 J_{CF} 254	100.3	160.8 J_{CF} 248	114.8	132.3	109.8	138.5	
$[Ir(dfppz)_2(\mathbf{2})][PF_6]$										
$[Ir(dfppz)_2(\mathbf{3})][PF_6]$	139.2[a]	128.0	148.0 J_{CF} 242	99.1	160.8 J_{CF} 228	115.8	131.8	108.9	138.1	
	C1	**C2**	**C3**	**C4**	**C5**	**C6**	**D3**	**D4**	**D5**	
$[Ir(dfppz)_2(pbpy)][PF_6]$	132.8/ 136.7	126.0	147.9 J_{CF} 256	98.0	159.1 J_{CF} 260	114.3	131.4	108.9	138.3	
$[Ir(dfppz)_2(\mathbf{1})][PF_6]$	134.2/ 138.1	127.0	149.0 J_{CF} 251	98.7	160.1 J_{CF} 245	115.2	132.3	109.7	139.0	
$[Ir(dfppz)_2(\mathbf{2})][PF_6]$	133.7[a]	124.9	147.2 J_{CF} 254	98.2	158.5 J_{CF} 252	113.6	131.7	108.7	138.9	
$[Ir(dfppz)_2(\mathbf{3})][PF_6]$										
	E2	**E3**	**E4**	**E5**	**E6**	**F2**	**F3**	**F4**	**F5**	**F6**
$[Ir(dfppz)_2(pbpy)][PF_6]$	157.2	124.9	127.5	140.0	150.1	164.2	122.7	140.2	129.1	165.6
$[Ir(dfppz)_2(\mathbf{1})][PF_6]$	157.7	122.4	165.7	125.8	150.5	158.3	120.4	165.9	127.2	166.3
$[Ir(dfppz)_2(\mathbf{2})][PF_6]$						157.9	120.6	163.9	127.0	164.4
$[Ir(dfppz)_2(\mathbf{3})][PF_6]$	149.3	105.9	156.3	109.4	149.8					
	G1	**G2/G6**	**G3/G5**	**G4**	**Me**	***C*^{t}Bu**				
$[Ir(dfppz)_2(pbpy)][PF_6]$	137.8	126.9/ 127.3	127.2/ 128.0	129.3						
$[Ir(dfppz)_2(\mathbf{1})][PF_6]$	139.1	128.0/ 128.5	128.0/ 129.0	130.2	30.8/ 30.7	36.45/ 36.40				
$[Ir(dfppz)_2(\mathbf{2})][PF_6]$					30.0	35.7				
$[Ir(dfppz)_2(\mathbf{3})][PF_6]$	138.2	126.6/ 127.3	127.3/ 127.4	128.5	40.0					

[a]For $[Ir(dfppz)_2(N^N)][PF_6]$ (N^N = pbpy, **1, 2, 3**), signal for C^{A1} only resolved in 151 MHz ^{13}C NMR spectra (298 K).

Table 4.1 indicates that there are correlations between the chemical shifts for a given carbon atom (e.g. A2 or A3) across the series of compounds. The cyclometallating carbon A1 is

strongly low-field shifted after complexation with an N^N ligand. In the dimer $[Ir_2(dfppz)_4Cl_2]$, carbon A1 lies *trans* to a chlorine atom, whereas after complexation the nitrogen of the bpy ligand is *trans* to carbon A1. The resonance of this carbon shifts from δ 115.0 ppm to δ 139.2 – 132.8 ppm. For $[Ir(dfppz)_2(pbpy)][PF_6]$ and $[Ir(dfppz)_2(\mathbf{1})][PF_6]$, where the two cyclometallating C^N ligands are non-equivalent, NOESY cross peaks helped to distinguish between pairs of rings A and C, and B and D. The NOESY spectrum shows cross peaks between the pair of protons A6 and E6, A6 and D5, and C6 and B5, respectively.

In $[Ir(dfppz)_2(pbpy)][PF_6]$, $[Ir(dfppz)_2(\mathbf{1})][PF_6]$ and $[Ir(dfppz)_2(\mathbf{2})][PF_6]$ the pendant phenyl rings in the bpy ligands undergo hindered rotation on the NMR timescale at 298 K. Upon cooling the sample down to 210 K, the broad signals start to split to show two separate signals for protons G2 and G6, and G3 and G4, respectively. The 500 MHz ^{1}H NMR spectrum of a CD_2Cl_2 solution of $[Ir(dfppz)_2(pbpy)][PF_6]$ at 210 K shows signals at δ 7.14 and 5.85 ppm (d, J = 7.6 Hz) from protons G2/G6 and at δ 7.12 and 6.79 ppm from protons G3/G5. At 298 K, the signals G3/G5 coalesce to a broad signal (FWHM ≈ 200 Hz) centred at δ 6.96 ppm. The signals of protons G2/G6 are still not fully collapsed giving rise to two very broad peaks, one centred at δ 6.0 ppm while the second signal is hidden under other signals at approximately δ 7.00 ppm.

Figure 4.1 depicts the 500 MHz ^{1}H NMR spectrum of a CD_2Cl_2 solution of $[Ir(dfppz)_2(\mathbf{2})][PF_6]$ at various temperatures. At 298 K, broad signals at δ 6.94 and 6.64 ppm arise from the coalescence of signals for pairs of resonances for $H^{G3/G5}$ and $H^{G2/G6}$ which are observed, respectively, at δ 7.08 and 6.75 ppm and δ 7.05 and 6.03 ppm at 210 K (Figure 4.1).

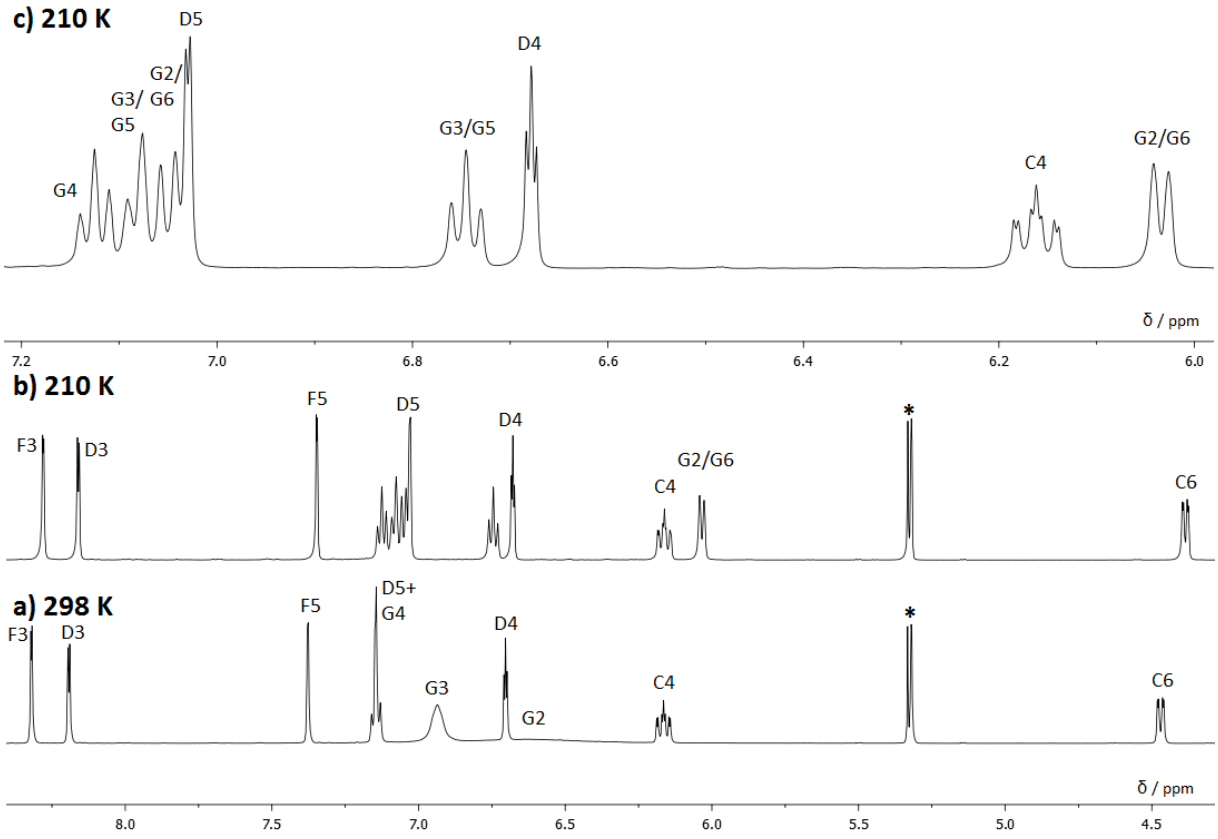

Figure 4.1 500 MHz ^{1}H NMR spectra of [Ir(dfppz)$_2$(2)][PF$_6$] in CD_2Cl_2 at a) 298 K and b) 210 K. The signal (δ 1.43 ppm) for the ^{t}Bu groups is not shown. Signals * = residual CH_2Cl_2 and $CDHCl_2$. c) Expansion of part of the spectrum shown in part b) showing the ring G proton signals.

In [Ir(dfppz)$_2$(**1**)][PF$_6$] the additional ^{t}Bu substituents have little effect on the dynamic process, because the substituents are on the periphery of the complex and do not affect the rotation of the phenyl ring.

In contrast to [Ir(ppy)$_2$(tpy)][PF$_6$] (see Section 5.3) there are fluorine atoms on the C^N ligands in the four complexes discussed in this chapter and therefore ^{19}F NMR spectra were recorded for the four complexes in CD_2Cl_2 solution. Starting with the symmetric compounds [Ir(dfppz)$_2$(**2**)][PF$_6$] and [Ir(dfppz)$_2$(**3**)][PF$_6$], the signals could be assigned. In [Ir(dfppz)$_2$(**2**)][PF$_6$] the proton decoupled spectrum shows a doublet at δ -73.7 ppm, which was assigned to the [PF$_6$]$^-$ anion (J_{PF} = 711 Hz), and two more doublets at δ -125.5 and -113.7 ppm, J_{FF} = 5.9 Hz. [Ir(dfppz)$_2$(**3**)][PF$_6$] show very similar signals. The proton coupled spectra show the further splitting of the signal at δ -125.5 and -113.7 ppm to a doublet of doublets, and triplet of doublets, respectively. The signal at lower frequency (δ -125 ppm) could be assigned to fluorine C3 (A3 in [Ir(dfppz)$_2$(**3**)][PF$_6$]) and the higher frequency signal to fluorine C5 (A5 in [Ir(dfppz)$_2$(**3**)][PF$_6$]).

4.3 Solid state structures

Several new X-ray structures were solved during the work on these complexes: [Ir$_2$(dfppz)$_4$Cl$_2$], [Ir(dfppz)$_2$(pbpy)][PF$_6$], [Ir(dfppz)$_2$(**2**)][PF$_6$], ligand **2** and [Ir(dfppz)$_2$(**3**)][PF$_6$].

Different crystal growing set-ups have been tried and several led to crystals that were used for X-ray structure determination.

4.3.1 $[Ir_2(dfppz)_4(\mu\text{-}Cl)_2]$

Single crystals of the iridium(III) dimer were grown by slow evaporation of a CH_2Cl_2 solution of the complex at room temperature. The dimer crystallizes as $[Ir_2(dfppz)_4(\mu\text{-}Cl)_2].CH_2Cl_2$ in the centrosymmetric space group *P*-1. In the unit cell there are two enantiomers of the dimer present: the Λ,Λ- and the Δ,Δ-form with two CH_2Cl_2 solvent molecules. As seen in other similar compounds, the N-donors of the two cyclometallating ligands are in a *trans*-arrangement. The bridging chlorine atoms therefore are *trans* to the C-atoms of the 2,4-difluorophenyl-rings. The two iridium atoms are crystallographically independent and the bond parameters of the iridium coordination sphere are given in the caption of Figure 4.2.

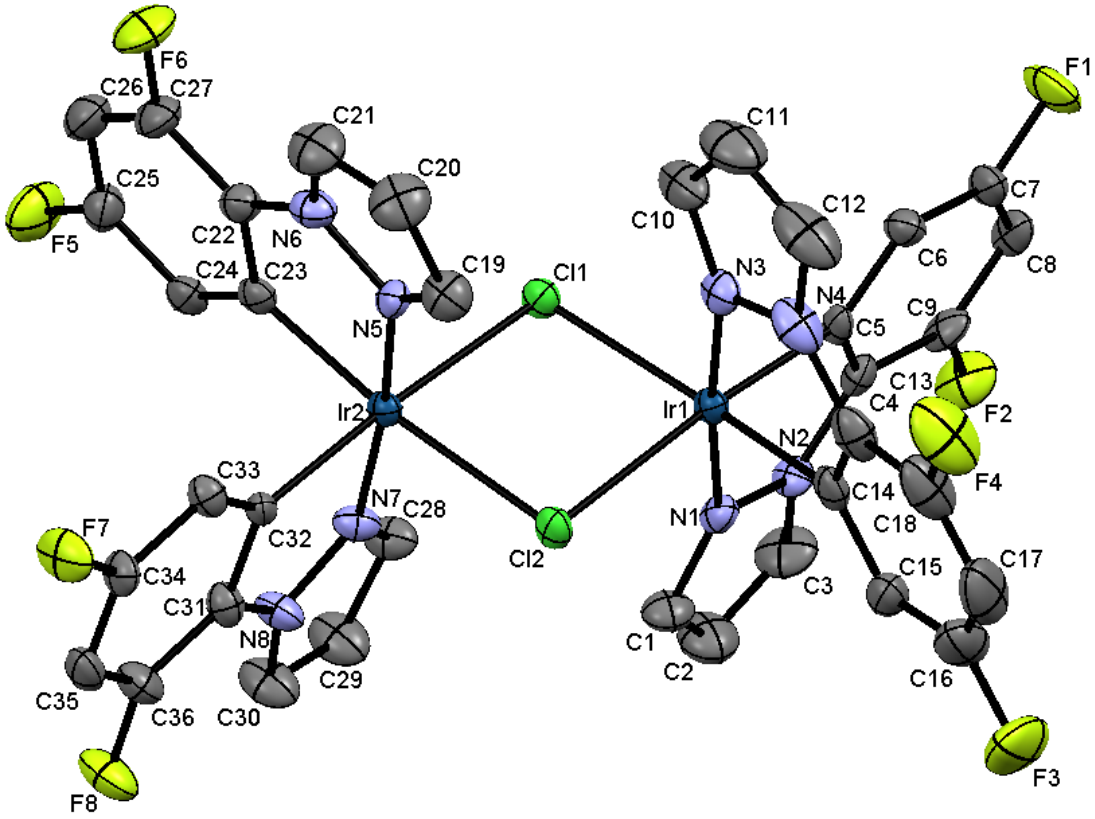

Figure 4.2 Structure of Λ,Λ-$[Ir_2(dfppz)_4(\mu\text{-}Cl)_2]$ in $[Ir_2(dfppz)_4(\mu\text{-}Cl)_2]\cdot CH_2Cl_2$ with ellipsoids plotted at 50% probability level; H atoms omitted. Selected bond lengths (in Å) and angles (in °): Ir1–C14 = 1.982(6), Ir1–C5 = 1.999(5), Ir1–N1 = 2.028(5), Ir1–N3 = 2.032(5), Ir1–Cl2 = 2.4870(15), Ir1–Cl1 = 2.4962(17), Ir2–C32 = 1.989(5), Ir2–C23 = 2.000(6), Ir2–N5 = 2.014(5), Ir2–N7 = 2.022(5), Ir2–Cl2 = 2.4856(17), Ir2–Cl1 = 2.4951(15); C5–Ir1–N1 = 80.5(2), C14–Ir1–N3 = 80.7(3), Cl2–Ir1–Cl1 = 83.39(5), Cl2–Ir2–Cl1 = 83.45(5), C23–Ir2–N5 = 80.8(2), C32–Ir2–N7 = 80.6(2).

The major interactions in the crystal packing are the face-to-face π-stacking between the difluorophenyl rings in adjacent molecules. There are two different packing interactions. The main interaction is between rings containing atoms C5 and $C32^{i}$ (symmetry code i = 1 + x, y, z). The planes through these rings subtend an angle of 2.6° and the inter-centroid distance is 3.68 Å. These contacts lead to chains of molecules that assemble along the *a*-axis (primary

stacking interactions in Figure 4.3). Between the chains there are additional face-to-face π-stacking interactions which are less efficient (secondary stacking interactions in Figure 4.3). These interactions are between the difluorophenyl rings containing atoms C14 and C23^{ii} (symmetry code ii = -1 + x, 1 + y, z). The angle between the least squares planes is bigger (8.2°) and the inter-centroid distance further (4.26 Å), making them less efficient. As discussed by Janiak[17] this stacking interaction is at the extreme end of the range. The solvent molecules in $[Ir_2(dfppz)_4(\mu\text{-}Cl)_2].CH_2Cl_2$ are ordered and participate in C...Cl and CH-π contacts, whereas the pyrazole rings only participate in intermolecular CH-F interactions.

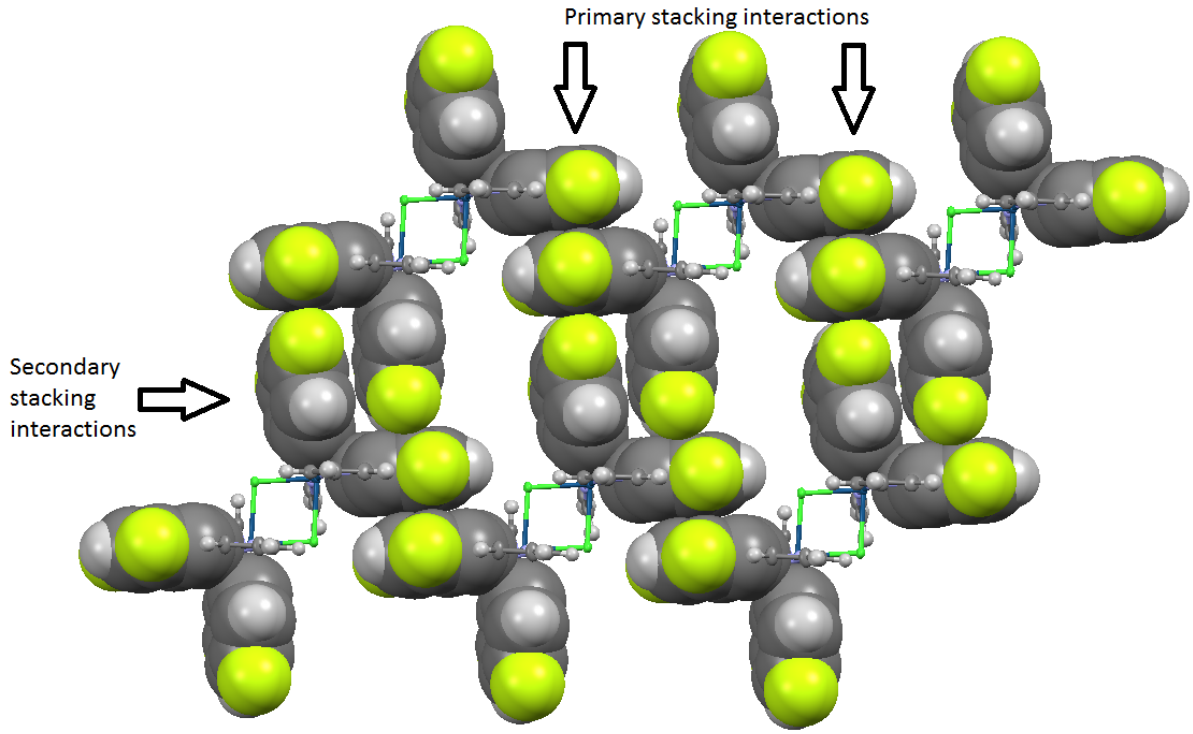

Figure 4.3 Assembly of chains of Λ,Λ-$[Ir_2(dfppz)_4(\mu\text{-}Cl)_2]$ molecules. Each chain runs parallel the a-axis (horizontal) and secondary stacking interactions lead to sheets in the ab-plane.

4.3.2 $[Ir(dfppz)_2(pbpy)][PF_6]$

From a CH_2Cl_2 solution of the complex, X-ray quality crystals of $4\{[Ir(dfppz)_2(pbpy)][PF_6]\}.3CH_2Cl_2$ were grown by solvent evaporation. The complex crystallizes in the centrosymmetric $P2_1/n$ space group with both enantiomers of $[Ir(dfppz)_2(pbpy)]^+$ in the unit cell and the structure of the Λ-$[Ir(dfppz)_2(pbpy)]^+$ cation is depicted in Figure 4.4. The atom Ir1 is in an octahedral environment and the N-donors of the two cyclometallating ligands are in a *trans*-arrangement, as expected and already seen in the structure of the precursor. The N-atoms of the bpy-rings are *trans* to the C-atoms of the 2,4-difluorophenyl rings. Both cyclometallating C^N ligands are almost planar. This is in contrast to the bpy ligand with an angle between the least squares planes of the two pyridine rings of 19.5°. The pendant phenyl ring of the bpy ligand is twisted through 57.0° with respect to the bonded pyridine ring. This non-planarity allows the free phenyl ring to undergo intramolecular face-to-face π-stacking with one of the difluorophenyl rings of one of the C^N ligands. The inter-centroid

separation is 3.44 Å and the angle between the least squares planes is 5.4°. This makes it a highly efficient interaction.

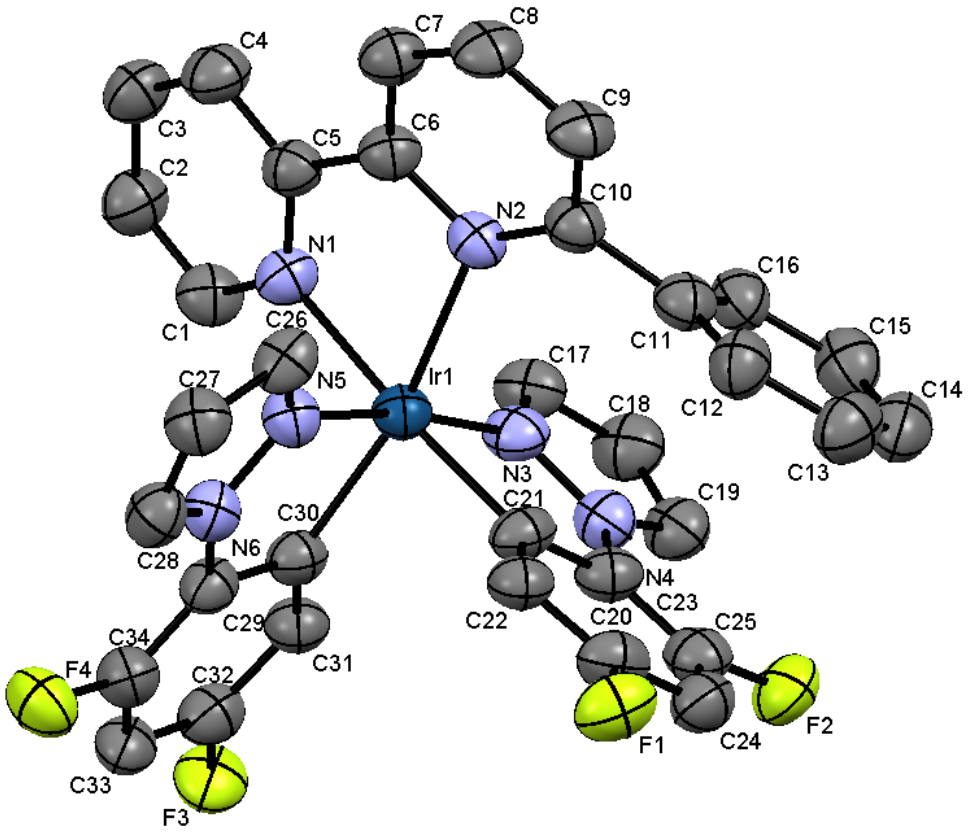

Figure 4.4 Structure of the Λ-$[Ir(dfppz)_2(pbpy)]^+$ cation in $4\{[Ir(dfppz)_2(pbpy)][PF_6]\}.3CH_2Cl_2$ with ellipsoids plotted at 50% probability level; H atoms omitted. Selected bond lengths (in Å) and angles (in °): Ir1–N3 = 2.021(7), Ir1–N5 = 2.022(6), Ir1–C30 = 2.031(8), Ir1–C21 = 2.035(8), Ir1–N1 = 2.140(7), Ir1–N2 = 2.191(6), N3–N4 = 1.375(10), N5–N6 = 1.357(9); N1–Ir1–N2 = 76.1(2), N3–Ir1–C21 = 79.6(3), N5–Ir1–C30 = 80.2(3).

A space-filling representation of the π-stacking interaction is depicted in Figure 4.5. Parallel to the horizontal b-axis there are chains of molecules of the same handedness, while adjacent chains have the opposite chirality. These chains are supported by CH...F hydrogen bonds (C26H26a...$F3^i$ = 2.46 Å, C26...$F3^i$ = 3.142(9) Å, C26 – H26a – $F3^i$ = 129°; symmetry code i = x, 1+y, z). The $[PF_6]^-$ anion and the solvent molecule are ordered and the crystal packing is dominated by the following contacts: $CH...F_{anion}$, $CH...F_{ligand}$, $Cl...\pi_{ligand}$, $F...\pi_{ligand}$.

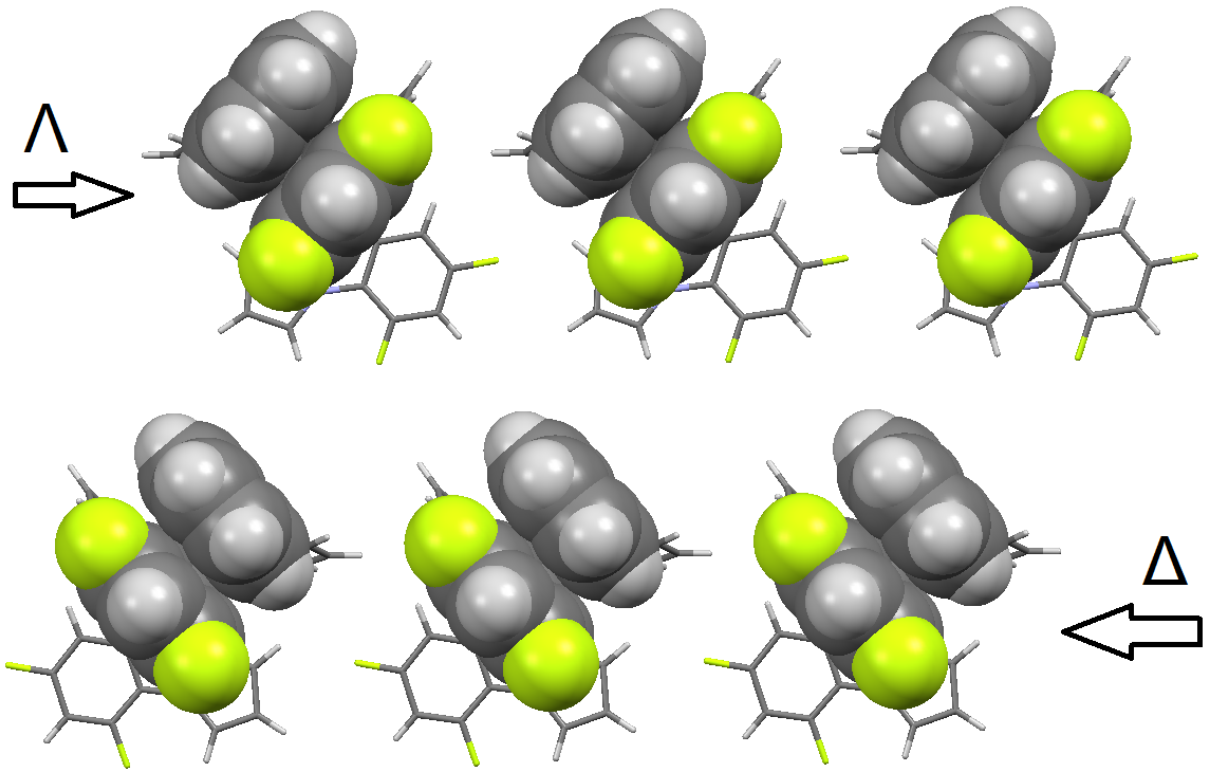

Figure 4.5 Association of $[Ir(dfppz)_2(pbpy)]^+$ cations of the same handedness into chains and intra-cation face-to-face π-stacking (see text).

4.3.3 Ligand 2 and $[Ir(dfppz)_2(2)][PF_6]$

Ligand **2** and $[Ir(dfppz)_2(\mathbf{2})][PF_6]$ have been structurally characterized. Crystals of the free ligand **2** (4,4'-di-*tert*-butyl-6,6'-diphenyl-2,2'-bipyridine) were isolated during the synthesis of the complex. The molecule crystallizes in the centrosymmetric *C*2/c space group. The bpy domain is planar and exhibits a *trans*-arrangement (Figure 4.6). The bond distances and bond angles are typical.[22] The angle between the least squares planes of the phenyl and pyridine rings is 24.6°.

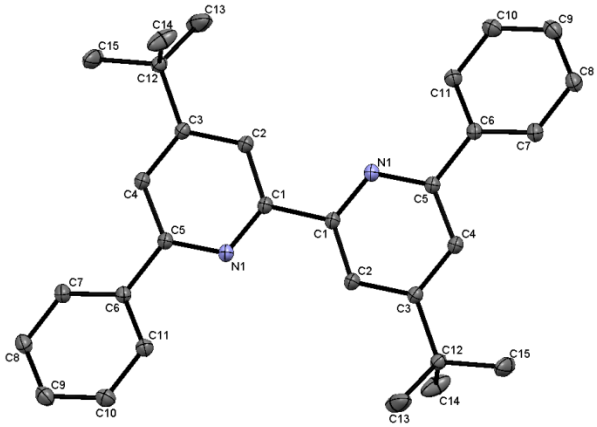

Figure 4.6 Structure of ligand 2 (4,4'-di-*tert*-butyl-6,6'-diphenyl-2,2'-bipyridine) with ellipsoids plotted at 50% probability level; H atoms omitted. Symmetry code i = 1/2 – x, 1/2 – y, 1 – z. Selected bond lengths (in Å): C1–C1i = 1.4943(10), C1–N1 = 1.3412(7), C5–N1 = 1.3414(7), C5–C6 = 1.4837(7), C3–C12 = 1.5297(7).

The pyridine rings of the free ligand undergo face-to-face π-π stacking in an offset manner. The pyridine ring containing atom N1 stacks with pyridine ring containing atom N1[ii] (symmetry code ii = ½ – x, 3/2 – y, 1 – z). The angle between the planes of these rings is 0° and the inter-plane and inter-centroid separations are 3.79 and 3.86 Å, respectively. Therefore these packing interactions are very efficient.[17]

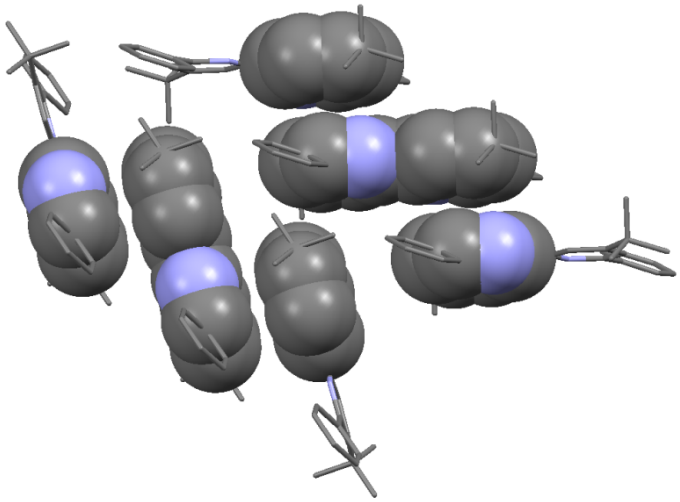

Figure 4.7 Packing of molecules of the free ligand 2, with the stacking interactions in the space-filling representation.

Crystals of the complex were grown from a CH_2Cl_2 solution by evaporation. [Ir(dfppz)$_2$(**2**)][PF_6].CH_2Cl_2 crystallizes in the $P2_1/c$ space group with both enantiomers of the complex present in the unit cell. Figure 4.8 shows the Δ-form of the cation. The iridium is in an octahedral coordination sphere and the bond parameters are similar to [Ir(dfppz)$_2$(pbpy)][PF_6]. The C^N ligands are almost planar, but the bpy ligand is twisted, analogous to [Ir(dfppz)$_2$(pbpy)][PF_6].

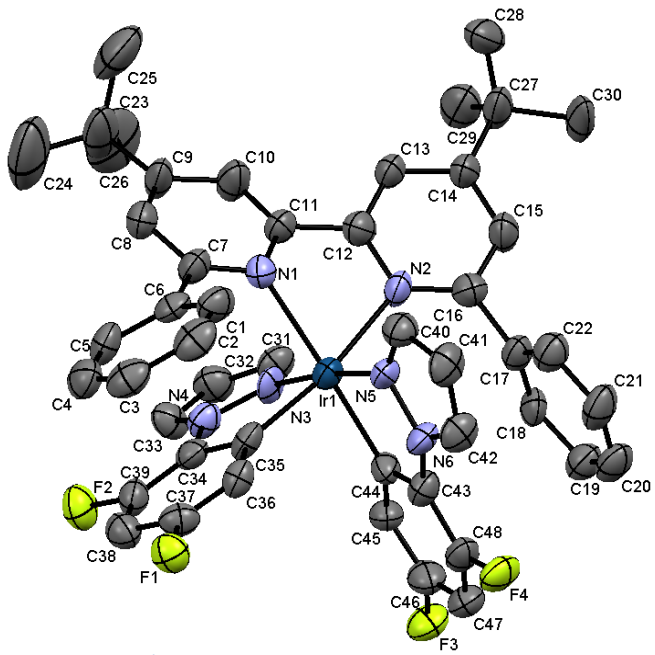

Figure 4.8 Structure of the Δ-[Ir(dfppz)$_2$(2)]$^+$ cation in [Ir(dfppz)$_2$(2)][PF_6].CH_2Cl_2 with ellipsoids plotted at 50% probability level; H atoms omitted. Selected bond lengths (in Å) and angles (in °): Ir1–N5 = 2.014(10), Ir1–C35 = 2.015(13), Ir1–N3 = 2.029(9), Ir1–C44 = 2.034(12), Ir1–N2 = 2.183(10), Ir1–N1 = 2.221(9), N3–N4 = 1.372(13), N5–N6 = 1.381(12); N2–Ir1–N1 = 76.4(3), C35–Ir1–N3 = 79.8(4), N5–Ir1–C44 = 79.2(4).

The twisting angle between the two pyridine rings is 22.0°, making it slightly greater than in [Ir(dfppz)$_2$(pbpy)][PF$_6$]. This can be explained by the presence of two, instead of only one, stacking interactions in [Ir(dfppz)$_2$(**2**)][PF$_6$]. These intra-cation face-to-face π-stacking interactions between the free phenyl ring and an adjacent cyclometallating difluorophenyl ring are highly efficient. The angles of the least squares planes between the rings containing C4/C38 and C20/C47 are 3.7 and 5.0° respectively and the inter-centroid distances are 3.46 and 3.47 Å, respectively.

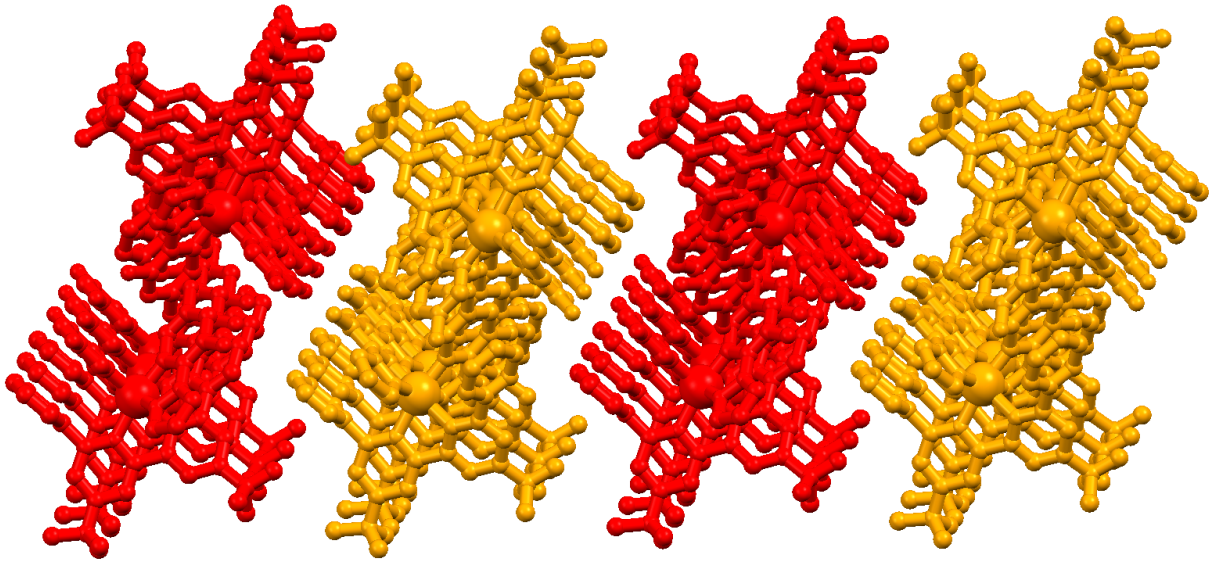

Figure 4.9 Packing of [Ir(dfppz)$_2$(2)]$^+$ cations in [Ir(dfppz)$_2$(2)][PF$_6$].CH$_2$Cl$_2$. Δ-cations are shown in red and Λ-cations in orange.

Figure 4.9 depicts the arrangement of the cations in the crystal structure. Due to the intra-molecular π-interactions between the pendant phenyl rings and the adjacent cyclometallating difluorophenyl rings, these cations are assembled into sheets parallel to the *bc*-plane. The sheets of cations are separated by sheets of interdigitated ligands.

The [PF$_6$]$^-$ anion and the CH$_2$Cl$_2$ solvent molecule are ordered, and CH...F contacts play a dominant role in the crystal packing.

4.3.4 [Ir(dfppz)$_2$(3)][PF$_6$]

From a CH$_2$Cl$_2$ solution of the bulk material, single crystals of [Ir(dfppz)$_2$(**3**)][PF$_6$].CH$_2$Cl$_2$ were grown by evaporation. The complex crystallizes in the centrosymmetric space group *P*-1 and in the unit cell both enantiomers are present. One of the cyclometallating [dfppz]$^-$ ligands in this structure is disordered. It has been modelled over two sites with 66.2% and 33.8% occupancies. In Figure 4.10 only the major occupancy sites are depicted. The bond parameters of the octahedral environment of the iridium atom (Ir1) are as expected, as they are within the ligands. In the dimethylamino groups of the bpy ligand, the environment of atoms N3 and N4 is consistent with sp^2 hybridization. The N-C bond lengths around these nitrogen atoms indicate conjugation of the aromatic π-system from the bpy ligand onto the dimethylamino groups. In the structures of [Ir(dfppz)$_2$(pbpy)][PF$_6$] and [Ir(dfppz)$_2$(**2**)][PF$_6$],

the trend of the bpy domain to twist more by addition of intra-molecular π-stacking has already been mentioned. This trend continues within the structure of [Ir(dfppz)$_2$(**3**)][PF$_6$] with angles of: 22.0° ([Ir(dfppz)$_2$(**2**)][PF$_6$], two phenyl rings) and 19.5° ([Ir(dfppz)$_2$(pbpy)][PF$_6$], one phenyl ring). For [Ir(dfppz)$_2$(**3**)][PF$_6$], the complex without any pendant phenyl rings, the angle between the planes of the pyridine rings is 15.2°. It is surprising that even in the absence of intra-molecular stacking interactions the bpy domain is non-planar. The inter-cation interactions appear to be the origin of the twisting in this compound.

The [PF$_6$]$^-$ ion is ordered. Similar to the three previously described structures in this chapter, the crystal packing is dominated by CH...F$_{anion}$ and CH...F$_{ligand}$ contacts. Contrary to the previously described structures in this chapter, the CH_2Cl_2 solvent molecule is disordered and has been modelled over two overlapping sites with occupancies of 63% and 37%.

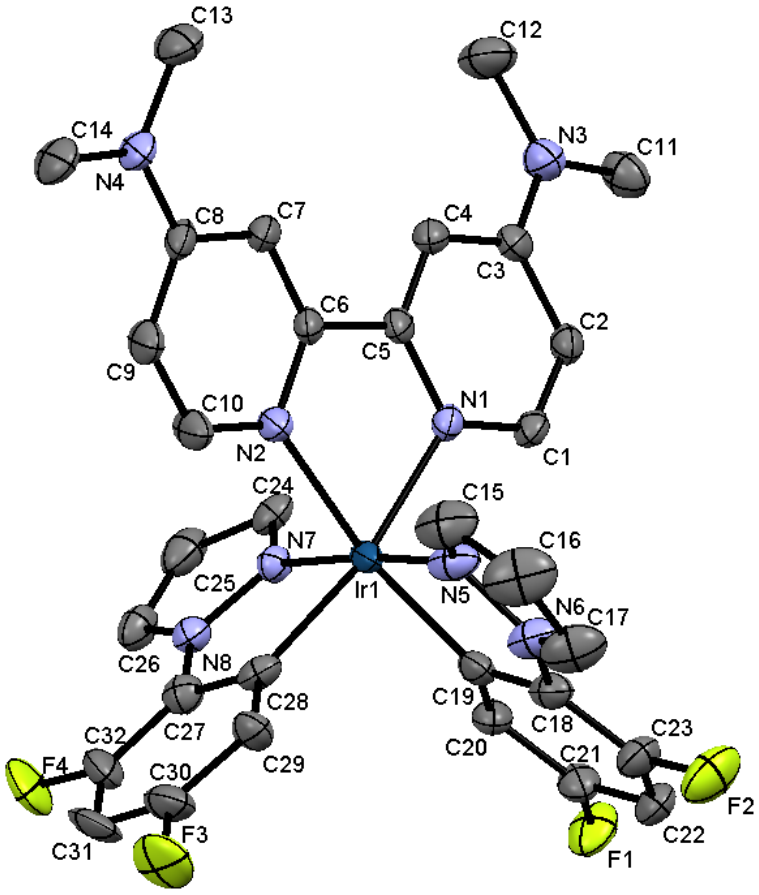

Figure 4.10 Structure of the Δ-cation in racemic [Ir(dfppz)$_2$(3)][PF$_6$].CH_2Cl_2 with ellipsoids plotted at 50% probability level; H atoms omitted and only the major occupancy sites for the disordered ligand containing atoms N7 and N8 are depicted. Selected bond lengths (in Å) and angles (in °): Ir1–N1 = 2.109(4), Ir1–N2 = 2.115(5), Ir1–N5 = 1.995(6), Ir1–C28 = 2.009(11), Ir1–N7 = 2.139(9), Ir1–C19 = 2.020(6), C8–N4 = 1.349(7), C3–N3 = 1.343(7), N3–C12 = 1.452(8), N3–C11 = 1.455(8), N4–C13 = 1.448(8), N4–C14 = 1.455(8); N1–Ir1–N2 = 76.20(18), C28–Ir1–N7 = 78.4(5), N5–Ir1–C19 = 80.0(2), C3–N3–C12 = 120.8(5), C3–N3–C11 = 120.1(5), C12–N3–C11 = 118.7(5), C8–N4–C13 = 121.7(5), C8–N4–C14 = 120.0(5), C13–N4–C14 = 117.9(5).

Crystallographic data for all compounds described in this section are listed in Table 4.2.

Table 4.2 Crystallographic data for ligand 2 and the complexes $[Ir_2(dfppz)_4(\mu\text{-}Cl)_2].CH_2Cl_2$, 4{$[Ir(dfppz)_2(pbpy)][PF_6]$} $.3CH_2Cl_2$, $[Ir(dfppz)_2(2)][PF_6].CH_2Cl_2$ and $[Ir(dfppz)_2(3)][PF_6].CH_2Cl_2$.

Compound	Ligand **2**	$[Ir_2(dfppz)_4(\mu\text{-}Cl)_2]$ $.CH_2Cl_2$	4{$[Ir(dfppz)_2(pbpy)]$ $[PF_6]$}$.3CH_2Cl_2$	$[Ir(dfppz)_2($**2**$)]$ $[PF_6].CH_2Cl_2$	$[Ir(dfppz)_2($**3**$)][PF_6]$ $.CH_2Cl_2$
Formula	$C_{30}H_{32}N_2$	$C_{37}H_{22}Cl_4F_8Ir_2N_8$	$C_{139}H_{94}Cl_6F_{40}Ir_4N_{24}P_4$	$C_{49}H_{44}Cl_2F_{10}IrN_6P$	$C_{33}H_{30}Cl_2F_{10}IrN_8P$
Formula weight / g mol^{-1}	420.60	1256.87	3965.84	1200.99	1022.74
Crystal colour and habit	colourless needle	yellow block	yellow block	yellow block	yellow block
Crystal system	monoclinic	triclinic	monoclinic	monoclinic	triclinic
Space group	*C*2/*c*	*P*–1	$P2_1/n$	$P2_1/c$	*P*–1
a, *b*, *c* / Å	19.8624(12)	10.753(3)	16.662(5)	20.8613(17)	9.5146(9)
	6.1354(3)	12.323(4)	10.561(3)	10.0629(5)	14.3727(12)
	19.9421(13)	16.058(4)	19.725(6)	25.126(2)	14.4945(14)
α, *β*, *γ*/ °	90	80.37(2)	90	90	102.341(7)
	106.045(5)	84.700(19)	92.00(3)	114.381(6)	102.295(8)
	90	65.47(2)	90	90	105.066(7)
U / $Å^3$	2335.6(2)	1907.9(9)	3468.9(18)	4804.2(6)	1792.4(3)
Dc / Mg m^{-3}	1.196	2.188	1.898	1.660	1.895
Z	4	2	1	4	2
μ(Mo-Kα) / mm^{-1}	0.069	7.329	4.102	3.005	4.010
T/ K	123	173	173	173	173
Refln. collected (R_{int})	87729 (0.052)	20996 (0.0755)	54439 (0.0696)	33704 (0.2023)	39217 (0.1096)
Unique refln.	6278	8332	7625	8485	6484
Refln. for refinement	5840	7239	6628	6560	6436
Parameters	145	532	497	628	646
Threshold	$I > 2.0\sigma$	$I > 2.0\sigma$	$I > 2.0\sigma$	$I > 2.0\sigma$	$I > 2.0\sigma$
*R*1 (*R*1 all data)	0.0517 (0.0560)	0.0399 (0.0476)	0.0581 (0.0668)	0.0876 (0.1085)	0.0436 (0.0438)
*wR*2 (*wR*2 all data)	0.0552 (0.0552)	0.0980 (0.1018)	0.1481 (0.1545)	0.2121 (0.2294)	0.1171 (0.1173)
Goodness of fit	1.0471	1.098	1.096	1.067	1.181

4.4 Photophysical studies of complexes in solution

The photophysical behaviour of the four complexes has been measured in aerated MeCN solutions. The electronic absorption spectra of $[Ir(dfppz)_2(pbpy)][PF_6]$, $[Ir(dfppz)_2($**1**$)][PF_6]$ and $[Ir(dfppz)_2($**2**$)][PF_6]$ are very similar, as can be seen in Figure 4.11. The relatively intense bands are at 247 and 307 nm ($[Ir(dfppz)_2(pbpy)][PF_6]$), 250 and 309 nm ($[Ir(dfppz)_2($**1**$)][PF_6]$) and 235, 275 (sh), 306 and 318 nm. All these absorptions are assigned to ligand-based π* ← π transitions. In $[Ir(dfppz)_2($**3**$)][PF_6]$ the NMe_2 groups extend the π-system of the bpy, therefore an enhancement of the absorption intensity is observed compared to the other three compounds, with maxima at 260, 287 and 352 nm.

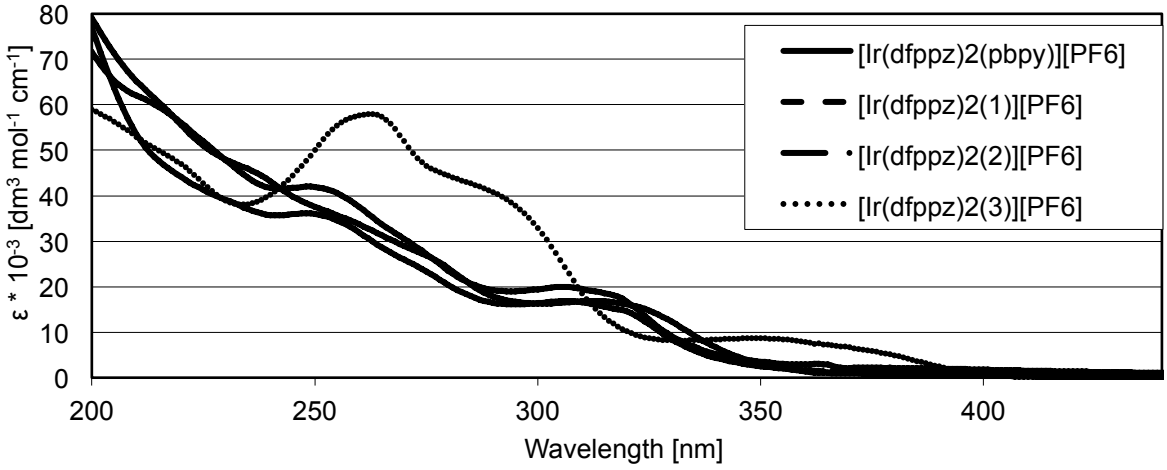

Figure 4.11 Absorption spectra of $[Ir(dfppz)_2(N\text{^}N)][PF_6]$ (N^N = pbpy, 1, 2, 3) in MeCN solutions (1.00 x 10^{-5} M).

Excitation between 280 and 310 nm leads to blue emissions in all four complexes, as depicted in Figure 4.12. The emission maxima are at 517, 505, 501 and 493 nm, with a broad and unstructured shape which is characteristic of complexes containing a combination of neutral diimine and cyclometallating ligands. The effect of the introduction of the fluorinated phenyl-pyrazole on the emission maximum can be seen by comparing $[Ir(dfppz)_2(pbpy)][PF_6]$ with $[Ir(ppy)_2(pbpy)][PF_6]$. The emission maximum of the latter is at 595 nm[18], whereas the former one emits at 517 nm. A similar blue shift in the emission spectrum can be observed on going from $[Ir(ppy)_2(\mathbf{3})][PF_6]$ (520 nm with a shoulder at 491 nm)[19] to $[Ir(dfppz)_2(\mathbf{3})][PF_6]$ (493 nm). The effect of exchanging pyridine with pyrazole in the cyclometallating ligands seems to have a very minor effect. $[Ir(dfppz)_2(\mathbf{3})][PF_6]$ emits at 493 nm with a shoulder at 463 nm compared to $[Ir(dfppz)_2(\mathbf{3})][PF_6]$ with emission only at 493 nm.

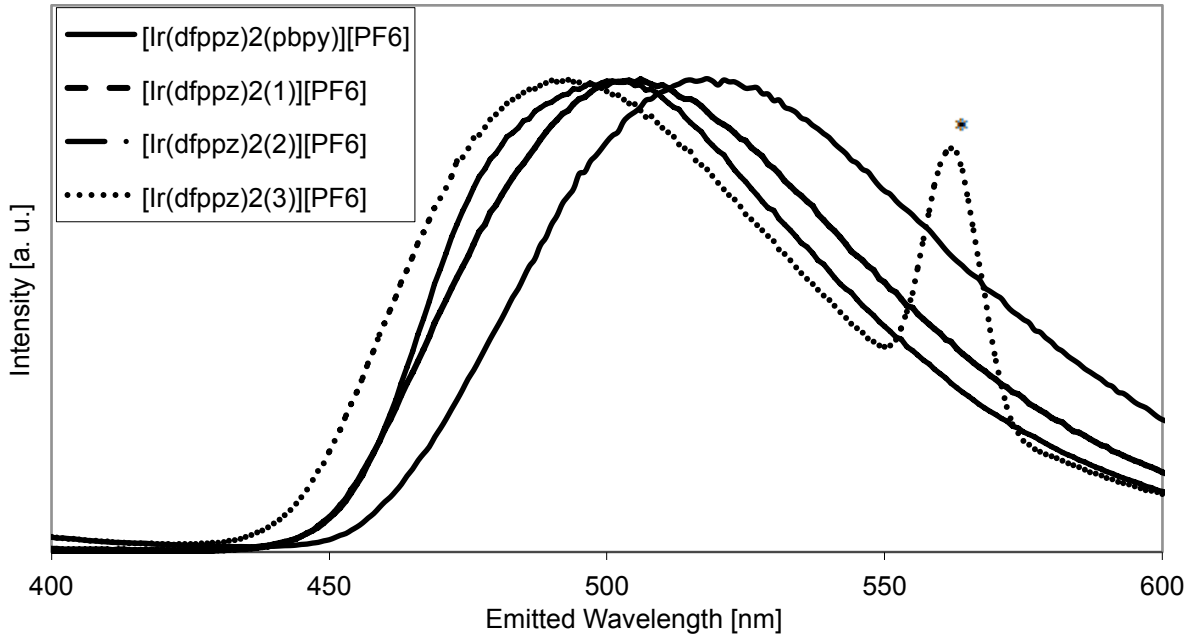

Figure 4.12 Normalized emission spectra of $[Ir(dfppz)_2(N^N)][PF_6]$ (N^N = pbpy, 1, 2, 3) in MeCN solution (1.00×10^{-5} M, 298 K).

The quantum yield measurements were performed on MeCN solutions of the complexes. Prior to measurement, the solutions were bubbled with argon for 15 minutes. $[Ir(dfppz)_2(\mathbf{3})][PF_6]$ has the highest quantum yield of 0.718, followed by $[Ir(dfppz)_2(pbpy)][PF_6]$ (0.491) and $[Ir(dfppz)_2(\mathbf{1})][PF_6]$ (0.424). Compound $[Ir(dfppz)_2(\mathbf{2})][PF_6]$ with the two intramolecular π-stacking interactions has the lowest quantum yield with 0.083.

4.5 Electrochemical studies

All four $[Ir(dfppz)_2(N^N)][PF_6]$ compounds are electrochemically active. The four compounds have been measured in MeCN solutions with 0.1 M $[^nBu_4N][PF_6]$ supporting electrolyte at a scan rate of 0.1 V s^{-1}. The cyclic voltammetric data with respect to Fc/Fc^+ are presented in

Table 4.3. Unless otherwise stated, the electrochemical processes are reversible or near-reversible. For all four complexes the reversible or quasi-reversible oxidation between +1.04 to +1.23 V was assigned to an iridium-centred process. $[Ir(dfppz)_2(\mathbf{3})][PF_6]$ shows two additional irreversible oxidations which arise from the dimethylamino groups forming radical cations. All four complexes show bpy-centred reversible reduction processes. Within the solvent accessible window (to -3.0 V) no reduction processes on the $[dfppz]^-$ ligands are observed, as the use of pyrazole induces a significant increase in LUMO energy compared to standard pyridine.[20] Comparison with literature values support our measurements, as $[Ir(dfppz)_2(4,4'\text{-}^tBu_2\text{-bpy})][PF_6]$ shows the iridium-centred oxidation at +1.25 V.[10] The fluorines on the C^N ligands act as electron-withdrawing groups and therefore shift the oxidation to more positive potentials compared to non-fluorinated C^N ligands.

Table 4.3 Cyclic voltammetric data with respect to Fc/Fc^+; MeCN solutions with $[^nBu_4N][PF_6]$ supporting electrolyte, and scan rate of 0.1 V s^{-1} (ir = irreversible; qr = quasi-reversible).

Compound	$E_{1/2}^{ox}$ / V	$E_{1/2}^{red}$ / V	$\Delta E_{1/2}$ / V
$[Ir(dfppz)_2(pbpy)][PF_6]$	+1.23	-1.75	2.98
$[Ir(dfppz)_2(\mathbf{1})][PF_6]$	+1.21	-1.83	3.04
$[Ir(dfppz)_2(\mathbf{2})][PF_6]$	$+1.22^{qr}$	-1.85, -2.46	3.07
$[Ir(dfppz)_2(\mathbf{3})][PF_6]$	$+1.04^{qr}$, $+1.47^{ir}$, $+1.57^{ir}$	-2.15	3.19

The $\Delta E_{1/2}$ values are in accord with the electrochemical values from previously reported blue emitting iridium(III) complexes (λ_{em} = 475 and $\Delta E_{1/2}$ = 3.07 V;[21] λ_{em} = 472 and $\Delta E_{1/2}$ = 3.15 V;7 λ_{em} = 452 and $\Delta E_{1/2}$ = 3.35 V).[21]

4.6 Device performances

The four compounds $[Ir(dfppz)_2(N^N)][PF_6]$ (N^N = pbpy, **1**, **2**, **3**) were further investigated in Valencia in the group of Henk J. Bolink. Some of the results are presented below (see Table 4.4).[22]

The efficiencies in thin films of the complex with polymethylmethacrylate (PMMA; 5% by weight) as well as in device configuration with ionic liquid (1-butyl-3methylimidazolium hexafluoridophosphate, [BMIM][PF_6]) are quantitative, with values up to 1.00. In thin films the quantum yields were characterized by emission maxima at 493, 492, 493 and 489 nm with quantum yields of 1.00, 0.99, 0.60, 0.89 for $[Ir(dfppz)_2(N^N)][PF_6]$ (N^N = pbpy, **1**, **2**, **3**), respectively. These quantum yields make the complexes amongst the most efficient ionic iridium emitters, and are in line with those previously reported for iridium(III) complexes bearing difluorophenylpyridine cyclometallating ligands together with a neutral diimine ligand with bulky groups.[19]

Complexes mixed with the ionic liquid [BMIM][PF_6] in a 4:1 molar ratio result in peak maxima of 510, 500, 504 and 510 nm with quantum yields of 0.89, 0.66, 0.15, 0.45 for

$[Ir(dfppz)_2(N^N)][PF_6]$ (N^N = pbpy, **1**, **2**, **3**), respectively. In the emission maxima the observed slight red-shift of the complexes mixed with an ionic liquid, compared to the thin films in PMMA, can be attributed to concentration effects. The lower quantum yield is due to the higher concentrations of the complexes in the film that promotes the self-quenching between molecules of the complex.

Table 4.4 Performances of the complexes in different environments.

Compound	Quantum yields of thin films	Quantum yields when mixed with ionic liquid	turn on time	Lifetime $t_{1/2}$	EQE
$[Ir(dfppz)_2(pbpy)][PF_6]$	100%	89%	3.8 h	12.2 h	0.16%
$[Ir(dfppz)_2(\mathbf{1})][PF_6]$	99%	66%	< 5 s	0.02 h	1.81%
$[Ir(dfppz)_2(\mathbf{2})][PF_6]$	60%	15%	0.4 h	4.4 h	0.70%
$[Ir(dfppz)_2(\mathbf{3})][PF_6]$	89%	45%	< 5 s	0.01 h	0.16%

These results are in accord with earlier measurements with fluorinated iridium complexes.[23]

Furthermore the four compounds have been tested in a LEC configuration.[22] The emission maxima are further red-shifted (see Figure 4.13). This strong red-shift observed in the electroluminescence emission compared to the photoluminescence emission is frequently observed in LECs using wide bandgap emitters. The origin of this effect is still not completely clear, but has been attributed to morphological effects and also to light-out coupling effects,[24] and therefore needs to be investigated further.

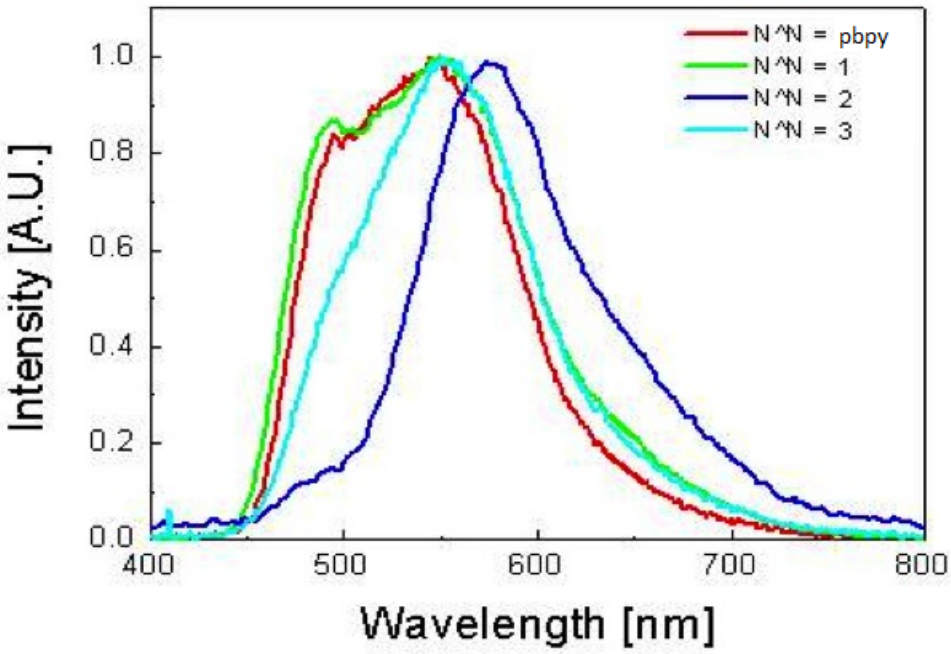

Figure 4.13 Electroluminescence spectra of ITO/PEDOT:PSS/$[Ir(dfppz)_2(N^N)][PF_6]$:[BMIM][PF_6] (4:1)/Al devices.

4.7 Conclusion and outlook

The synthesis and characterization of the four complexes was successful. The combined modification on the cyclometallating ligand with electron-withdrawing substituents and on the N^N ligand with electron-releasing ^{t}Bu or NMe_2 substituents shifted the emission maxima of the complexes towards the blue region of the visible spectrum, as expected. The crystal structures of the ligand **2**, the precursor $[Ir_2(dfppz)_4(\mu\text{-}Cl)_2]\cdot CH_2Cl_2$, and the complexes $\{[Ir(dfppz)_2(pbpy)][PF_6]\}.3CH_2Cl_2$, $[Ir(dfppz)_2(\mathbf{2})][PF_6].CH_2Cl_2$ and $[Ir(dfppz)_2(\mathbf{3})][PF_6].CH_2Cl_2$ were determined and confirm the dominant packing interactions in these compounds to be intermolecular face-to-face π-π stacking and intra-cation stacking. The latter stacking interactions involve the pendant phenyl substituents in the cations of $[Ir(dfppz)_2(phpy)][PF_6]$, $[Ir(dfppz)_2(\mathbf{1})][PF_6]$ and $[Ir(dfppz)_2(\mathbf{2})][PF_6]$. In solution the rotation of the phenyl is hindered on the NMR time-scale at room temperature. The four complexes are blue emitters in solution, in thin films and with ionic liquid. But in LEC configuration there is a red shift about 50 nm of the electroluminescence spectra with respect to the photoluminescence spectra in solution. This phenomenon needs to be investigated further. All the complexes can be used for the generation of electroluminescence devices without the addition of additives such as charge transporting molecules.

Unfortunately, the four complexes did not show long device lifetimes. One possible explanation could be cleavage of the fluorine radicals of the $[dfppz]^-$ ligands through electrical aging as also seen in iridium complexes for applications in OLEDs.[25] The current research in our group is to replace the fluorine with other electron-withdrawing substituents, as the fluorine has a negative influence upon the lifetime of the device. Unfortunately, this will result in more complicated synthetic procedures when compared to the fluorine-compounds.

4.8 Experimental

4.8.1 [Ir(dfppz)$_2$(pbpy)][PF$_6$]

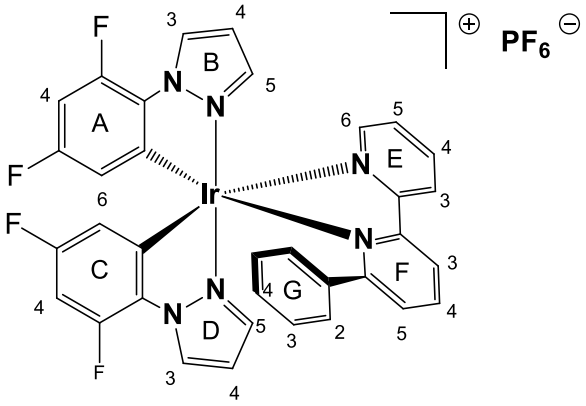

[Ir$_2$(dfppz)$_4$(μ-Cl)$_2$] (70.0 mg, 0.060 mmol) and 6-phenyl-2,2'-bipyridine (28.0 mg, 0.121 mmol) were added to methanol (15 cm^3) in an argon flushed vial. The yellow suspension was heated in a microwave reactor for 2 h (120 °C, 12 bar). The reaction mixture was cooled to room temperature and an excess of solid NH_4PF_6 was added. The mixture was stirred for 1.5 h at room temperature and then evaporated to dryness. The product was purified by column chromatography (silica/ CH_2Cl_2 changing to CH_2Cl_2 : MeOH 100 : 3 followed by alumina with the same eluents). [Ir(dfppz)$_2$(pbpy)][PF$_6$] was isolated as a yellow solid (79.3 mg, 0.0855 mmol, 71.2%). *^{1}H NMR* (600 MHz, CD_2Cl_2, 298 K) δ/ppm 8.52 (dd, J = 8.1, 1.2 Hz, 1H, H^{F3}), 8.45 (d, J = 8.1 Hz, 1H, H^{E3}), 8.36 (d, J = 2.9 Hz, 1H, H^{D3}), 8.30 (t, J = 7.9 Hz, 1H, H^{F4}), 8.24 (d, *J* = 2.9 Hz, 1H, H^{B3}), 8.21 (overlapping m, 2H, H^{E6+E5}), 7.60 (dd, J = 7.8, 1.2 Hz, 1H, H^{F5}), 7.52 (ddd, J = 7.5, 5.6, 1.2 Hz, 1H, H^{E4}), 7.26 (d, J = 2.3 Hz, 1H, H^{D5}), 7.13 (t, J = 7.5 Hz, 1H, H^{G4}), 6.96 (br, H^{G3}), 6.78 (t, J = 2.6 Hz, 1H, H^{B5}), 6.62 (m, 1H, H^{A4}), 6.57 (t, J = 2.7 Hz, 1H, H^{B4}), 6.38 (d, J = 2.4 Hz, 1H, H^{B5}), 6.22 (m, 1H, H^{C4}), 5.99 (v br, H^{G2}), 5.46 (m, 1H, H^{A6}), 4.95 (m, 1H, H^{C6}). *^{13}C NMR* (126 MHz, CD_2Cl_2, 298 K): δ/ppm 165.6 (C^{F6}), 164.2 (C^{F2}), 160.0 (C^{A5}), 159.1 (C^{C5}), 157.2 (C^{E2}), 150.1 (C^{E6}), 148.3 (C^{A3}), 147.9 (C^{C3}), 140.2 (C^{F4}), 140.0 (C^{E5}), 138.3 (C^{D5}), 137.8 (C^{G1}), 137.4 (C^{B5}), 131.7 (C^{B3}), 131.4 (C^{D3}), 129.3 (C^{G4}), 129.1 (C^{F5}), 128.0 ($C^{G3/G5}$), 127.5 (C^{E4}), 127.3 ($C^{G2/G6}$), 127.2 ($C^{G3/G5}$), 126.9 ($C^{G2/G6}$), 126.5 (C^{A2}), 126.0 (C^{C2}), 124.9 (C^{E3}), 122.7 (C^{F3}), 114.3 (C^{C6}),114.1 (C^{A6}), 108.9 (C^{B4+D4}), 99.7 (C^{A4}), 98.0 (C^{C4}). *^{19}F{^{1}H} NMR* (376 MHz, CD_2Cl_2, 298 K) δ/ppm −74.1 (d, J_{PF} = 711 Hz, $[PF_6]^-$), −112.3 (d, J_{FF} = 6.5 Hz, $F^{C5/A5}$), −115.0 (d, J_{FF} = 6.1 Hz, $F^{C5/A5}$), −124.3 (d, J_{FF} = 6.4 Hz, $F^{C3/A3}$), −125.4 (d, J_{FF} = 6.0 Hz, $F^{C3/A3}$). *IR* (solid, ν/cm^{-1}): 3164 (w), 3084 (w), 1617 (m), 1608 (m), 1577 (m), 1560 (m), 1510 (w), 1478 (s), 1450 (m), 1445 (m), 1420 (s), 1338 (w), 1309 (w), 1259 (m), 1253 (m), 1230 (w), 1182 (w), 1167 (m), 1122 (w), 1110 (s), 1074 (m), 1039 (s), 987 (s), 965 (w), 917 (w), 894 (w), 880 (w), 839 (s), 825 (s), 815 (s), 780 (m), 758 (m), 749 (s), 737 (s), 718 (m), 699 (m), 645 (m), 626 (s), 621 (m), 610 (s). *MS* (ESI, m/z): 783.2 $[M - PF_6]^+$ (calc. 783.2). *UV-Vis* λ/nm (ε/dm^3 mol^{-1} cm^{-1}) (MeCN, 1.00 × 10^{-5} mol dm^{-3}) 247 (36 100), 307 (17 000). *Luminescence* (MeCN, 1.00 × 10^{-5} mol dm^{-3}, λ_{ex} = 307 nm): λ_{em} = 517 nm. *Quantum yield* (MeCN, degassed with argon, λ_{ex} = 250 nm, integration range: 445 – 800 nm): 0.491. *Elem. Anal*. calcd. for. $C_{34}H_{22}F_{10}IrN_6P{\cdot}CH_2Cl_2$ (1012.69) C 41.51, H 2.39, N, 8.30; found C 41.09, H 2.36, N 8.13.

4.8.2 [Ir(dfppz)$_2$(1)][PF$_6$]

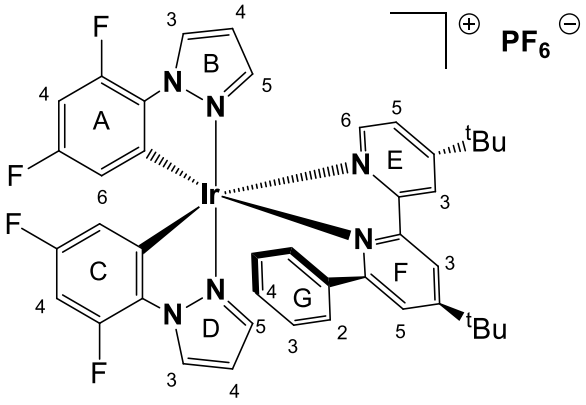

[Ir$_2$(dfppz)$_4$(μ-Cl)$_2$] (70.0 mg, 0.060 mmol) and 4,4'-di-*tert*-butyl-6-phenyl-2,2'-bipyridine (41.5 mg, 0.121 mmol) were added to methanol (15 cm^3) in an argon flushed vial, and the yellow suspension was heated in a microwave reactor for 2 h (120 °C, 11 bar). The reaction mixture was cooled to room temperature and solid NH_4PF_6 was added. After 20 h, no precipitation had occurred and so an excess of $AgPF_6$ was added and the mixture stirred for 1 h. Solvent was then removed, and the crude material was purified twice by column chromatography (silica/CH_2Cl_2 changing to CH_2Cl_2:MeOH 100:3 followed by alumina with the same eluents). [Ir(dfppz)$_2$(**1**)][PF$_6$] was isolated as a yellow solid (89.0 mg, 0.0856 mmol, 71.3%). *^{1}H NMR* (500 MHz, CD_2Cl_2, 298 K) δ/ppm 8.36 (d, J = 2.8 Hz, 1H, H^{D3}), 8.31 (d, J = 2.0 Hz, 1H, H^{F3}), 8.28 (overlapping, 2H, H^{E3+B3}), 8.07 (d, J = 5.8 Hz, 1H, H^{E6}), 7.53 (d, J = 1.9 Hz, 1H, H^{F5}), 7.48 (m, 1H, H^{E5}), 7.24 (d, J = 2.1 Hz, 1H, H^{D5}), 7.14 (t, J = 7.5 Hz, 1H, H^{G4}), 6.95 (br, 2H, H^{G3}), 6.77 (t, J = 2.6 Hz, 1H, H^{D4}), 6.61 (m, 1H, H^{A4}), 6.59 (t, J = 2.8 Hz, 1H, H^{B4}), 6.37 (d, J = 2.5 Hz, 1H, H^{B5}), 6.21 (m, 1H, H^{C4}), 6.03 (v br, H^{G2}), 5.47 (m, 1H, H^{A6}), 4.93 (m, 1H, H^{C6}), 1.51 (s, 9H, H^{Me}, ring F), 1.45 (s, 9H, H^{Me}, ring E). *^{13}C NMR* (126 MHz, CD_2Cl_2, 298 K): δ/ppm 166.3 (C^{F6}), 165.9 (C^{F4}), 165.7 (C^{E4}), 158.3 (C^{F2}), 160.8 (C^{A5}), 160.1 (C^{C5}), 157.7 (C^{E2}), 150.5 (C^{E6}), 149.4 (C^{A3}), 149.0 (C^{C3}), 139.1 (C^{G1}), 139.0 (C^{D5}), 138.5 (C^{B5}), 132.3 (2C, C^{B3+D3}), 130.2 (C^{G4}), 129.0 ($C^{G3/G5}$), 128.5 ($C^{G2/G6}$), 128.0 (2C, $C^{G2/G6+G3/G5}$), 127.4 (C^{A2}), 127.2 (C^{F5}), 127.0 (C^{C2}), 125.8 (C^{E5}), 122.4 (C^{E3}), 120.4 (C^{F3}), 115.2 (C^{C6}), 114.8 (C^{A6}), 109.8 (C^{B4}), 109.7 (C^{D4}), 100.3 (C^{A4}), 98.7 (C^{C4}), 36.45 (C^{tBu}, ring F), 36.40 (C^{tBu}, ring E), 30.8 (C^{Me}, ring F), 30.7 (C^{Me}, ring E). *^{19}F{^{1}H} NMR* (376 MHz, CD_2Cl_2, 298 K) δ/ppm −74.2 (d, J_{PF} = 711 Hz, $[PF_6]^-$), −112.4 (d, J_{FF} = 6.2 Hz, $F^{C5/A5}$), −115.1 (d, J_{FF} = 5.9 Hz, $F^{C5/A5}$), −124.5 (d, J_{FF} = 6.2 Hz, $F^{C3/A3}$), −125.5 (d, J_{FF} = 5.9 Hz, $F^{C3/A3}$). *IR* (solid, ν/cm^{-1}): 3177 (w), 2956 (w), 1611 (m), 1580 (m), 1542 (w), 1480 (s), 1438 (w), 1419 (s), 1369 (w), 1337 (w), 1309 (w), 1251 (m), 1166 (w), 1125 (w), 1106 (m), 1073 (m), 1037 (s), 987 (s), 963 (w), 908 (w), 825 (s), 804 (s), 771 (m), 752 (m), 743 (s), 703 (s), 655 (w), 625 (m), 602 (s). *MS* (ESI, m/z): 895.4 $[M - PF_6]^+$ (calc. 895.3). *UV-Vis* λ/nm (ε/dm^3 mol^{-1} cm^{-1}) (MeCN, 1.00 × 10^{-5} mol dm^{-3}): 218 sh (57 500), 250 (42 000), 309 (19 900). *Luminescence* (MeCN, 1.00 × 10^{-5} mol dm^{-3}, λ_{ex} = 305 nm): λ_{em} = 505 nm. *Quantum yield* (MeCN, degassed with argon, λ_{ex} = 250 nm, integration range: 440 – 800 nm): 0.424. *Elem. Anal.* calcd. for $C_{42}H_{38}F_{10}IrN_6P{\cdot}0.75CH_2Cl_2$ (1103.67): C 46.52, H 3.61, N, 7.61; found C 46.51, H 3.63, N 7.64.

4.8.3 [Ir(dfppz)$_2$(2)][PF$_6$]

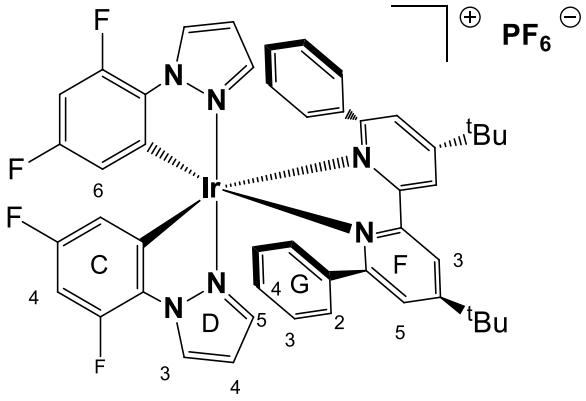

[Ir$_2$(dfppz)$_4$(μ-Cl)$_2$] (100.0 mg, 0.0853 mmol), 4,4'-di-*tert*-butyl-6,6'-diphenyl-2,2'-bipyridine (75.3 mg, 0.179 mmol) and AgPF$_6$ (45.3 mg, 0.179 mmol) were combined with methanol (15 cm^3) in an argon flushed vial. This was placed in a microwave reactor for 2 h at 120 °C (P = 13 bar). The vial was removed from the reactor and CH_2Cl_2 (3 cm^3) was added. The reaction mixture was heated for further 15 min at 100 °C (P = 11 bar) in the microwave reactor. The yellow-green solution was cooled to room temperature and an excess of solid NH_4PF_6 was added. The mixture was stirred for 1 h at room temperature and then evaporated to dryness. The product was purified by chromatography (column, alumina with CH_2Cl_2 changing to CH_2Cl_2:MeOH 100:5, then preparative TLC, alumina, CH_2Cl_2:MeOH 100:1.5). [Ir(dfppz)$_2$(**2**)][PF$_6$] was isolated as a yellow solid (99.6 mg, 0.089 mmol, 52.3%). *^{1}H NMR* (500 MHz, CD_2Cl_2, 298 K) δ/ppm 8.32 (d, J = 2.1 Hz, 2H, H^{F3}), 8.19 (d, J = 2.9 Hz, 2H, H^{D3}), 7.38 (d, J = 2.0 Hz, 2H, H^{F5}), 7.14 (overlapping m, 4H, H^{G4+D5}), 6.94 (br, 4H, H^{G3}), 6.70 (t, J = 2.6 Hz, 2H, H^{D4}), 6.64 (v br., H^{G2}), 6.16 (m, 2H, H^{C4}), 4.47 (m, 2H, H^{C6}), 1.48 (s, 18H, H^{Me}, ring F). *^{13}C NMR* (126 MHz, CD_2Cl_2, 298 K): δ/ppm 164.4 (C^{F6}), 163.9 (C^{F4}), 157.9 (C^{F2}), 158.5 (C^{C5}), 147.2 (C^{C3}), 138.2 (C^{G1}), 138.9 (C^{D5}), 131.7 (C^{D3}), 128.5 (C^{G4}), 127.4 ($C^{G3/G5}$), 127.3 (2C, $C^{G2/G6+G3/G5}$), 127.0 (C^{F5}), 126.6 ($C^{G2/G6}$), 124.9 (C^{C2}), 120.6 (C^{F3}), 113.6 (C^{C6}), 108.7 (C^{D4}), 98.2 (C^{C4}), 35.7 (C^{tBu}, ring F), 30.0 (C^{Me}, ring F). *^{19}F{^{1}H} NMR* (376 MHz, CD_2Cl_2, 298 K) δ/ppm −73.7 (d, J_{PF} = 711 Hz, $[PF_6]^-$), −113.7 (d, J_{FF} = 5.9 Hz, F^{C5}), −125.5 (d, J_{FF} = 5.9 Hz, F^{C3}). *IR* (solid, ν/cm^{-1}): 3152 (w), 3091 (w), 2968 (w), 2874 (w), 1613 (m), 1584 (m), 1544 (w), 1500 (w), 1480 (m), 1440 (w), 1419 (m), 1398 (m), 1369 (w), 1338 (w), 1307 (w), 1251 (m), 1215 (w), 1166 (w), 1125 (w), 1105 (m), 1070 (m), 1037 (m), 986 (s), 961 (w), 914 (w), 880 (w), 829 (s), 819 (s), 801 (m), 754 (s), 697 (s), 662 (w), 626 (m). *MS* (ESI, m/z): 971.5 $[M - PF_6]^+$ (calc. 971.3). *UV-Vis* λ/nm (ε/dm^3 mol^{-1} cm^{-1}) (MeCN, 1.00 × 10^{-5} mol dm^{-3}): 235 (45 900), 274 (27 300), 306 (16 850), 318sh (15 000). *Luminescence* (MeCN, 1.00 × 10^{-5} mol dm^{-3}, λ_{ex} = 310 nm): λ_{em} = 501 nm. *Quantum yield* (MeCN, degassed with argon, λ_{ex} = 250 nm, integration range: 440 – 800 nm): 0.086. *Elem. Anal*. calcd. for $C_{42}H_{38}F_{10}IrN_6P{\cdot}0.25CH_3OH$ (1047.98): C 51.56, H 3.86, N, 7.48; found C 51.57, H 3.93, N 7.55.

4.8.4 [Ir(dfppz)$_2$(3)][PF$_6$]

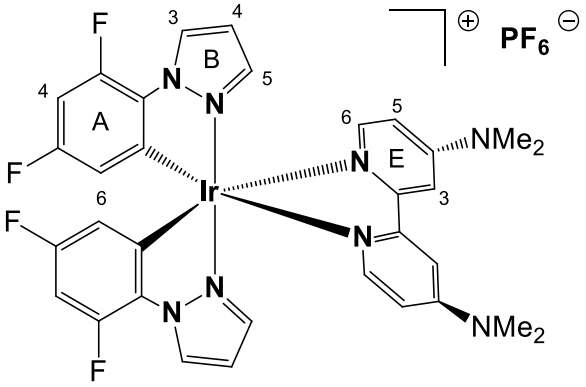

[Ir$_2$(dfppz)$_4$(μ-Cl)$_2$] (70.0 mg, 0.060 mmol) and 4,4'-bis(dimethylamino)-2,2'-bipyridine (29.2 mg, 0.121 mmol) were added to methanol (15 cm^3) in an argon flushed vial, and this was heated in a microwave reactor for 2 h (120 °C, 11 bar). The yellow solution was cooled to room temperature and an excess of solid NH_4PF_6 was added. The mixture was stirred for 1.5 h at room temperature and then evaporated to dryness. The crude material was purified by column chromatography (silica/CH_2Cl_2 changing to CH_2Cl_2:MeOH 100:3 followed by alumina with the same eluents). [Ir(dfppz)$_2$(**3**)][PF$_6$] was isolated as a yellow-green solid (50.5 mg, 0.0539 mmol, 44.8%). *^{1}H NMR* (500 MHz, CD_2Cl_2, 298 K) δ/ppm 8.36 (d, J = 2.8 Hz, 2H, H^{B3}), 7.53 (d, J = 6.7 Hz, 2H, H^{E6}), 7.30 (d, J = 2.6 Hz, 2H, H^{E3}), 6.93 (d, J = 2.1 Hz, 2H, H^{B5}), 6.67 (m, 2H, H^{A4}), 6.59 (t, J = 2.6 Hz, 2H, H^{B4}), 6.49 (dd, J = 6.7, 2.6 Hz, 2H, H^{E5}), 5.78 (m, 2H, H^{A6}), 3.19 (s, 12H, H^{Me}, ring E). *^{13}C NMR* (126 MHz, CD_2Cl_2, 298 K): δ/ppm 160.8 (C^{A5}), 156.3 (C^{E4}), 149.8 (C^{E6}), 149.3 (C^{E2}), 148.0 (C^{A3}), 138.1 (C^{B5}), 131.8 (C^{B3}), 128.0 (C^{A2}), 115.8 (C^{A6}), 109.4 (C^{E5}), 108.9 (C^{B4}), 105.9 (C^{E3}), 99.1 (C^{A4}), 40.0 (C^{Me}, ring E). *^{19}F{^{1}H} NMR* (376 MHz, CD_2Cl_2, 298 K) δ/ppm −74.1 (d, J_{PF} = 711 Hz, $[PF_6]^-$), −114.2 (d, J_{FF} = 5.9 Hz, F^{A5}), −125.3 (d, J_{FF} = 5.5 Hz, F^{A3}). *IR* (solid, ν/cm^{-1}): 3166 (w), 2928 (w), 1612 (s), 1585 (m), 1576 (m), 1544 (m), 1512 (w), 1474 (m), 1434 (m), 1420 (m), 1380 (m), 1337 (w), 1309 (w), 1285 (m), 1253 (m), 1226 (w), 1187 (w), 1165 (w), 1108 (m), 1072 (m), 1034 (s), 1016 (m), 987 (s), 962 (w), 916 (w), 834 (s), 825 (s), 808 (s), 803 (s), 746 (m), 740 (m), 710 (w), 655 (w), 626 (m), 602 (s). *MS* (ESI, m/z): 971.5 $[M - PF_6]^+$ (calc. 971.3). *UV-Vis* λ/nm (ε/dm^3 mol^{-1} cm^{-1}) (MeCN, 1.00 × 10^{-5} mol dm^{-3}): 216 sh (48 800), 260 (42 000), 352 (8600). *Luminescence* (MeCN, 1.00 × 10^{-5} mol dm^{-3}, λ_{ex} = 280 nm): λ_{em} = 493 nm. *Quantum yield* (MeCN, degassed with argon, λ_{ex} = 260 nm, integration range: 430 – 800 nm): 0.718. *Elem. Anal.* calcd. for $C_{42}H_{38}F_{10}IrN_6P{\cdot}0.75CH_2Cl_2$ (1103.67): C 39.28, H 2.97, N, 11.19; found C 39.24, H 2.86, N 11.28.

[1] M. S. Lowry, J. I. Goldsmith, J. D. Slinker, R. Rohl, R. A. Pascal, G. G. Malliaras, S. Bernhard, *Chem. Mater.,* 2007, **17**, 5712.
[2] Md. K. Nazzeruddin, R. T. Weigh, Z. Zhou, C. Klein, Q. Wang, F. De Angelis, S. Fantacci, M. Graetzel, *Inorg. Chem.,* 2006*,* **45**, 9245.
[3] J. D. Slinker, A. A. Gorodetsky, M. S. Lowry, J. J. Wang, S. Parker, R. Rohl, S. Bernhard, G. G. Malliaras, *J. Am. Chem. Soc.*, 2004, **126**, 2763.
[4] T. Hu, L. He, L. Duan, Y. Qiu, *J. Mater. Chem.*, 2012, **22**, 4206.
[5] See for example: F. Neve, A. Crispini, S. Campagna, S. Serroni*, Inorg. Chem*., 1999, **38**, 2250 and references cited therein.
[6] H. C. Su, H. F. Chen, F. C. Fang, C. C. Liu, C. C. Wu, K. T. Wong, Y. H. Liu, S. M. Peng, *J. Am. Chem. Soc*, 2008, **130**, 3413.
[7] L. He, J. Qiao, L. Duan, G. Dong, D. Zhang, L. Wang, Y. Qiu, *Chem. Mater.*, 2010, **22**, 3535.
[8] M. Lepeltier, T. K.-M. Lee, K. K.-W, Lo, L. Toupet, H. Le Bozec, V. Guerchais, *Eur. J. Inorg. Chem.*, 2005, **110**.
[9] A. B. Tamayo,B. D. Alleyne, P. I. Djurovich, S. Lamansky, I. Tsyba, N. N. Ho, R. Bau, M. E. Thompson, *J. Am. Chem*. *Soc*., 2003, **125**, 7377.
[10] A. B. Tamayo, S. Garon, T. Sajoto, P. I. Djurovich, I. M. Tsyba, R. Bau, M. E. Thompson, *Inorg. Chem*., 2005, **44**, 8723.
[11] C.-H. Yang, S.-W. Li, Y. Chi, Y.-M. Cheng, Y.-S. Yeh, P.-T. Chou, G.-H. Lee, C.-H. Wang, C.-F. Shu, *Inorg. Chem.*, 2005, **44**, 7770.
[12] K. Dedeian, J. Shi, N. Shepherd, E. Forsythe, D. C. Moron, *Inorg. Chem*, 2005, **44**, 4445.
[13] C.-J. Chang, C.-H. Yang, K. Chen, Y. Chi, C.-F. Shu, M.-L. Ho, Y.-S. Yeh, P.-T. Chou, *Dalton Trans*., 2007, 1881.
[14] N. M. Shavaleev, R. Scopelliti, E. Baranoff, M. Grätzel, Md. K. Nazeeruddin, *Inorg. Chim. Acta*, 2012, **383**, 316.
[15] G.-G. Shan, H.-B. Li, Z.-C. Mu, D.-X. Zhu, Z.-M. Su, Y. Liao, *J. Organomet. Chem.*, 2012, **702**, 27.
[16] G.-G. Shan, H.-B. Li, H.-T. Cao, D.-X. Zhu, P. Li, Z.-M. Su, Y. Liao, *Chem. Commun.*, 2012, **48**, 2000.
[17] C. Janiak, *J. Chem. Soc., Dalton Trans.,* 2000, 3885.
[18] R. D. Costa, E. Ortí, H. J. Bolink, S. Graber, C. E. Housecroft, E. C. Constable, *Adv. Funct. Mater.*, 2010, **20**, 1511.
[19] F. De Angelis, S. Fantacci, N. Evans, C. Klein, S. M. Zakeeruddin, J.-E. Moser, K. Kalyanasundaram, H. J. Bolink, M. Grätzel, M. K. Nazeeruddin, *Inorg. Chem.*, 2007, **46**, 5989.
[20] T. Sajoto, P. I. Djurovich, A. Tamayo, M. Yousufuddin, R. Bau, M. E. Thompson, *Inorg. Chem.*, 2005, **44**, 7992.
[21] L. He, L. Duan, J. Qiao, R. Wang, P. Wei, Y. Qiu, *Adv. Funct. Mater*., 2008, **18**, 2123.
[22] E. Baranoff, H. J. Bolink, E. C. Constable, M. Delgado, D. Häussinger, C. E. Housecroft, M. K. Nazeeruddin, M. Neuburger, E. Ortí, G. E. Schneider, D. Tordera, R. M. Walliser, J. A. Zampese, *Dalton Trans*., 2013, **42**, 1073.
[23] H. J. Bolink, E. Coronado, R. D. Costa, N. Lardies, E. Ortí, *Inorg. Chem*., 2008, **47**, 9149.
[24] H. J. Bolink, L. Cappelli, S. Cheylan, E. Coronado, R. D. Costa, N. Larpdiés, M. K. Nazeeruddin, E. Ortí, *J. Mater. Chem. Soc.*, 2004, **17**, 5032.
[25] S. Schmidbauer, A. Hohenleutner, B. König, *Adv. Mater.*, 2013, DOI: 10.1002/adma.201205022.

Chapter 5

5. Introducing terpyridine ligands in iridium(III) complexes and moving the emission maximum towards the red region of the visible spectrum

5.1. Introduction

A wide variety of cationic iridium(III) complexes incorporating N^N ligands based on 2,2'-bpy and its derivatives are known. But only one iridium(III) complex with a tpy as N^N ligand on an iridium(III) complex has been reported so far: $[Ir(ppy)_2(ttpy)][PF_6]$ with ttpy = 4'-(4-tolyl)-2,2':6',2''-terpyridine.[1] The complex shows an emission maximum in the red-orange region (λ_{em} = 625 nm) exhibiting a low quantum yield in MeCN solution (0.017). Unfortunately, no crystal structure of this complex has been reported.

This raises the question: does the pendant pyridine ring of the tpy unit undergo similar face-to-face π-π stacking as is seen in the complexes incorporating pbpy and its derivatives (see e.g. Chapters 3 and 4)? The effect of this change to the photophysical and electrochemical properties and to the performance in LEC devices has not yet been investigated.

While working with tpy, contrary to the previous chapter (see Chapter 4), the idea in this chapter was to achieve red/orange emitters. The bandgap between the HOMO and LUMO was designed to be small in order to achieve a shift in the emission spectrum to the red region of the visible light. The methods to shift these energy levels are the exact opposite to a blue-shift. To achieve a smaller band gap, the HOMO needs to be destabilized, thus increasing its energy level, and/or the LUMO needs to be stabilized, i.e. lowering its energy level. To destabilize the HOMO, electron-donating substituents are widely used and to destabilize the LUMO, electron-withdrawing substituents are attached on the ancillary ligand.[2, 3] The change on the ancillary ligand is the introduction of another pyridine ring on the 4'-position of the tpy ligand. In comparison to the complex containing a simple tpy ligand, complexes with an extended tpy π-system will have a destabilized LUMO and therefore yield a red-shift in the emission maximum. In addition to the change on the ancillary ligand, the effect of introduction of bulky side-groups on the cyclometallating ligands was also investigated. Finally, the effect of the methylation of the 4'-pyridyl ring was studied.

To date, red-emitting iridium(III) complexes have been reported with emission maxima at 656 nm[4] or 687 nm.[5] The quantum yields of these complexes are 0.20 and 0.02 respectively. The aim was to synthesise complexes, which emit in the red region and which exhibit a relatively good quantum yield.

5.2. Results and discussion

The five complexes $[Ir(ppy)_2(tpy)][PF_6]$, $[Ir(dmppz)_2(tpy)][PF_6]$, $[Ir(dmppz)_2(\mathbf{4})][PF_6]$, $[Ir(ppy)_2(\mathbf{4})][PF_6]$ and $[Ir(dmppz)_2(\mathbf{5})][PF_6]_2$, (Scheme 5.1) were prepared by the established methodology[6] of treating a dichlorido-bridged iridium(III) dimer with two equivalents of an N^N ligand. The reactions were performed in a microwave reactor followed by precipitation with ammonium hexafluoridophosphate, and the purification was done by column chromatography.

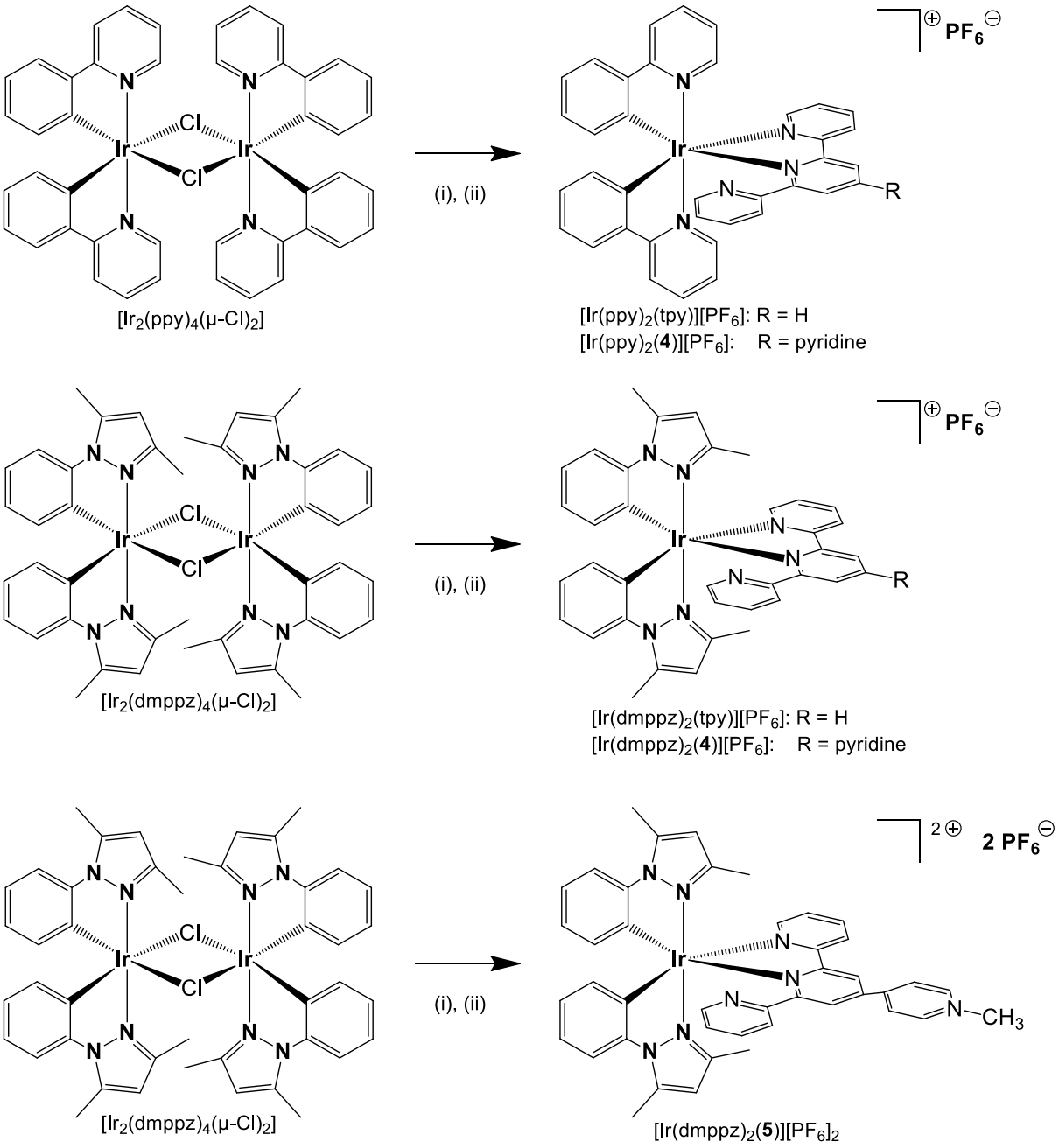

Scheme 5.1 Syntheses of the complexes described in this chapter. Conditions: (i) tpy, 4 or 5, MeOH, microwave, 120°C, 2h; (ii) $[NH_4][PF_6]$, 30 – 60 min.

The yields ranged from 47.6% for $[Ir(ppy)_2(tpy)][PF_6]$ to 98.1% for $[Ir(dmppz)_2(tpy)][PF_6]$. The ESI mass spectrum of each of the complexes showed a peak that was assigned to the [M –

$PF_6]^+$ ion and the observed isotope patterns were in accord with those simulated. The elemental analyses could be fitted by the addition of up to one solvent molecule.

The NMR spectroscopic assignments were done with routine 2D techniques (COSY, NOESY, HMBC and HMQC). An example of the assignment will be shown with $[Ir(ppy)_2(tpy)][PF_6]$ (see Section 5.3.).

Unlike in the previous sections, all complexes do not contain a C_2 axis. Therefore the environments of the two cyclometallating C^N ligands are non-equivalent and this can be seen in the NMR spectra (e.g. Figure 5.1).

5.3. NMR spectroscopic assignment of $[Ir(ppy)_2(tpy)][PF_6]$

The structure of $[Ir(ppy)_2(tpy)][PF_6]$ is shown in Scheme 5.2 with the ring labels for the NMR assignments. Starting with previously discussed symmetric complexes, comparison of NMR spectroscopic data (see Sections 3.2 and 4.2) leads to the assumption that the high-field doublet can be assigned to proton A6. With a pendant phenyl (see Chapters 3 and 4) or pyridine ring, the two cyclometallating ligands are non-equivalent. This leads to different rings A and C and the two high-field doublets were initially both labelled A6/C6. The COSY spectrum helped to identify the spin systems for all rings. In the NOESY spectrum, the cross-peaks between protons A3/C3 and B3/D3 helped to identify the two different C^N ligands. With a NOESY cross-peak between ring G and D, ring D could be identified. This led directly to the identification of rings C, B and A. NOESY crosspeaks between proton G3 and F5, and F3 and E3 identified the tpy ligand.

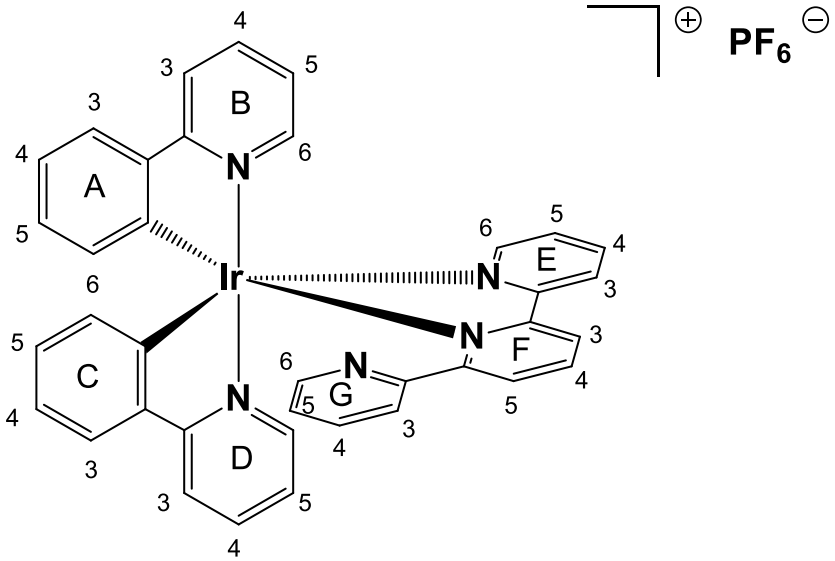

Scheme 5.2 $[Ir(ppy)_2(tpy)][PF_6]$ with ring labelling for NMR spectroscopy

The ^1H NMR spectrum of $[Ir(ppy)_2(tpy)][PF_6]$ was measured in CD_2Cl_2 and the proton spectrum is depicted in Figure 5.1. The peaks are labelled with the corresponding proton.

The only significantly broadened signal is for proton B6 at δ 8.87 ppm. The broadening originates from hydrogen bonding between the lone-pair of the free nitrogen of ring G with proton B6. The crystal structure of $[Ir(ppy)_2(tpy)][PF_6]$ shows that proton B6 is only 2.57 Å away from the nitrogen of the free pyridine in the solid state (see Figure 5.4). Going to the other C^N ligand in $[Ir(ppy)_2(tpy)][PF_6]$ it is quite obvious that proton D6 is less shifted towards the low-field region. This is an evidence of the different chemical environments of protons B6 and D6.

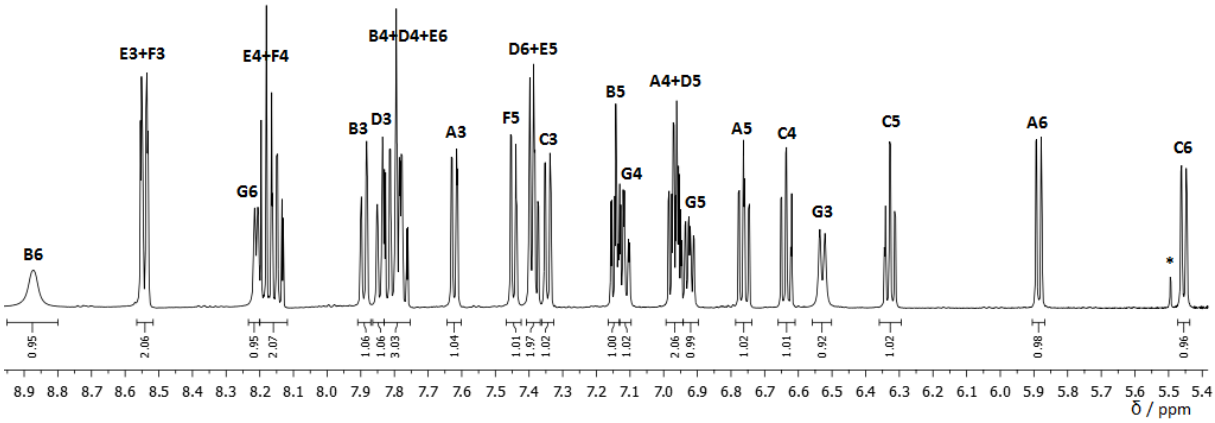

Figure 5.1 ^{1}H NMR spectrum of $[Ir(ppy)_2(tpy)][PF_6]$ (500 MHz, CD_2Cl_2, 298 K, TMS)

The full assignment was done using COSY, NOESY, HMQC and HMBC spectroscopy.

Correlation spectroscopy (COSY) led to the identification of the individual ring systems, in which cross peaks show correlations between protons e.g. C5 and C6 (Figure 5.2, grey line). The proton C5 also shows a cross-peak with proton C4 (black line) whereas proton A6 shows a cross-peak with proton A5.

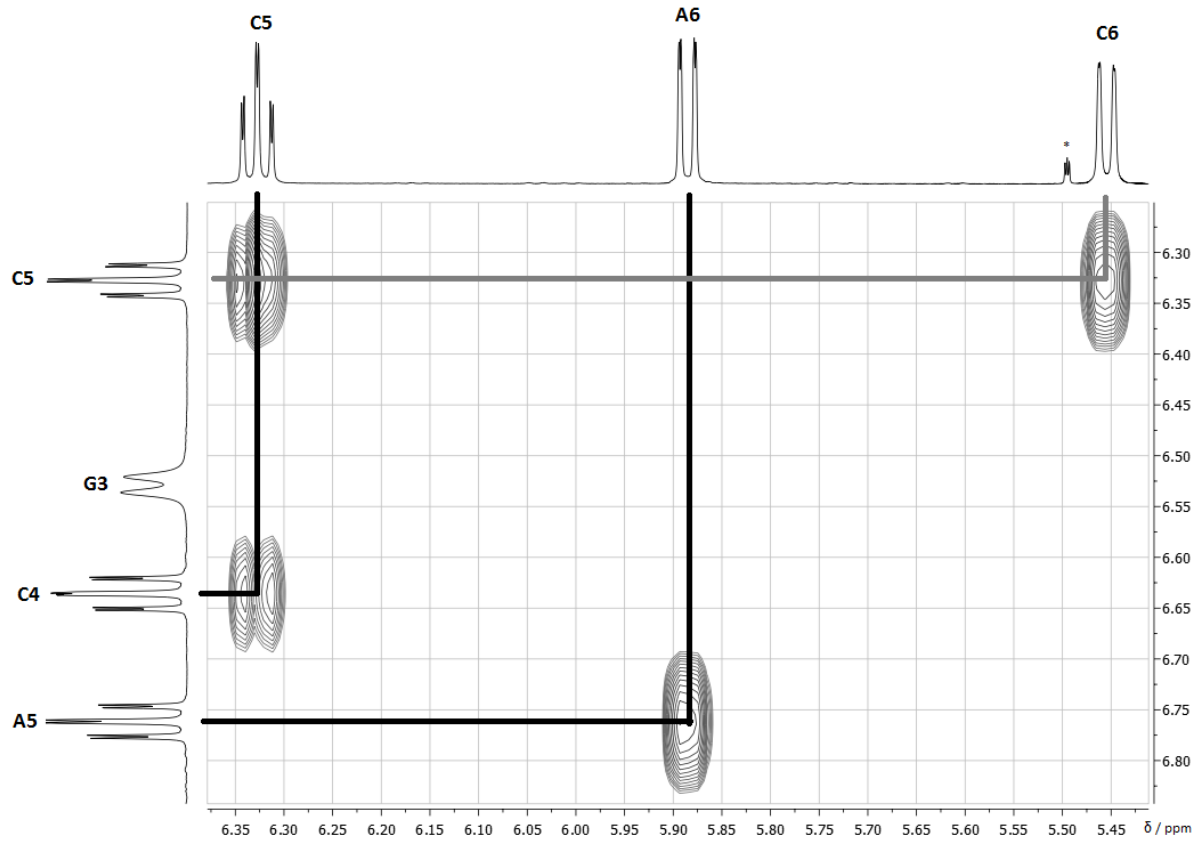

Figure 5.2 Region of the COSY spectrum of $[Ir(ppy)_2(tpy)][PF_6]$ (500 MHz, CD_2Cl_2, 298 K, TMS)

As previously discussed, NOESY spectra helped to identify the bonded ring systems. A region of the NOESY spectrum is depicted in Figure 5.3. Proton G3 shows a strong cross-peak with proton F5 (Figure 5.3, black lines) and a much weaker cross-peak with proton C3 (Figure 5.3, grey lines). The latter interaction is from the face-to-face π-stacked rings C and G.

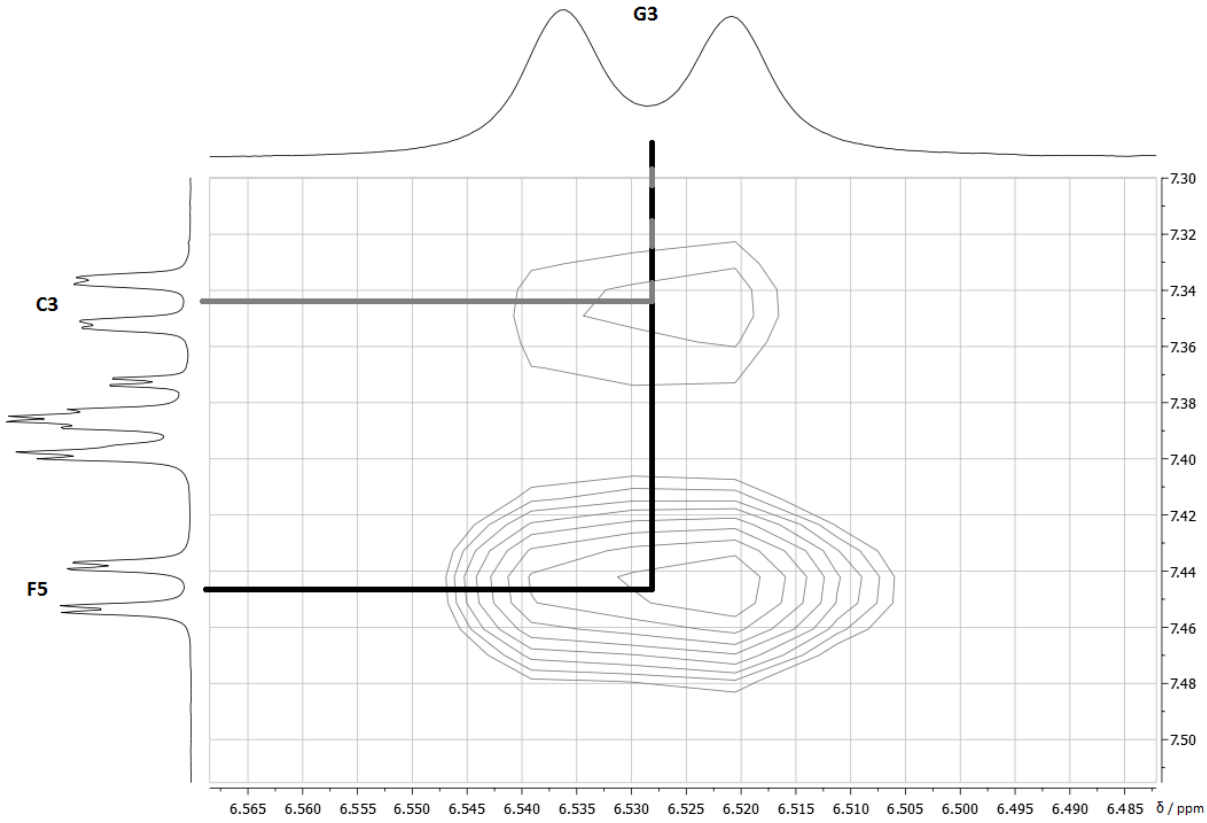

Figure 5.3 Region of the 2D-NOESY spectrum of $[Ir(ppy)_2(tpy)][PF_6]$ (500 MHz, CD_2Cl_2, 298 K, TMS)

Using HMQC and HMBC, the carbon peaks were assigned; e.g. proton C3 shows a $^4J_{CH}$ correlation with carbon D2 in HMBC.

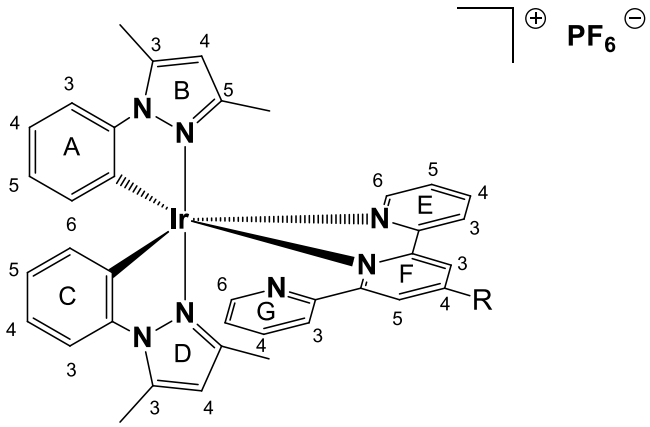

Scheme 5.3 Ring labelling and atom numbering for NMR spectroscopic assignments of $[Ir(dmppz)_2(tpy)][PF_6]$, $[Ir(dmppz)_2(4)][PF_6]$ and $[Ir(dmppz)_2(5)][PF_6]_2$.

Comparison of the NMR spectroscopic data indicates that there are correlations between the chemical shifts for a given carbon atom across the series of compounds. The similarities of the C^N ligands in $[Ir(ppy)_2(tpy)][PF_6]$ and $[Ir(ppy)_2(\mathbf{4})][PF_6]$, and in $[Ir(dmppz)_2(tpy)][PF_6]$, $[Ir(dmppz)_2(\mathbf{4})][PF_6]$ and $[Ir(dmppz)_2(\mathbf{5})][PF_6]_2$ lead to comparable chemical shifts for a given carbon atom. The cyclometallating carbon atoms A1 and C1 are strongly low-field shifted by changing the C^N ligands from $[ppy]^-$ to $[dmppz]^-$. The resonances of these carbons shift from δ 130.4 – 133.2 ppm to δ 146.7 – 150.4 ppm. In compounds $[Ir(ppy)_2(tpy)][PF_6]$ and

$[Ir(ppy)_2(\mathbf{4})][PF_6]$ the chemical shifts of carbons A6 and C6 differ only about 1.8 ppm, whereas carbons B6 and D6 differ about 4.5 ppm. This supports the effect of an interaction between B6 and pyridine ring G.

In the blue emitting iridium(III) complexes of the previous chapter (see Chapter 4) the proton signals of the pendant phenyl rings are broad, due to their ability to undergo hindered rotation on the NMR timescale. In contrast with the introduction of an additional 4'-pyridyl ring H in compounds $[Ir(ppy)_2(\mathbf{4})][PF_6]$, $[Ir(dmppz)_2(\mathbf{4})][PF_6]$ and $[Ir(dmppz)_2(\mathbf{5})][PF_6]_2$ sharp proton signals in the NMR spectra are observed, as these do not have different NMR environments and do not coalesce.

5.4. Solid state structures

Crystals of good X-ray quality could be grown for compounds $[Ir(ppy)_2(tpy)][PF_6]$, $[Ir(dmppz)_2(tpy)][PF_6]$ $[Ir(dmppz)_2(\mathbf{4})][PF_6]$ and $[Ir(dmppz)_2(\mathbf{5})][PF_6]_2$. Unfortunately for $[Ir(ppy)_2(\mathbf{4})][PF_6]$, the crystals grew in very thin needles yielding a structure of poor quality.

Table 5.1 Crystallographic data of the five complexes.

Compound	$4\{[Ir(ppy)_2(tpy)][PF_6]\}.2.5C_4H_{10}O.1.5MeCN.3H_2O$	$[Ir(dmppz)_2(tpy)][PF_6]$	$2\{[Ir(ppy)_2(\mathbf{4})][PF_6]\}.C_4H_{10}O.CH_2Cl_2$	$[Ir(dmppz)_2(\mathbf{4})][PF_6].CH_2Cl_2$	$[Ir(dmppz)_2(\mathbf{5})][PF_6]_2.2CH_2Cl_2$
Formula	$C_{161}H_{143.5}F_{24}Ir_4N_{21.5}O_{5.5}P_4$	$C_{37}H_{33}F_6IrN_7P$	$C_{89}H_{72}Cl_2F_{12}Ir_2N_{12}OP_2$	$C_{43}H_{38}Cl_2F_6IrN_8P$	$C_{45}H_{43}C_{l4}F_{12}IrN_8P_2$
Formula weight / g mol^{-1}	3816.16	912.89	2070.87	1074.90	1319.83
Crystal colour and habit	yellow block	yellow block	orange needle	orange block	red block
Crystal system	triclinic	monoclinic	triclinic	triclinic	triclinic
Space group	*P*-1	$P2_1/n$	*P*-1	*P*-1	*P*-1
a, b, c / Å	13.770(2)	12.7713(7)	10.641(2)	10.8170(7)	9.0099(16)
	17.615(3)	21.4055(16)	18.025(4)	13.5418(8)	14.026(3)
	18.315(2)	12.8079(8)	21.629(4)	14.6844(9)	20.222(5)
α, β, γ/ °	85.763(12)	90	88.86(3)	94.081(2)	101.420(16)
	85.821(11)	94.874(5)	82.15(3)	100.297(2)	96.000(16)
	64.441(11)	90	81.97(3)	103.316(2)	99.536(14)
U / $Å^3$	4086.4(10)	3488.7(4)	4069.3(14)	2045.2(2)	2445.4(8)
*D*c / Mg m^{-3}	1.548	1.738	1.690	1.745	1.792
Z	1	4	2	2	2
μ(Mo-Kα) / mm^{-1}	3.372	3.944	3.457	-	3.104
μ(Cu-Kα) / mm^{-1}	-	-	-	8.510	-
T/ K	173	173	173	123	173
Refln. collected (R_{int})	93421 (0.1519)	93669 (0.0726)	50153 (0.2647)	46149 (0.0286)	26234 (0.0704)
Unique refln.	16046	10141	14413	7238	10145
Refln. for refinement	13628	9710	9184	7171	8551
Parameters	1048	473	1084	554	682
Threshold	$I > 2.0\sigma$	$I > 2.0\sigma$	$I > 2.0\sigma$	$I > 2.0\sigma$	$I > 2.0\sigma$
*R*1 (*R*1 all data)	0.0523 (0.0605)	0.0234 (0.0251)	0.0995 (0.1535)	0.0227 (0.0229)	0.0442 (0.0600
*wR*2 (*wR*2 all data)	0.1393 (0.1464)	0.0575 (0.0582)	0.1963 (0.2328)	0.0596 (0.0598)	0.0879 (0.0926)
Goodness of fit	1.080	1.167	1.043	1.100	1.042

5.4.1. $[Ir(ppy)_2(tpy)][PF_6]$

From a MeCN solution of the complex layered with Et_2O, X-ray quality crystals of $4\{[Ir(ppy)_2(tpy)][PF_6]\}.2.5Et_2O.1.5MeCN.3H_2O$ were grown by diffusion. The compound crystallizes in the triclinic space group *P*-1 with two independent cations (labelled A and B) in the asymmetric unit. Whereas cation A is in the Λ-form, cation B is in the Δ-form. Cation B is depicted in Figure 5.4; bond lengths and angles in cation A are very similar to those in cation B. The atoms Ir1A and Ir1B are in octahedral environments and the N-donors of the two cyclometallating $[ppy]^-$ ligands are in a *trans*-arrangement. The N-atoms of the tpy ligand are *trans* to the C-atoms of the $[ppy]^-$ ligands. The $[ppy]^-$ ligands are all almost planar (angles of the least squares planes within each $[ppy]^-$ ligand are below 6.2°). This is in contrast to the tpy ligands with angles between the least squares planes of the bonded pyridine rings of 18.2 and 18.3° (for cation A and B). The pendant pyridine ring is twisted through 56.2 and 62.0° in A and B, with respect to the pyridine ring to which it is bonded. This non-planarity allows the free pyridine ring to engage in intramolecular face-to-face π-stacking with one of the phenyl rings of one of the $[ppy]^-$ ligands. The inter-centroid separations are 3.50 and 3.45 Å and the angle between the least squares planes are 11.0 and 7.23°. All these values are very similar to the stacking interactions in $[Ir(ppy)_2(pbpy)][PF_6]$ (inter-centroid separations: 3.48 Å; twisting angle: 7.5°).[7]

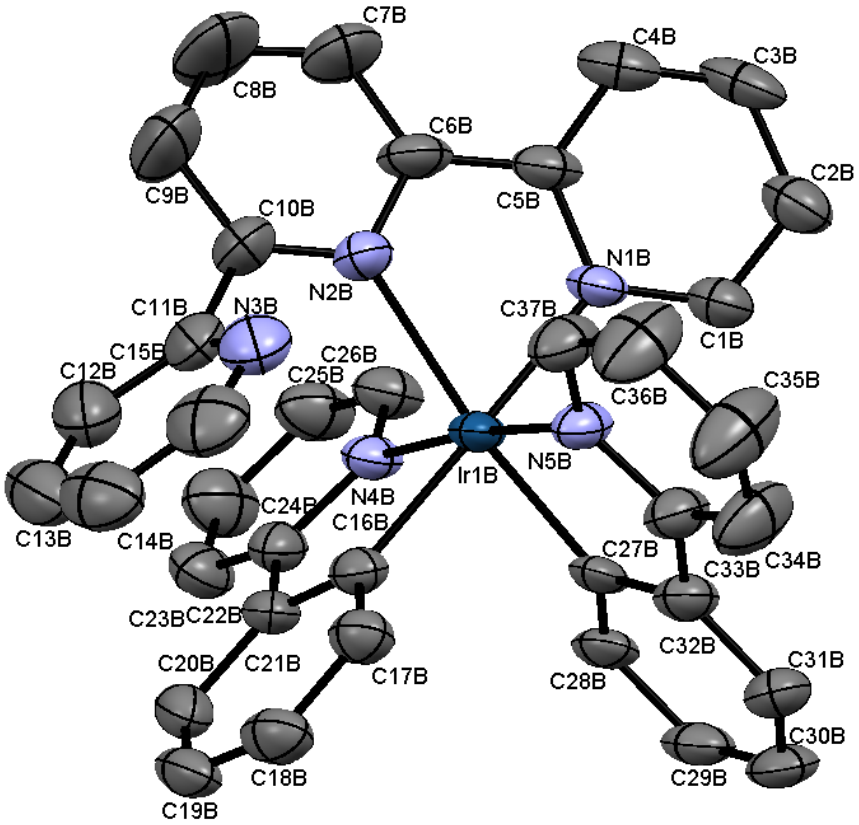

Figure 5.4 Structure of the Δ-$[Ir(ppy)_2(tpy)]^+$ cation (cation B) in $4\{[Ir(ppy)_2(tpy)][PF_6]\}.2.5Et_2O.1.5MeCN.3H_2O$ with ellipsoids plotted at 50% probability level; H atoms omitted. Selected bond lengths (in Å) and angles (in °): Ir1A–C27A: 1.994(6), Ir1A–C16A: 2.018(6), Ir1A–N5A: 2.042(5), Ir1A–N4A: 2.049(5), Ir1A–N1A: 2.130(5), Ir1A–N2A: 2.214(5); N1A–Ir1A–N2A: 76.4(2), N4A–Ir1A–C16A: 80.3(2), N5A–Ir1A–C27A: 81.1(2). Selected bond lengths (in Å) and angles (in °): Ir1B–C27B: 2.015(6), Ir1B–C16B: 2.023(6), Ir1B–N5B: 2.023(4), Ir1B–N4B 2.033(4), Ir1B–N1B: 2.128(5), Ir1B–N2B: 2.220(5); N1B–Ir1B–N2B: 76.1(2), N4B–Ir1B–C16B: 79.9(2), N5B–Ir1B–C27B: 80.5(2).

The crystal packing consists of parallel layers of cations which are alternated by layers of anions together with the solvent molecules. The layers of cations consist of alternating rows of molecules A and B. Each row consists of alternating molecules of Δ- and Λ-handedness. Figure 5.5 depicts one layer of the cations.

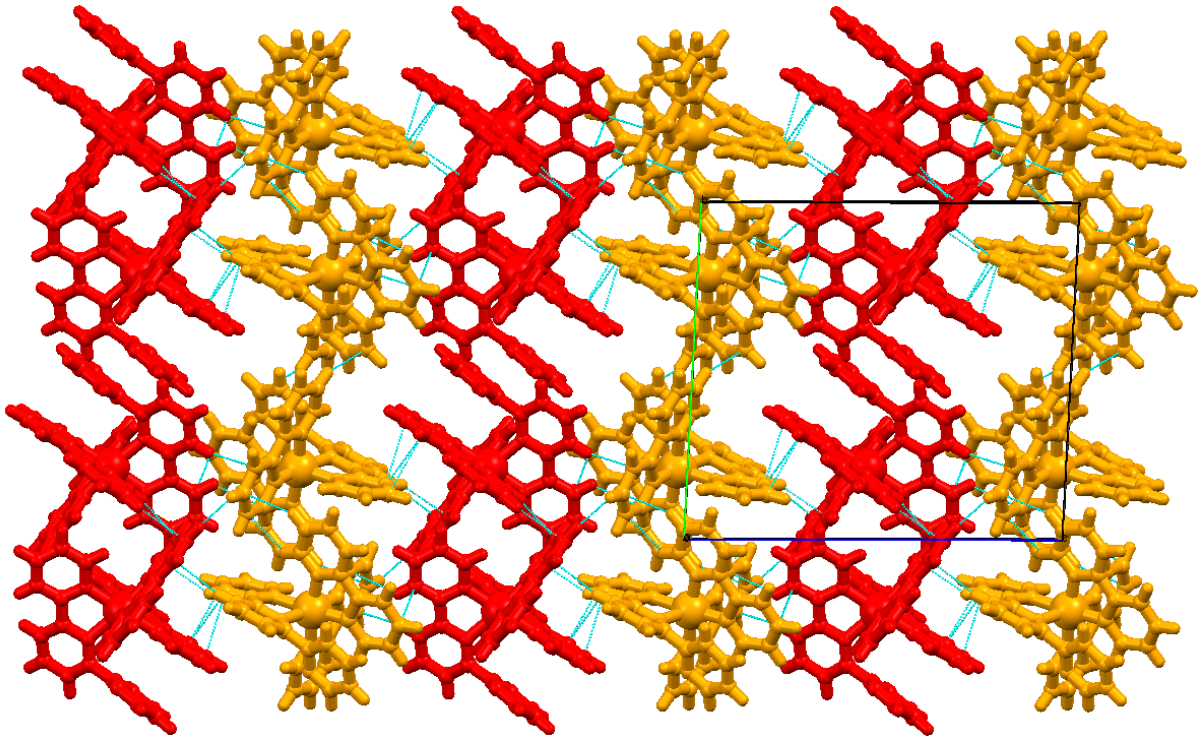

Figure 5.5 Packing interactions of $[Ir(ppy)_2(tpy)][PF_6]$ lead to layers of rows of molecules A (yellow) and B (red). Within each row the cations alternate Δ- and Λ-handedness.

Meaningful packing interactions consist of edge-to-face π-interactions. These interactions lead to a grid-like array of the molecules in $[M(tpy)_2]^{n+}$ complexes,[8] but instead of having a complex with two tridentate ligands, $[Ir(ppy)_2(tpy)][PF_6]$ has three bidentate ligands. The interactions are between a ring containing atom C7B and a ring containing atom C31A and between a ring containing atom C7A and a ring containing $C31B^{i}$ (symmetry code i = x, y, z + 1). The C-H...phenyl ring centroid distances are 3.00 and 3.04 Å and the C-H are pointing directly towards the centre of the phenyl ring. These distances are bigger and the molecules are less densely packed than in crystal structures with tpy embrace nets reported in the literature.[9, 10]

The other inter-cation contacts are out of the range for distances and angles to be π-π interactions as discussed by Janiak.[11] Additionally, there are cation...anion contacts which stabilize the crystal packing. The cations, anions and one Et_2O solvent molecule are ordered and the other solvent molecules were calculated with fractional occupancies: the second Et_2O molecules with 25%, the MeCN with 75% and the three water molecules with 50% occupancy each.

5.4.2. [Ir(dmppz)$_2$(tpy)][PF$_6$]

X-ray quality crystals of [Ir(dmppz)$_2$(tpy)][PF$_6$] were grown from a solution of CH_2Cl_2 by diffusion. The structure of Δ-[Ir(dmppz)$_2$(tpy)]$^+$ is depicted in Figure 5.6. The complex crystallizes in the monoclinic space group $P2_1/n$ with both enantiomers of the cation in the unit cell. The atom Ir1 is in an octahedral environment and the N-donors of the two cyclometallating ligands are in a *trans*-arrangement. The cyclometallating [dmppz]$^-$ ligands are less planar than the [ppy]$^-$ ligands in [Ir(ppy)$_2$(tpy)][PF$_6$], with twisting angles of the least squares planes within each ligand of 7.2 and 9.9°. The twisting angle between the two bonded pyridine rings in the tpy ligand is 14.8°, while the pendant pyridine ring is twisted about 69.6° with respect to the pyridine ring to which it is bonded. This twisting allows the pendant pyridine ring to undergo face-to-face π-stacking with the phenyl rings of one of the [dmppz]$^-$ ligands. The twisting angle between the least squares planes of the involved rings is 10.1° with an inter-centroid distance of 3.41 Å, making it an efficient interaction.[11]

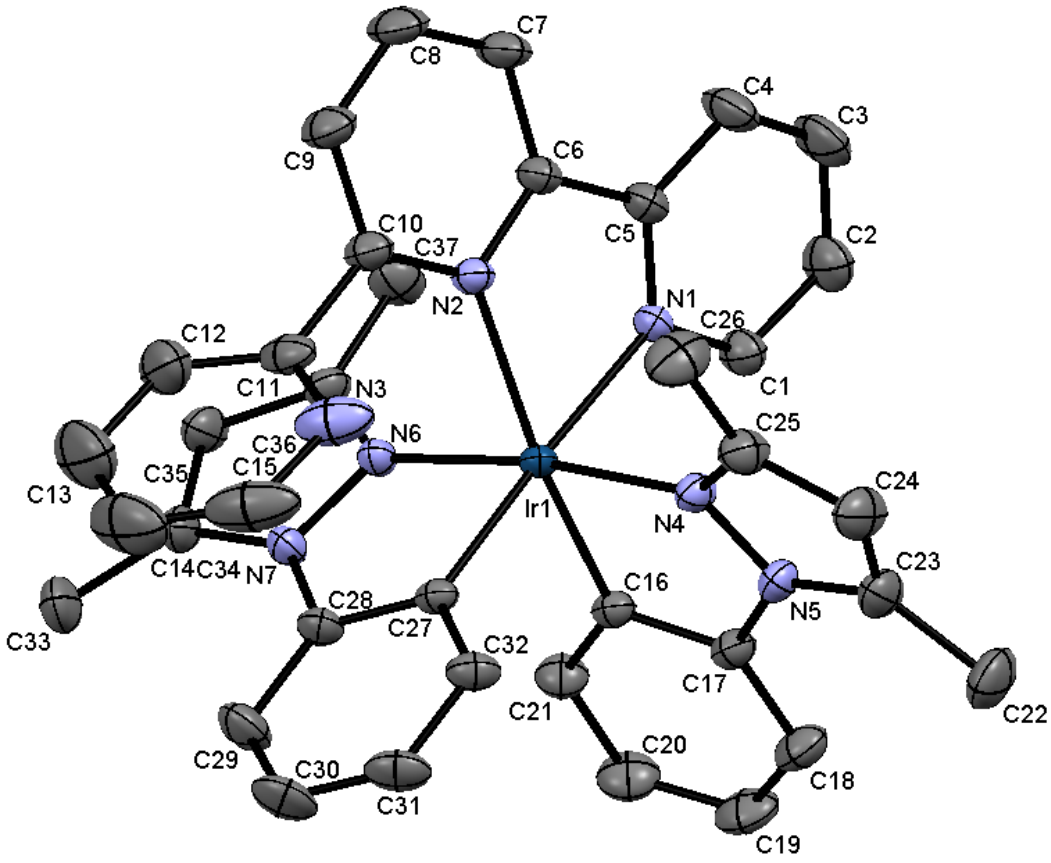

Figure 5.6 Structure of the Δ-cation B of [Ir(dmppz)$_2$(tpy)]$^+$ with ellipsoids plotted at 50% probability level; H atoms omitted. Selected bond lengths (in Å) and angles (in °): Ir1–C16: 2.003(2), Ir1–C27: 2.011(2), Ir1–N6: 2.025(2), Ir1–N4: 2.028(2), Ir1–N1: 2.140(2), Ir1–N2: 2.221(2); N1–Ir1–N2: 75.9(1), N4–Ir1–C16: 79.6(1), N6–Ir1–C27: 79.6(1).

The crystal packing is dominated by cation – anion interactions with F...H distances between 2.3 and 3.3 Å (see Figure 5.7).

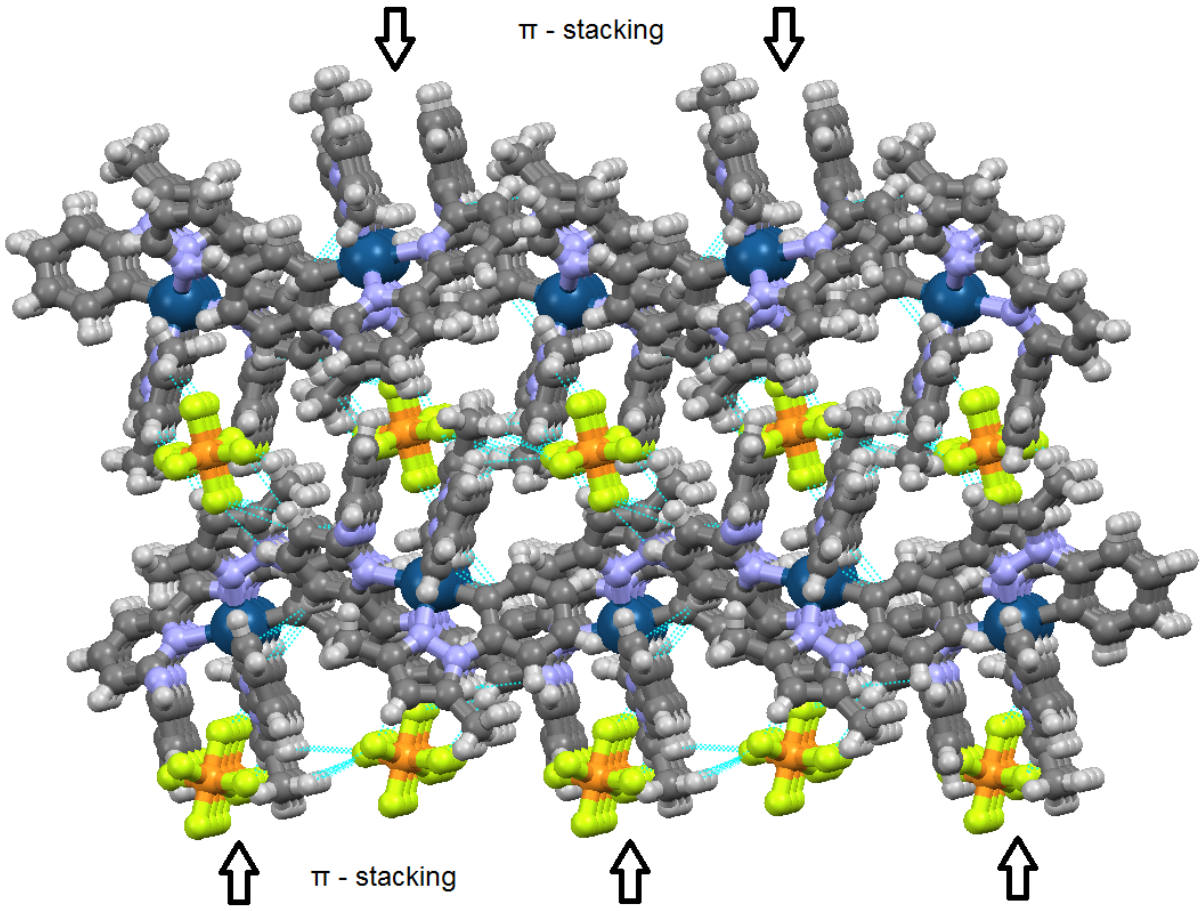

Figure 5.7 Crystal packing within $[Ir(dmppz)_2(tpy)][PF_6]$. The arrows point at the intramolecular π-stacking interactions.

Both ions are well resolved and ordered and there are no additional solvent molecules in the crystal structure.

5.4.3. $[Ir(ppy)_2(4)][PF_6]$

From a CH_2Cl_2 solution of the complex layered with Et_2O, X-ray quality crystals of $2\{[Ir(ppy)_2(\mathbf{4})][PF_6]\}.Et_2O.CH_2Cl_2$ were grown by diffusion. There are two independent cations (labelled A and B) in the asymmetric unit, both in the Λ-form. The structure of the Λ-cation of cation B is depicted in Figure 5.8; molecule A looks very similar. The crystals were very thin needles and diffraction was extremely weak, leading to a R factor relatively high (9.95%).

The complex crystallizes in the triclinic centrosymmetric *P*-1 space group with both enantiomers of cations A and B in the unit cell. Both atoms Ir1A and Ir1B are in an octahedral environment and the N-donors of the two cyclometallating ligands are in a *trans*-arrangement. All cyclometallating $[ppy]^-$ ligands are almost planar, with a twisting angle between the least squares planes below 4.4°. This is in contrast to the tpy ligands with angles between the least squares planes of the two bonded pyridine rings of 17.7 and 20.0° in cation A and B. The pendant pyridine rings, containing atoms N3A and N3B, of the tpy ligands are twisted through 47.8 and 50.7° with respect to the bonded pyridine ring. This

non-planarity allows the free pyridine ring to undergo intramolecular face-to-face π-stacking with one of the phenyl rings of one of the cyclometallating ligands. The inter-centroid separations are 3.56 and 3.54 Å and the angles between the least squares planes are 14.5 and 8.3° in molecule A and B, respectively. Whereas in cation B the interaction is highly efficient, the twisting angle in cation A is rather big as discussed by Janiak[11]. Janiak sets the limits for π-stacking interactions at 3.8 Å distance and a twisting angle between the stacking rings at 20°.

The 4'-pyridyl rings, containing atoms N4A and N4B, are twisted through 25.6 and 21.8° with respect to the pyridine ring to which it is bonded.

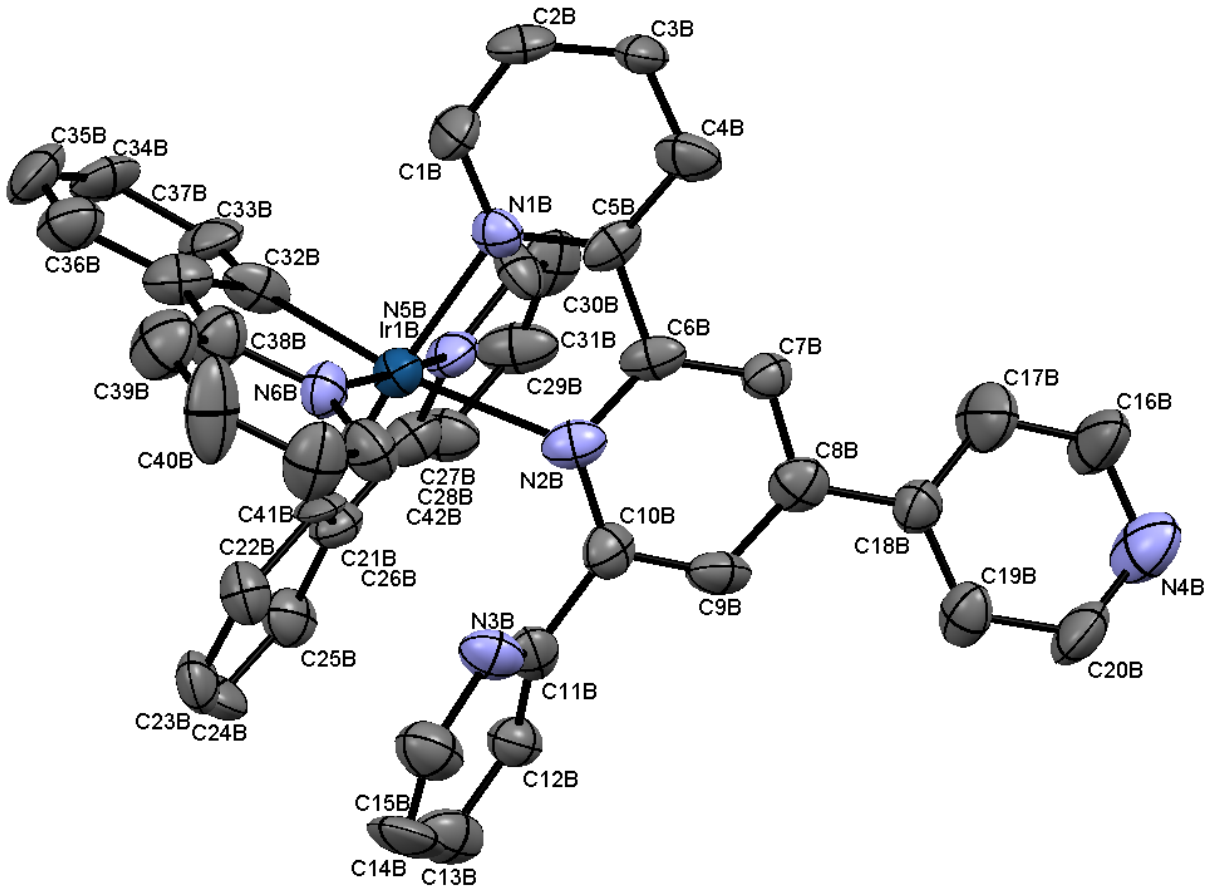

Figure 5.8 Structure of Λ-cation of 2{[Ir(ppy)$_2$(4)][PF$_6$]}.Et$_2$O.CH$_2$Cl$_2$ with ellipsoids plotted at 50% probability level; H atoms omitted. Selected bond lengths (in Å) and bond angles (in °): Ir1A–C32A: 1.945(2), Ir1A–C21A: 1.996(2), Ir1A–N6A: 2.032(1), Ir1A–N5A: 2.056(2), Ir1A–N1A: 2.124(1), Ir1A–N2A: 2.210(1);), N1A–Ir1A–N2A: 74.9(5), N5A–Ir1A–C21A: 82.0(8), N6A–Ir1A–C32A: 79.6(6). Selected bond lengths (in Å) and bond angles (in °): Ir1B–C32B: 1.93(2), Ir1B–C21B: 1.98(1), Ir1B–N5B: 2.03(1), Ir1B–N6B: 2.04(1), Ir1B–N1B: 2.11(1), Ir1B–N2B: 2.21(1); N1B–Ir1B–N2B: 75.1(5), N5B–Ir1B–C21B: 80.6(6), N6B–Ir1B–C32B: 80.2(6).

The crystal packing is dominated by interactions between cations and anions, cations and solvent molecules, anions and solvent molecules and by interactions between cations (e.g. N4A...H12A-C12B^{i} at a distance of 2.65 Å; symmetry code i = 1 – x, -y, 1 – z). The pendant pyridine rings are not involved in intermolecular face-to-face stacking interactions. The packing interactions lead to alternating sheets of cations A and B. Within the sheets the cations are of alternating handedness (see Figure 5.9).

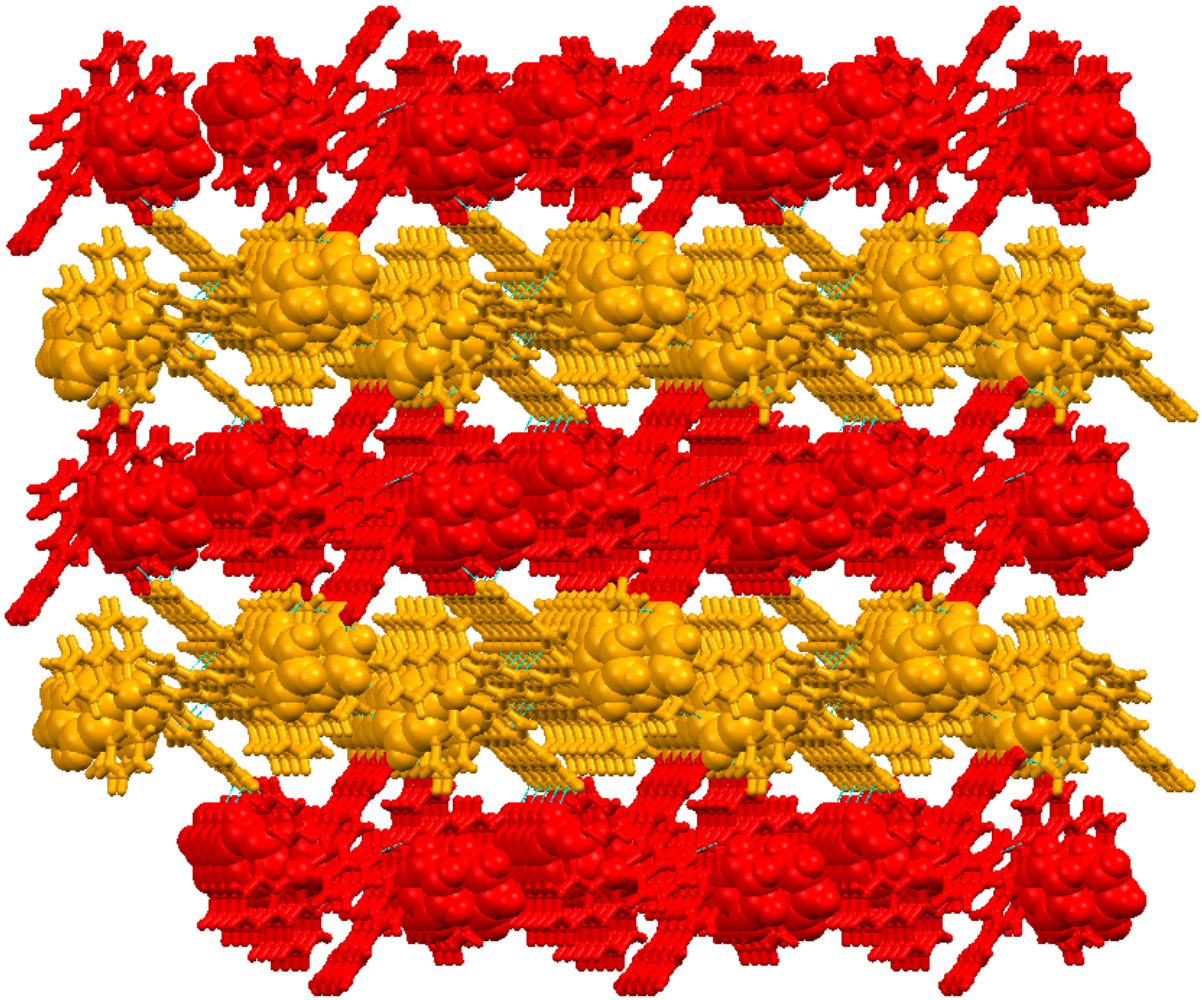

Figure 5.9 Crystal packing of [Ir(ppy)$_2$(4)][PF$_6$] consists of alternating sheets of molecules A (orange) and B (red), each with alternating Δ- and Λ-forms.

All the molecules are ordered and both solvent molecules are with full occupancy.

5.4.4. [Ir(dmppz)$_2$(4)][PF$_6$]

From a CH_2Cl_2 solution of the complex, X-ray quality crystals of [Ir(dmppz)$_2$(**4**)][PF$_6$].CH_2Cl_2 were grown by diffusion. The complex crystallizes in the triclinic *P*-1 space group with both enantiomers of the cation in the unit cell and the Δ-[Ir(dmppz)$_2$(**4**)]$^+$ cation is depicted in Figure 5.10. The atom Ir1 is in an octahedral environment with the N-donors in a *trans*-arrangement. Similar to [Ir(dmppz)$_2$(tpy)][PF$_6$] (see section 5.4.2), the [dmppz]$^-$ ligands are less planar than the [ppy]$^-$ ligands in other compounds. Within the tpy ligand, the twisting angles and distances are similar to [Ir(dmppz)$_2$(tpy)][PF$_6$]. The angles between the least squares planes of the phenyl and pyrazole rings are 5.8 and 8.6°. The twisting angle of the bonded pyridine rings within the tpy ligand is 17.2°. The pendant pyridine ring of the tpy ligand, containing atom N3, is twisted through 62.7° with respect to the pyridine ring it is attached to, and this non-planarity allows the free pyridine ring to undergo intramolecular face-to-face π-stacking with the phenyl ring of one of the C^N ligands. The inter-centroid separation is 3.55 Å and the angle between the least squares planes is 8.0°, making it a

highly efficient interaction. The 4'-pyridyl ring, containing atom N4, is twisted through 14.4° with respect to the pyridine ring to which it is bonded. This value is significantly smaller than in $[Ir(ppy)_2(\mathbf{4})][PF_6]$.

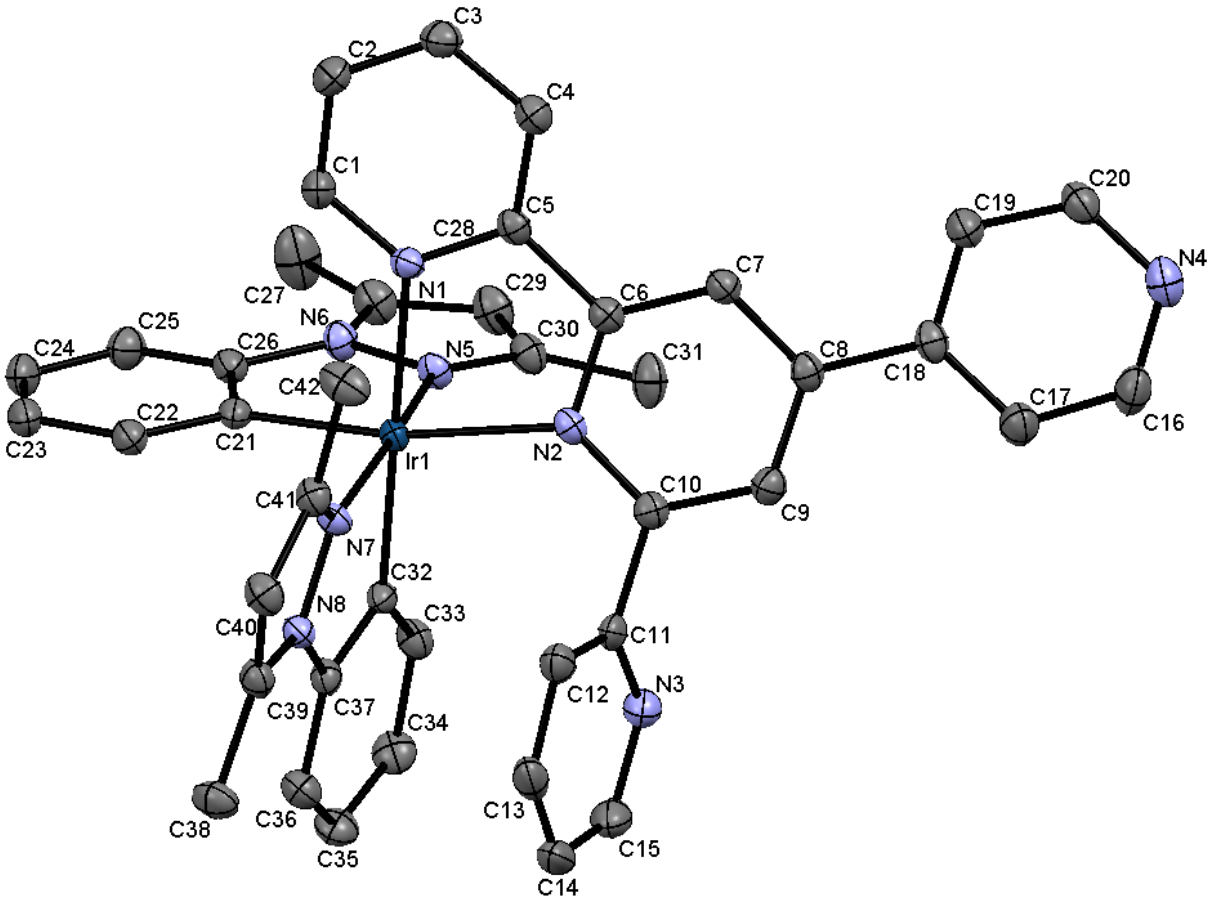

Figure 5.10 Structure of the Δ-cation in $[Ir(dmppz)_2(4)][PF_6].CH_2Cl_2$ with ellipsoids plotted at 50% probability level; H atoms omitted. Selected bond lengths (in Å) and bond angles (in °): Ir1–C21: 2.008(3), Ir1–C32: 2.015(3), Ir1–N7: 2.031(2), Ir1–N5: 2.051(2), Ir1–N1: 1.134(2), Ir1–N2: 2.206(2); N1–Ir1–N2: 75.8(1), N5–Ir1–C21: 79.6(1), N7–Ir1–C32: 79.6(1).

The packing interactions between the cations consist of hydrogen bonds between atoms N3...H29A^{i} (2.63 Å), N3...H31A^{i} (2.66 Å; symmetry code i = 2 – x, 1 – y, 1 – z), and N4...H40A^{ii} (2.70 Å; symmetry code ii = x, y, z – 1) and face-to-face π-stacking interactions between the two enantiomers of the cation. The enantiomers embrace each other yielding sheets of cations of alternating Δ- and Λ-cations (see Figure 5.11). This embracing is supported by C...H contacts between atoms C19 and H34A^{i} (2.79 Å; symmetry code i = 2 – x, 1 – y, 1 – z) and between atoms C22 respectively C23 and H36A^{iii} (2.74 and 2.76 Å rsp.; symmetry code iii = 2 – x, 1 – y, 2 – z).

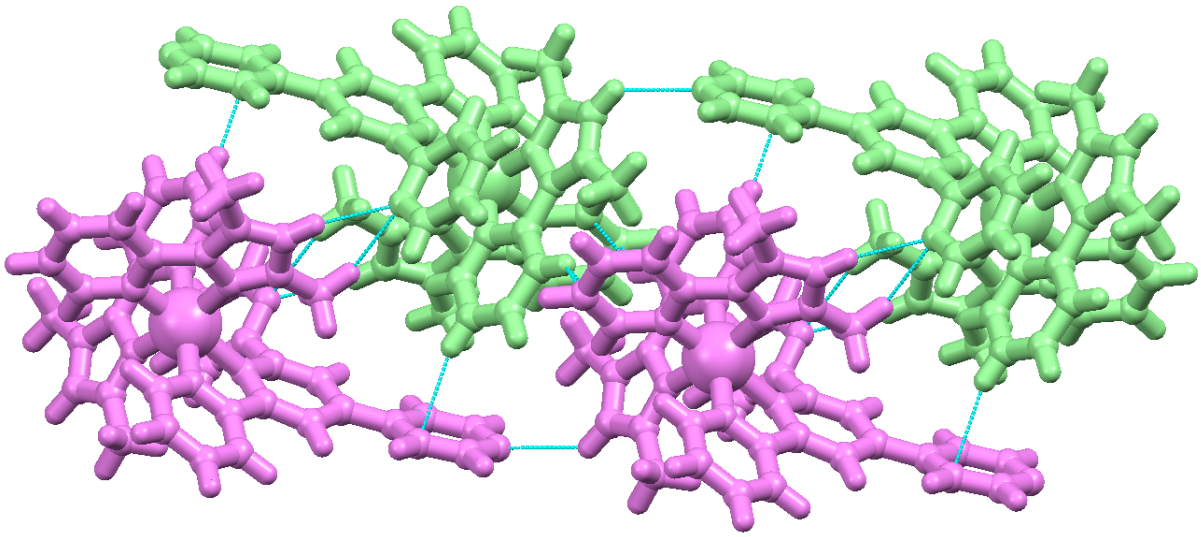

Figure 5.11 Packing interactions in between Δ- (purple) and Λ-cations (green) of $[Ir(dmppz)_2(4)]^+$.

There are intermolecular CH...π interactions between the methyl groups and the pyrazole rings of the $[dmppz]^-$ ligands, containing atoms N5, N6 and $C27^i$ (symmetry code i = 1 – x, 1 – y, 1 – z). These $[dmppz]^-$ ligands are not involved in the intramolecular stacking interactions. The least squares planes of the pyrazole rings are parallel (symmetry imposed by an inversion centre) at a distance of 3.61 Å and the distance between a centroid and the carbon atom of the methyl group is 3.72 Å (see Figure 5.12), being on the very edge of the range discussed by Janiak.[11]

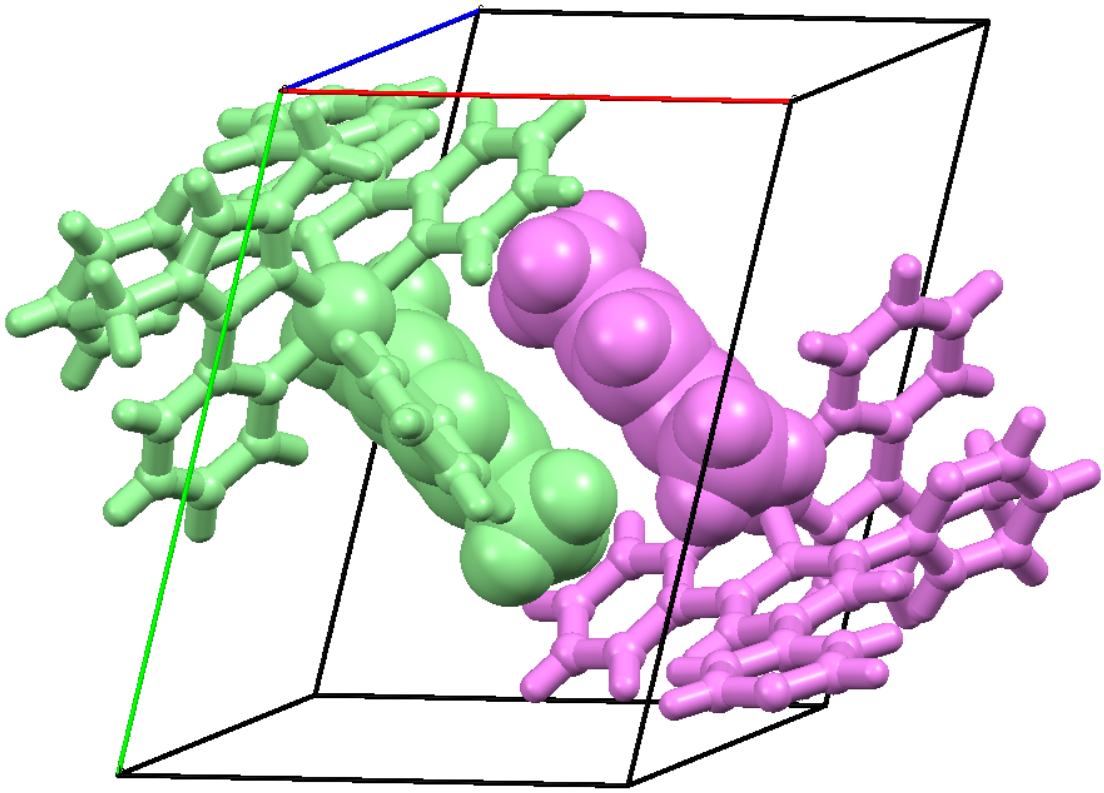

Figure 5.12 Face-to-face stacking interactions between the two Δ- (purple) and Λ-enantiomers (green) in the unit cell of $[Ir(dmppz)_2(4)][PF_6].CH_2Cl_2$.

The arrangement of the interacting cations in the crystal consists of horizontal sheets of cations with alternating Δ- and Λ-handedness (see Figure 5.13). The sheets of cations are interleaved by anions and solvent molecules. The anions and solvent molecules are omitted but would be between the layers of cations. The crystal packing interactions are between cations, anions and CH_2Cl_2.

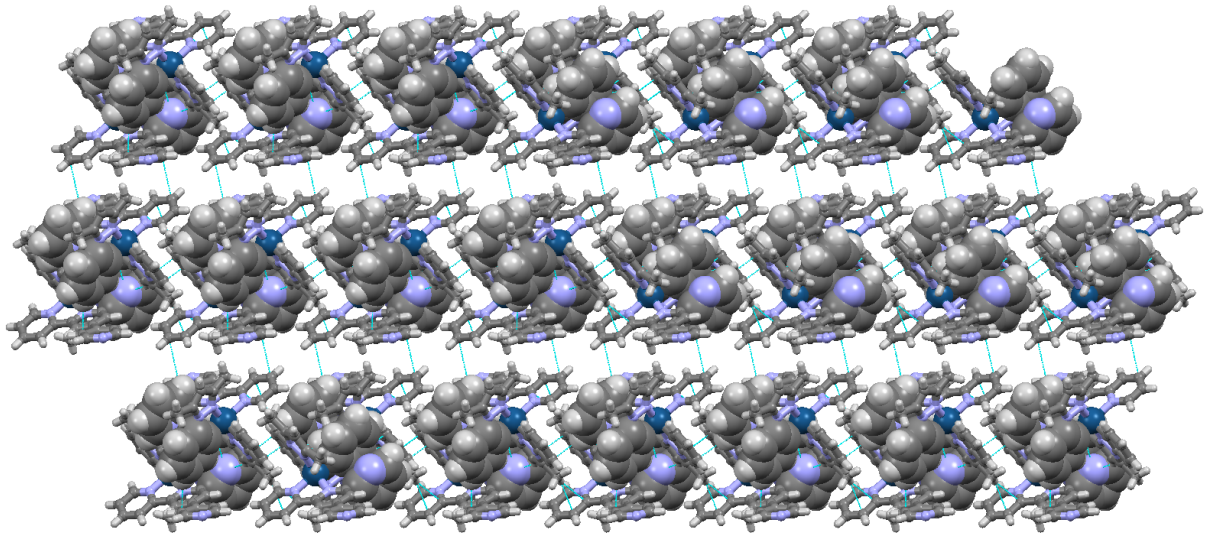

Figure 5.13 Sheets of cations of $[Ir(dmppz)_2(4)][PF_6].CH_2Cl_2$. Between the layers are the anions and solvent molecules (omitted for clarity).

In the crystal structure, all the cation, anions and solvent molecules are ordered and in full occupancy.

5.4.5. $[Ir(dmppz)_2(5)][PF_6]_2$

From a CH_2Cl_2 solution of the complex, X-ray quality crystals of $[Ir(dmppz)_2(\mathbf{5})][PF_6]_2.2CH_2Cl_2$ were grown by diffusion. The Δ-$[Ir(dmppz)_2(\mathbf{5})]^+$ cation is depicted in Figure 5.14. The complex crystallizes in the triclinic *P*-1 space group with both enantiomers of the cation in the unit cell. The atom Ir1 is in an octahedral environment with the N-donors in a *trans*-arrangement. Comparison with $[Ir(dmppz)_2(\mathbf{4})][PF_6]$ shows the following differences. One of the $[dmppz]^-$ ligands is almost planar with an angle between the least squares planes within the two rings of 4.0°, whereas the other cyclometallating ligand is twisted about 13.5°. The twisting angle of the bonded pyridine rings within the tpy ligand is 8.3°. This is half of the value of $[Ir(dmppz)_2(\mathbf{4})][PF_6]$. The pendant pyridine ring of the tpy ligand, containing atom N3, is twisted through 78.2° with respect to the pyridine ring to which it is bonded. This non-planarity allows the free pyridine ring to undergo intramolecular face-to-face π-stacking with one of the phenyl rings of the C^N ligands. The inter-centroid separation is 3.44 Å and the angle between the least squares planes is 8.4°. This makes it an efficient interaction. The 4'-pyridyl ring, containing atom N4, is twisted through 36.1° with respect to the pyridine ring to which it is bonded, compared to 14.4° within $[Ir(dmppz)_2(\mathbf{4})][PF_6]$ and 21.8 and 25.6° within $[Ir(ppy)_2(\mathbf{4})][PF_6]$.

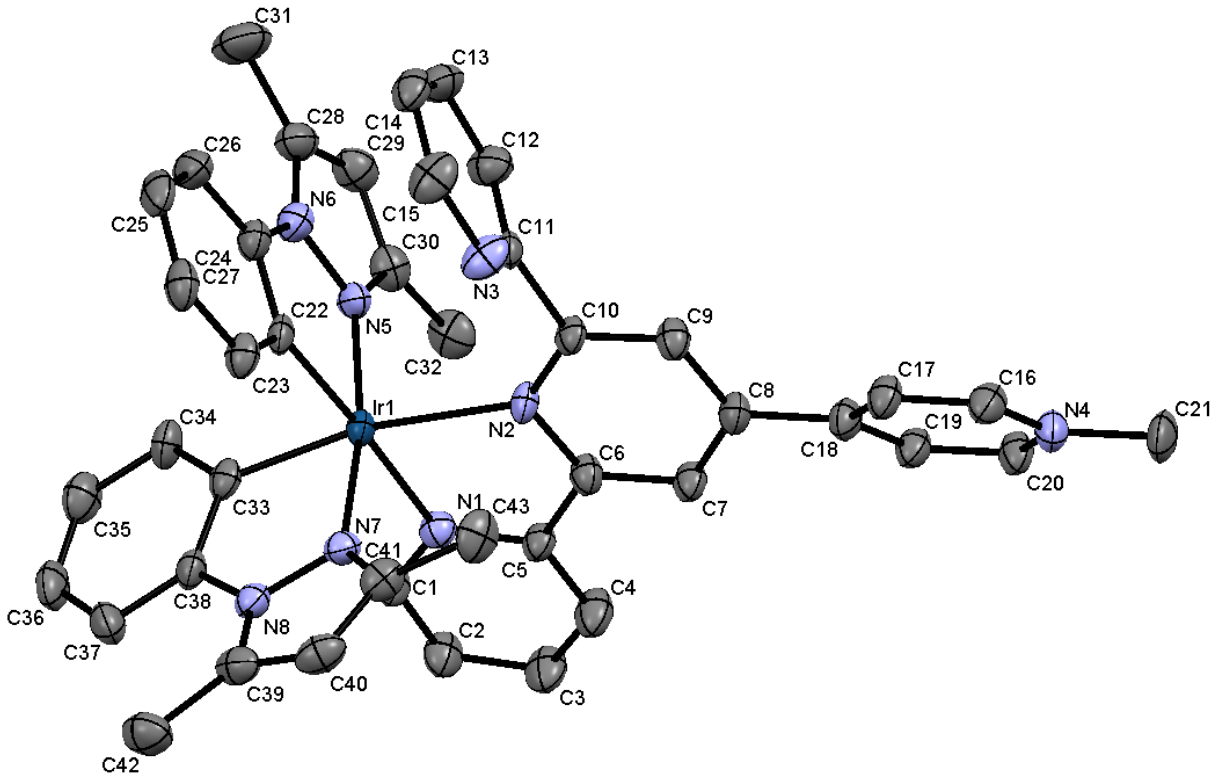

Figure 5.14 Structure of the Δ-cation in $[Ir(dmppz)_2(5)][PF_6]_2.2CH_2Cl_2$ with ellipsoids plotted at 50% probability level; H atoms omitted. Selected bond lengths (in Å) and bond angles (in °): Ir1–C33: 1.991(5), Ir1–N5: 2.018(5), Ir1–C22: 2.024(5), Ir1–N7: 2.045(5), Ir1–N1: 2.152(4), Ir1–N2: 2.214(4); N1–Ir1–N2: 75.7(2), N5–Ir1–C22: 79.3(2), N7–Ir1–C33: 80.0(2).

In contrast to the crystal packing of $[Ir(dmppz)_2(\mathbf{4})][PF_6]$, in $[Ir(dmppz)_2(\mathbf{5})][PF_6]_2$ the cations do not embrace one another. There are intermolecular π-interactions between protons H42C and H42C^i and the pyrazole rings of the $[dmppz]^-$ ligands, containing atoms N7, N8 and N7^i and N8^i (symmetry code i = 1 – x, 1 – y, 1 – z). These C^N ligands are not involved in the intramolecular stacking interactions. The least squares planes of the pyrazole rings are parallel (symmetry imposed by an inversion centre) at a distance of 3.41 Å. The H...pyrazole ring centroid separation is 2.65 Å and the proton is pointing towards the centre of the pyrazole ring. This packing interaction leads to vertical columns of cations with alternating Δ- and Λ-handedness (see Figure 5.15).

Packing interactions between the Me-group of the tpy ligand with the two cyclometallating phenyl rings lead to rows and finally to sheets of cations with the same handedness (some interaction distances: C21...C38^i: 3.755(8), C21...C24^i: 3.391(9) Å; symmetry code i = x – 1, y – 1, z). The holes between the sheets contain the anions and solvent molecules (see Figure 5.15). The F...H distances are between 2.7 and 3.1 Å.

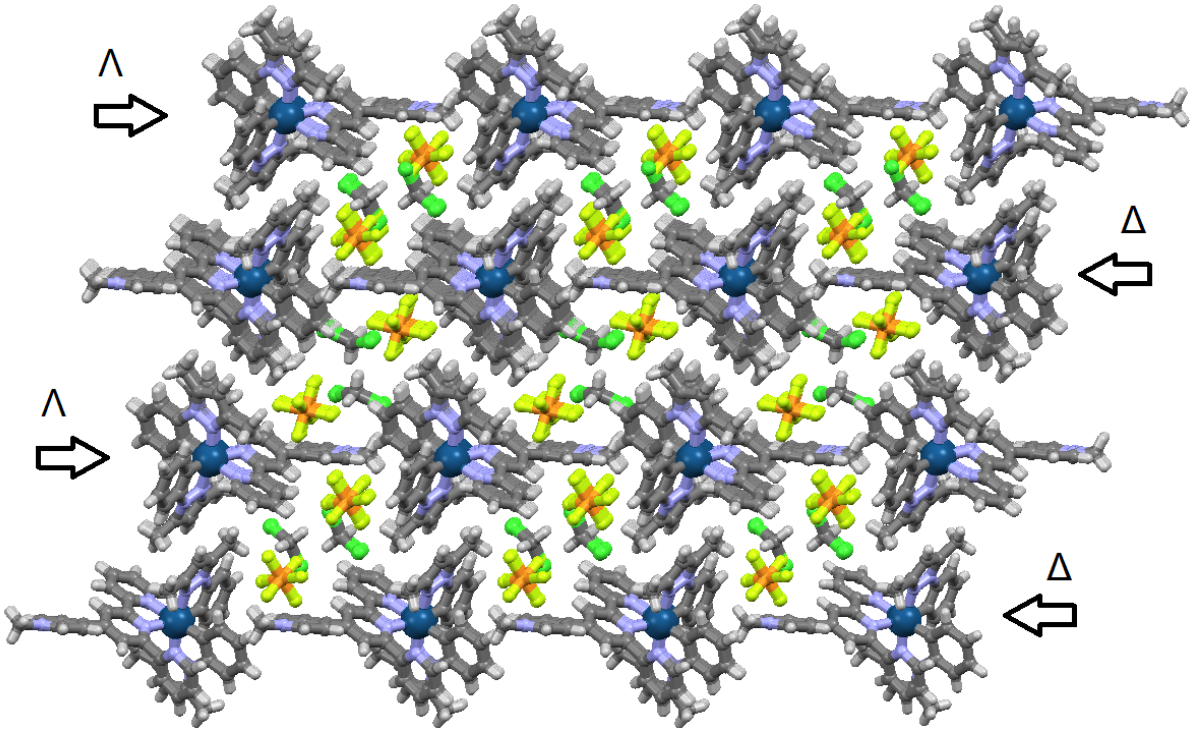

Figure 5.15 Packing interactions in $[Ir(dmppz)_2(5)][PF_6]_2$.

The cation, anion and one of the CH_2Cl_2 molecules are ordered, whereas the second CH_2Cl_2 molecule was modelled over two sites with occupancies of 0.53 and 0.47.

5.5. Photophysical studies

The photophysical behaviour of the five complexes has been measured in aerated CH_2Cl_2 solutions. The electronic absorption spectra of $[Ir(ppy)_2(tpy)][PF_6]$, $[Ir(dmppz)_2(tpy)][PF_6]$, $[Ir(ppy)_2(\mathbf{4})][PF_6]$, $[Ir(dmppz)_2(\mathbf{4})][PF_6]$ and $[Ir(dmppz)_2(\mathbf{5})][PF_6]_2$ are comparable (see Figure 5.16). The spectra show intense bands in the UV region at 250 to 300 nm and less intense bands at lower energy. The relatively intense bands are at 261 and 375 nm ($[Ir(ppy)_2(tpy)][PF_6]$), 258 and 350 nm ($[Ir(ppy)_2(\mathbf{4})][PF_6]$), 250, 290 and 350 nm ($[Ir(dmppz)_2(tpy)][PF_6]$), 253, 320 and 350 nm ($[Ir(dmppz)_2(\mathbf{4})][PF_6]$) and 256, 315 and 400 nm ($[Ir(dmppz)_2(\mathbf{5})][PF_6]_2$). The high energy absorption bands are assigned to spin-allowed ligand-based $\pi^* \leftarrow \pi$ transitions. The less intense, lower energy absorptions are assigned to typical spin-allowed metal-to-ligand charge transfer transitions (MLCT).[12, 13, 14] Comparison of $[Ir(ppy)_2(tpy)][PF_6]$ with $[Ir(ppy)_2(pbpy)][PF_6]$ indicates only a small effect on the absorption spectrum, when changing the pendant phenyl ring to a pyridine ring.7

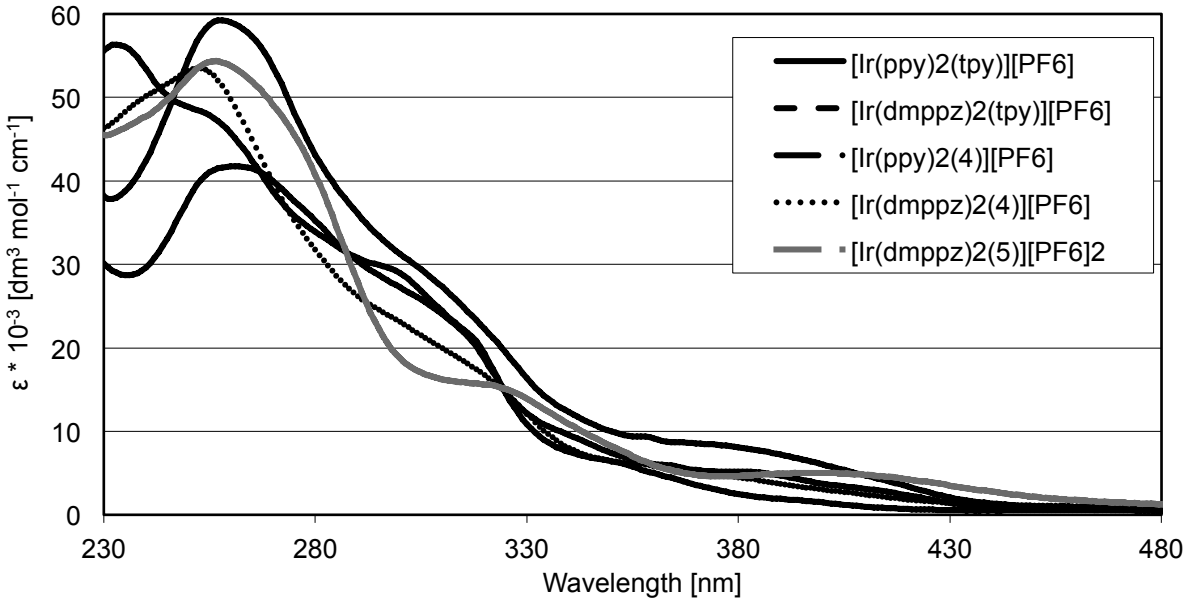

Figure 5.16 Absorption spectra of the four red emitting complexes in CH_2Cl_2 (c = 1.00 x 10^{-5} M).

Excitation between 250 to 260 nm leads to orange to red emissions in four of the five complexes (Figure 5.17). Completely different is the emission spectrum of $[Ir(dmppz)_2(\mathbf{5})][PF_6]_2$. Starting from $[Ir(dmppz)_2(\mathbf{4})][PF_6]$, the effect of the methylation of the 4'-pyridyl ring did not lead to a further red shift in the emission spectrum. Excitation at 260 nm leads to an emission maximum at 358 nm.

The emission maxima of the other four complexes are in the orange region 590 nm ($[Ir(ppy)_2(tpy)][PF_6]$) and 599 nm ($[Ir(dmppz)_2(tpy)][PF_6]$) and in the red region at 620, 640 nm ($[Ir(ppy)_2(\mathbf{4})][PF_6]$) and 642 nm ($[Ir(dmppz)_2(\mathbf{4})][PF_6]$), with a broad and unstructured shape which is characteristic of complexes containing a combination of neutral diimine and cyclometallating ligands. The effect of the $[dmppz]^-$ ligands instead of the $[ppy]^-$ ligands is a slight red shift. Comparison of $[Ir(ppy)_2(tpy)][PF_6]$ with $[Ir(ppy)_2(pbpy)][PF_6]$ shows only minimal effect on the emission spectrum by the change of the pbpy ligand to the tpy ligand (590 nm to 595 nm).[7, 15] The introduction of the 4'-pyridyl ring and therefore the extension of the aromatic system on the N^N ligand, leads to a red-shift of the emission maximum of almost 50 nm. There are only a few iridium(III) based compounds known with an emission maximum at longer wavelengths up to 687 nm.[4, 13]

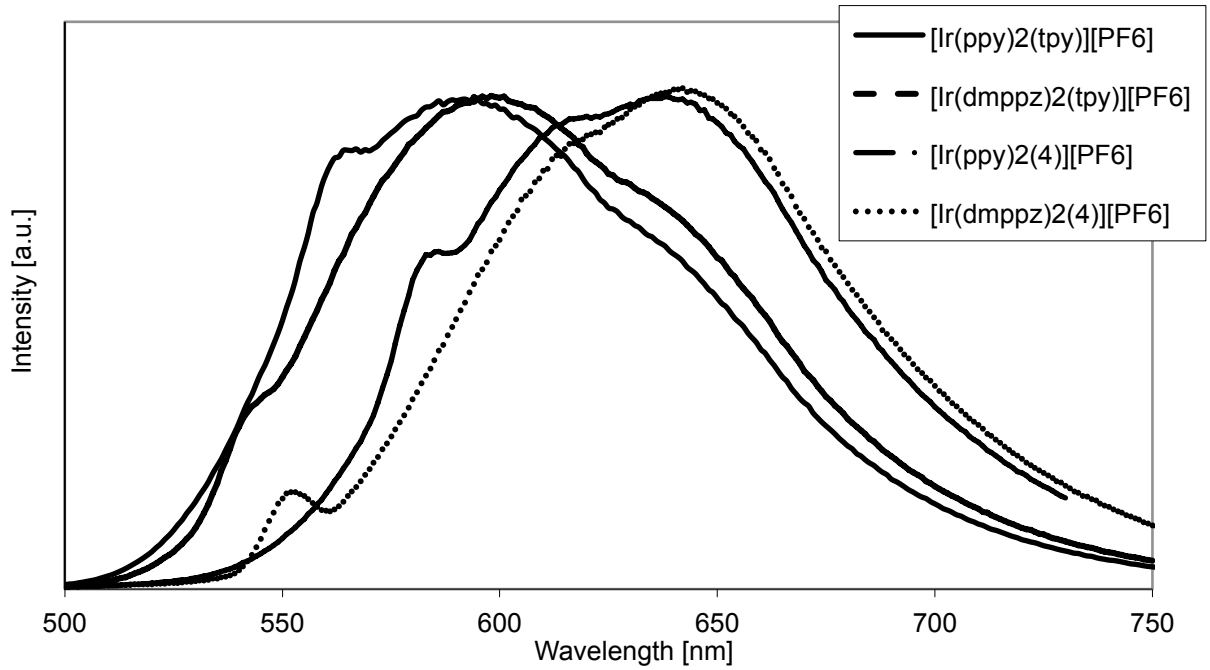

Figure 5.17 Emission spectra of the orange and red emitting complexes in CH_2Cl_2.

Quantum yield measurements were performed on CH_2Cl_2 solutions of the complexes. Prior to the measurements, the solutions were degassed with argon for 15 minutes. All the orange-red emitting complexes show low quantum yield values. The change of the cyclometallating ligand from $[ppy]^-$ to $[dmppz]^-$ enhances the quantum yield. Comparing the influence by changing the pendant phenyl ring to a pyridine ring, the quantum yield is lowered about ⅓, from 3% to 1.7%.7 The quantum yield of the deepest red emitter in the series is 0.062 (λ_{em} = 642 nm), which is comparable with other reported red emitting compounds (λ_{em} = 656 nm, QY = 0.20 and λ_{em} = 687 nm, QY = 0.02).4, [13, 14]

5.6. Electrochemical studies

All five complexes are electrochemically active. The complexes have been measured in CH_2Cl_2 solutions with 0.1 M $[^nBu_4N][PF_6]$ supporting electrolyte at a scan rate of 0.1 V s^{-1}. The cyclic voltammetric data with respect to internal Fc/Fc^+ are presented in Table 5.2. Unless otherwise stated, the electrochemical processes are reversible or near-reversible. For all five complexes the reversible or quasi reversible oxidations between +0.79 and +0.90 were assigned to an iridium-centred process. Upon changing pyridine to dimethylpyrazole in the C^N ligand, the oxidation potential is lowered by about 0.08 V. This is in line with the red shift in the emission maxima of the complexes.

All five complexes show ligand centred quasi reversible reduction processes. The trend upon the introduction of the pyridine ring shows a decrease of the reduction potential of more than 0.1 V, which is also consistent with the red-shift in the emission maxima spectra.

Table 5.2 Cyclic voltammetric data with respect to Fc/Fc^+; CH_2Cl_2 solutions with $[^nBu_4N][PF_6]$ supporting electrolyte, and scan rate of 0.1 V s^{-1} (ir = irreversible; qr = quasi-reversible).

Compound	$E_{1/2}^{ox}$ / V	$E_{1/2}^{red}$ / V	$\Delta E_{1/2}$ / V
$[Ir(ppy)_2(tpy)][PF_6]$	$+0.90^{ir}$	-1.82^{qr}	2.72
$[Ir(dmppz)_2(tpy)][PF_6]$	$+0.82^{ir}$	-1.87^{qr}	2.69
$[Ir(ppy)_2(\mathbf{4})][PF_6]$	$+0.88^{ir}$	-1.71^{qr}	2.59
$[Ir(dmppz)_2(\mathbf{4})][PF_6]$	$+0.79^{qr}$	-1.71^{qr}	2.50
$[Ir(dmppz)_2(\mathbf{5})][PF_6]_2$	$+0.88^{qr}$	-1.30^{qr}, -2.07^{ir}	2.18

The $\Delta E_{1/2}$ values of the complexes are in accord with the emission maxima, except $[Ir(dmppz)_2(\mathbf{5})][PF_6]_2$. The smaller this value, the more red-shifted is the emission maximum of the complex. Comparison with an iridium(III) compound with the emission maximum at 656 nm and the corresponding $\Delta E_{1/2}$ of 2.23 V shows that the measured cyclic voltammetric values are in line with their results.4 A second oxidation around +1 V is observed in all five complexes. It appears to be reasonable to assume that this originates from the oxidation of chloride ion.

5.7. Device performances

The photo- and electroluminescent properties of the four red emitting complexes have been tested in devices (iTMC:$[BMIM][PF_6]$ 4:1, see Table 5.3). Unfortunately, not all performed in devices under an applied bias. The photoluminescence emission maxima are comparable with the solution emission maxima of the four red-emitting complexes. Under applied current (2 mA), only $[Ir(ppy)_2(tpy)][PF_6]$ and $[Ir(dmppz)_2(tpy)][PF_6]$ exhibited electroluminescent behaviour. For $[Ir(ppy)_2(\mathbf{4})][PF_6]$ a higher current (4 mA) had to be applied and the emission maximum was strongly red-shifted compared to the EL of the other two complexes (see Figure 5.18).

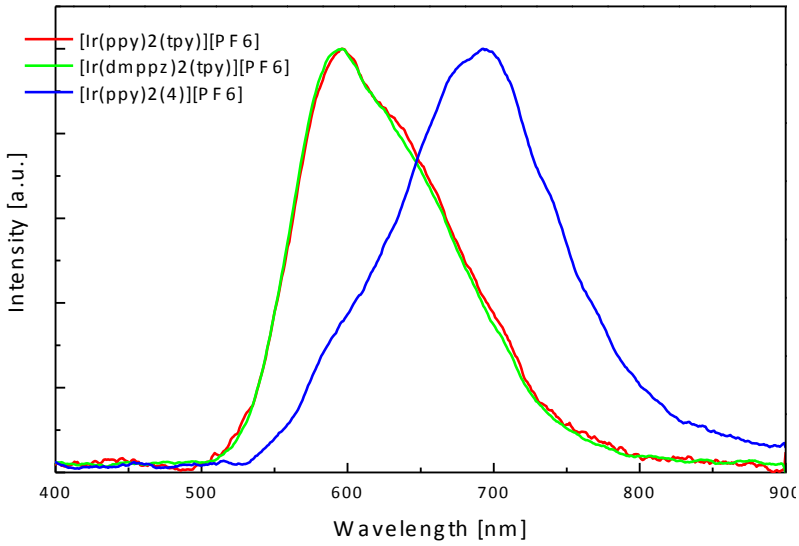

Figure 5.18 Electroluminescence spectra of the complexes $[Ir(ppy)_2(tpy)][PF_6]$, $[Ir(dmppz)_2(tpy)][PF_6]$ and $[Ir(ppy)_2(4)][PF_6]$.

This is often observed and still not fully explained (see Section 4.6). The photoluminescent quantum yields are in agreement of the device performances (e.g. EQE, Table 5.3), but overall the EQEs are very low.

Table 5.3 Device performances of the complexes. *: measured under a current of 4 mA (instead of 2 mA).

iTMC	PL λ_{max}	Solid state PLQY	turn on time t_{on}	EL λ_{max}	EQE
$[Ir(ppy)_2(tpy)][PF_6]$	590 nm	11.8%	<1min	598 nm	<0.1%
$[Ir(dmppz)_2(tpy)][PF_6]$	597 nm	8.7%	30 min	600 nm	<0.1%
$[Ir(ppy)_2(\mathbf{4})][PF_6]$	641 nm	4.8%	--	695 nm*	--
$[Ir(dmppz)_2(\mathbf{4})][PF_6]$	637 nm	6.6%	--	--	--

5.8. Conclusion and outlook

The synthesis and characterization of five complexes containing tpy-based ancillary ligands was successful. The combined modification of the cyclometallating ligand by the change of pyridine to dimethylpyrazole and the extension of the aromatic system going from a bpy to a tpy ligand shifted the PL emission maxima of the complexes to the red region of the visible spectrum. The introduction of a charge on ligand **4** through methylation of the 4'-pyridyl ring, did not yield a further red-shift of the emission maximum.

Crystal structures of all compounds were determined and confirm the intramolecular face-to-face π-stacking interaction of the pendant pyridine ring, similar to that seen with a pendant phenyl ring in iridium(III) complexes incorporating pbpy derivatives (see Chapter 4).

In addition, the free nitrogen of the pendant pyridine ring undergoes a hydrogen bridge to the proton at the 6 position of the pyridine ring of one of the cyclometallating ligands.

The four orange-red emitting complexes have been sent to Valencia for further investigation. Unfortunately only two of the complexes exhibited electroluminescent behaviour. Therefore further investigation on these complexes or similar red emitting compounds is needed.

5.9. Experimental

5.9.1. $[Ir(ppy)_2(tpy)][PF_6]$

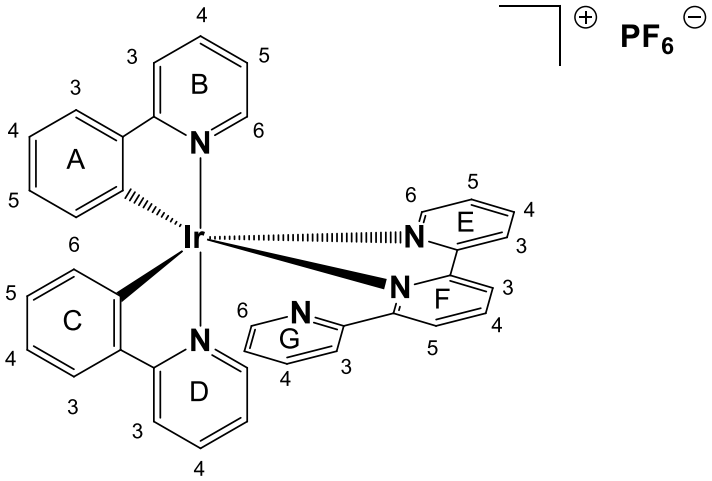

A yellow suspension of $[Ir_2(ppy)_4(\mu\text{-}Cl)_2]$ (100.0 mg, 0.0933 mmol) and 2,2':6',2''-terpyridine (43.8 mg, 0.188 mmol) in methanol (15 mL) was heated in a microwave reactor for 30 minutes at 120°C (P = 13 bar). The orange solution was then cooled to room temperature, and solid NH_4PF_6 (excess) was added. The mixture was stirred for 30 minutes at room temperature and then evaporated to dryness. The crude material was purified by column chromatography (Merck aluminium oxide 90; CH_2Cl_2 changing to CH_2Cl_2:MeOH = 100:5). The solid was redissolved in dichloromethane with some methanol and overlayered with diethyl ether for recrystallization. $[Ir(ppy)_2(tpy)][PF_6]$ was isolated as an orange solid (78.4 mg, 0.0892 mmol, 47.6%).^{1}*H NMR* (500 MHz, CD_2Cl_2, 298 K) δ/ppm 8.87 (s, 1H, H^{B6}), 8.54 (m, 2H, H^{F3+E3}), 8.21 (d, *J* = 4.6 Hz, 1H, H^{G6}), 8.22 – 8.11 (m, 2H, H^{F4+E4}), 7.91 – 7.86 (m, 1H, H^{B3}), 7.84 (d, *J* = 7.9 Hz, 1H, H^{D3}), 7.81 (ddd, *J* = 8.5, 7.7, 1.6 Hz, 1H, H^{B4}), 7.81 – 7.74 (m, 2H, H^{D4+E6}), 7.62 (dd, *J* = 7.8, 1.2 Hz, 1H, H^{A3}), 7.45 (dd, *J* = 7.7, 1.2 Hz, 1H, H^{F5}), 7.39 (m, 1H, H^{D6+E5}), 7.34 (dd, *J* = 7.8, 1.2 Hz, 1H, H^{C3}), 7.18 – 7.11 (m, 1H, H^{B5}), 7.12 (td, *J* = 7.7, 1.7 Hz, 1H, H^{G4}), 7.01 – 6.93 (m, 2H, H^{A4+D5}), 6.92 (ddd, *J* = 7.6, 4.9, 1.0 Hz, 1H, H^{G5}), 6.76 (td, *J* = 7.5, 1.4 Hz, 1H, H^{A5}), 6.67 – 6.60 (m, 1H, H^{C4}), 6.53 (d, *J* = 7.7 Hz, 1H, H^{G3}), 6.33 (td, *J* = 7.5, 1.3 Hz, 1H, H^{C5}), 5.89 (dd, *J* = 7.7, 0.9 Hz, 1H, H^{A6}), 5.47 – 5.44 (m, 1H, H^{C6}). ^{13}*C NMR* (126 MHz, CD_2Cl_2, 298 K) δ/ppm 168.7 (C^{D2}), 167.0 (C^{B2}), 163.4 (C^{F6}), 157.5 (C^{E2}), 157.4 (C^{F2}), 156.4 (C^{G2}), 152.9 (C^{B6}), 150.9 (C^{E6}), 150.4 (C^{C1}), 148.7 (C^{G6}), 148.4 (C^{D6}), 146.7 (C^{A1}), 143.6 (C^{A2}), 142.9 (C^{C2}), 140.4 (C^{F4}), 139.9 (C^{E4}), 138.7 (C^{D4}), 138.6 (C^{B4}), 136.9 (C^{G4}), 132.9 (C^{C6}), 131.1 (C^{A6}), 131.0 (C^{A5}), 130.5 (C^{C5}), 129.5 (C^{F5}), 128.2 (C^{E5}), 125.8 (C^{E3}), 125.2 (C^{A3}), 124.7 (C^{G5}), 124.6 (C^{F3}), 124.4 (C^{C3}), 123.3 (C^{B5}), 123.2 (2C, C^{A4+D5}), 123.1 (C^{G3}), 121.3 (C^{C4}), 119.9 (C^{D3}), 119.8 (C^{B3}). *IR* (solid, ν/cm^{-1}): 3090 (w), 2921 (w), 2852 (w), 2350 (w), 1778 (w), 1608 (m), 1583 (m), 1478 (m), 1452 (m), 1420 (m), 1317 (w), 1270 (w), 1155 (s), 1137 (s), 1065 (w), 1030 (w), 991 (w), 955 (w), 886 (w), 836 (s), 825 (s), 775 (m), 757 (s), 739 (m), 729 (m), 722 (m), 697 (m), 630 (m), 602 (s). *MS* (ESI, m/z): 734.2 $[M\text{-}PF_6]^+$ (calc. 734.2). *UV-Vis* λ / nm (ε / $dm^3\ mol^{-1}\ cm^{-1}$) (CH_2Cl_2, 2.50×10^{-5} mol dm^{-3}): 261 (48'700), 375 (6'100). *Luminescence* (CH_2Cl_2, c = 2.50 x 10^{-5} mol dm^{-3}, λ_{ex} = 260 nm): λ_{em} = 590 nm. *Quantum yield* (CH_2Cl_2, degassed with argon, λ_{ex} = 255 nm, integration range: 540 – 800 nm): 0.017. *Elem. Anal.* calcd. for

$C_{37}H_{27}N_5IrPF_6.0.25H_2O$ (883.33) C 50.31, H 3.14, N, 7.93; found C 50.31, H 3.16, N 7.97. *Electrochemistry* vs. Fc/Fc^+: E_1^{ox}: +0.90 V/ir, E_1^{red}: -1.89 V/-1.74[q] V.

5.9.2. [Ir(dmppz)$_2$(tpy)][PF$_6$]

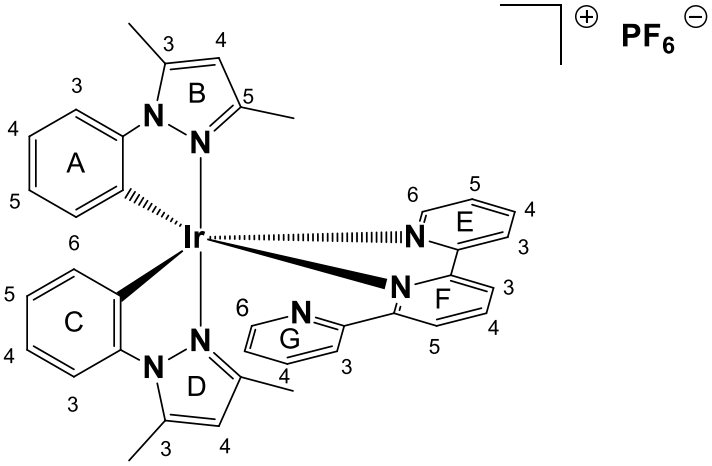

A yellow suspension of $[Ir_2(dmppz)_4(\mu\text{-}Cl)_2]$ (114.0 mg, 0.100 mmol) and 2,2':6',2''-terpyridine (46.9 mg, 0.201 mmol) in methanol (15 mL) was heated in a microwave reactor for 1 hour at 120°C (P = 14 bar). The orange solution was then cooled to room temperature, and solid NH_4PF_6 (excess) was added. The mixture was stirred for 1 hour at room temperature and then evaporated to dryness. The crude material was purified by column chromatography (Merck aluminium oxide 90; CH_2Cl_2 changing to CH_2Cl_2:MeOH = 100:5). $[Ir(dmppz)_2(tpy)][PF_6]$ was isolated as an orange solid (179.2 mg, 196.2 mmol, 98.1%). *^{1}H NMR* (500 MHz, CD_2Cl_2, 298 K) δ/ppm 8.55 (dd, *J* = 8.2, 1.3 Hz, 1H, H^{F3}), 8.51 (d, *J* = 8.2 Hz, 1H, H^{E3}), 8.24 (t, *J* = 7.9 Hz, 1H, H^{F4}), 8.11 – 8.06 (m, 2H, H^{E4+G6}), 7.76 (ddd, *J* = 5.5, 1.6, 0.7 Hz, 1H, H^{E6}), 7.48 (dd, *J* = 7.7, 1.3 Hz, 1H, H^{F5}), 7.35 (ddd, *J* = 7.6, 5.5, 1.2 Hz, 1H, H^{E5}), 7.29 (dd, *J* = 8.2, 1.0 Hz, 1H, H^{A3}), 7.14 (td, *J* = 7.7, 1.7 Hz, 1H, H^{G4}), 6.97 (ddd, *J* = 8.1, 7.4, 1.4 Hz, 1H, H^{A4}), 6.92 (dd, *J* = 8.2, 0.8 Hz, 1H, H^{C3}), 6.88 – 6.83 (m, 2H, H^{G5}), 6.73 (td, *J* = 7.5, 1.2 Hz, 1H, H^{A5}), 6.57 (ddd, *J* = 8.2, 7.4, 1.4 Hz, 1H, H^{C4}), 6.42 (td, *J* = 7.4, 1.1 Hz, 1H, H^{C5+G3}), 6.15 (s, 1H, H^{D4}), 6.05 (s, 1H, H^{B4}), 5.99 (dd, *J* = 7.6, 1.4 Hz, 1H, H^{A6}), 5.74 (dd, *J* = 7.5, 1.3 Hz, 1H, H^{C6}), 2.79 (s, 3H, $H^{CH3\text{-}D3}$), 2.69 (s, 3H, $H^{CH3\text{-}B3}$), 1.81 (s, 3H, $H^{CH3\text{-}B5}$), 1.52 (s, 3H, $H^{CH3\text{-}D5}$). *^{13}C NMR* (126 MHz, CD_2Cl_2, 298 K) δ/ppm 164.4 (C^{F6}), 157.8 (C^{F2}), 157.6 (C^{E2}), 154.9 (C^{G2}), 150.8 (C^{B5}), 150.5 (C^{D5}), 150.4 (C^{E6}), 148.9 (C^{G6}), 144.6 (C^{C2}), 144.4 (C^{A2}), 142.0 (C^{B3}), 141.5 (C^{D3}), 140.4 (C^{F4}), 139.7 (C^{E4}), 135.7 (C^{G4}), 134.4 (C^{C6}), 133.2 (C^{C1}), 133.0 (C^{A6}), 130.8 (C^{A1}), 130.3 (C^{F5}), 128.0 (C^{E5}), 126.2 (C^{A5}), 125.3 (C^{E3}), 124.9 (C^{C5}), 124.6 (C^{G5}), 123.9 (2C, C^{A4+F3}), 123.1 (C^{G3}), 121.9 (C^{C4}), 113.2 (C^{A3}), 112.6 (C^{C3}), 110.8 (C^{B4}), 110.5 (C^{D4}), 15.1 ($C^{CH3\text{-}D3}$), 14.8 ($C^{CH3\text{-}B3}$), 12.9 ($C^{CH3\text{-}D5}$), 12.5 ($C^{CH3\text{-}B5}$). *IR* (solid, v/cm^{-1}): 2920 (w), 2366 (w), 1988 (w), 1696 (w), 1604 (w), 1568 (w), 1553 (m), 1471 (m), 1445 (w), 1428 (w), 1397 (w), 1372 (w), 1312 (w), 1296 (w), 1274 (w), 1234 (w), 1192 (w), 1167 (w), 1150 (w), 1122 (w), 1075 (w), 1036 (w), 992 (w), 925 (w), 906 (w), 884 (w), 835 (s), 823 (m), 771 (w), 744 (m), 732 (m), 717 (m), 691 (w), 636 (m). *MS* (ESI, m/z): 768.2 $[M\text{-}PF_6]^+$ (calc. 768.2). *UV-Vis* λ / nm (ε / dm^3 mol^{-1} cm^{-1}) (CH_2Cl_2, 2.50 × 10^{-5} mol dm^{-3}): 250 (53'000), 290 (33'300), 350 (7'200). *Luminescence* (CH_2Cl_2, c = 2.50 x 10^{-5} mol dm^{-}

^{3}, λ_{ex} = 250 nm): λ_{em} = 599 nm. *Elem. Anal*. calcd. for $C_{37}H_{33}N_7IrPF_6 \cdot 0.5H_2O$ (921.89) C 48.20, H 3.72, N, 10.64; found C 48.15, H 3.60, N 10.55. *Quantum yield* (CH_2Cl_2, degassed with argon, λ_{ex} = 250 nm, integration range: 520 – 800 nm): 0.075. *Electrochemistry* vs. Fc/Fc^+: E_1^{ox}: +0.82 V/ir, E_1^{red}: -1.95 V/-1.78^{q} V.

5.9.3. [Ir(ppy)$_2$(4)][PF$_6$]

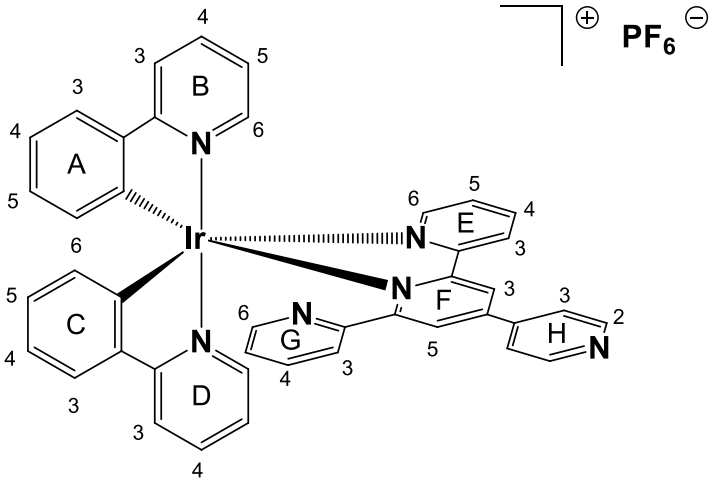

A yellow suspension of $[Ir_2(ppy)_4(\mu\text{-}Cl)_2]$ (107.6 mg, 0.100 mmol) and 4'-pyridine-2,2':6',2''-terpyridine (62.4 mg, 0.201 mmol) in methanol (15 mL) was heated in a microwave reactor for 30 minutes at 120°C (P = 14 bar). The red solution was then cooled to room temperature, and solid NH_4PF_6 (excess) was added. The mixture was stirred for 1 hour at room temperature, filtered and washed with water (3 x 25 mL) and diethyl ether (3 x 25 mL). The red solid was redissolved in dichloromethane with some methanol and overlayered with n-hexane for recrystallization twice. After washing with diethyl ether [Ir(ppy)$_2$(**4**)][PF$_6$] was isolated as a red solid (145 mg, 0.152 mmol, 76.1%). *^{1}H NMR* (500 MHz, CD_2Cl_2, 298 K) δ/ppm 8.94 (d, *J* = 4.3 Hz, 1H, H^{B6}), 8.80 (d, *J* = 2.0 Hz, 1H, H^{F3}), 8.79 (dd, *J* = 4.5, 1.7 Hz, 2H, H^{H2}), 8.75 (d, *J* = 8.3 Hz, 1H, H^{E3}), 8.25 (d, *J* = 4.4 Hz, 1H, H^{G6}), 8.22 – 8.17 (m, 1H, H^{E4}), 7.91 (ddd, *J* = 8.3, 1.3, 0.7 Hz, 1H, H^{B3}), 7.86 (d, *J* = 7.9 Hz, 1H, H^{D3}), 7.84 – 7.75 (m, 5H, $H^{B4+D4+E6+H3}$), 7.67 (d, *J* = 1.9 Hz, 1H, H^{F5}), 7.64 (dd, *J* = 7.9, 1.2 Hz, 1H, H^{A3}), 7.44 (ddd, *J* = 5.9, 1.2, 0.5 Hz, 1H, H^{D6}), 7.42 (ddd, *J* = 7.6, 5.5, 1.2 Hz, 1H, H^{E5}), 7.37 (dd, *J* = 7.8, 1.1 Hz, 1H, H^{C3}), 7.18 – 7.11 (m, 2H, H^{B5+G4}), 7.02 – 6.92 (m, 3H, $H^{A4+D5+G5}$), 6.77 (td, *J* = 7.5, 1.4 Hz, 1H, H^{A5}), 6.65 (ddd, *J* = 7.8, 7.3, 1.2 Hz, 1H, H^{C4}), 6.60 (d, *J* = 7.7 Hz, 1H, H^{G3}), 6.34 (td, *J* = 7.5, 1.3 Hz, 1H, H^{C5}), 5.90 (dd, *J* = 7.7, 0.8 Hz, 1H, H^{A6}), 5.47 (dd, *J* = 7.6, 0.8 Hz, 1H, H^{C6}). *^{13}C NMR* (126 MHz, CD_2Cl_2, 298 K) δ/ppm 168.6 (C^{D2}), 167.0 (C^{B2}), 164.2 (C^{F6}), 158.6 (C^{F2}), 156.9 (C^{E2}), 156.2 (C^{G2}), 152.9 (C^{B6}), 151.1 (C^{H2}), 150.9 (C^{E6}), 150.3 (C^{C1}), 149.3 (C^{H4}), 148.9 (C^{G6}), 148.5 (C^{D6}), 146.9 (C^{A1}), 143.6 (2C, C^{A2+F4}), 142.9 (C^{C2}), 140.0 (C^{E4}), 138.7, (C^{D4}) 138.6 (C^{B4}), 136.7 (C^{G4}), 132.9 (C^{C6}), 131.1 (C^{A6}), 131.0 (C^{A5}), 130.5 (C^{C5}), 128.5 (C^{E5}), 126.9 (C^{F5}), 126.3 (C^{E3}), 125.2 (C^{A3}), 124.8 (C^{G5}), 124.3 (C^{C3}), 123.4 (2C, C^{A4+B5}), 123.3 (C^{D5}) 123.2 (C^{G3}), 122.2 (C^{H3}), 122.1 (C^{F3}), 121.4 (C^{C4}), 120.0 (C^{D3}), 119.9 (C^{B3}). *IR* (solid, ν/cm^{-1}): 3043 (w), 2344 (w), 1607 (m), 1583 (m), 1535 (w), 1477 (m), 1439 (w), 1419 (m), 1398 (m), 1316 (w), 1270 (w), 1228 (w), 1164 (w), 1065 (w), 1031 (w), 993 (w), 879 (w), 828 (s), 788 (m), 754 (m), 728 (m), 668 (m),

624 (m), 602 (m). *MS* (ESI, m/z): 811.3 $[M\text{-}PF_6]^+$ (calc. 810.9). *UV-Vis* λ/nm (ε / $dm^3\ mol^{-1}\ cm^{-1}$) (CH_2Cl_2, 2.50×10^{-5} mol dm^{-3}): 258 (68'100), 350 (11'400). *Luminescence* (CH_2Cl_2, c = 2.50 x 10^{-5} mol dm^{-3}, λ_{ex} = 250 nm): λ_{em} = 620 and 640 nm. *Quantum yield* (CH_2Cl_2, degassed with argon, λ_{ex} = 260 nm, integration range: 540 – 800 nm): 0.029. *Elem. Anal*. calcd. for $C_{42}H_{32}N_6IrPF_6.H_2O$ (973.9) C 51.80, H 3.31, N, 8.63; found C 51.85, H 3.23, N 8.64. *Electrochemistry* vs. Fc/Fc^+: E_1^{ox}: +0.88 V/irr, E_1^{red}: -1.81 V/-1.60[q] V.

5.9.4. [Ir(dmppz)$_2$(4)][PF$_6$]

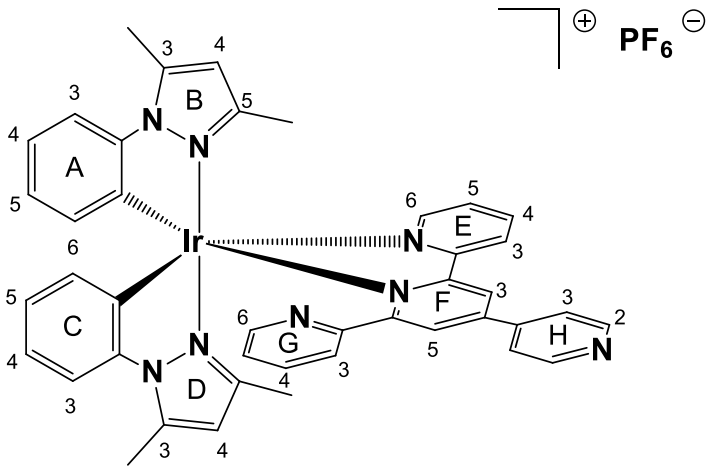

A yellow suspension of $[Ir_2(dmppz)_4(\mu\text{-}Cl)_2]$ (114.0 mg, 0.100 mmol) and 4'-pyridine-2,2':6',2''-terpyridine (62.4 mg, 0.201 mmol) in methanol (15 mL) was heated in a microwave reactor for 30 minutes at 120°C (P = 11 bar). The red solution was then cooled to room temperature, and solid NH_4PF_6 (excess) was added. The mixture was stirred for 30 minutes at room temperature. As no precipitation occurred an excess of $AgPF_6$ was added and stirred for further 30 minutes, followed by evaporation to dryness. The crude material was purified twice by column chromatography (Merck aluminium oxide 90 followed by Fluka Silica 60; CH_2Cl_2 changing to CH_2Cl_2:MeOH = 100:5). $[Ir(dmppz)_2(\mathbf{4})][PF_6]$ was isolated as red solid (135.0 mg, 0.136 mmol, 68.0%). *^{1}H NMR* (500 MHz, CD_2Cl_2, 298 K) δ/ppm 8.84 – 8.82 (m, 2H, H^{H2}), 8.79 (d, *J* = 2.0 Hz, 1H, H^{F3}), 8.72 (d, *J* = 8.2 Hz, 1H, H^{E3}), 8.16 – 8.11 (m, 2H, H^{E4+G6}), 7.84 – 7.81 (m, 2H, H^{H3}), 7.79 (ddd, *J* = 5.5, 1.6, 0.7 Hz, 1H, H^{E6}), 7.72 (d, *J* = 1.9 Hz, 1H, H^{F5}), 7.39 (ddd, *J* = 7.6, 5.5, 1.2 Hz, 1H, H^{E5}), 7.31 (dd, *J* = 8.2, 1.0 Hz, 1H, H^{A3}), 7.16 (td, *J* = 7.7, 1.7 Hz, 1H, H^{G4}), 6.98 (ddd, *J* = 8.2, 7.4, 1.4 Hz, 1H, H^{A4}), 6.93 (dd, *J* = 8.2, 0.8 Hz, 1H, H^{C3}), 6.88 (ddd, *J* = 7.7, 4.9, 1.1 Hz, 1H, H^{G5}), 6.74 (td, *J* = 7.5, 1.2 Hz, 1H, H^{A5}), 6.58 (ddd, *J* = 8.2, 7.4, 1.4 Hz, 1H, H^{C4}), 6.50 (s, 1H, H^{G3}), 6.44 (td, *J* = 7.4, 1.1 Hz, 1H, H^{C5}), 6.15 (s, 1H, H^{D4}), 6.06 (s, 1H, H^{B4}), 6.00 (dd, *J* = 7.6, 1.4 Hz, 1H, H^{A6}), 5.76 (dd, *J* = 7.5, 1.3 Hz, 1H, H^{C6}), 2.79 (s, 3H, $H^{CH3\text{-}D3}$), 2.70 (s, 3H, $H^{CH3\text{-}B3}$), 1.90 (s, 3H, $H^{CH3\text{-}B5}$), 1.54 (s, 3H, $H^{CH3\text{-}D5}$). *^{13}C NMR* (126 MHz, CD_2Cl_2, 298 K) δ/ppm 165.1 (C^{F6}), 159.0 (C^{F2}), 157.3 (C^{E2}), 154.7 (C^{G2}), 151.4 (C^{H2}), 150.8 (C^{B5}), 150.6 (C^{E6}), 150.5 (C^{D5}), 149.4 (C^{H4}), 149.1 (C^{G6}), 144.6 (C^{C2}), 144.4 (C^{A2}), 143.5 (C^{F4}), 142.1 (C^{B3}), 141.5 (C^{D3}), 139.9 (C^{E4}), 135.7 (C^{G4}), 134.5 (C^{C6}), 133.2 (C^{C1}), 133.0 (C^{A6}), 130.8 (C^{A1})2, 128.3 (C^{E5}), 127.7 (C^{F5}), 126.3 (C^{A5}), 125.6 (C^{E3}), 125.0 (C^{C5}), 124.8 (C^{G5}), 124.0 (C^{A4}), 123.2 (C^{G3}), 122.1 (C^{H3}), 122.0 (C^{C4}), 121.4 (C^{F3}), 113.3 (C^{A3}), 112.6 (C^{C3}), 110.9 (C^{B4}), 110.5 (C^{D4}), 15.1 ($C^{CH3\text{-}D3}$), 14.8 ($C^{CH3\text{-}B3}$), 13.0 ($C^{CH3\text{-}D5}$), 12.8 ($C^{CH3\text{-}B5}$). *IR* (solid, ν/cm^{-1}): 3131 (w), 3054 (w), 2162 (w),

1700 (m), 1585 (m), 1549 (m), 1541 (m), 1471 (s), 1442 (m), 1420 (m), 1398 (s), 1373 (m), 1276 (m), 1263 (m), 1239 (m), 1168 (w), 1143 (m), 1068 (w), 1037 (m), 995 (m), 903 (m), 860 (m), 830 (s), 820 (s), 792 (s), 786 (s), 753 (s), 742 (s), 730 (s), 717 (s), 703 (s), 694 (s), 659 (m), 622 (s), 612 (s), 608 (s). *MS* (ESI, m/z): 845.3 $[M\text{-}PF_6]^+$ (calc. 845.3). *UV-Vis* λ/nm (ε / dm^3 mol^{-1} cm^{-1}) (CH_2Cl_2, 5.00 x 10^{-5} mol dm^{-3}): 253 (64'600), 320 (20'900), 350 (8'400). *Luminescence* (CH_2Cl_2, c = 2.50 x 10^{-5} mol dm^{-3}, λ_{ex} = 256 nm): λ_{em} = 642 nm. *Quantum yield* (CH_2Cl_2, degassed with argon, λ_{ex} = 250 nm, integration range: 520 – 810 nm): 0.062. *Elem. Anal*. calcd. for $C_{42}H_{36}N_8IrPF_6.0.5CH_2Cl_2$ (1032.44) C 48.44, H 3.61, N, 10.85; found C 48.64, H 3.53, N 10.53. *Electrochemistry* vs. Fc/Fc^+: E_1^{ox}: +0.86 V/+0.71^q V, E_1^{red}: -1.79 V/-1.63^q V.

5.9.5. $[Ir(dmppz)_2(5)][PF_6]_2$

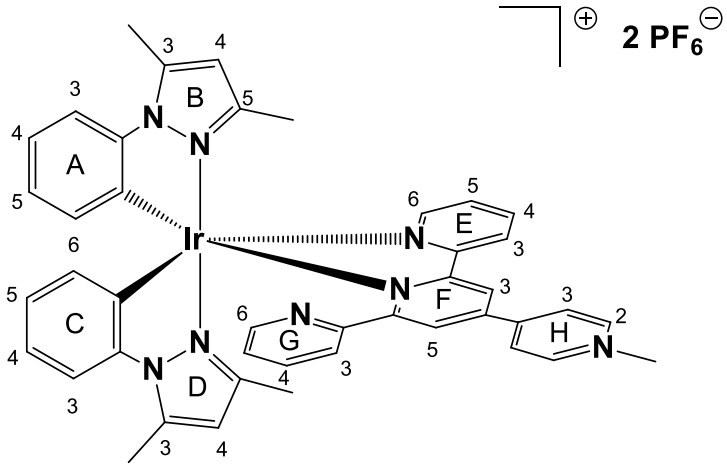

A yellow suspension of $[Ir_2(dmppz)_4(\mu\text{-}Cl)_2]$ (114.0 mg, 0.100 mmol) and 4'-methyl-pyridine-2,2':6',2''-terpyridine hexafluoridophosphate (98.8 mg, 0.21 mmol) in methanol (15 mL) was heated in a microwave reactor for 90 minutes at 120°C (P = 14 bar). The red solution was then cooled to room temperature, and solid NH_4PF_6 (excess) was added. The mixture was stirred for 30 minutes at room temperature and the red precipitate was collected. The crude material was purified twice by column chromatography (Merck aluminium oxide 90 followed by Fluka Silica 60; CH_2Cl_2 changing to CH_2Cl_2:MeOH = 100:4). $[Ir(dmppz)_2(\mathbf{5})][PF_6]_2$ was isolated as red solid (124.0 mg, 0.127 mmol, 63.6%). *^1H NMR* (500 MHz, CD_2Cl_2, 298 K) δ/ppm 9.03 (d, *J* = 2.0 Hz, 1H, H^{F3}), 8.88 (d, *J* = 8.3 Hz, 1H, H^{E3}), 8.80 (d, *J* = 6.9 Hz, 2H, H^{H2}), 8.60 (d, *J* = 7.0 Hz, 2H, H^{H3}), 8.14 (dq, *J* = 4.9, 1.3 Hz, 2H, H^{E4+G6}), 7.85 (d, *J* = 1.9 Hz, 1H, H^{F5}), 7.79 (m, 1H, H^{E6}), 7.39 (ddd, *J* = 7.6, 5.5, 1.1 Hz, 1H, H^{E5}), 7.32 (dd, *J* = 8.2, 1.0 Hz, 1H, H^{A3}), 7.22 (m, 1H, H^{G4}), 6.98 (m, 1H, H^{A4}), 6.92 (m, 2H, H^{C3+G5}), 6.73 (td, *J* = 7.5, 1.1 Hz, 1H, H^{A5}), 6.63 (s, 1H, H^{G3}), 6.59 (m, 1H, H^{C4}), 6.45 (td, *J* = 7.4, 1.1 Hz, 1H, H^{C5}), 6.14 (s, 1H, H^{D4}), 6.07 (s, 1H, H^{B4}), 5.99 (dd, *J* = 7.6, 1.3 Hz, 1H, H^{A6}), 5.76 (dd, *J* = 7.5, 1.3 Hz, 1H, H^{C6}), 4.47 (s, 3H, $H^{CH3\text{-}H1}$), 2.78 (s, 3H, $H^{CH3\text{-}D3}$), 2.71 (s, 3H, $H^{CH3\text{-}B3}$) , 1.93 (s, 3H, $H^{CH3\text{-}B5}$), 1.53 (s, 3H, $H^{CH3\text{-}D5}$). *^{13}C NMR* (126 MHz, CD_2Cl_2, 298 K) δ/ppm 165.5 (C^{F6}), 160.0 (C^{F2}), 156.9 (C^{E2}), 154.0 (C^{G2}),152.1 (C^{H4}), 151.1 (C^{B5}), 150.6 (C^{D5}), 150.4 (C^{E6}), 149.1 (C^{G6}), 146.3 (C^{H2}), 144.7 (C^{F4}), 144.5 (C^{C2}), 144.3 (C^{A2}), 142.1 (C^{B3}), 141.6 (C^{D3}), 140.1 (C^{E4}), 136.0 (C^{G4}), 134.6 (C^{C6}), 133.0 (2C, C^{A6+C1}), 130.4 (C^{A1}), 128.6 (C^{E5}), 128.1 (C^{F5}), 127.6 (C^{H3}), 126.5 (C^{E3}), 126.3 (C^{A5}), 125.1 (2C, C^{C5+G5}),

124.1 (C^{A4}), 123.4 (C^{G3}), 122.2 (C^{C4}), 122.1 (C^{F3}), 113.3 (C^{A3}), 112.6 (C^{C3}), 110.9 (C^{B4}), 110.6 (C^{D4}), 49.4 ($C^{CH3\text{-}H1}$), 15.2 ($C^{CH3\text{-}D3}$), 14.8 ($C^{CH3\text{-}B3}$), 13.1 ($C^{CH3\text{-}B5}$), 13.0 ($C^{CH3\text{-}D5}$). *IR* (solid, v/cm^{-1}): 3657 (w), 3131 (w), 3054 (w), 1646 (w), 1617 (w), 1570 (w), 1553 (w), 1528 (w), 1471 (s), 1444 (w), 1414 (w), 1398 (w), 1375 (w), 1337 (w), 1276 (w), 1270 (w), 1225 (w), 1195 (w), 1146 (w), 1122 (w), 1093 (w), 1059 (w), 1035 (w), 993 (w), 822 (s), 816 (s), 789 (s), 773 (s), 743 (s), 731 (w), 719 (w), 692 (w), 657 (w), 601 (s). *MS* (ESI, m/z): 1005.3 $[M\text{-}PF_6]^+$ (calc. 1005.3), 860.3 $[M\text{-}2PF_6]^+$ (calc. 860.3), 535.2 $[Ir(dmppz)_2]^+$ (calc. 535.2), 430.2 $[M\text{-}2PF_6]^{2+}$ (calc. 430.2). *UV-Vis* λ/nm (ε / dm^3 mol^{-1} cm^{-1}) (CH_2Cl_2, 2.50 × 10^{-5} mol dm^{-3}): 256 (64'000), 315 (19'000), 400 (6'000). *Luminescence* (CH_2Cl_2, c = 2.50 x 10^{-5} mol dm^{-3}, λ_{ex} = 245 nm): λ_{em} = 359 nm. *Quantum yield* (CH_2Cl_2, degassed with argon, λ_{ex} = 255 nm, integration range: 520 – 800 nm): 0.01. *Elem. Anal.* calcd. For $C_{43}H_{39}IrN_8P_2F_{12}.0.5NH_4Cl$ (1176.72) C 43.89, H 3.51, N 10.12; found C 43.52, H 3.52, N 10.34. *Electrochemistry*: E_1^{ox}: +0.88 V/irr, E_1^{red}: -1.37 V/1.23^q V, E_2^{red}: -2.07 V/irr.

[1] F. Neve, A. Crispini, S. Campagna and S. Serroni*, Inorg. Chem*., 1999, **38**, 2250.

[2] L. He, J. Qiao, L. Duan, G. F. Dong, D. Q. Zhang, L. D. Wang, Y. Qiu, *Adv. Funct. Mater.,* 2009, **19***,* 2950.

[3] R. D. Costa, F. J. Cespedes-Guirao, E. Ortí, H. J. Bolink, J. Gierschner, F. Fernandez-Lazaro, A. Sastre-Santos, *Chem. Commun.,* 2009, 3886.

[4] H.-C. Su, H.-F. Chen, F.-C. Fang, C.-C. Liu, C.-C. Wu, K.-T. Wong, Y.-H. Liu, S.-M. Peng, *J. Am. Chem. Soc.,* 2008*,* **130**, 3413.

[5] J. L. Rodríguez-Redondo, R. D. Costa, E. Ortí, A. Sastre-Santos, H. J. Bolink, F. Fernández-Lázaro, *Dalton Trans.*, 2009, 9787.

[6] See for example: F. Neve, A. Crispini, S. Campagna and S. Serroni*, Inorg. Chem*., 1999, **38**, 2250 and references cited therein.

[7] H. J. Bolink, E. Coronado, R. D. Costa, E. Ortí, M. Sessolo, S. Graber, K. Doyle, M. Neuburger, C. E. Housecroft, E. C. Constable, *Adv. Mater.*, 2008, **20**, 3910.

[8] J. McMurtrie, I. Dance, *Cryst. Eng. Comm.*, 2005, **7**, 35, 216.

[9] M. L. Scudder, H. A. Goodwin, I. G. Dance, *New J. Chem.*, 1999, **23**, 695.

[10] E. C. Constable, K. Harris, C. E. Housecroft, M. Neuburger, J. A. Zampese, *CrystEngComm.,* 2010, **12**, 2949.

[11] C. Janiak, *J. Chem. Soc., Dalton Trans.,* 2000, 3885.

[12] A. B. Tamayo, S. Garon, T. Sajoto, P. I. Djurovich, I. M. Tsyba, R. Bau, M. E. Thompson, *Inorg. Chem.*, 2005, **44**, 8723.

[13] J. L. Rodríguez-Redondo, R. D. Costa, E. Ortí, A. Sastre-Santos, H. J. Bolink, F. Fernández-Lázaro, *Dalton Trans.*, 2009, 9787.

[14] F. Kessler, R. D. Costa, D. Di Ceso, R. Scopelliti, E. Ortí, H. J. Bolink, S. Meier, W. Sarfert, M. Grätzel, Md. K. Nazeeruddin, E. Baranoff, *Dalton Trans.*, 2012, **41**, 180.

[15] R. D. Costa, E. Ortí, H. J. Bolink, S. Graber, C. E. Housecroft, E. C. Constable, *Adv. Funct. Mater.*, 2010, **20**, 1511.

Chapter 6

6. Iridium(III) complexes with further terpyridine ligands

6.1. Introduction

In this chapter, the studies from the previous chapter (see Chapter 5)[1] are extended. In Chapter 5, tpy and some of its derivatives were used as ancillary ligands. In this chapter, other tpy ligands have been used to synthesize new iridium(III) complexes. The cyclometallating ligands are $[ppy]^-$ for all four complexes discussed in this chapter.

The ancillary ligands consist of a tpy unit with a phenyl ring at the 4'-position. On the *para*-position of the phenyl ring, there are different heteroatom groups attached (see Scheme 6.1). The introduction of the phenyl ring extends the π-conjugation of the ancillary ligand and should therefore yield a red-shift of the emission maximum of the complexes. Furthermore, the influence of the heteroatom groups will be investigated in order to determine the effect on the photophysical and electrochemical properties of the iridium(III) complexes. In addition, the complexes have been used to prepare LEC devices and their properties under a LEC configuration have been investigated.

6.2. Results and discussion

Four complexes $[Ir(ppy)_2(\mathbf{6})][PF_6]$, $[Ir(ppy)_2(\mathbf{7})][PF_6]$, $[Ir(ppy)_2(\mathbf{8})][PF_6]$ and $[Ir(ppy)_2(\mathbf{9})][PF_6]$ were prepared by treating a dichlorido bridged iridium(III) dimer with two equivalents of an N^N ligand (Scheme 6.1).[2] The reactions were performed in a microwave reactor followed by precipitation with ammonium hexafluoridophosphate and silver hexafluoridophosphate, and the purification was done by recrystallization or column chromatography.

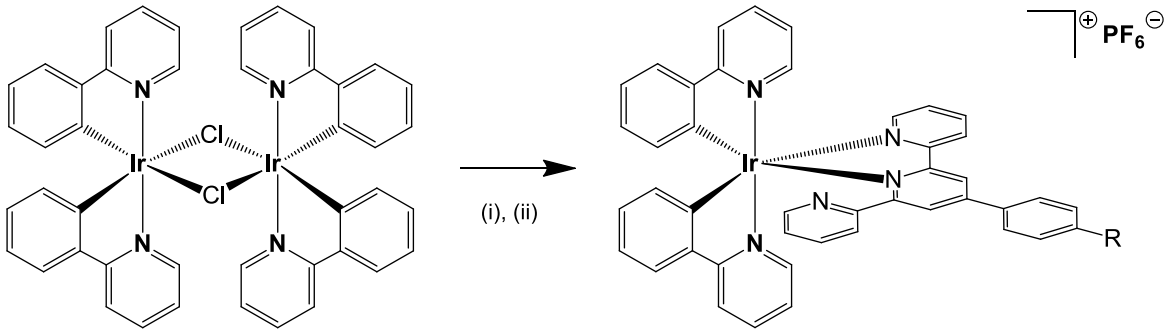

$[Ir_2(ppy)_4(\mu\text{-}Cl)_2]$

$[Ir(ppy)_2(\mathbf{6})][PF_6]$: R = NH_2
$[Ir(ppy)_2(\mathbf{7})][PF_6]$: R = OCH_3
$[Ir(ppy)_2(\mathbf{8})][PF_6]$: R = SCH_3
$[Ir(ppy)_2(\mathbf{9})][PF_6]$: R = OH

Scheme 6.1 Syntheses of the complexes described in this chapter. Conditions: (i) ligand 6, 7, 8 or 9, MeOH, microwave (2hr, 120 °C); (ii) $[NH_4][PF_6]$ (30 – 60 min).

The yields ranged from 79.5% ([Ir(ppy)$_2$(**9**)][PF$_6$]) to 97.2% ([Ir(ppy)$_2$(**6**)][PF$_6$]). The ESI mass spectrum of each of the complexes showed a peak that was assigned to the [M – PF$_6$]$^+$ ion and the observed isotope patterns were in accordance with those simulated.

The NMR spectroscopic assignments were done using routine 1D and 2D techniques (COSY, NOESY, HMBC and HMQC). Due to the presence of pendant pyridine rings, the C^N ligands appear non-equivalent for all complexes. This leads to very similar ^{1}H and ^{13}C NMR spectra to those already discussed in Chapter 5 (see Section 5.3). Full assignments are given in the experimental section.

6.3. Solid state structures

Table 6.1 Crystallographic data for complexes [Ir(ppy)$_2$(6)][PF$_6$], [Ir(ppy)$_2$(7)][PF$_6$], [Ir(ppy)$_2$(8)][PF$_6$] and [Ir(ppy)$_2$(9)][PF$_6$].

Compound	[Ir(ppy)$_2$(**6**)][PF$_6$] .2CH$_2$Cl$_2$	{4[Ir(ppy)$_2$(**7**)][PF$_6$]} .2Et$_2$O.CH$_3$CN	2{[Ir(ppy)$_2$(**8**)][PF$_6$]} .CH$_3$CN.2H$_2$O	[Ir(ppy)$_2$(**9**)][PF$_6$] .2CH$_2$Cl$_2$
Formula	$C_{45}H_{36}Cl_4F_6IrN_6P$	$C_{184}H_{148}F_{24}Ir_4N_{22}O_5P_4$	$C_{90}H_{73}F_{12}Ir_2N_{11}O_2P_2S_2$	$C_{45}H_{36}Cl_4F_6IrN_6P$
Formula weight / g mol^{-1}	1139.79	4096.00	2079.12	12414.77
Crystal colour and habit	orange plate	yellow block	orange block	yellow block
Crystal system	monoclinic	monoclinic	monoclinic	monoclinic
Space group	*P*2$_1$/*n*	*C*$_2$/*c*	*P*2$_1$/*n*	*P*2$_1$/*n*
a, *b*, *c* / Å	10.2803(4)	55.632(4)	14.5443(10)	13.4211(15)
	12.4470(4)	10.5213(11)	14.7612(10)	53.159(6)
	33.7717(12)	34.013(2)	19.8943(14)	17.941(2)
α, *β*, *γ*/ ^{o}	90	90	90	90
	93.369(2)	124.848(4)	104.707(4)	108.3520(10)
	90	90	90	90
U / Å^3	4313.9(3)	16338(2)	4131.2(5)	12149(2)
*D*c / Mg m^{-3}	1.755	1.665	1.668	1.697
Z	4	4	2	1
μ(Mo-Kα) / mm^{-1}	3.448	3.381	3.392	2.350
T/ K	123	173	123	123
Refln. collected (R_{int})	31698 (0.0542)	163250 (0.0969)	134040 (0.0425)	130556 (0.0707)
Unique refln.	8021	20080	12026	30721
Refln. for refinement	6667	18711	10753	21221
Parameters	622	1220	570	1775
Threshold	*I* > 2.0*σ*	*I* > 2.0*σ*	*I* > 2.0*σ*	*I* > 2.0*σ*
*R*1 (*R*1 all data)	0.0476 (0.0673)	0.0286 (0.0320)	0.0194 (0.0247)	0.0658 (0.1034)
*wR*2 (*wR*2 all data)	0.0993 (0.1155)	0.0605 (0.0617)	0.0444 (0.0471)	0.1732 (0.2047)
Goodness of fit	1.151	1.195	1.047	1.099

6.3.1. [Ir(ppy)$_2$(6)][PF$_6$]

X-ray quality crystals of the complex were grown from a solution of CH$_2$Cl$_2$, layered with Et$_2$O by diffusion. The complex crystallizes as [Ir(ppy)$_2$(**6**)][PF$_6$].2CH$_2$Cl$_2$ in the monoclinic centrosymmetric *P*2$_1$/n space group. In the asymmetric unit there is one cation, one anion and two solvent molecules. The atom Ir1 is in an octahedral environment and the N-donors of the two cyclometallating ligands are in a *trans*-arrangement, as expected and already

seen in similar compounds.[4, 5] The two N-donors of the tpy ligand are *trans* to the C-atoms of the cyclometallating phenylpyridine rings. Both cyclometallating C^N ligands are almost planar, with angles between the least squares planes of 2.7 and 4.5°, whereas the angle between the least squares planes of the N^N ligand is 9.4°. The pendant phenyl ring of the tpy ligand is twisted through 64.2° with respect to the bonded pyridine ring. This non-planarity allows the free pyridine ring to undergo intramolecular face-to-face π-stacking with one of the phenyl rings of one of the C^N ligands. The inter-centroid separation is 3.31 Å and the angle between the least squares planes is 10.9°. The distance would make it a very efficient interaction, but the angle is rather large, as discussed by Janiak[3]. Janiak sets the limits for π-stacking interactions to distances up to 3.8 Å between the stacking rings and the tilting angles between the rings have to be below 20°. These values are also very similar to the intramolecular stacking interactions with a pendant phenyl ring[4]. Both enantiomers are in the unit cell and the Λ-$[Ir(ppy)_2(\mathbf{6})]^+$ cation is depicted in Figure 6.1.

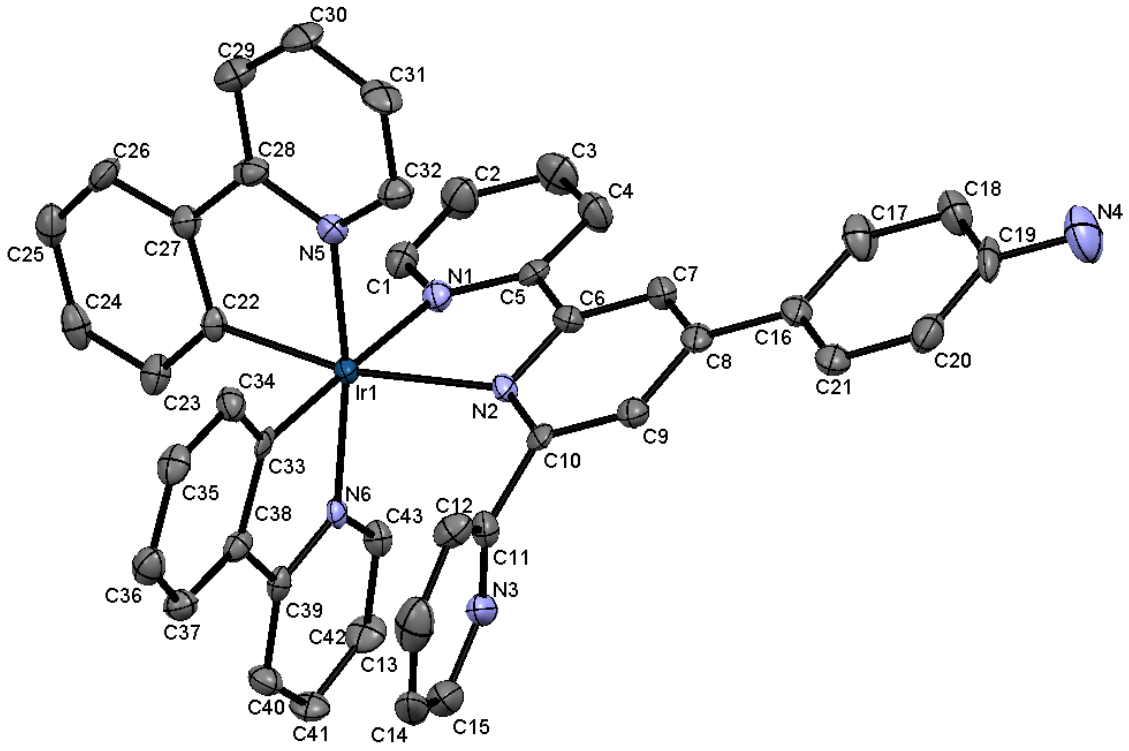

Figure 6.1 Structure of Λ-$[Ir(ppy)_2(6)]^+$ with ellipsoids plotted at 50% probability level; H atoms omitted. Selected bond lengths (in Å) and bond angles (in °): Ir1–C33: 2.012(5), Ir1–C22: 2.013(5), Ir1–N6: 2.039(4), Ir1–N5: 2.057(4), Ir1–N1: 2.153(4), Ir1–N2: 2.204(4); N1–Ir1–N2: 76.0(2), N5–Ir1–C22: 80.5(2), N6–Ir1–C33: 80.3(2).

The crystal packing is dominated by intermolecular face-to-face π-stacking between a Λ- and a Δ-cation. The stacking interaction is between the planar rings, the pyridine ring containing atom N2 and the pendant phenyl ring containing atom C16, with another molecule containing atomes $N2^i$ and $C16^i$ (symmetry code 1 – x, -y, 2 – z). The alignment of the mean squares planes of the stacked rings is parallel (symmetry imposed by an inversion centre) with a separation of 3.36 Å between the planes. The inter-centroid separation is 3.62 Å, making it a very efficient stacking interaction. This packing interaction leads to sheets of chains of Λ- and Δ-cations parallel to the b axis (Figure 6.2).

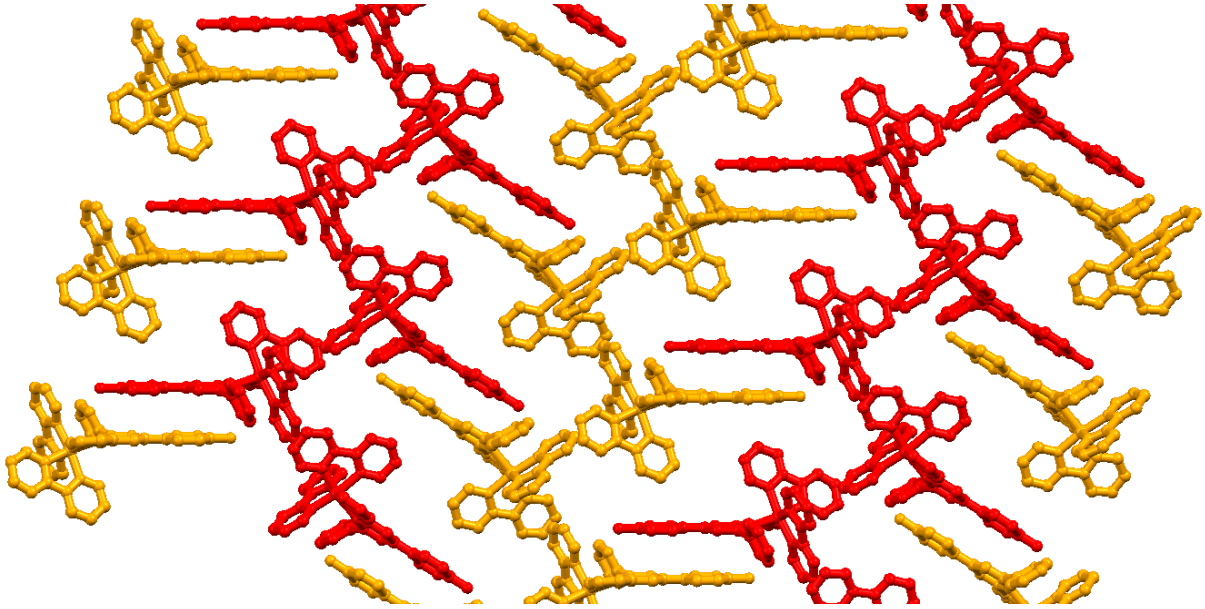

Figure 6.2 Packing interactions between $[Ir(ppy)_2(6)]^+$ cations with different handedness, viewed along the a-axis. Face-to-face π-stacking between the tpy-phenyl rings of cations with Δ- (red) and Λ-forms (orange). The hydrogen atoms, anions and solvent molecules are omitted.

Sandwiched between these sheets are $[PF_6]^-$ anions and CH_2Cl_2 solvent molecules. Each $[PF_6]^-$ anion supports the packing by CH…F hydrogen bonds to five different cations and to one solvent molecule, with F…H distances between 2.15 to 2.67 Å. The free phenyl ring containing atom C16 undergoes a π-interaction with proton H30A^i at a C-H…phenyl ring centroid distance of 2.47 Å. The amino group of the tpy ligand undergoes hydrogen bonding to the pendant pyridine ring of an adjacent cation with a distance of 2.68 Å between H4B and N3^i (symmetry code i = 1 – x, –y, 2 – z). Additionally atom N4 undergoes an interaction with atom H43A^i at a distance of 3.03 Å. The crystal packing is dominated by the following contacts: $CH…F_{anion}$, $CH…\pi_{ligand}$, $N…HC_{ligand}$, $Cl…HC_{ligand}$. The cation, anion and one of the CH_2Cl_2 molecules are ordered, whereas the second solvent molecule is disordered and has been modelled over 3 sites of occupancies 0.5, 0.25 and 0.25.

6.3.2. $[Ir(ppy)_2(7)][PF_6]$

Single crystals were grown over a number of days from a MeCN solution of $[Ir(ppy)_2(\mathbf{7})][PF_6]$ which was layered with Et_2O. The complex crystallizes as $\{4[Ir(ppy)_2(\mathbf{7})][PF_6]\}.2Et_2O.MeCN$ in the monoclinic centrosymmetric space group *C*2/*c*. There are two independent cations (A and B) in the asymmetric unit, both are in an octahedral environment, both are in the Λ-form and the cation B is depicted in Figure 6.3. Cations A and B are very similar, having only minor differences in the environments of the atoms Ir1A and Ir1B. In the unit cell, both enantiomers of both independent cations are present.

For atoms Ir1A and Ir1B the N-donors of the cyclometallating C^N ligand are mutually *trans*. For Ir1A, both C^N ligands are planar with torsion angles between the least squares planes

below 5.9°. The least squares planes of the two coordinated pyridine rings of the tpy ligand are twisted about 13.7°. The pendant pyridine ring is strongly twisted about 64.4°. For Ir1B the values differ a little. Both C^N ligands are planar, with torsion angles between the least squares planes below 3.0°. The least squares planes of the two coordinated pyridine rings of the tpy ligand are twisted about 14.1°. The pendant pyridine ring is strongly twisted about 60.5°.

This strong deviation of planarity within the tpy ligand is similar to that seen in [Ir(ppy)$_2$(**6**)][PF$_6$], and allows the pendant pyridine ring to undergo intramolecular face-to-face π-stacking with the phenyl ring of the cyclometallating [ppy]$^-$ ligand containing atom C34A or C23B, in cation A or B respectively. The twisting angle between the least squares planes are 3.4° or 8.0°, respectively. The inter-centroid distances are 3.49 and 3.42 Å for molecule A and B, respectively, being well in the range discussed by Janiak3 and comparable with [Ir(ppy)$_2$(**6**)][PF$_6$].

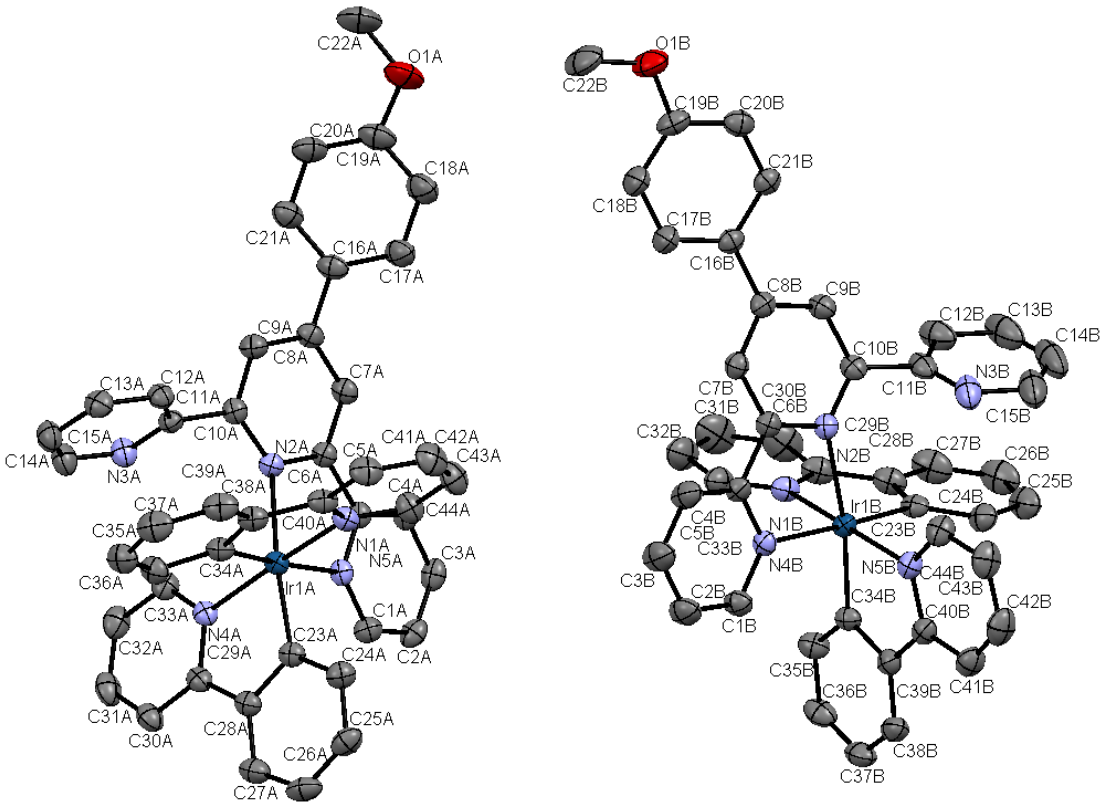

Figure 6.3 Structure of Λ-cations A and B of [Ir(ppy)$_2$(7)]$^+$ with ellipsoids plotted at 50% probability level; H atoms omitted. Selected bond lengths (in Å) and bond angles (in °): Ir1A–C23A: 1.996(3), Ir1A–C34A: 2.015(3), Ir1A–N4A: 2.040(2), Ir1A–N5A: 2.058(2), Ir1A–N1A: 2.122(2), Ir1A–N2A: 2.206(2); N1A–Ir1A–N2A: 76.0(1), N4A–Ir1A–C23A: 80.6(1), N5A–Ir1A–C23A: 80.2(2). Selected bond lengths (in Å) and bond angles (in °): Ir1B–C34B: 2.002(3), Ir1B–C23B: 2.016(3), Ir1B–N5B: 2.041(2), Ir1B–N4B: 2.053(2), Ir1B–N1B: 2.140(2), Ir1B–N2B: 2.211(2); N1B–Ir1B–N2B: 76.2(1), N4B–Ir1B–C23B: 80.4(1), N5B–Ir1B–C34B: 80.5(1).

However, upon examination of the crystal packing, the effect of changing the substituent on the tpy ligand can be seen. By changing the amino group of the tpy ligand to a methoxy group, intermolecular π-stacking interactions of the phenyl ring, as seen in [Ir(ppy)$_2$(**6**)][PF$_6$],

are prevented (see Figure 6.4 and Figure 6.2). This leads to a different arrangement of the cations in the crystal structure.

The crystal packing is dominated by the following interactions. Between two molecules of B the methoxy groups undergo hydrogen bonding with a distance between atoms O1B and H22E^{i} of 2.77 Å (symmetry code i = 1 – x, -1 – y, 1 – z). Additionally there are edge-to-face π-interactions between molecules A and B with the same handedness. Molecule A shows an edge-to-face π-stacking interaction between the phenyl ring of one [ppy]$^-$ ligand containing atom C23A and protons of the phenyl ring of the other [ppy]$^-$ ligand with a C-H41A^{ii}…phenyl ring centroid distance of 2.91 Å (symmetry code ii = 3/2 – x, y + ½, 3/2 – z). Between two molecules of B, protons H27B^{iii} and H30B^{iii} of the [ppy]$^-$ ligand (symmetry code iii = 1 – x, y, 3/2 – z) and the phenyl ring of the tpy ligand containing atom C16B show interaction with a C-H…phenyl ring centroid distance of 3.03 Å. These edge-to-face stacking interactions are very similar to the one discussed in Chapter 5 (see Section 5.4.1 [Ir(ppy)$_2$(tpy)][PF$_6$]). Between the cations, there are anions and solvent molecules undergoing meaningful contacts between cations and anions with H…F distances between 2.26 and 2.66 Å (similar to the previous sections).

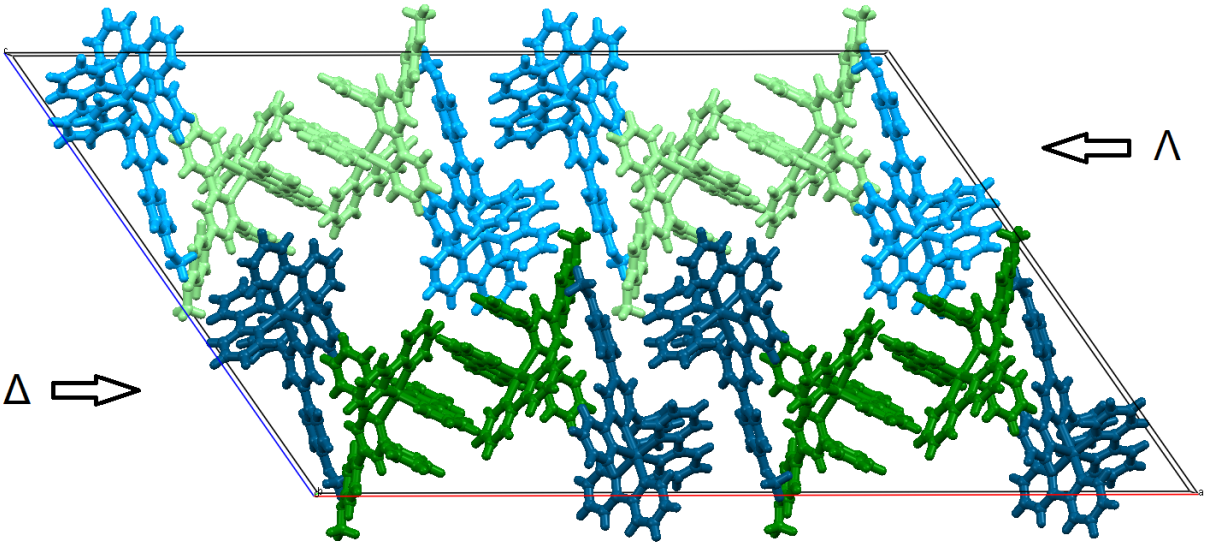

Figure 6.4 Packing interactions in one unit cell of [Ir(ppy)$_2$(7)][PF$_6$], viewed along b axis. Molecules A (green) and B (blue) alternate. Additionally there are rows of molecules with the same handedness. The Δ-form are with dark colours, the Λ-form are presented with light colours. Anions and solvent molecules are omitted.

All cations are ordered. The anions show a rotational disorder and are modelled over sites of 0.54:0.46 and 0.60:0.40 occupancies. The Et$_2$O solvent molecule is disordered as well and calculated over sites of 0.5:0.5 occupancies, whereas the MeCN solvent molecule is ordered.

6.3.3. [Ir(ppy)$_2$(8)][PF$_6$]

X-ray quality crystals were grown from a MeCN solution of [Ir(ppy)$_2$(**8**)][PF$_6$], layered with Et$_2$O. The complex crystallizes as 2{[Ir(ppy)$_2$(**8**)][PF$_6$]}.MeCN.2H$_2$O in the monoclinic centrosymmetric space group $P2_1/n$. Both enantiomers are present in the unit cell and the Λ-

cation is depicted in Figure 6.5. Similar to the previously discussed compounds, the atom Ir1 is in an octahedral environment with the N-donors of the cyclometallating $[ppy]^-$ ligand in a *trans*-configuration. The cyclometallating C^N ligands are almost planar (angles between the least square planes are below 2.6°), the two coordinated pyridine rings within the tpy ligand are twisted about 25.3°, which is much greater than within all other similar compounds. The bonded pyridine ring is twisted about 45° out of the Ir–N bond-axis, which is significantly bigger than the previous compounds described in this chapter. The least square planes between the pendant pyridine ring and the pyridine ring to which it is bonded is twisted about 41.9°, which is significantly smaller than in $[Ir(ppy)_2(\mathbf{7})][PF_6]$. This leads to a less efficient intramolecular face-to-face π-stacking interaction: the twisting angle of the least squares planes between the pyridine and phenyl rings is 12.1° with a inter-centroid distance of 3.60 Å. The twisting angle of the least squares planes of the pendant phenyl ring and the pyridine ring to which it is bonded is 44.0°.

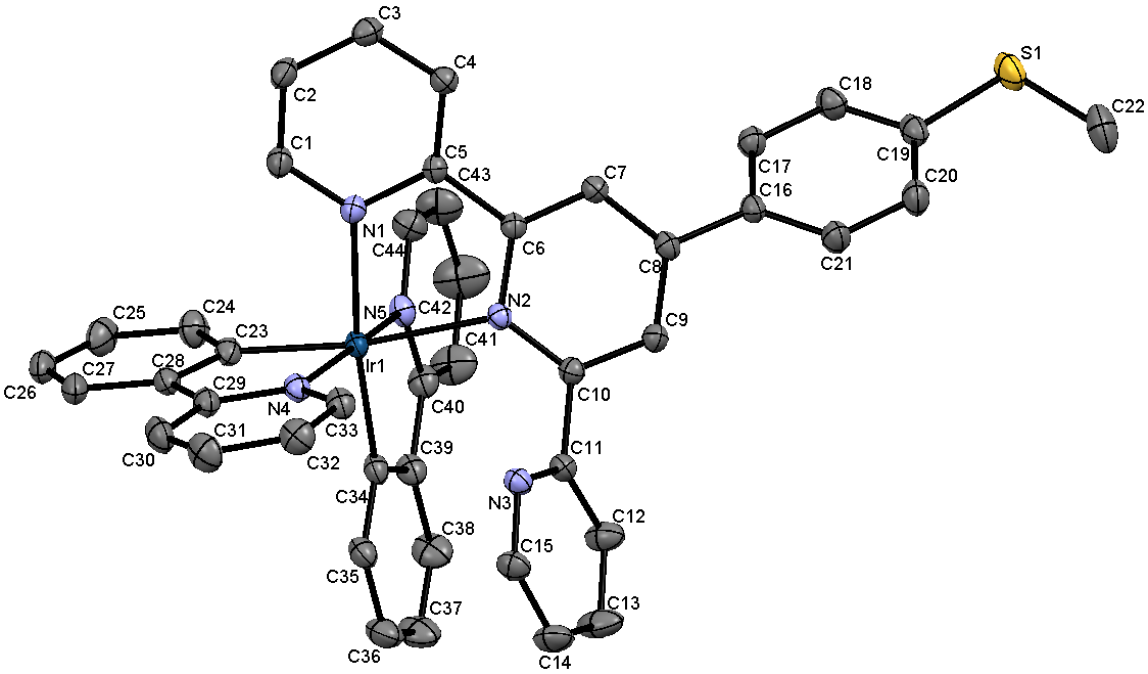

Figure 6.5 Structure of Λ-2{$[Ir(ppy)_2(8)][PF_6]$}.MeCN.$2H_2O$ with ellipsoids plotted at 50% probability level; H atoms omitted. Selected bond lengths (in Å) and bond angles (in °): Ir1–C23: 2.004(1), Ir1–C34: 2.014(1), Ir1–N5: 2.050(1), Ir1–N4: 2.053(1), Ir1–N1: 2.129(1), Ir1–N2: 2.230(1); N1–Ir1–N2: 76.2(0), N4–Ir1–C23: 80.4(1), N5–Ir1–C34: 80.4(1).

The unit cell consists of two Δ- and two Λ-cations, four anions, two MeCN and four water molecules. Pairs of independent Δ- and Λ-cations embrace one another with close C...H and N...H contacts within the tpy ligands (H4A...N3i = 2.47 Å, C4...N3i = 3.15 Å, C4...C10i = 3.37 Å, symmetry code i = 2 – x, 2 – y, 1 – z, see Figure 6.6).

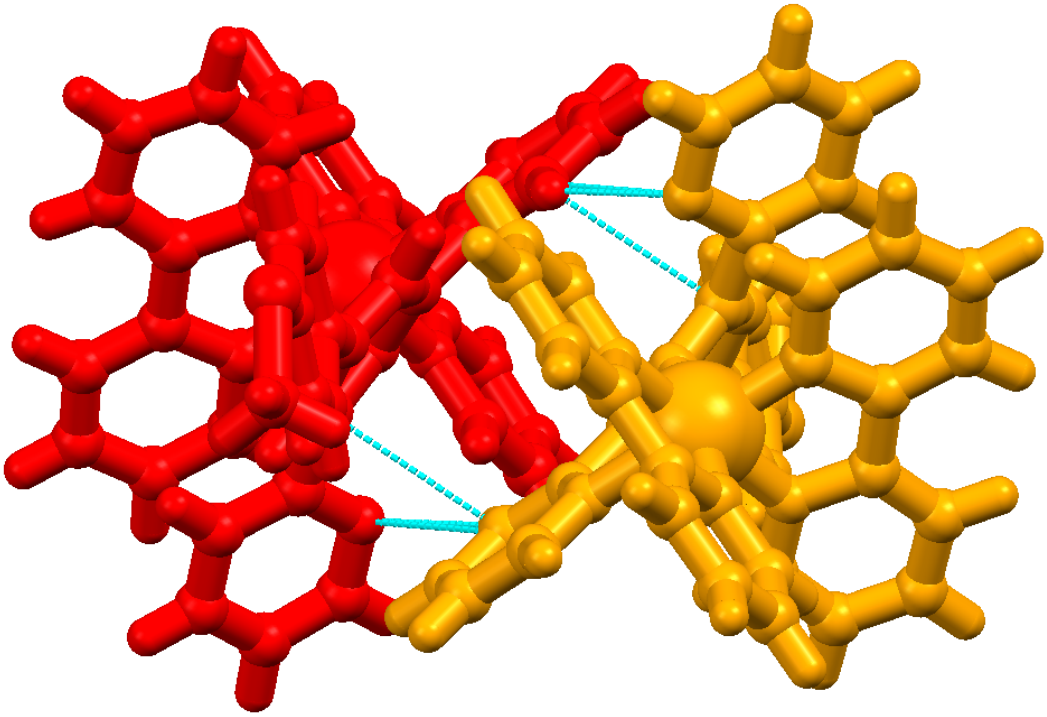

Figure 6.6 Packing of Δ- (red) and Λ-cations (orange) in $[Ir(ppy)_2(8)][PF_6]$ showing the C…H and N…H contacts between a pair of independent cations.

Other crystal packing interactions are cation – anion contacts: H...F contacts are at distances between 2.42 to 2.64 Å. These packing interactions lead to parallel alignments (symmetry imposed by an inversion centre) of the phenyl rings of the tpy ligand, but the inter-centroid distances (4.07 Å) are out of the range discussed by Janiak for π-stacking interactions (< 3.8 Å).3 An overview of the crystal packing is depicted in Figure 6.7.

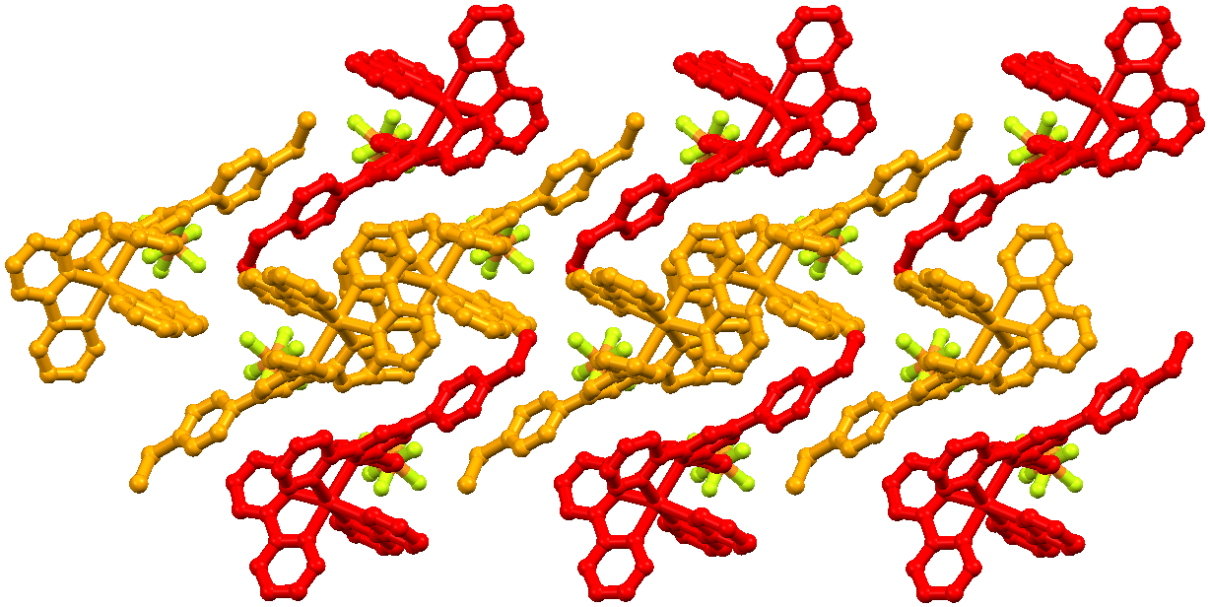

Figure 6.7 Crystal packing in $[Ir(ppy)_2(8)][PF_6]$ with parallel alignments of the phenyl rings between Δ- (red) and Λ-forms (orange).

The cations and the anions are ordered whereas the solvent molecules have been modelled as a 50% occupancy MeCN and two 50% occupancy water molecules.

6.3.4. $[Ir(ppy)_2(9)][PF_6]$

After several attempts, crystals of $[Ir(ppy)_2(\mathbf{9})][PF_6]$ were grown from a solution of MeCN and CH_2Cl_2. Unfortunately, the crystals led only to poor structural data. The structure confirms the presence of the complex, the iridium atom is in an octahedral environment with the N-donors of the cyclometallating $[ppy]^-$ ligands mutually *trans*. The pendant pyridine ring of the tpy ligand undergoes intramolecular face-to-face π-stacking with one of the $[ppy]^-$ ligands.

6.4. Photophysical properties

In general, the four complexes show photophysical similarities to the reported complex with a tolyl-tpy ligand.1 The photophysical behaviour of the four complexes has been measured in CH_2Cl_2. The electronic absorption spectra show similarities between $[Ir(ppy)_2(\mathbf{8})][PF_6]$ and $[Ir(ppy)_2(\mathbf{9})][PF_6]$ through the whole spectrum, and between $[Ir(ppy)_2(\mathbf{6})][PF_6]$ and $[Ir(ppy)_2(\mathbf{7})][PF_6]$ mainly in the UV region (see Figure 6.8). All four complexes show relatively intense bands between λ 240 and 410 nm. These absorptions are assigned to ligand-based π* ← π and π* ← n transitions. The phenyl ring on the tpy ligand extends the π-conjugation, leading to the bigger range for these transitions.5 At higher wavelengths, there are the MLCT transitions, with much lower intensities. This is mainly seen in $[Ir(ppy)_2(\mathbf{6})][PF_6]$ at 475 nm (inset in Figure 6.8). The more electron donating the substituent, the more shifted is the absorption band around 380 nm towards lower energies.[5] $[Ir(ppy)_2(\mathbf{7})][PF_6]$ and $[Ir(ppy)_2(\mathbf{9})][PF_6]$ show very similar spectra in this region, both having an oxygen atom on the tpy ligand. $[Ir(ppy)_2(\mathbf{8})][PF_6]$ has a sulfur atom instead and this leads to a shift in the absorption bands to lower energy. Changing to the nitrogen atom in $[Ir(ppy)_2(\mathbf{6})][PF_6]$, the electron donating effect is further increased, yielding a shift of the band around 370 nm to lower energy to 386 nm.

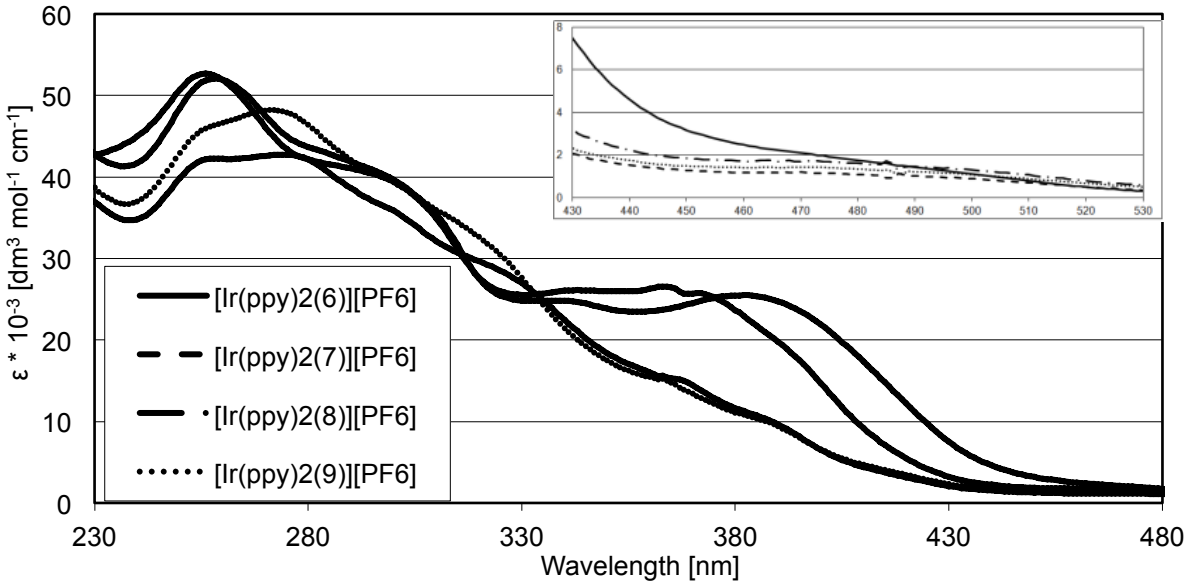

Figure 6.8 Absorption spectra in aerated CH_2Cl_2 solutions (c = 1.00 x 10^{-5} M, 298 K), with an inset to zoom to the MLCT region between 430 and 530 nm.

Excitation between λ 255 and 360 nm leads to an orange emission for all four complexes (Figure 6.9). The emission maxima are 580, 589, 595 and 590 nm, with the broad and unstructured shape, which has been seen before in complexes containing a combination of neutral diimine and cyclometallating ligands.[1, 4, 6] The effect of changing the substituent on the phenyl ring of the tpy ligand does not significantly affect the emission maxima. All four emission maxima are similar to the simple $[Ir(ppy)_2(tpy)][PF_6]$ compound (see Section 5.5).

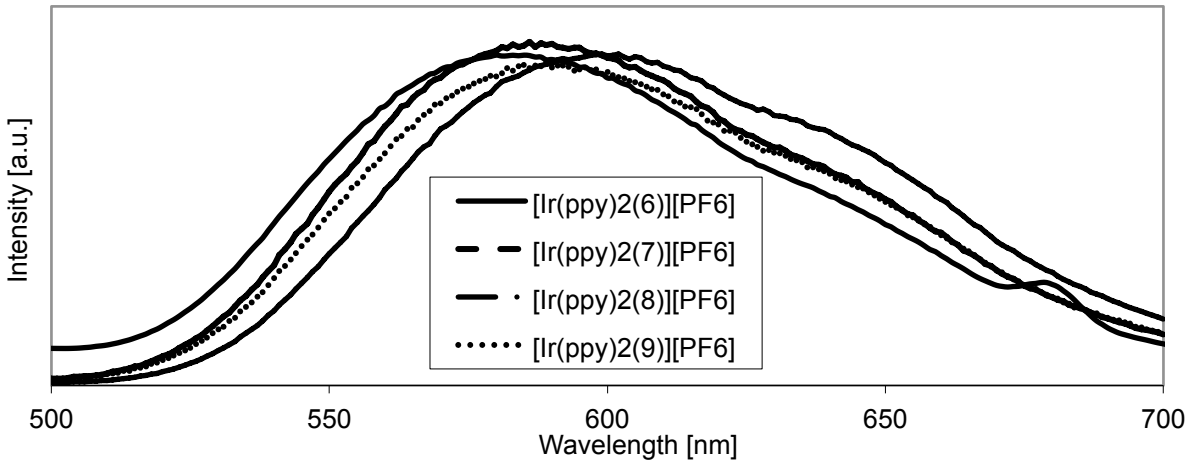

Figure 6.9 Normalized emission spectra of complexes $[Ir(ppy)_2(6)][PF_6]$, $[Ir(ppy)_2(7)][PF_6]$, $[Ir(ppy)_2(8)][PF_6]$ and $[Ir(ppy)_2(9)][PF_6]$ in CH_2Cl_2 solutions (c = 1.00 x 10^{-5} M, 298 K).

The quantum yield measurements were performed on CH_2Cl_2 solutions of the complexes, which had been bubbled with argon for 15 minutes prior to the measurements. $[Ir(ppy)_2(\mathbf{6})][PF_6]$ shows the highest quantum yield of this series of complexes (9.9%), whereas the other three complexes are around 6%. These quantum yields are significantly higher than the compound with the tolyl-tpy ligand (1.7%).1 This difference can be explained with the emission maximum being at 625 nm. The general trend for cationic iridium

complexes towards further red emission maxima leads to lower quantum yields (see Section 5.5).[5, 7]

6.5. Electrochemical properties

All four complexes are electrochemically active. Cyclic voltammetry for all complexes have been measured in CH_2Cl_2 solutions with 0.1 M [^{n}Bu$_4$N][PF_6] supporting electrolyte at a scan rate of 0.1 V s^{-1}. The cyclic voltammetric data with respect to internal Fc/Fc^+ are presented in Table 6.2. Unless otherwise stated, the electrochemical processes are reversible or near-reversible. For all four complexes the reversible or quasi reversible oxidations between +0.74 V and +0.84 V was assigned to an iridium-centred process. Changing the substituent on the tpy ligand has only a minor effect on the first oxidation potential.

All four complexes show ligand centred quasi-reversible reduction processes. Similar to the metal centred oxidation the reduction processes are not affected by changing the substituents on the tpy ligands.

Table 6.2 Cyclic voltammetric data with respect to Fc/Fc^+; CH_2Cl_2 solutions with 0.1 M [^{n}Bu$_4$N][PF_6] supporting electrolyte, and scan rate of 0.1 V s^{-1} (ir = irreversible; qr = quasi-reversible).

Compound	$E_{1/2}^{ox}$ / V	$E_{1/2}^{red}$ / V	$\Delta E_{1/2}$ / V
[Ir(ppy)$_2$(**6**)][PF_6]	+0.74^{ir}	–1.74^{ir}, –2.05^{qr}	2.48
[Ir(ppy)$_2$(**7**)][PF_6]	+0.77^{qr}	–1.85^{qr}	2.62
[Ir(ppy)$_2$(**8**)][PF_6]	+0.84^{ir}	–1.82^{qr}	2.66
[Ir(ppy)$_2$(**9**)][PF_6]	+0.75^{ir}	–1.86^{qr}, –2.15^{ir}	2.61

The $\Delta E_{1/2}$ values of the complexes are in accord with the previously mentioned observations. All the four complexes show emission maxima in the orange region around 600 nm and they all have similar $\Delta E_{1/2}$ values. Comparison with the archetype4 [Ir(ppy)$_2$(pbpy)][PF_6] and with the complexes discussed in Chapter 3 (see Section 3.5), show comparable values in the emission spectra as well as in the electrochemical processes. A second oxidation around +0.95 V is observed in all four complexes. It appears to be reasonable to assume that this originates from the quasi-reversible oxidation of chloride ion.

6.6. Device performances

All four complexes have been tested in thin films with ionic liquid for their photoluminescent and electroluminescent properties, similar to the previously described complexes. Compared to the solution PL emission maxima, in thin films with ionic liquid (iTMC:[BMIM][PF_6] 4:1) the emission maxima are slightly red-shifted (λ_{em} = 600, 591, 604, 593 nm).

This red-shift is even stronger when changing to electroluminescence (λ_{em} = 632, 602, 620, 625 nm). The short turn-on times (below 6 min) show the good ionic mobility of the complexes and therefore the injection of electrons and holes is good as well. In LEC devices, the performances are poor. Some data are presented in Table 6.3.

Table 6.3 Device performances of the complexes (see text).

iTMC	PL λ_{em} [nm]	PLQY	turn on time t_{on}	Luminance$_{max}$ [cd/m^2]	EL λ_{em} [nm]	EQE
[Ir(ppy)$_2$(**6**)][PF$_6$]	600	4.6%	<1min	1	632	< 0.1%
[Ir(ppy)$_2$(**7**)][PF$_6$]	591	23.5%	3.6min	54	602	0.3%
[Ir(ppy)$_2$(**8**)][PF$_6$]	604	15.8%	6 min	29	620	0.2%
[Ir(ppy)$_2$(**9**)][PF$_6$]	593	11.3%	<1min	60	625	0.4%

The low luminance maximum of [Ir(ppy)$_2$(**6**)][PF$_6$] compared to the other three complexes is an indication that the amino group has a negative effect on the device performance and should therefore be avoided in complexes. Currently, this compound is still under further investigation (e.g. theoretical studies) in order to fully understand this observation.

6.7. Conclusion and outlook

Changing the substituents on the tpy ligand with a phenyl spacer in between, seems to have only minor effects on the photophysical and electrochemical properties in these iridium(III) complexes.

Enhanced rigidity of the complexes in the polypyridine ligands, e.g. through reduced rotational freedom of the phenyl spacer, could lead to a stronger dependence between the photophysical and electrochemical properties of the complex and the structural differences.

6.8. Experimental

6.8.1. [Ir(ppy)$_2$(6)][PF$_6$]

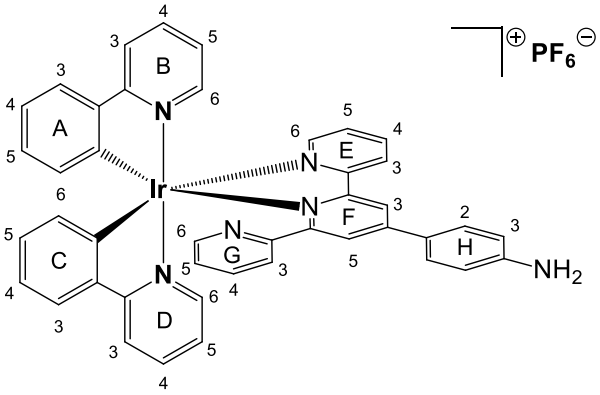

A yellow suspension of [Ir$_2$(ppy)$_4$(μ-Cl)$_2$] (107.2 mg, 0.100 mmol) and 4'-aniline-2,2':6',2''-terpyridine (65.7 mg, 0.201 mmol) in methanol (15 mL) was heated in a microwave reactor for 2 hours at 120°C (P = 15 bar). The orange solution was then cooled to room temperature, and solid sodium NH_4PF_6 (excess) was added. The mixture was stirred for 1 hr at room temperature to give an orange solid, solvent was evaporated to dryness. The crude material was dissolved in dichloromethane followed by an upper layer of diethyl ether. The flask was left to stand for 2 days in which a crystalline solid formed. After decanting the solvent mixture [Ir(ppy)$_2$(**6**)][PF$_6$] was isolated as an orange-red solid (190 mg, 0.196 mmol, 97.2%). *^{1}H NMR* (500 MHz, CD_2Cl_2, 298 K) δ/ppm 8.90 (s, 1H, H^{B6}), 8.62 (d, *J* = 6.5 Hz, 1H, H^{F3}), 8.61 (s, 1H, H^{E3}), 8.22 (d, *J* = 4.6 Hz, 1H, H^{G6}), 8.17 – 8.12 (m, 1H, H^{E4}), 7.90 – 7.84 (m, 2H, H^{B3+D3}), 7.79 (tdd, *J* = 16.0, 7.8, 1.5 Hz, 3H, $H^{B4+D4+E6}$), 7.72 – 7.68 (m, 2H, H^{H2}), 7.62 (dd, *J* = 7.9, 1.2 Hz, 1H, H^{A3}), 7.56 (d, *J* = 2.0 Hz, 1H, H^{F5}), 7.45 (dd, *J* = 5.7, 0.5 Hz, 1H, H^{D6}), 7.39 – 7.34 (m, 2H, H^{E5+C3}), 7.14 (m, 1H, H^{B5}), 7.12 (td, *J* = 7.8, 1.8 Hz, 1H, H^{G4}), 6.99 – 6.94 (m, 2H, H^{A4+D5}), 6.92 (ddd, *J* = 7.6, 4.9, 1.1 Hz, 1H, H^{G4}), 6.82 – 6.79 (m, 2H, H^{H3}), 6.77 (td, *J* = 7.5, 1.3 Hz, 1H, H^{A5}), 6.64 (td, *J* = 7.7, 1.2 Hz, 1H, H^{C4}), 6.54 (d, *J* = 7.6 Hz, 1H, H^{G3}), 6.33 (td, *J* = 7.5, 1.3 Hz, 1H, H^{C5}), 5.91 (dd, *J* = 7.7, 0.9 Hz, 1H, H^{A6}), 5.47 (dd, *J* = 7.6, 0.7 Hz, 1H, H^{C6}), 3.65 (s, 2H, H^{NH2}). *^{13}C NMR* (126 MHz, CD_2Cl_2, 298 K) δ/ppm 168.8 (C^{D2}), 167.1 (C^{B2}), 163.3 (C^{F6}), 157.7 (C^{E2}), 157.5 (C^{F2}), 156.7 (C^{G2}), 152.7 (C^{B6}), 151.6 (C^{F4}), 150.8 (2C, C^{E6+H4}), 150.7 (C^{C1}), 148.6 (C^{G6}), 148.4 (C^{D6}), 147.5 (C^{A1}), 143.7 (C^{A2}), 142.8 (C^{C2}), 139.7 (C^{E4}), 138.6 (C^{D4}), 138.5 (C^{B4}), 136.6 (C^{G4}), 132.8 (C^{C6}), 131.1 (C^{A6}), 130.9 (C^{A5}), 130.4 (C^{C5}), 129.2 (C^{H2}), 128.0 (C^{E5}), 125.5 (C^{E3}), 125.1 (C^{A3}), 124.9 (C^{F5}), 124.5 (C^{G5}), 124.3 (C^{C3}), 123.9 (C^{H1}), 123.3 (C^{B5}), 123.2 (C^{D5}), 123.1 (2C, C^{A4+G3}), 121.2 (C^{C4}), 120.1 (C^{F3}), 119.9 (C^{D3}), 119.8 (C^{B3}), 115.7 (C^{H3}). *IR* (solid) ν/cm^{-1} 3393 (w, $\nu_{Aniline}$), 3048 (w, $\nu_{Aniline}$), 2356 (w), 1700 (m), 1597 (m), 1583 (m), 1521 (w), 1474 (m), 1412 (w), 1364 (w), 1305 (w), 1254 (w), 1228 (w), 1189 (w), 1164 (w), 1064 (w), 1030 (w), 1003 (w), 942 (w), 879 (w), 828 (s), 803 (m), 788 (m), 753 (m), 728 (m), 668 (m), 602 (s). *MS* (ESI, m/z): 825.4 [M-PF$_6$]$^+$ (calc. 825.2). *UV-Vis* λ/nm (ε/dm^3 mol^{-1} cm^{-1}) (CH_2Cl_2, 1.00 × 10^{-5} mol dm^{-3}): 259 (52'100), 339 (24'800), 382 (25'500), 475 (2'100). *Luminescence* (CH_2Cl_2, c = 1.00 x 10^{-5} mol dm^{-3}, λ_{ex} = 255 nm): λ_{em} = 580 nm. *Quantum yield* (CH_2Cl_2, degassed with argon, λ_{ex} = 260 nm, integration range: 500 – 800 nm): 0.099. *Elem. Anal.* calcd. for

$C_{43}H_{32}N_6IrPF_6 \cdot 1.5H_2O$ (996.96) C 51.80, H 3.54, N, 8.43; found C 51.87, H 3.48, N 8.38. *Electrochemistry*: E_1^{ox}: +0.74 V/irr, E_1^{red}: -1.36 V/irr, E_2^{red}: -2.07 V/-2.02^q V.

6.8.2. [Ir(ppy)$_2$(7)][PF$_6$]

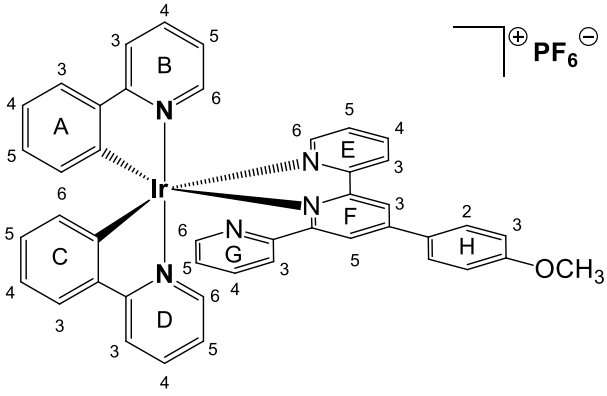

A yellow suspension of $[Ir_2(ppy)_4(\mu\text{-}Cl)_2]$ (107.2 mg, 0.100 mmol) and 4'-phenyl-*p*-methoxy-2,2':6',2''-terpyridine (67.5 mg, 0.199 mmol) in methanol (15 mL) was heated in a microwave reactor for 2 hours at 120°C (P = 12 bar). The orange solution was then cooled to room temperature, and solid NH_4PF_6 (excess) was added. The mixture was stirred for 30 minutes at room temperature. As no precipitate appeared, $AgPF_6$ (excess) was added, the stirring continued for 1 hour and then the mixture was evaporated to dryness. The crude material was purified twice by column chromatography (Merck aluminium oxide 90 and Fluka Silica 60; CH_2Cl_2 changing to CH_2Cl_2:MeOH = 100:2). [Ir(ppy)$_2$(**7**)][PF$_6$] was isolated as an orange solid (159 mg, 0.162 mmol, 81.2%). *^{1}H NMR* (500 MHz, CD_2Cl_2, 298 K) δ/ppm 8.89 (s, 1H, H^{B6}), 8.67 (d, *J* = 2.0 Hz, 1H, H^{F3}), 8.65 (d, *J* = 8.3 Hz, 1H, H^{E3}), 8.22 (d, *J* = 4.5 Hz, 1H, H^{G6}), 8.17 (ddd, *J* = 8.2, 7.7, 1.6 Hz, 1H, H^{E4}), 7.88 (dd, *J* = 1.3, 0.7 Hz, 1H, H^{B3}), 7.86 (d, *J* = 6.9 Hz, 1H, H^{D3}), 7.85 – 7.82 (m, 2H, H^{H2}), 7.82 – 7.75 (m, 3H, $H^{B4+D4+E6}$), 7.62 (dd, *J* = 7.9, 1.2 Hz, 1H, H^{A3}), 7.61 (d, *J* = 1.9 Hz, 1H, H^{F5}), 7.45 (dd, *J* = 5.8, 0.5 Hz, 1H, H^{D6}), 7.39 (ddd, *J* = 7.6, 5.5, 1.2 Hz, 1H, H^{E5}), 7.36 (dd, *J* = 7.8, 1.1 Hz, 1H, H^{C3}), 7.14 (ddd, *J* = 7.4, 5.9, 1.5 Hz, 1H, H^{B5}), 7.12 (dd, *J* = 8.3, 6.9 Hz, 1H, H^{G4}), 7.11 – 7.07 (m, 2H, H^{H3}), 7.00 – 6.95 (m, 2H, H^{A4+D5}), 6.93 (ddd, *J* = 7.6, 4.9, 0.9 Hz, 1H, H^{G5}), 6.77 (td, *J* = 7.5, 1.3 Hz, 1H, H^{A5}), 6.67 – 6.62 (m, 1H, H^{C4}), 6.55 (d, *J* = 7.6 Hz, 1H, H^{G3}), 6.34 (td, *J* = 7.4, 1.3 Hz, 1H, H^{C5}), 5.90 (dd, *J* = 7.8, 0.8 Hz, 1H, H^{A6}), 5.47 (dd, *J* = 7.6, 0.6 Hz, 1H, H^{C6}), 3.88 (s, 3H, H^{CH3}). *^{13}C NMR* (126 MHz, CD_2Cl_2, 298 K) δ/ppm 168.8 (C^{D2}), 167.1 (C^{B2}), 163.6 (C^{F6}), 162.9 (C^{H4}), 157.8 (C^{F2}), 157.5 (C^{E2}), 156.6 (C^{G2}), 152.8 (C^{B6}), 151.5 (C^{F4}), 150.9 (C^{E6}), 150.6 (C^{C1}), 148.5 (C^{D6}), 148.3 (C^{G6}), 147.3 (C^{A1}), 143.7 (C^{A2}), 142.8 (C^{C2}), 139.8 (C^{E4}), 138.6 (C^{D4}), 138.5 (C^{B4}), 137.1 (C^{G4}), 132.8 (C^{C6}), 131.1 (C^{A6}), 131.0 (C^{A5}), 130.5 (C^{C5}), 129.4 (C^{H2}), 128.2 (C^{E5}), 127.5 (C^{H1}), 125.9 (C^{F5}), 125.7 (C^{E3}), 125.1 (C^{A3}), 124.6 (C^{G5}), 124.3 (C^{C3}), 123.3 (3C, $C^{A4+B5+G3}$), 123.2 (C^{D5}), 121.3 (C^{C4}), 121.1 (C^{F3}), 119.9 (C^{D3}), 119.8 (C^{B3}), 115.6 (C^{H3}), 56.2 (C^{CH3}). *IR* (solid): ν/cm^{-1} = 3042 (w, ν_{OMe}), 2344 (w), 1700 (m), 1603 (s), 1583 (s), 1517 (m), 1476 (s), 1459 (m), 1437 (m), 1424 (m), 1420 (m), 1410 (m), 1399 (m), 1366 (w), 1303 (m), 1268 (m), 1247 (s), 1231 (m), 1181 (m), 1164 (m), 1122 (w), 1095 (w), 1065 (w), 1030 (m), 1003 (m), 994 (w), 879 (w), 828 (s), 828 (s), 804 (s), 788 (s), 753 (s), 727 (s). *MS* (ESI, m/z): 840.3 $[M\text{-}PF_6]^+$ (calc. 840.2). *UV-Vis* λ/nm (ε/dm^3 mol^{-1} cm^{-1}) (CH_2Cl_2, 1.00 × 10^{-5}

mol dm^{-3}): 258 (42'200), 274 (42'700), 365 (15'300), 386 (10'500). *Luminescence* (CH_2Cl_2, c = 1.00 x 10^{-5} mol dm^{-3}, λ_{ex} = 320 nm): λ_{em} = 589 nm. *Quantum yield* (CH_2Cl_2, degassed with argon, λ_{ex} = 260 nm, integration range: 520 – 800 nm): 0.061. *Elem. Anal.* calcd. for $C_{44}H_{33}N_5OIrPF_6 \cdot H_2O$ (1002.96) C 52.69, H 3.52, N, 6.98; found C 52.55, H 3.40, N 6.92. *Electrochemistry*: E_1^{ox}: +0.83 V/+0.70[q] V, E_1^{red}: -1.94 V/-1.76[q] V.

6.8.3. [Ir(ppy)$_2$(8)][PF$_6$]

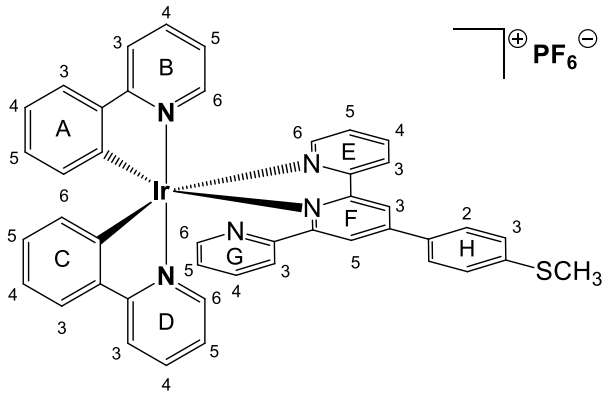

A yellow suspension of [$Ir_2(ppy)_4(\mu\text{-}Cl)_2$] (107.2 mg, 0.100 mmol) and 4'-phenyl-*p*-thiomethyl-2,2':6',2''-terpyridine (70.7 mg, 0.199 mmol) in methanol (15 mL) was heated in a microwave reactor for 2 hours at 120°C (P = 13 bar). The red solution was then cooled to room temperature, and solid NH_4PF_6 (excess) was added. The mixture was stirred for 30 minutes at room temperature. As no precipitate appeared $AgPF_6$ (excess) was added, the stirring continued for 1 hour and then the mixture was evaporated to dryness. The crude material was purified twice by column chromatography (Merck aluminium oxide 90 and Fluka Silica 60; CH_2Cl_2 changing to CH_2Cl_2:MeOH = 100:2). [Ir(ppy)$_2$(**8**)][PF_6] was isolated as a pale orange solid (180.0 mg, 0.179 mmol, 90.2%). *^{1}H NMR* (500 MHz, CD_2Cl_2, 298 K) δ/ppm 8.86 (s, 1H, H^{B6}), 8.70 (d, *J* = 1.9 Hz, 1H, H^{F3}), 8.66 (d, *J* = 8.2 Hz, 1H, H^{E3}), 8.23 (d, *J* = 4.7 Hz, 1H, H^{G6}), 8.17 (td, *J* = 8.0, 1.6 Hz, 1H, H^{E4}), 7.88 (t, *J* = 8.2 Hz, 2H, H^{B3+D3}), 7.83 – 7.76 (m, 5H, $H^{B4+D4+E6+H2}$), 7.65 (s, 1H, H^{F5}), 7.62 (dd, *J* = 7.9, 1.1 Hz, 1H, H^{A3}), 7.46 (d, *J* = 5.5 Hz, 1H, H^{D6}), 7.43 – 7.38 (m, 3H, H^{C3+H3}), 7.37 (dd, *J* = 7.8, 1.0 Hz, 1H, H^{C3}), 7.20 – 7.12 (m, 2H, H^{B5+G4}), 7.02 – 6.94 (m, 3H, $H^{A4+D5+G5}$), 6.78 (td, *J* = 7.5, 1.3 Hz, 1H, H^{A5}), 6.65 (td, *J* = 7.8, 1.2 Hz, 1H, H^{C4}), 6.57 (d, *J* = 7.3 Hz, 1H, H^{G3}), 6.35 (td, *J* = 7.5, 1.2 Hz, 1H, H^{C5}), 5.90 (dd, *J* = 7.7, 0.9 Hz, 1H, H^{A6}), 5.49 (d, *J* = 7.8 Hz, 1H, H^{C6}), 2.55 (s, 3H, H^{CH3}). *^{13}C NMR* (126 MHz, CD_2Cl_2, 298 K) δ/ppm 168.7 (C^{D2}), 167.1 (C^{B2}), 157.9 (C^{F2}), 157.4 (C^{E2}), 152.8 (C^{G2}), 152.6 (C^{B6}), 151.3 (C^{F4}), 150.9 (C^{E6}), 150.5 (C^{C1}), 148.6 (C^{D6}), 148.1 (C^{G6}), 147.2 (C^{A1}), 144.3 (C^{H4}), 143.7 (C^{A2}), 142.9 (C^{C2}), 139.8 (C^{E4}), 138.7 (C^{D4}), 138.6 (C^{B4}), 136.9 (C^{G4}), 132.9 (C^{C6}), 131.3 (C^{H1}), 131.1 (C^{A6}), 131.0 (C^{A5}), 130.5 (C^{C5}), 128.4 (C^{E5}), 128.1 (C^{H2}), 126.8 (C^{H3}), 126.3 (C^{F5}), 125.8 (C^{E3}), 125.1 (C^{A3}), 124.8 (C^{G5}), 124.4 (C^{C3}), 123.4 (2C, C^{B5+G3}), 123.3 (C^{A4}), 123.2 (C^{D5}), 121.3 (2C, C^{C4+F3}), 119.9 (C^{D3}), 119.8 (C^{B3}), 15.3 (C^{CH3}). *IR* (solid): ν/cm^{-1} = 3038 (w, ν_{SMe}), 1700 (w), 1607 (s), 1583 (s), 1565 (m), 1476 (s), 1420 (m), 1393 (m), 1364 (w), 1317 (w), 1307 (w), 1269 (w), 1255 (w), 1228 (w), 1164 (m), 1099 (m), 1064 (w), 1030 (m), 993 (w), 960 (w), 879 (w), 831 (s), 831 (s), 785 (m), 753 (s), 727 (s), 710 (m), 666 (w), 627 (s), 610 (s), 603 (m). *MS* (ESI, m/z): 856.3 [M-PF_6]$^+$

(calc. 856.2). *UV-Vis* λ/nm (ε/dm^3 mol^{-1} cm^{-1}) (CH_2Cl_2, 1.00 × 10^{-5} mol dm^{-3}): 256 (52'700), 288 (41'200), 343 (26'100), 364 (26'600), 372 (25'700), 394 (18'000). *Luminescence* (CH_2Cl_2, c = 1.00 x 10^{-5} mol dm^{-3}, λ_{ex} = 325 nm): λ_{em} = 595 nm. *Quantum yield* (CH_2Cl_2, degassed with argon, λ_{ex} = 255 nm, integration range: 520 – 800 nm): 0.068. *Elem. Anal.* calcd. for $C_{44}H_{33}IrN_5SPF_6 \cdot 1.5H_2O$ (1028.19) C 51.41, H 3.53, N, 6.81; found C 51.41, H 3.27, N 6.81. *Electrochemistry*: E_1^{ox}: +0.84 V/irr, E_1^{red}: -1.90 V/-1.73^q V.

6.8.4. [Ir(ppy)$_2$(9)][PF$_6$]

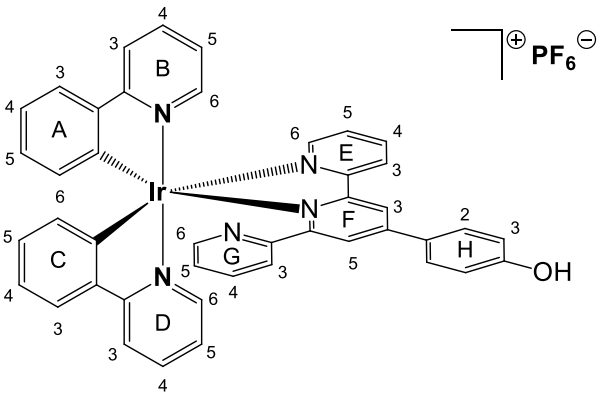

A yellow suspension of [Ir$_2$(ppy)$_4$(μ-Cl)$_2$] (107.2 mg, 0.100 mmol) and 4'-phenyl-*p*-hydroxy-2,2':6',2''-terpyridine (64.7 mg, 0.199 mmol) in methanol (15 mL) was heated in a microwave reactor for 2 hours at 120°C (P = 13 bar). The orange solution was then cooled to room temperature, and solid NH_4PF_6 (excess) was added. The mixture was stirred for 30 minutes at room temperature. As no precipitate appeared $AgPF_6$ (excess) was added, the stirring continued for 1 hour and then the mixture was evaporated to dryness. The crude material was purified twice by column chromatography (Merck aluminium oxide 90, CH_2Cl_2 changing to CH_2Cl_2:MeOH:MeCN = 100:5:5 and Fluka Silica 60; CH_2Cl_2 changing to CH_2Cl_2:MeOH = 100:3). [Ir(ppy)$_2$(**9**)][PF$_6$] was isolated as an orange solid (154.0 mg, 0.158 mmol, 79.5%). *^{1}H NMR* (500 MHz, CD_2Cl_2, 298 K) δ/ppm 8.98 (br, 1H, H^{B6}), 8.68 (d, *J* = 8.3 Hz, 1H, H^{E3}), 8.58 (d, *J* = 2.0 Hz, 1H, H^{F3}), 8.48 (s, 1H, H^{OH}), 8.21 (d, *J* = 2.5 Hz, 1H, H^{G6}), 8.16 (ddd, *J* = 8.2, 7.7, 1.6 Hz, 1H, H^{E4}), 7.89 (m, 1H, H$^{B3/D3}$), 7.86 (m, 1H, H$^{B3/D3}$), 7.82 (m, 3H, H$^{B4+D4+E6}$), 7.59 (dd, *J* = 7.8, 1.2 Hz, 1H, H^{A3}), 7.56 (m, 2H, H^{H2}), 7.54 (d, *J* = 6.0 Hz, 1H, H^{D6}), 7.43 (d, *J* = 1.9 Hz, 1H, H^{F5}), 7.38 (m, 2H, H^{E5+C3}), 7.17 (m, 2H, H^{B5+G4}), 7.03 – 6.95 (m, 3H, H$^{D5+G5+A4}$), 6.80 (td, *J* = 7.5, 1.4 Hz, 1H, H^{A5}), 6.71 (d, *J* = 8.6 Hz, 2H, H^{H3}), 6.66 (ddd, *J* = 7.8, 7.3, 1.2 Hz, 1H, H^{C4}), 6.56 (s, 1H, , H^{G3}), 6.38 (td, *J* = 7.5, 1.2 Hz, 1H, H^{C5}), 5.91 (m, 1H, H^{A6}), 5.53 (d, *J* = 7.5 Hz, 1H, H^{C6}). *^{13}C NMR* (126 MHz, CD_2Cl_2, 298 K) δ/ppm 168.7 (C^{D2}), 167.2 (C^{B2}), 160.4 (C^{F6}), 160.0 (C^{H4}), 157.5 (C^{F2}), 157.3 (C^{E2}), 155.5 (C^{G2}), 151.9 (C^{B6}), 151.1 (C^{F4}), 150.9 (C^{C1}), 150.8 (C^{E6}), 149.1 (C^{D6}), 148.2 (C^{G6}), 147.4 (C^{A1}), 143.7 (C^{A2}), 143.2 (C^{C2}), 139.8 (C^{E4}), 138.7 (C$^{B4/D4}$), 138.6 (C$^{B4/D4}$), 137.2 (C^{G4}), 132.5 (C^{C6}), 131.0 (C^{A5}), 130.9 (C^{A6}), 130.5 (C^{C5}), 129.4 (C^{H2}), 128.2 (C^{E5}), 126.0 (C^{H1}), 125.9 (C^{F5}), 125.8 (C^{E3}), 125.1 (2C, C^{A3+G5}), 124.6 (C^{C3}), 123.9 (C^{G3}), 123.8 (C^{B5}), 123.3 (C^{A4}), 123.2 (C^{D5}), 121.3 (C^{C4}), 120.9 (C^{F3}), 120.0 (2C, C^{B3+D3}), 117.49 (C^{H3}). *IR* (solid): ν/cm^{-1} = 3043 (w, ν_{OH}), 2601 (w), 2162 (w), 1663 (w), 1607 (s), 1583 (s), 1520 (m), 1477 (s), 1438 (m), 1419 (m), 1404 (m), 1367 (w), 1319 (w), 1285 (m), 1270 (m), 1233 (m), 1163 (m), 1042 (m), 1031

(m), 1025 (m), 1009 (m), 830 (s), 828 (s), 805 (s), 790 (s), 755 (s), 739 (s), 730 (s), 627 (s), 618 (s) cm^{-1}. *MS* (ESI, m/z): 826.3 $[M\text{-}PF_6]^+$ (calc. 826.2). *UV-Vis* λ/nm (ε/dm^3 mol^{-1} cm^{-1}) (CH_2Cl_2, 1.00 × 10^{-5} mol dm^{-3}): 256 (52'700), 364 (26'600). *Luminescence* (CH_2Cl_2, c = 1.00 x 10^{-5} mol dm^{-3}, λ_{ex} = 360 nm): λ_{em} = 590 nm. *Quantum yield* (CH_2Cl_2, degassed with argon, λ_{ex} = 270 nm, integration range: 490 – 815 nm): 0.058. *Elem. Anal.* calcd. for $C_{43}H_{31}IrN_5OPF_6 \cdot 4H_2O$ (1042.98) C 49.52, H 3.77, N 6.71; found C 48.92, H 3.37, N 6.61. *Electrochemistry*: E_1^{ox}: +0.75 V/irr, E_1^{red}: -1.90 V/-1.81[q] V, E_2^{red}: -2.15 V/irr.

[1] F. Neve, A. Crispini, S. Campagna and S. Serroni*, Inorg. Chem*., 1999, **38**, 2250.
[2] See for example: F. Neve, A. Crispini, S. Campagna and S. Serroni*, Inorg. Chem*., 1999, **38**, 2250 and references cited therein.
[3] C. Janiak, *J. Chem. Soc., Dalton Trans.,* 2000, 3885.
[4] H. J. Bolink, E. Coronado, R. D. Costa, E. Ortí, M. Sessolo, S. Graber, K. Doyle, M. Neuburger, C. E. Housecroft, E. C. Constable, *Adv. Mater.*, 2008, **20**, 3910.
[5] A. B. Tamayo, S. Garon, T. Sajoto, P. I. Djurovich, I. M. Tsyba, R. Bau, M. E. Thompson, *Inorg. Chem.*, 2005, **44**, 8723.
[6] J. D. Slinker, J. Rivnay, J. S. Moskowitz, J. B. Parker, S. Bernhard, H. D. Abruña, G. G. Malliaras, *J. Mater. Chem.*, 2007, **17**, 2976.
[7] M. L. Scudder, H. A. Goodwin, I. G. Dance, *New J. Chem.*, 1999, **23**, 695.

Chapter 7

7. Exploring the stereochemical complexity of octahedral iridium(III) complexes

7.1. Introduction

Starting from the archetypical bis-chelate iridium(III) dimer $[Ir_2(ppy)_4(\mu\text{-}Cl)_2]$,[1, 2] the aim of this chapter is to investigate multinuclear complexes comprising polygons or polyhedra in which the vertices are $\{Ir(ppy)_2\}$ units and the edges are bridging ligands such as 2,3'-, 2,4'- or 4,4'-bpy.[3] There are 6 possible isomers of bipyridine (see Scheme 7.1).

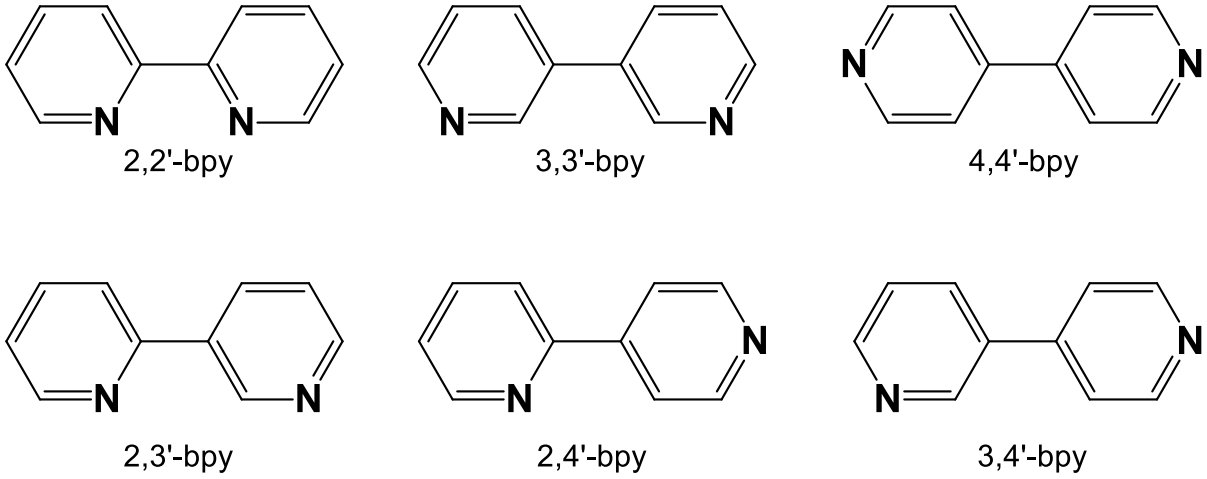

Scheme 7.1 The isomers of bipyridine.

The ligands chosen were 2,4'-bpy and 4,4'-bpy. In 2,4'-bpy the relative positions of the two *N*-donors are unlikely to permit the ligand to adopt a bridging mode on grounds of steric hindrance, whereas with 4,4'-bpy multinuclear complexes can be expected. The chelating behaviour of 2,2'-bpy has already been discussed in previous chapters (see Chapters 2 and 3).

Although there is a wide variety of cationic iridium(III) complexes, reactions with non-chelating bpy have not previously been reported.[4] Reactions with bis(pyridine) ligands (L) containing linkers between the pyridine domains lead to complexes of the type $[\{Ir_2(ppy)_2Cl\}_2(\mu\text{-}L)]$ or $[\{Ir_2(ppy)_2\}_2(\mu\text{-}L)_2]^{2+}$.[5]

7.2. Results and discussion

7.2.1. $[Ir(ppy)_2(2,4'\text{-bpy})Cl]$

The reaction was performed similarly to the other previously described complexation reactions. Reacting $[Ir_2(ppy)_4(\mu\text{-}Cl)_2]$ dimer with two equivalents of 2,4'-bpy under microwave conditions resulted in the formation of yellow crystals of $[Ir(ppy)_2(2,4'\text{-bpy})Cl]$ in 71.4% yield (Scheme 7.2). The ESI mass spectrum showed peaks at m/z 657.2 $[M - Cl]^+$ and 501.1 $[Ir(ppy)_2]^+$ and the observed isotope patterns were in accord with those simulated.

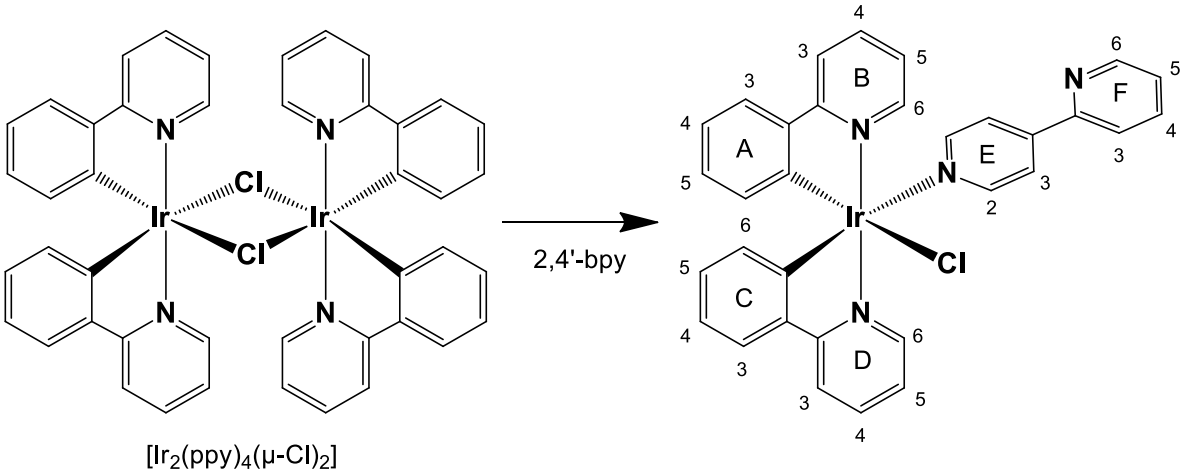

Scheme 7.2 Synthesis of [Ir(ppy)$_2$(2,4'-bpy)Cl] with atom labelling for NMR spectroscopic assignments. The reaction yields a racemic product, only the Λ-enantiomer is shown.

The absence of a C_2 axis in the complex results in each proton environment in the {Ir(ppy)$_2$} unit being unique. The ^{1}H NMR spectrum (shown in Figure 7.1) is consistent with this fact. Comparison with the spectrum of the free 2,4'-bpy ligand indicates that the major shifts are associated with the 4-pyridyl ring E. This strongly indicates that the ligand has coordinated through the less-hindered nitrogen instead of the 2-pyridyl ring.

The ^{1}H and ^{13}C NMR spectra were assigned using COSY, NOESY, HMQC and HMBC spectroscopy. The assignment of the cyclometallating rings A, B, C and D was performed with the help of NOESY cross peaks between the pairs of protons A6 and D6, C3 and D3, and A3 and B3. The proximity of protons B6 and D6 to the chlorido ligand results in the dramatic difference in their chemical shifts (see Figure 7.1). This is also seen in the solid state structure which is discussed later (see Figure 7.4).

At room temperature, proton signals from ring E are broad while the signals from ring F are sharp and well resolved. The extremely broad resonance for protons E2 is centred at δ 9.05 ppm (see inset of Figure 7.1). The resonance for protons E3 is centred at δ 7.85 ppm, with a line-width at half-height of approximately 15 Hz. Upon cooling the CD_2Cl_2 solution of the complex from 298 K to 213 K, the proton signals of ring E split. The resonance for proton E3 at δ 7.85 ppm splits into two signals at δ 7.96 ppm and δ 7.67 ppm. The signal for proton E2 at δ 9.05 ppm gives rise to two broadened doublets ($J \approx 5$ Hz) at δ 9.85 ppm and δ 8.13 ppm. This indicates (similar to the pendant phenyl and pyridine rings discussed in previous chapters) that the 2,4'-bpy ligand undergoes hindered rotation about the Ir-N bond, but there is free rotation on the NMR timescale about the C-C bond between the two pyridine rings within the ligand.

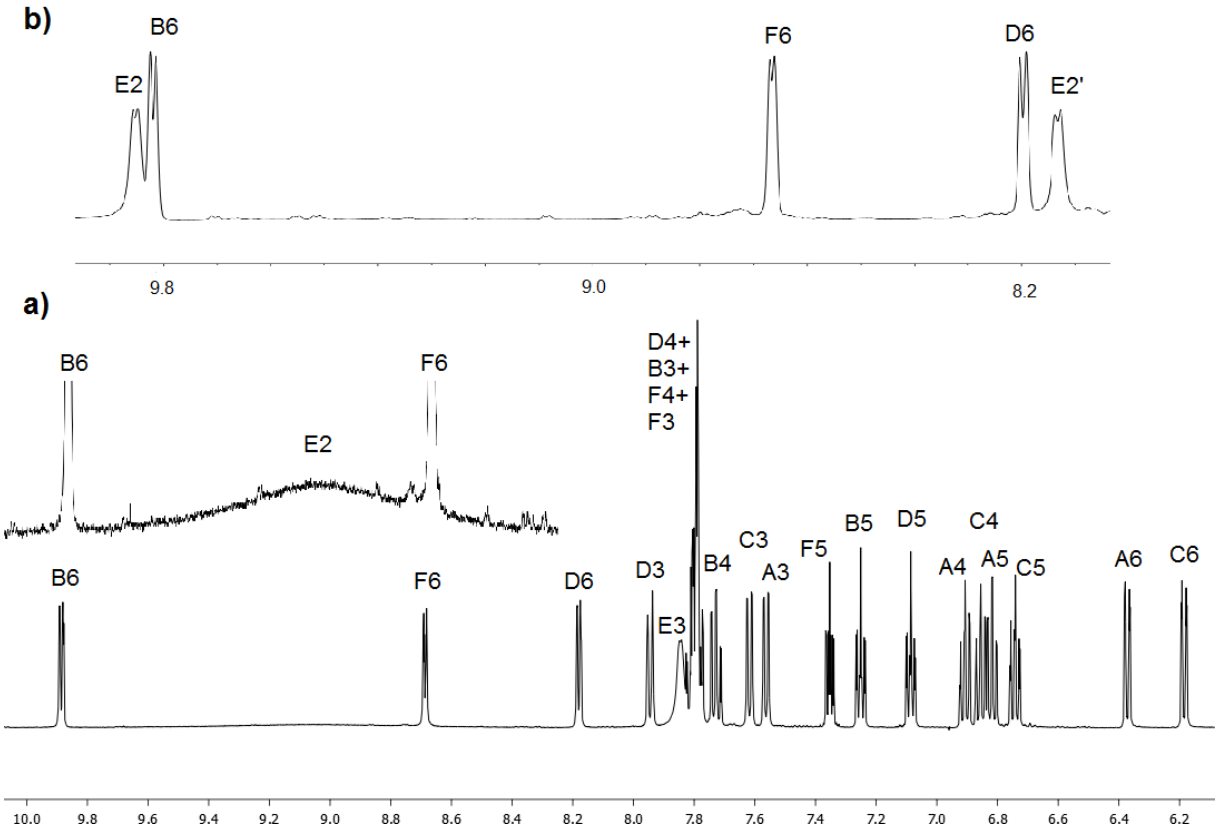

Figure 7.1 500 MHz ^{1}H NMR spectra of [Ir(ppy)$_2$(2,4'-bpy)Cl] in CD_2Cl_2 a) at 298 K, b) at 213 K.

In the ^{13}C NMR spectrum, the broadness of the proton signal prevents the observation of an HMQC cross-peak. The E2 carbon was assigned to a broadened resonance at δ 152.6 ppm.

7.2.2. [Ir(ppy)$_2$(2,4'-bpy)Cl] in DMSO

Dissolution of [Ir$_2$(ppy)$_4$(μ-Cl)$_2$] in DMSO leads to cleavage of the chlorido bridges and the formation of racemic [Ir(ppy)$_2$Cl(DMSO)]. [6, 7, 8] Three complexes were found in the literature which are closely related to [Ir(ppy)$_2$Cl(DMSO)]. In each of the reported compounds, structural data confirm an S-bound DMSO.6, [9, 10]

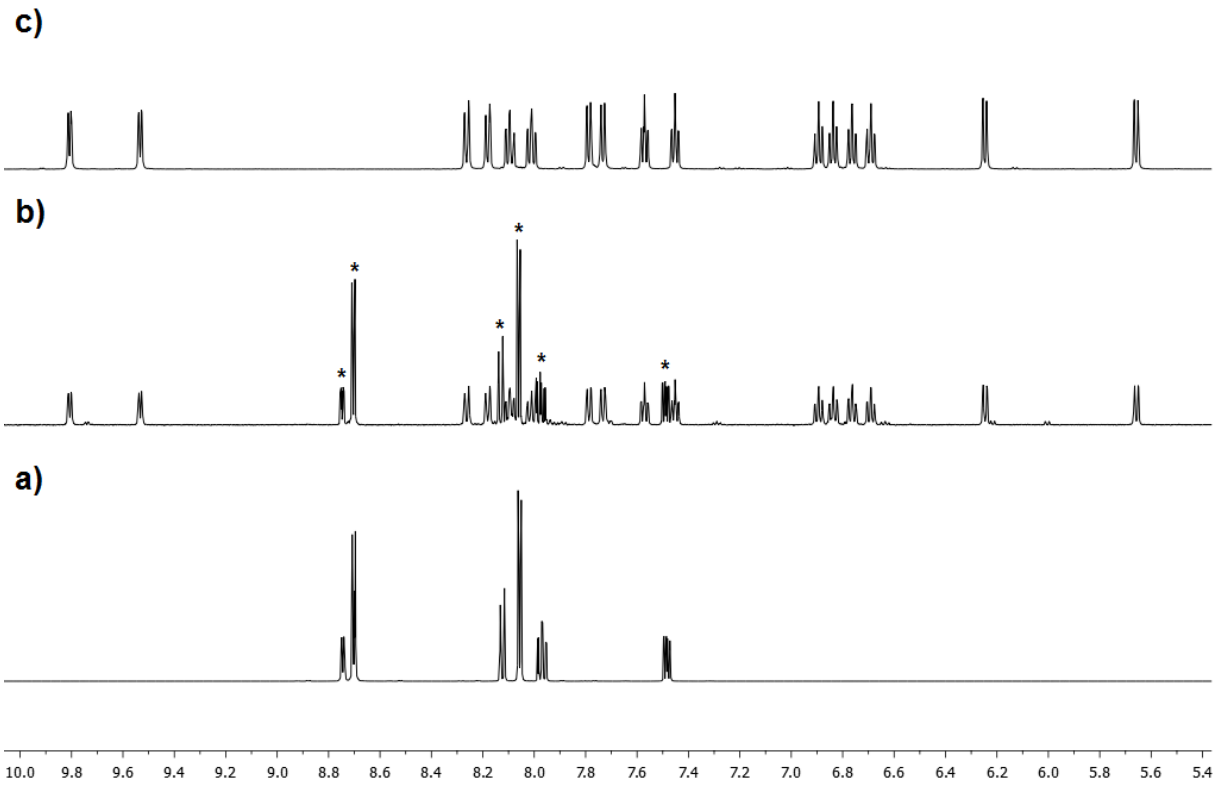

Figure 7.2 500 MHz ^{1}H NMR spectra in DMSO-d_6 at 298 K of a) free 2,4'-bpy ligand, b) [Ir(ppy)$_2$(2,4'-bpy)Cl] with resonances due to the 2,4'-bpy marked *, c) [Ir$_2$(ppy)$_4$(μ-Cl)$_2$]

The ^{1}H NMR spectrum of [Ir(ppy)$_2$(2,4'-bpy)Cl] dissolved in DMSO-d_6 is depicted in Figure 7.2. Integration of the peaks is consistent with the compound. Comparison of the two proton NMR spectra of the same compound in different solvents shows significant differences (compare Figure 7.1 and Figure 7.2). Most obvious are the following changes:

- The 2,4'-bpy protons show sharp resonances.
- The [ppy]$^-$ ligands are still non-equivalent confirming the absence of a C_2 axis in the iridium(III) complex on an NMR timescale.
- The presence of two high frequency signals at δ 9.85 and 9.81 ppm.

The high frequency signals are assigned to protons H$^{B6/D6}$ of the cyclometallating [ppy]$^-$ ligands. Whereas the chemical shifts of these two protons show similarity, the corresponding signals in [Ir(ppy)$_2$(2,4'-bpy)Cl] are significantly separated: δ 9.89 and 8.18 ppm. The resonances of a free 2,4'-bpy in a DMSO-d_6 solution show direct coincidence with those of [Ir(ppy)$_2$(2,4'-bpy)Cl], while the remaining signals in the ^{1}H NMR spectrum are coincident with those of a DMSO-d_6 solution of [Ir$_2$(ppy)$_4$(μ-Cl)$_2$] (Figure 7.2), i.e. the cleavage product described in the literature6. All these data indicate that when [Ir(ppy)$_2$(2,4'-bpy)Cl] is dissolved in DMSO, the solvent displaces the 2,4'-bpy ligand rather than the chlorido ligand. The proposed solution species is therefore [Ir(ppy)$_2$(DMSO-d_6)Cl] rather than [Ir(ppy)$_2$(2,4'-bpy)(DMSO-d_6)]Cl. Several attempts to prepare and isolate a bulk sample or grow crystals of [Ir(ppy)$_2$(DMSO-d_6)Cl] were unsuccessful. The electrospray ionization mass spectrum of a

DMSO/MeOH solution of the bulk [Ir(ppy)$_2$(2,4'-bpy)Cl] exhibits peaks at m/z 657.0, 578.9 and 500.9, which are consistent with the [Ir(ppy)$_2$(2,4'-bpy)]$^+$, [Ir(ppy)$_2$(DMSO)]$^+$ and [Ir(ppy)$_2$]$^+$ ions, respectively.

7.2.3. [Ir(ppy)$_2$(2,4'-bpy)$_2$][PF$_6$]

Several attempts towards the bulk synthesis of [Ir(ppy)$_2$(2,4'-bpy)$_2$][PF$_6$] were unsuccessful. In the course of studying the species obtained from the dissolution of [Ir(ppy)$_2$(2,4'-bpy)Cl] in DMSO (i.e. [Ir(ppy)$_2$(DMSO)Cl] + 2,4'-bpy) precipitation of a hexafluoridophosphate salt was attempted. After stirring a sample of [Ir(ppy)$_2$(2,4'-bpy)Cl] in DMSO for 1 hr, an excess of aqueous NH_4PF_6 was added, but NMR spectroscopic data for the crude precipitated material revealed a mixture of products which could not be isolated. X-ray quality crystals grew in the NMR tube from the solution above the crude precipitate. The highest mass peak in the mass spectrum of the crystals dissolved in a solution of CH_2Cl_2 and MeOH was observed at m/z 813.2, showing the right isotope pattern of the [Ir(ppy)$_2$(2,4'-bpy)$_2$]$^+$ ion. This composition was confirmed by a single crystal structure analysis (see Figure 7.6).

7.2.4. [{Ir(ppy)$_2$Cl}$_2$(μ-4,4'-bpy)]

Among bridging ligands, 4,4'-bpy is ubiquitous[11, 12, 13] and it is used extensively for the assembly of molecular squares and other polygons. The studies with the 2,4'-bpy ligand produced [Ir(ppy)$_2$(2,4'-bpy)Cl] and [Ir(ppy)$_2$(2,4'-bpy)$_2$][PF$_6$]. In moving to 4,4'-bpy, the focus was how the reaction pathway would change. Targets included binuclear [{Ir(ppy)$_2$Cl}$_2$(μ-4,4'-bpy)] or cyclic {Ir(ppy)$_2$(4,4'-bpy)}$_n$ assemblies. With the former as an objective, the reaction of [Ir$_2$(ppy)$_4$(μ-Cl)$_2$] with one equivalent of 4,4'-bpy in MeOH was carried out under microwave conditions. The reaction product was an orange solid, which was poorly soluble in common solvents such as MeCN, MeOH, CH_2Cl_2 and $CHCl_3$. For the electrospray ionization mass spectrum a very dilute MeOH/CH_2Cl_2 solution was introduced into the spectrometer, exhibiting peak envelopes at m/z 1192.9, 657.2 and 501.1, which were assigned to [M – Cl]$^+$, [Ir(ppy)$_2$(4,4'-bpy)]$^+$ and [Ir(ppy)$_2$]$^+$, respectively, and the observed isotope patterns agreed with those simulated for these ions. Elemental analysis of the bulk sample indicated a bulk formulation of [Ir$_2$(ppy)$_4$Cl$_2$(μ-4,4'-bpy)].2H$_2$O. The proposed structure of the complex is shown in Scheme 7.3.

The poor solubility of the material hampered numerous attempts to grow X-ray quality crystals of [Ir$_2$(ppy)$_4$Cl$_2$(μ-4,4'-bpy)].

The bulk sample was slightly soluble in DMSO. Figure 7.3 shows the ^{1}H NMR spectra of [Ir$_2$(ppy)$_4$(μ-Cl)$_2$] (c), [Ir$_2$(ppy)$_4$Cl$_2$(μ-4,4'-bpy)] (b) and free 4,4'-bpy (a), all in DMSO-*d*$_6$. Integration of the peaks of [Ir$_2$(ppy)$_4$Cl$_2$(μ-4,4'-bpy)] is consistent with the assumption. These data confirm that 4,4'-bpy was present in the initial complex. But they also indicate, that DMSO displaces the 4,4'-bpy ligand in a similar manner to the behaviour of [Ir(ppy)$_2$(2,4'-

bpy)Cl]. After the subtraction of the two peaks arising from the free 4,4'-bpy, the remaining signals are identical to those of [Ir(ppy)$_2$Cl(DMSO)] (Figure 7.3 c).

Similarly, the ^{13}C NMR spectrum of the bulk sample in DMSO-d_6 is a superimposition of the ^{13}C spectrum of free 4,4'-bpy and [Ir(ppy)Cl(DMSO)].3 The observations are summarized in Scheme 7.3. The electrospray mass spectrum of a DMSO/MeOH solution of the bulk [Ir$_2$(ppy)$_4$Cl$_2$(μ-4,4'-bpy)] exhibits peaks at m/z 657.2, 579.1 and 501.1, which is consistent with the [Ir(ppy)$_2$(4,4'-bpy)]$^+$, [Ir(ppy)$_2$(DMSO)]$^+$ and [Ir(ppy)$_2$]$^+$ ions, respectively.

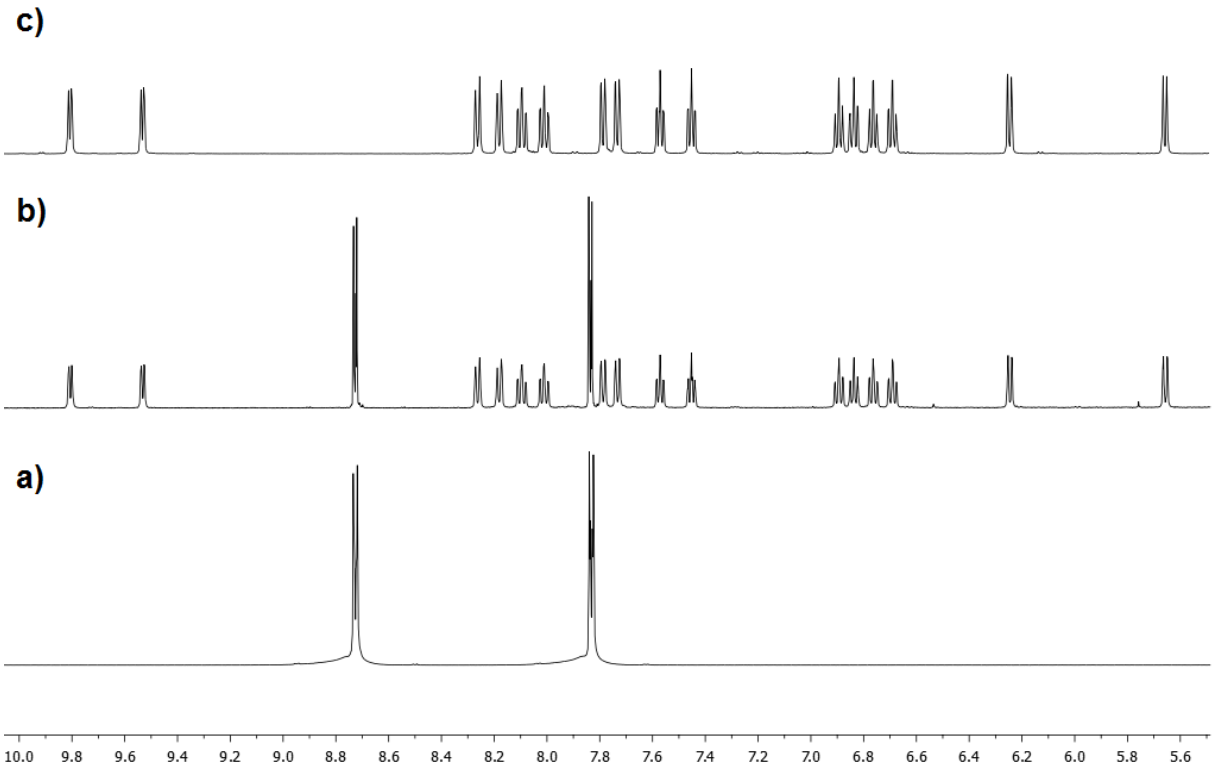

Figure 7.3 ^{1}H NMR spectra in DMSO-d_6 a) the free 4,4'-bpy ligand, b) [{Ir$_2$(ppy)$_2$(Cl)}$_2$(μ-4,4'-bpy)], c) [Ir$_2$(ppy)$_4$(μ-Cl)$_2$] (298 K, 500 MHz, TMS).

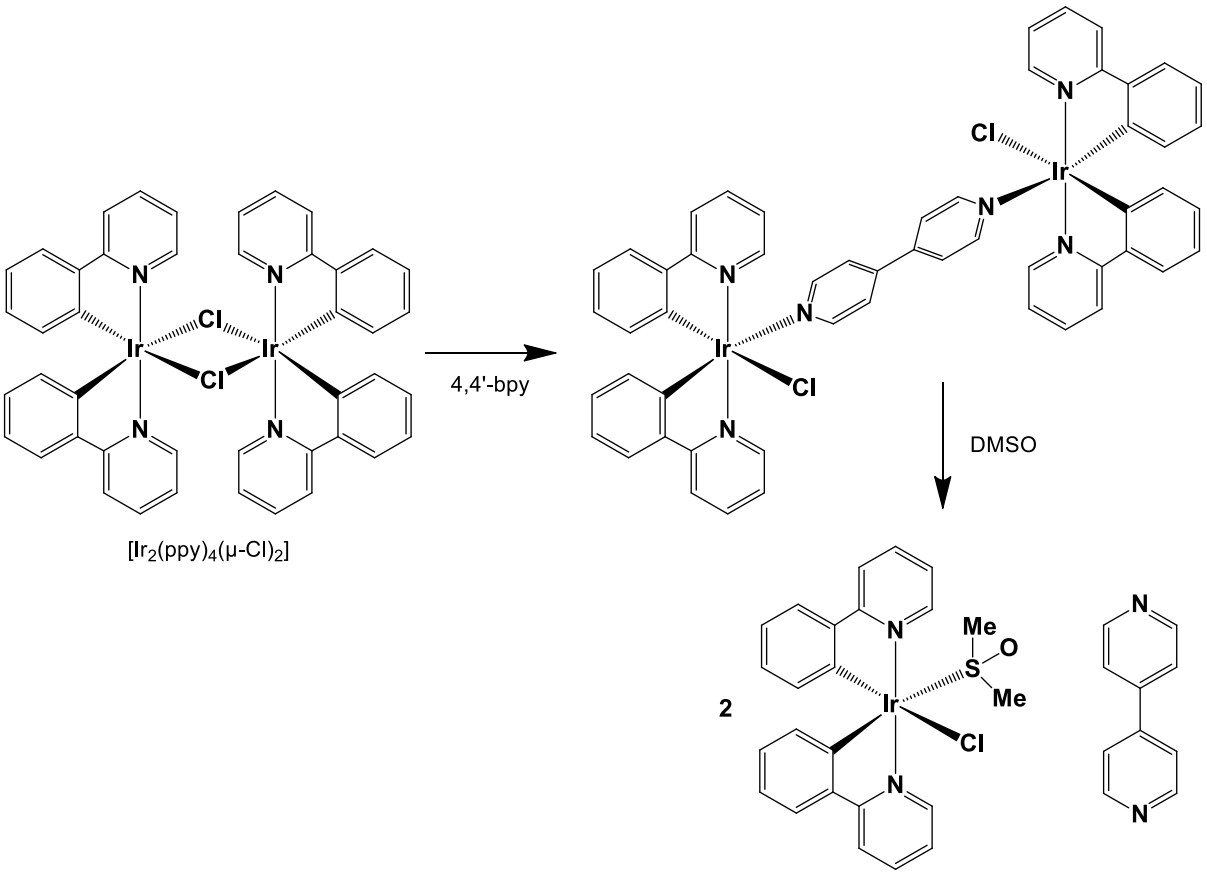

Scheme 7.3 Proposed pathway of the reaction of $[Ir_2(ppy)_4(\mu\text{-}Cl)_2]$ with one equivalent of 4,4'-bpy followed by ligand exchange in DMSO.

7.2.5. $[Ir(ppy)_2(tbpy)Cl]$

In an attempt to synthesize a model compound for the results described above, $[Ir(ppy)_2(tbpy)Cl]$ was selected. Unfortunately the compound appears unstable in solution. Several trials to isolate the desired product failed. Dissolution of the crude product in CH_2Cl_2 followed by layering with Et_2O yielded single crystals of good X-ray quality.

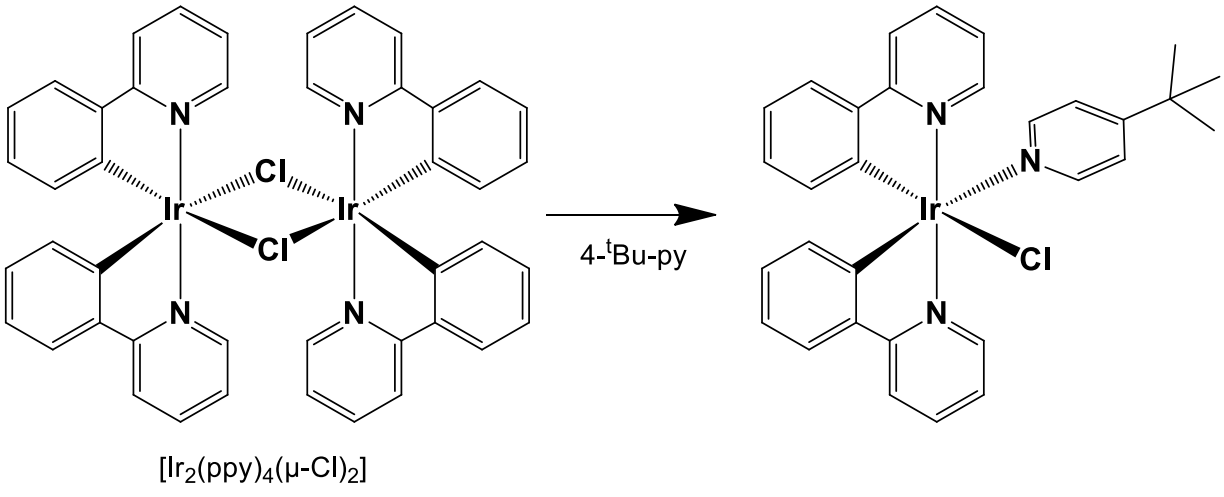

Scheme 7.4 Synthesis of $[Ir(ppy)_2(tbpy)Cl]$.

Upon redissolution of these crystals in a solution of CD_2Cl_2 the complex appears to fall apart, showing a mixture of products in the NMR spectrum. The highest mass peak in the ESI mass spectrum of the crystals in MeOH was observed at m/z 636.2, showing the right isotope pattern for the $[Ir(ppy)_2(tbpy)]^+$ ion. This composition was confirmed by a single crystal structure analysis (see Figure 7.10).

7.3. Solid state structures

7.3.1. [Ir(ppy)$_2$(2,4'-bpy)Cl]

Single crystals of $[Ir(ppy)_2(2,4'\text{-bpy})Cl]$ were grown directly from the crude reaction mixture in the microwave vial while standing at room temperature over night. The complex crystallizes from a racemic mixture spontaneously as $[Ir(ppy)_2(2,4'\text{-bpy})Cl]$ in the chiral, monoclinic space group $P2_1$. The selected crystal for X-ray structure determination only contains the Δ-enantiomer. In the unit cell there are two Δ-enantiomers without any solvent molecules. The iridium(III) ion in the complex is 6-coordinate with two cyclometallating $[ppy]^-$ ligands having the N-donor atoms in a *trans* configuration, which is in agreement with previously reported complexes containing similar $\{Ir(ppy)_2\}$-units.[14]

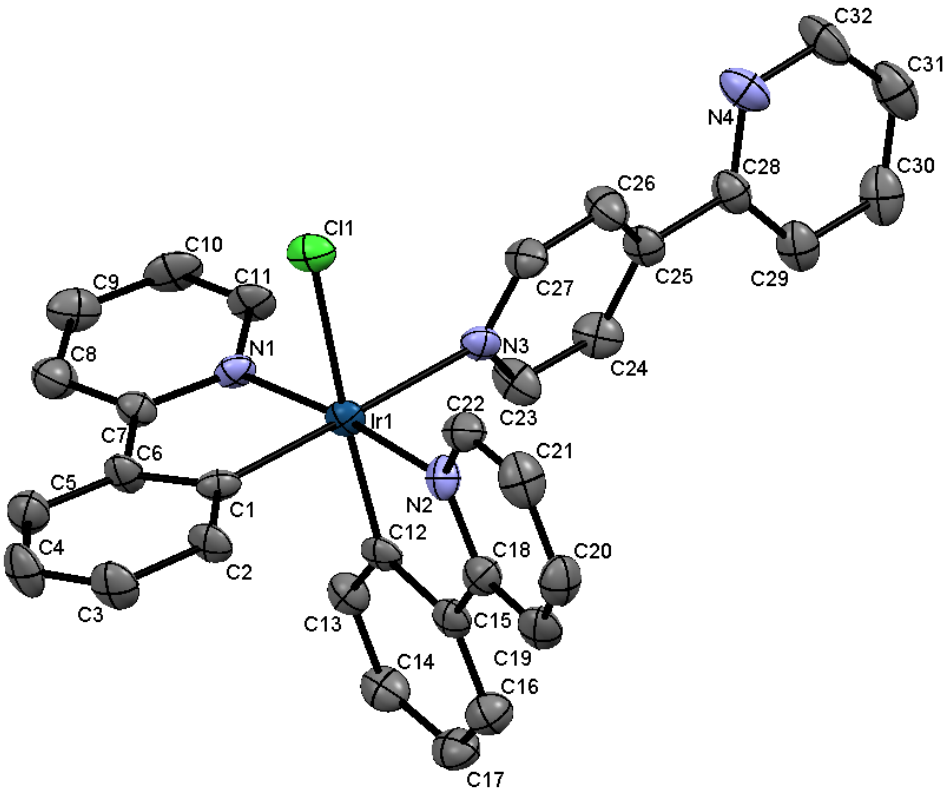

Figure 7.4 Structure of Δ-[Ir(ppy)$_2$(2,4'-bpy)Cl] (ellipsoids at 50% probability level; H atoms omitted for clarity). Selected bond lengths (in Å) and angles (in °): Ir1–C12 = 1.986(6), Ir1–C1 = 1.992(8), Ir1–N2 = 2.043(6), Ir1–N1 = 2.047(6), Ir1–N3 = 2.215(6), Ir1–Cl1 = 2.4622(18); C1–Ir1–N1 = 80.4(3), C12–Ir1–N2 = 80.7(3), N3–Ir1–Cl1 = 89.63(18), N2–Ir1–N1 = 173.3(3), C1–Ir1–N3 = 175.9(3), C12–Ir1–Cl1 = 175.4(2).

To minimize steric Cl...H interactions between atoms Cl1 and H27A (C...H distance = 2.62 Å), the coordinated 4'-pyridine ring is twisted 23.2(4)° out of the meridional-plane containing

atoms Ir1, C12, Cl1 and N3. The deviation of each atom from the plane is smaller than 0.06 Å. This intramolecular contact is shorter than the intermolecular hydrogen bonds of the chlorido ligand and is therefore significant (see Table 7.1).

Table 7.1 Hydrogen bonds involving the chlorido ligand in $[Ir(ppy)_2(2,4'\text{-bpy})Cl]$.

Contact	CH...Cl (Å)	C...Cl (Å)	C-H...Cl (°)	Symmetry code*
C22H22a...Cl	2.65	3.311(9)	127	
C27H27a...Cl	2.62	3.24(1)	123	
C10H10a...Cl1*	2.68	3.632(7)	176	2 – x, –½ + y, 1 – z
C16H16a...Cl*	2.86	3.476(9)	124	–1 + x, y, z
C32H32a...Cl*	2.74	3.588(8)	149	2 – x, –½ + y, 2 – z

The other packing interactions are face-to-face π-stacking between the pyridine ring of one of the cyclometallating ligands containing atom N2 with the pendant pyridine ring containing $N4^i$ (symmetry code i = 1 – x, ½ + y, 2 – z) which lie over each other. The distance between the centroids is 3.57 Å with an interplane angle of 9.1° which reduces the efficiency of this interaction (see Figure 7.5).

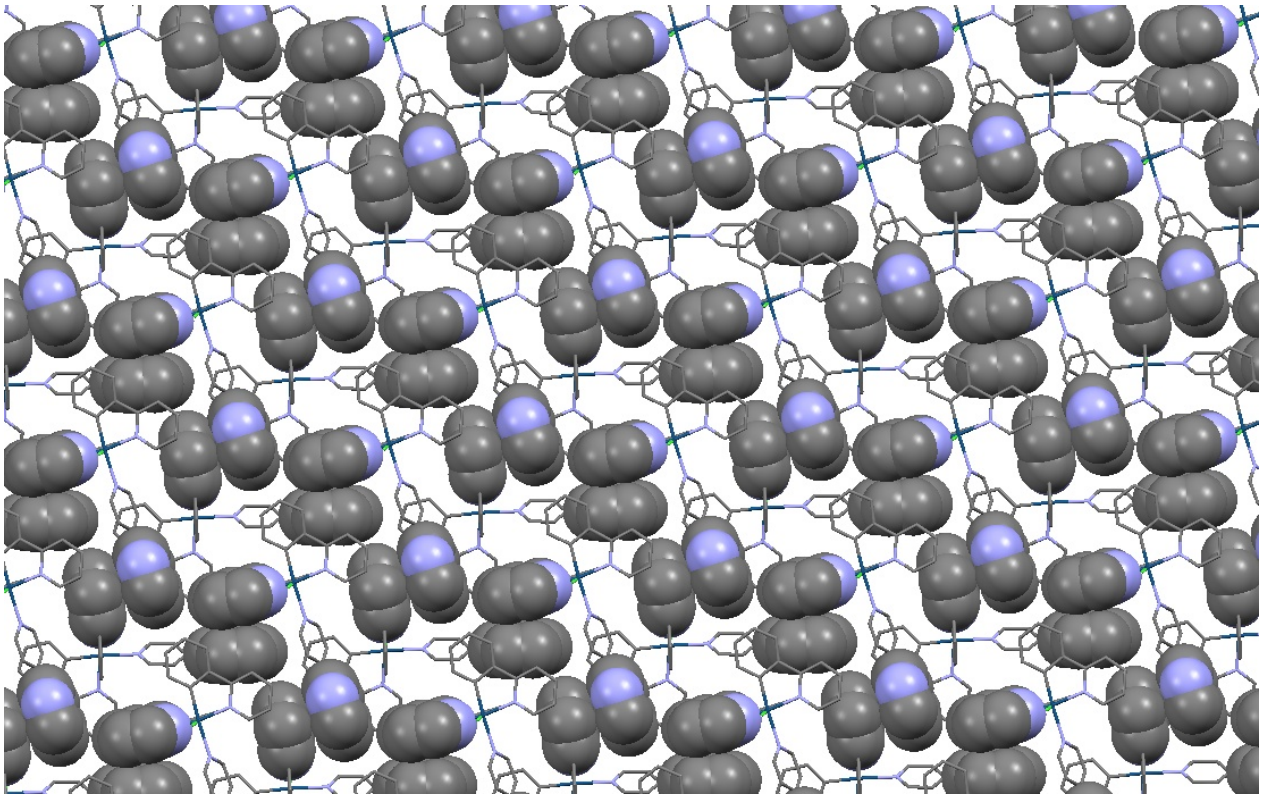

Figure 7.5 Packing interactions within $[Ir(ppy)_2(2,4'\text{-bpy})Cl]$, face-to-face π-stacking interactions in space filling representation.

7.3.2. $[Ir(ppy)_2(2,4'\text{-}bpy)_2][PF_6]$

Single crystals of $[Ir(ppy)_2(2,4'\text{-}bpy)_2][PF_6]$ were grown by evaporation in the NMR tube from the solution of the crude precipitate. They are racemic and crystallize in the monoclinic centrosymmetric space group *C*2/*c* with two independent half-cations in the asymmetric unit. The second half of each cation is generated by a two-fold rotation axis.

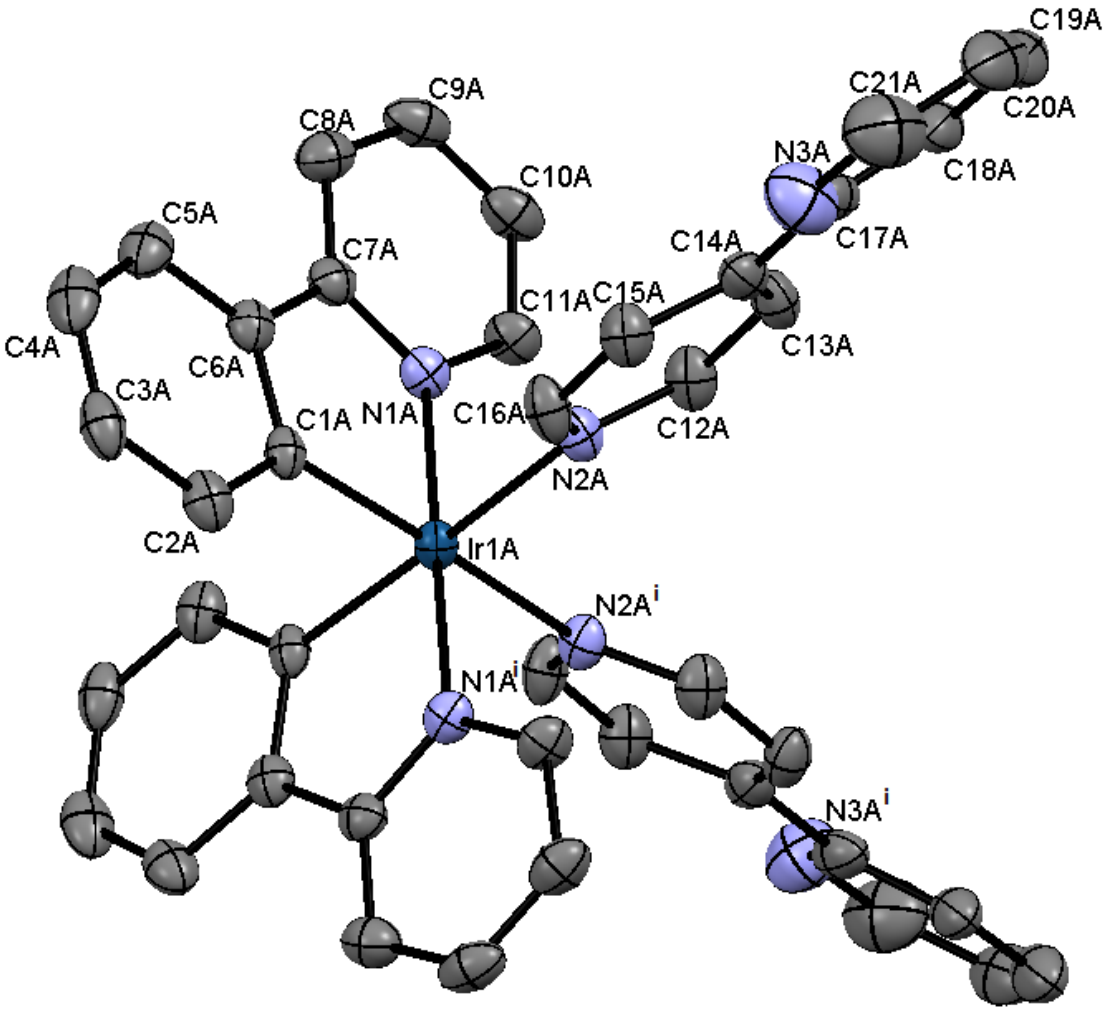

Figure 7.6 Structure of one of the independent Δ-$[Ir(ppy)_2(2,4'\text{-}bpy)_2]^+$ cations (cation A) in $[Ir(ppy)_2(2,4'\text{-}bpy)_2][PF_6]$ (ellipsoids at 50% probability level; H atoms omitted for clarity). Symmetry code i = 1 – x, y, ½ – z. Selected bond lengths (in Å) and angles (in °) in cation A: Ir1A–C1A = 2.010(4), Ir1A–N1A = 2.040(4), Ir1A–N2A = 2.182(4); C1A–Ir1A–N1A = 80.41(16), N1A–Ir1A–N2A = 84.80(14), N2A–Ir1A–N2A^{i} = 97.0(2), N1A–Ir1A–N1A^{i} = 179.7(2). Selected bond lengths (in Å) and angles (in °) in cation B: Ir1B–C1B–2.005(4), Ir1B– N1B = 2.030(4), Ir1B–N2B = 2.176(3); C1B–Ir1B–N1B = 80.35(16), N1B–Ir1B–N2B = 87.40(13), N2B–Ir1B–N2B^{i} = 93.55(18), N1B–Ir1B–N1B = 174.3(2).

Cation A possesses Δ-handedness and is depicted in Figure 7.6; bond parameters are given in the caption for both cations. Cation B possesses Λ-handedness. The second enantiomer of each pair is present in the unit cell.

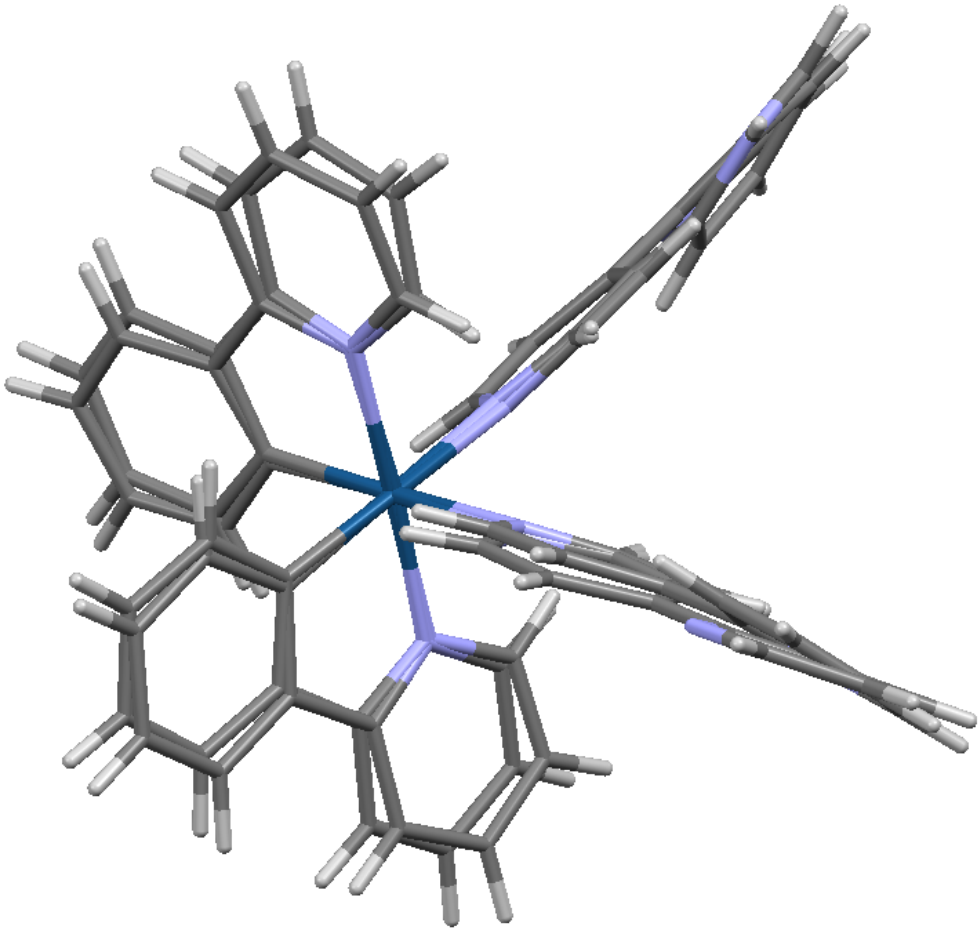

Figure 7.7 Overlay of the two independent cations A and B, after inversion of one of the cations of $[Ir(ppy)_2(2,4'\text{-}bpy)_2][PF_6]$.

An overlay of the two cations after inversion of one is depicted in Figure 7.7 and shows that the orientation of the pendant pyridine rings containing atoms N3A and N3B is the main difference. Both atoms Ir1A and Ir1B are in octahedral coordination environments, and the *trans* arrangement of the N-donors of the cyclometallating $[ppy]^-$ ligands are as expected. The monodentate 2,4'-bpy ligands are coordinated through the 4-pyridyl ring. The 2,4'-bpy ligands are not planar and the planes of the two pyridine rings in cation A subtend an angle of 9.8(3)°, while the corresponding angle in cation B is 14.8(3)°. This small deviation from planarity allows each of atoms N3A and N3B in the pendant pyridine ring to form intramolecular hydrogen bonds with the ortho-CH unit of the adjacent ring (C15AH15A. . .N3A = 2.49 Å, C13BH13B. . .N3B = 2.50 Å). Pairs of independent Δ- and Λ-cations embrace one another with close CH...C_π contacts (H21B...C9A^{ii} = 2.77 Å, H13B...C5A^{ii} = 2.87 Å; see Figure 7.8 a).[15, 16] Between pairs of 2,4'-bpy ligand in adjacent Δ- and Λ-cations face-to-face π-interactions are an important contribution to the crystal packing (see Figure 7.8 b). The distance between the centroid of the pyridine ring containing atom C20A and the least squares planes through the ligand containing atoms N2B^{iii} and C20B^{iii} is 3.30 Å, with an angle of 6.7° between the planes. This is also an important interaction, although the alignment of the π-systems is not ideal for an efficient stacking contact. Janiak has pointed out that the extent of ring slippage is often large in interactions between bpy-based ligand.[17]

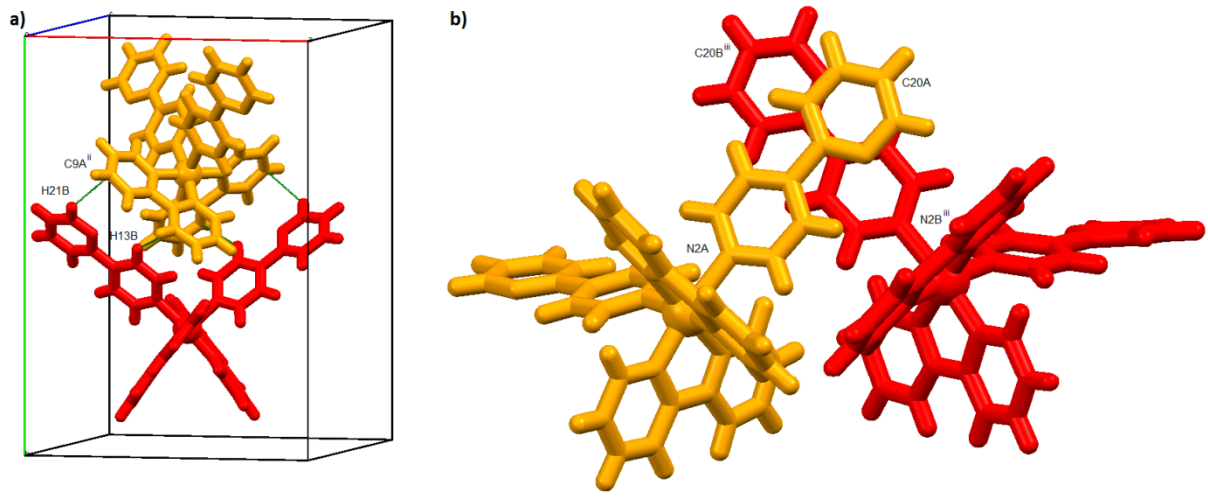

Figure 7.8 Packing of Δ- and Λ-cations in $[Ir(ppy)_2(2,4'\text{-}bpy)_2][PF_6]$. a) CH...$C_\pi$ contacts between a pair of independent cations A (Δ-chirality) and B (Λ-chirality) (symmetry code ii = 1 – x, y, ½ – z); atom H13B makes a contact to C5A^{ii}. b) Face-to-face interaction of 2,4'-bpy units in adjacent cations; symmetry code iii = ½ – x, -½ + y, ½ – z.

The role of the face-to-face interactions in the packing of the Δ- and Λ-cations is depicted in Figure 7.9 a (shown in space-filling representation). The overall assembly in the crystal lattice can be described in terms of sheets of Δ-A and Λ-B cations interleaved by sheets of Λ-A and Δ-B cations (Figure 7.9 b). The $[PF_6]^-$ anion is ordered, and the cation...anion packing interactions are dominated by extensive CH...F contacts.

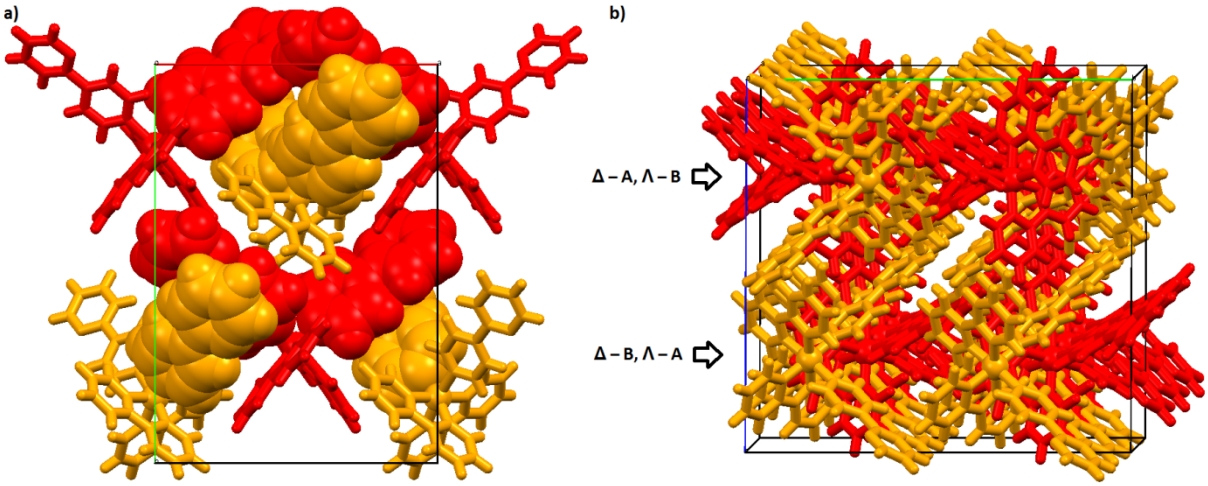

Figure 7.9 Packing of Δ- and Λ-cations in $[Ir(ppy)_2(2,4'\text{-}bpy)_2][PF_6]$. a) View down the c-axis showing π-stacking of pairs of 2,4'-bpy ligands (see text). b) Packing into sheets of Δ-A and Λ-B cations interleaved by sheets of Λ-A and Δ-B cations.

7.3.3. [Ir(ppy)$_2$(tbpy)Cl]

Attempts at the bulk synthesis of [Ir(ppy)$_2$(tbpy)Cl] failed due to the instability of the compound in solution. Dissolving the crude material in CH_2Cl_2 and carefully layering with Et_2O yielded after several days crystals with good X-ray quality of the desired compound. Racemic [Ir(ppy)$_2$(tbpy)Cl].H_2O crystallizes in the triclinic centrosymmetric space group *P*-1. Both enantiomers are present in the unit cell together with two water molecules. The iridium(III) atom in the centre is 6-coordinate with two cyclometallating $[ppy]^-$ ligands having the N-donor atoms in *trans* configuration.

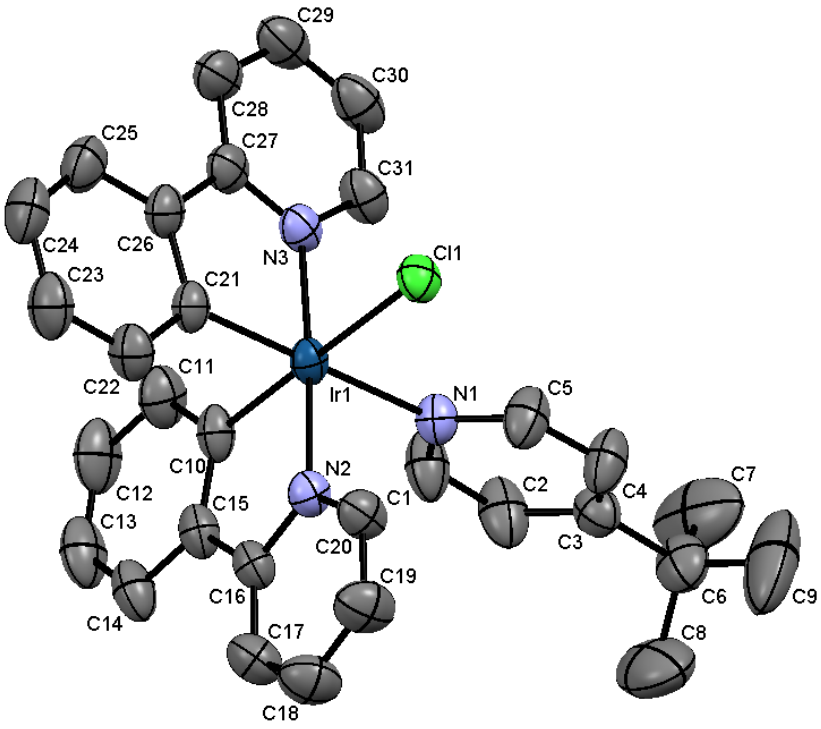

Figure 7.10 Structure of [Ir(ppy)$_2$(tbpy)Cl] in the monohydrate (ellipsoids at 50% probability level; H atoms omitted for clarity). Selected bond lengths (in Å) and angles (in °): Ir1–C10 = 1.994(4), Ir1–C21 = 2.006(4), Ir1–N2 = 2.047(3), Ir1–N3 = 2.052(3), Ir1–N1 = 2.211(3), Ir1–Cl1 = 2.4851(10); C21–Ir1–N3 = 80.4(1), C10–Ir1–N2 = 80.4(1), N1–Ir1–Cl1 = 90.67(8), N2–Ir1–N3 = 176.6(1), C21–Ir1–N1 = 177.4(1), C10–Ir1–Cl1 = 175.5(1).

To minimize steric Cl...H interactions between atoms Cl1 and H5A (distance = 2.57 Å), the monodentate pyridine ring is twisted 14.0(3)° out of the meridional-plane containing atoms Ir1, C10, Cl1 and N1 with a deviation of each atom from the plane < 0.06 Å. This intramolecular contact is shorter than the intermolecular hydrogen bonds of the chlorido ligand and is therefore significant (see Table 7.2, compare with Table 7.1).

Table 7.2 Hydrogen bonds involving the chlorido ligand in [Ir(ppy)$_2$(tbpy)Cl].

Contact	CH...Cl (Å)	C...Cl (Å)	C-H...Cl (°)	Symmetry code*
C20H20a...Cl	2.68	3.35(5)	128	
C5H5a...Cl	2.57	3.27(5)	130	
C29H29a...Cl*	2.84	3.60(5)	138	–x, 1 – y, 1 – z
C7H7a...Cl2*	2.81	3.78(1)	168	x, –1 + y, z

The dominant packing interactions are face-to-face π-stacking between the pyridine ring of one of the cyclometallating ligands containing atom N3 with the same pyridine ring of another complex (atom $N3^{i}$, symmetry code i = -x, -y, 1 – z). The planes are parallel and the distance between the planes is 3.51 Å making these interactions very efficient. The stacking pyridine rings are in sheets, separated by the ^{t}Bu groups (see Figure 7.11).

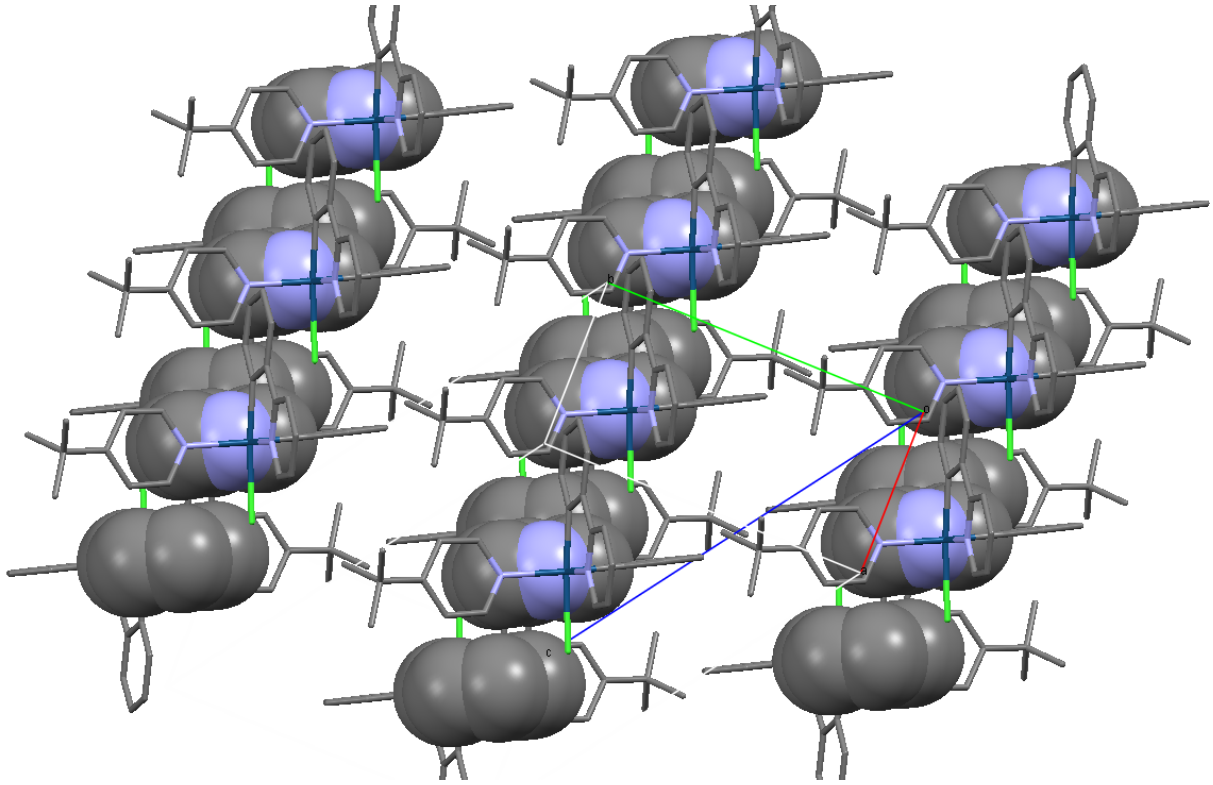

Figure 7.11 Packing interactions within $[Ir(ppy)_2(tbpy)Cl]$, face-to-face π-stacking interactions in space filling representation.

Table 7.3 Crystallographic data of the complexes.

Compound	[Ir(ppy)$_2$(2,4'-bpy)Cl]	[Ir(ppy)$_2$(2,4'-bpy)$_2$][PF$_6$]	[Ir(ppy)$_2$(tbpy)Cl].H$_2$O
Formula	$C_{32}H_{24}ClIrN_4$	$C_{42}H_{32}F_6IrN_6P$	$C_{31}H_{29}ClIrN_3.H_2O$
Formula weight / g mol^{-1}	692.22	957.93	689.26
Crystal colour and habit	yellow needle	yellow block	yellow needle
Crystal system	monoclinic	monoclinic	triclinic
Space group	$P2_1$ Flack parameter = 0	$C2/c$	P-1
a, b, c / Å	9.4396(19) 13.441(3) 10.057(2)	15.6496(15) 21.8929(14) 21.161(2)	8.0367(14) 11.543(2) 16.501(3)
α, β, γ/ ^{o}	90 93.24(3) 90	90 97.158(8) 90	76.154(14) 86.264(14) 73.679(14)
U / Å^3	1273.9(4)	7193.7(11)	1426.5(4)
Dc / mg m^{-3}	1.805	1.769	1.600
Z	2	8	2
μ(Mo-Kα) / mm^{-1}	5.375	3.830	4.801
T/ K	173	173	173
Refln. collected (R_{int})	40977 (0.1412)	54929 (0.0733)	42498 (0.0973)
Unique refln.	5018	8062	7042
Refln. for refinement	4905	7031	6647
Parameters	343	506	346
Threshold	$I > 2.0\sigma$	$I > 2.0\sigma$	$I > 2.0\sigma$
R1 (R1 all data)	0.0361 (0.0370)	0.0368 (0.0456)	0.0323 (0.0347)
wR2 (wR2 all data)	0.0924 (0.0931)	0.0788 (0.0819)	0.0736 (0.0748)
Goodness of fit	1.070	1.175	1.117

7.4. Photophysical studies

As only [Ir(ppy)$_2$(2,4'-bpy)Cl] could be synthesized and purified in large enough quantities, photophysical studies of only this compound were performed in solutions of CH_2Cl_2 (see Figure 7.12). The absorption spectrum shows the maximum at 265 nm, originating from ligand transitions with an additional weak MLCT band around 400 nm. The photoluminescence emission spectrum shows, under excitation at 368 nm, a maximum at 502 nm, an additional peak at 462 nm, a shoulder at 534 nm with a long tail towards the red region. The quantum yield measurement was performed on a CH_2Cl_2 solution of [Ir(ppy)$_2$(2,4'-bpy)Cl], which had been bubbled with argon for 15 minutes prior to the measurement. The quantum yield of this complex is 24.1% (λ_{ex} = 270 nm). It is necessary to use a tightly closed measurement cell, as this value and the excited state lifetime decrease strongly with time after bubbling with argon.

Studies for thin films and LEC or OLED devices in Valencia failed due to solubility issues.

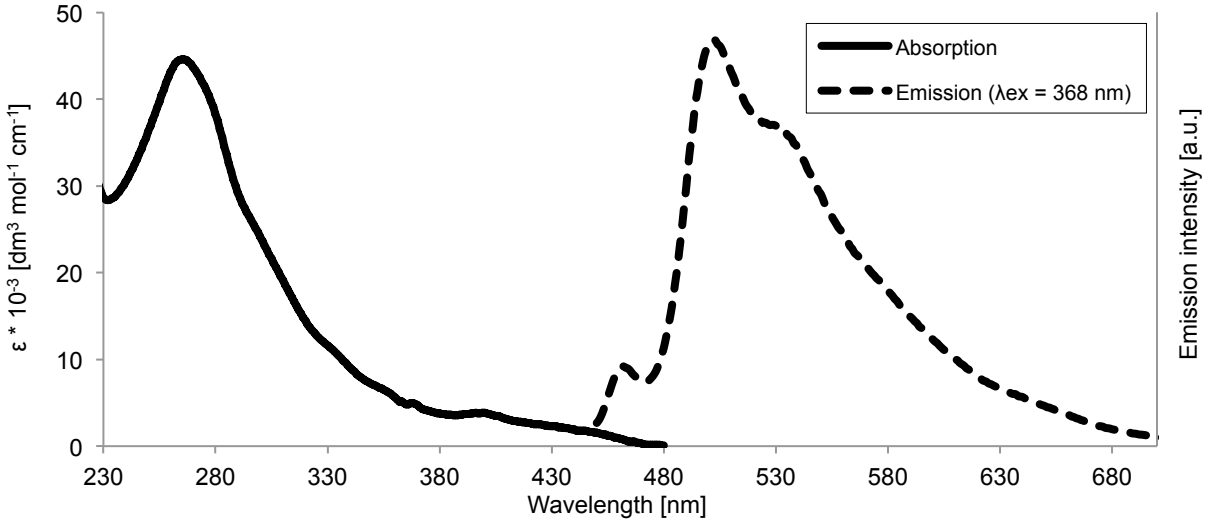

Figure 7.12 Absorption and emission spectrum of $[Ir(ppy)_2(2,4'\text{-bpy})Cl]$ in CH_2Cl_2 solutions (1.00×10^{-5} M)

7.5. Conclusion and outlook

In this chapter, the focus has not been on the photophysical properties of the synthesized iridium(III) compounds but on their stereochemical complexity. Commonly little is mentioned except for the *trans* arrangement of the nitrogen atoms in the $[ppy]^-$ ligands. But here the stereochemical consequences of the stereogenic $\{Ir(ppy)_2\}$-core in $[Ir(ppy)_2XY]$ and $[Ir(ppy)_2X_2]^+$ (X = pyridine and its derivatives, Y = halogen atom) species has been investigated. $[Ir(ppy)_2(2,4'\text{-bpy})Cl]$, $[Ir(ppy)_2(2,4'\text{-bpy})_2][PF_6]$, $[\{Ir(ppy)_2Cl\}_2(\mu\text{-}4,4'\text{-bpy})]$ and $[Ir(ppy)_2(tbpy)Cl]$ have been prepared and characterized. In solution, the coordinated 2,4'-bpy ligand in $[Ir(ppy)_2(2,4'\text{-bpy})Cl]$ undergoes hindered rotation about the Ir-N bond at 298 K on the NMR timescale, but there is free rotation about the C-C bond between the two pyridine rings. On crystallization, racemic $[Ir(ppy)_2(2,4'\text{-bpy})Cl]$ spontaneously resolves and the single crystal structure of the Δ-enantiomer has been determined. Dimethyl sulfoxide displaces 2,4'-bpy from $[Ir(ppy)_2(2,4'\text{-bpy})Cl]$, and 4,4'-bpy from $[\{Ir(ppy)_2Cl\}_2(\mu\text{-}4,4'\text{-bpy})]$, and ^1H NMR spectroscopic data for these complexes have been discussed.

7.6. Experimental

7.6.1. [Ir(ppy)$_2$(2,4'-bpy)Cl]

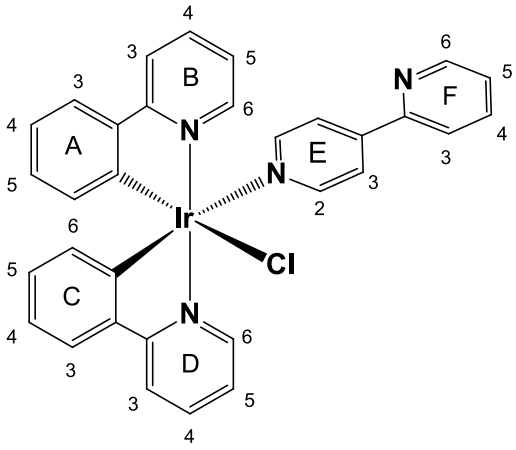

A yellow suspension of [Ir$_2$(ppy)$_4$(μ-Cl)$_2$] (122 mg, 0.114 mmol) and 2,4'-bipyridine (36.2 mg, 0.232 mmol) in methanol (15 mL) was heated in a microwave reactor for 4 h at 120 °C (P = 14 bar). After cooling to room temperature, the yellow solution was left standing for 7 h during which time yellow crystals of [Ir(ppy)$_2$(2,4'-bpy)Cl] formed (113 mg, 0.163 mmol, 71.5%). ^{1}H NMR (500 MHz, CD_2Cl_2, 298 K, TMS) δ 9.89 (ddd, J = 5.8, 1.5, 0.7 Hz, 1H, H^{B6}), 9.05 (v. br., 2H, H^{E2}), 8.69 (ddd, J = 4.8, 1.6, 1.1 Hz, 1H, H^{F6}), 8.18 (ddd, J = 5.8, 1.5, 0.7 Hz, 1H, H^{D6}), 7.95 (d, J = 7.9 Hz, 1H, H^{D3}), 7.85 (br, 2H, H^{E3}), 7.82–7.76 (m, 4H, $H^{F3+B3+F4+D4}$), 7.73 (ddd, J = 8.1, 7.4, 1.6 Hz, 1H, H^{B4}), 7.62 (dd, J = 7.7, 1.2 Hz, 1H, H^{C3}), 7.56 (dd, J = 7.7, 1.3 Hz, 1H, H^{A3}), 7.35 (ddd, J = 6.6, 4.8, 1.8 Hz, 1H, H^{F5}), 7.25 (ddd, J = 7.3, 5.8, 1.5 Hz, 1H, H^{B5}), 7.09 (ddd, J = 7.3, 5.8, 1.4 Hz, 1H, H^{D5}), 6.91 (ddd, J = 7.8, 7.3, 1.2 Hz, 1H, H^{A4}), 6.86 (ddd, J = 7.8, 7.3, 1.2 Hz, 1H, H^{C4}), 6.82 (td, J = 7.4, 1.4 Hz, 1H, H^{A5}), 6.74 (td, J = 7.4, 1.4 Hz, 1H, H^{C5}), 6.37 (dd, J = 7.6, 0.8 Hz, 1H, H^{A6}), 6.19 (dd, J = 7.6, 0.8 Hz, 1H, H^{C6}). ^{13}C NMR (126 MHz, CD_2Cl_2, 298 K) δ 168.8 (C^{D2}), 168.3 (C^{B2}), 153.6 (C^{F2}), 152.6 (br, C^{E2}), 151.4 (C^{B6}), 151.2 (C^{A1}), 150.8 (C^{F6}), 149.7 (C^{D6}), 149.4 (C^{C1}), 147.5 (C^{E4}), 144.8 ($C^{A2/C2}$), 144.7 ($C^{A2/C2}$), 137.8 ($C^{B4/D4/F4}$), 137.6 ($C^{B4/D4/F4}$), 137.3 ($C^{B4/D4/F4}$), 132.6 (C^{C6}), 131.9 (C^{A6}), 130.7 (C^{A5}), 129.6 (C^{C5}), 124.9 (C^{F5}), 124.8 (C^{A3}), 124.3 (C^{C3}), 123.0 ($C^{B5/D5}$), 122.95 (C^{E3}), 122.6 ($C^{B5/D5}$), 121.8 (C^{F3}), 121.6 ($C^{A4/C4}$), 121.55 ($C^{A4/C4}$), 119.7 (C^{D3}), 118.9 (C^{B3}). IR (solid, ν, cm^{-1}) 3427 (w), 3364 (w), 3254 (w), 3036 (w), 2991 (w), 1672 (w), 1653 (w), 1605 (m), 1582 (m), 1558 (s), 1477 (m), 1431 (m), 1412 (m), 1369 (w), 1315 (w), 1267 (w), 1217 (m), 1153 (m), 1061 (w), 1028 (m), 1014 (w), 851 (w), 783 (m), 754 (s), 731 (s). ESI-MS: *m/z* 657.2 $[M\text{-}Cl]^+$ (calc. 657.2), 501.1 $[Ir(ppy)_2]^+$ (calc. 501.1). UV–Vis (CH_2Cl_2, 1.00 * 10^{-5} mol dm^{-3}) λ /nm (ε/dm^3 mol^{-1} cm^{-1}) 265 (44'600), 398 (3'800). Emission (CH_2Cl_2, 1.00 * 10^{-4} mol dm^{-3}, λ_{ex} = 368 nm): λ_{em} = 462, 502, 534 nm. $C_{32}H_{24}ClIrN_4.H_2O$ requires C, 54.11; H, 3.69; N, 7.89. Found: C, 53.69; H, 3.63; N, 7.81.

7.6.2. [Ir(ppy)$_2$(2,4'-bpy)$_2$][PF$_6$]

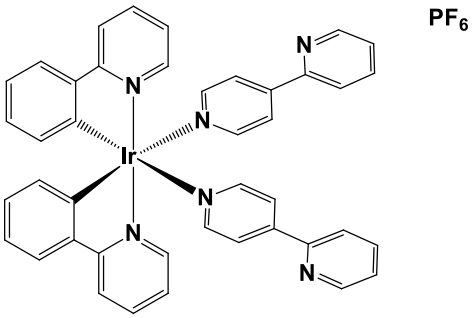

[Ir(ppy)$_2$(2,4'-bpy)Cl] (58.4 mg, 0.0844 mmol) was dissolved in DMSO (10 mL) and the solution was stirred for 1 h at room temperature. Aqueous NH_4PF_6 (excess) was added and the mixture was stirred for 1 h. Extraction with CH_2Cl_2 and H_2O resulted in a mixture of products as seen by NMR spectroscopy, but yellow X-ray quality crystals of [Ir(ppy)$_2$(2,4'-bpy)$_2$][PF$_6$] grew in an NMR-tube of the crude material. Attempts at bulk synthesis failed. ESI-MS (CH_2Cl_2/MeOH) m/z 813.2 $[M\text{-}PF_6]^+$ (calc. 813.2), 657.2 $[Ir(ppy)_2(bpy)]^+$ (calc. 657.2), 501.1 $[Ir(ppy)_2]^+$ (calc. 501.1).

7.6.3. [{Ir(ppy)$_2$Cl}$_2$(μ-4,4'-bpy)]

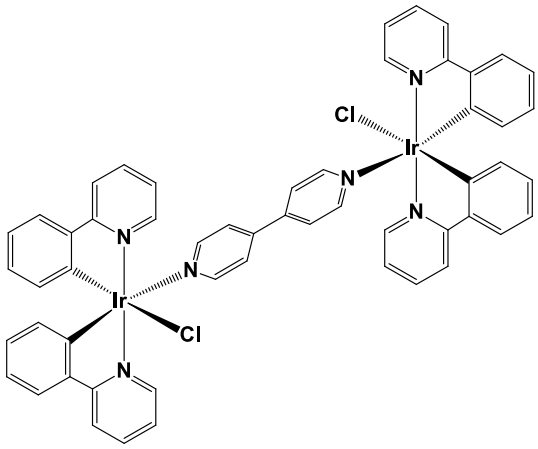

A yellow suspension of [Ir$_2$(ppy)$_4$(μ-Cl)$_2$] (50.2 mg, 0.0468 mmol) and 4,4'-bipyridine (7.4 mg, 0.047 mmol) in methanol (15 mL) was heated in a microwave reactor for 2 h at 120 °C (P = 14 bar). The orange precipitate of [{Ir(ppy)$_2$Cl}$_2$(μ-4,4'-bpy)] was collected by filtration (46.1 mg, 0.0375 mmol, 80.2%). IR (solid, ν, cm^{-1}) 3038 (m), 3017 (m), 1606 (m), 1582 (m), 1560 (m), 15 50 (m), 1476 (s), 1418 (s), 1408 (m), 1321 (m), 1268 (m), 1217 (s), 1162 (m), 1122 (w), 1107 (w), 1084 (w), 1065 (m), 1030 (s), 983 (w), 966 (w), 929 (w), 875 (m), 857 (w), 818 (s), 791 (m), 771 (s), 753 (s), 742 (s), 727 (s), 668 (s), 633 (s), 601 (s). ESI-MS (MeOH/CH_2Cl_2): m/z 1192.9 $[M\text{-}Cl]^+$ (calc. 1193.2), 657.2 $[Ir(ppy)_2(bpy)]^+$ (calc. 657.2), 501.1 $[Ir(ppy)_2]^+$ (calc. 501.1). $C_{54}H_{40}Cl_2Ir_2N_6.2H_2O$ requires C, 51.30; H, 3.51; N, 6.65. Found: C, 51.24; H, 3.28; N, 6.69. NMR spectroscopic data: see text.

7.6.4. [Ir(ppy)$_2$(tbpy)Cl]

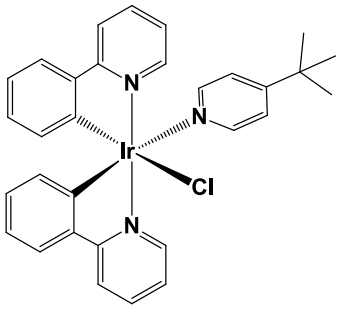

A yellow suspension of [$Ir_2(ppy)_4(\mu\text{-}Cl)_2$] (107 mg, 0.100 mmol) and *tert*-butylpyridine (27.0 mg, 0.200 mmol) in methanol (15 mL) was heated in a microwave reactor for 4 h at 120 °C (P = 9 bar). After cooling to room temperature, the yellow mixture was put in the freezer (-20 °C) for 48 hrs. The precipitate was filtered and washed with cold methanol (-20 °C). A mixture of products as seen by NMR spectroscopy was isolated. The mixture was dissolved in CH_2Cl_2 and overlayered with Et_2O. A few crystals of X-ray quality could be isolated of [Ir(ppy)$_2$(tbpy)Cl]. Redissolving the crystals in CD_2Cl_2 for NMR spectroscopy resulted in dissociation of the product to a mixture of compounds. ESI-MS (MeOH) m/z 636.2 $[M\text{-}PF_6]^+$ (calc. 636.2), 501.1 $[Ir(ppy)_2]^+$ (calc. 501.1).

---

[1] S. Sprouse, K. A. King, P. J. Spellane, R. J. Watts, *J. Am. Chem. Soc.*, 1984, **106**, 6647.

[2] T. Hu, L. He, L. Duan. Y. Qiu, *J. Mater. Chem.*, 2012, **22**, 4206.

[3] See for example: R. Chakrabarty, P. S. Mukherjee, P. J. Stang, *Chem. Rev.*, 2011, **111**, 6810, and references therein.

[4] E. C. Constable, C. E. Housecroft, G. E. Schneider, J. A. Zampese, *Polyhedron*, 2013, **52**, 530.

[5] V. Chandrasekhar, T. Hajra, J. K. Bera, S. M. W. Rahaman, N. Satumtira, O. Elbjeirami, M. A. Omary, *Inor. Chem.*, 2012, **51**, 1319.

[6] S. Kappaun, S. Sax, S. Eder, K. C. Möller, K. Waich, F. Niedermair, R. Saf, K. Mereiter, J. Jacob, K. Müllen, E. J. W. List, C. Slugovc, *Chem. Mater.,* 2007, **19**, 1209.

[7] A. Santoro, A. M. Prokhorov, V. N. Kozhevnikov, A. C. Whitwood, B. Donnio, J. A. G. Williams, D. W. Bruce, *J. Am. Chem. Soc.*, 2011, **133**, 5248.

[8] E. Baranoff, B. F. E. Curchod, J. Frey, R. Scopelliti, F. Kessler, I. Tavernelli, U. Rothlisberger, M. Grätzel, Md. K. Nazeeruddin, *Inorg. Chem*., 2012, **51**, 215.

[9] S. Bettington, M. Tavasli, M. R. Bryce, A. S. Batsanov, A. L. Thompson, H. A. Al Attar, F. B. Dias, A. P. Monkman, *J. Mater. Chem*., 2006, **16,** 1046.

[10] A. S. Batsanov, S. Bettington, M. R. Bryce, Private communication to the CSD, refcode OBAVEU.

[11] E. C. Constable, in: P. A. Gale, J. W. Steed (Eds.), Supramolecular Chemistry, *vol.6*, Wiley, Chichester, 2010, 3073.

[12] See for example: K. Biradha, M. Sarkar, L. Rajput, *Chem. Commun*., 2006, 4169 and references therein.

[13] See for example: H. W. Roesky, M. Andruh, *Coord. Chem. Rev*., 2003, **236**, 91 and references therein.

[14] I. J. Bruno, J.C. Cole, P. R. Edgington, M. K. Kessler, C. F. Macrae, P. McCabe, J. Pearson, R. Taylor, *Acta Crystallogr*., Sect. B, 2002, **58**, 389.

[15] M. Nishio, *CrystEngComm*, 2004*,* **6**, 130.

[16] M. Nishio, Y. Umezawa, K. Honda, S. Tsuboyama, H. Suezawa, *CrystEngComm,* 2009, **11**, 1757.

[17] F. O. Garces, K. A. King, R. J. Watts, *Inorg. Chem.,* 1988, **27**, 3464.

Chapter 8

8. Conclusion and outlook

In this PhD thesis, a series of new iridium(III) complexes was successfully synthesized and characterized. Many of the complexes have been characterized by NMR spectroscopy, MS, EA and IR as well as by X-ray analysis. The hindered rotation of the pendant aromatic rings of the ancillary ligands was investigated using variable temperature NMR spectroscopy. In addition, many of the complexes were investigated in thin-film and/or LEC configuration.

A key issue concerning LEC performance (e.g. the maximum luminance) is the absence of small and mobile anions. It was determined that chloride plays an important role in decreasing the luminance output of a LEC device. A facile technique to prove the absence of chloride anions is described (see Chapter 2). Upon changing the size and molecular mass of the anions, their mobility under an applied bias has successfully been changed (see Section 3.6).The emission maximum of iridium(III) complexes was successfully shifted towards the blue region upon modifications of both the ancillary and the cyclometallating ligands. In solution and thin-films, these blue-emitting complexes exhibited quantum yields up to 100% (see Section 4.6). The introduction of ancillary ligands containing tpy units allowed a face-to-face π-stacking interaction of the pendant pyridine ring with one of the C^N ligands, as was also seen with the pendant phenyl rings introduced into bpy ligands. Upon the extension of the π-conjugation system of the ancillary tpy ligand, the emission maximum could be shifted to the red region of the visible spectrum (see Chapters 5 and 6). Finally, the stereochemical complexity of the octahedral environment of iridium(III) atoms was investigated and trials towards making multinuclear species have successfully been carried out.

There are many ways to achieve an overall white emission. In a similar fashion to LCD screens, one possibility is to mix 3 complexes which emit at different wavelengths (red, green, blue). Another approach is to mix only 2 complexes (e.g. orange and sky-blue). However, to be able to achieve a stable white emission, blue and red iridium(III) emitters with good colour purity and high efficiency are required. A blue emitting ($[Ir(dfppz)_2(\mathbf{3})][PF_6]$, λ_{em} = 493 nm, QY = 0.72) and a red emitting complex ($[Ir(dmppz)_2(\mathbf{4})][PF_6]$, λ_{em} = 642 nm, QY = 0.062) have been mixed in different ratios (from 1:0.002 to 1:6.5) in a solution of dichloromethane (see Figure 8.1), analogous to reported measurements in thin films.[1]

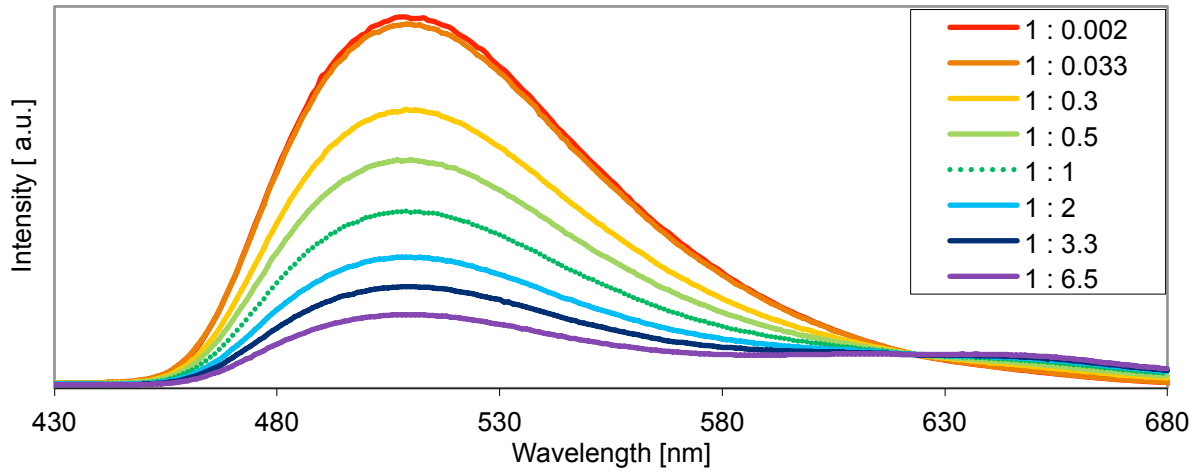

Figure 8.1 Mixing $[Ir(dfppz)_2(3)][PF_6]$ and $[Ir(dmppz)_2(4)][PF_6]$ in a solution of DCM (c = 1E-5 M, λ_{ex} = 350 nm) at different ratios.

With an excess of the blue emitting complex, due to the high quantum yield, the blue emission is dominant. Upon addition of more of the red emitting complex, a second emission around 640 nm begins to appear, while the blue emission decreases. It has to be mentioned, that the quantum yields of the two complexes are very different, and therefore it is more likely to observe a blue emission, than a red emission, even though the energy of the emitted wavelength is higher for the blue than the red emission.

These measurements are only a proof of principle and need further efforts to achieve an overall white emission.

Another possibility to achieve white emission, besides mixing two emitting salts, is to synthesize a system where both the cation and anion are emitting iridium(III) complexes (see Scheme 8.1). Preliminary studies have focused only on preparation of anionic iridium(III) complexes with a non-emitting cation, e.g. sodium or potassium. The substituents on both ions must be carefully selected, in order to get an overall white emission. A very important part will be the quantum yields of the two ions, as the overall emission will depend on it. Due to lack of time, this route has not yet been fully investigated, but would be interesting to follow in the future.

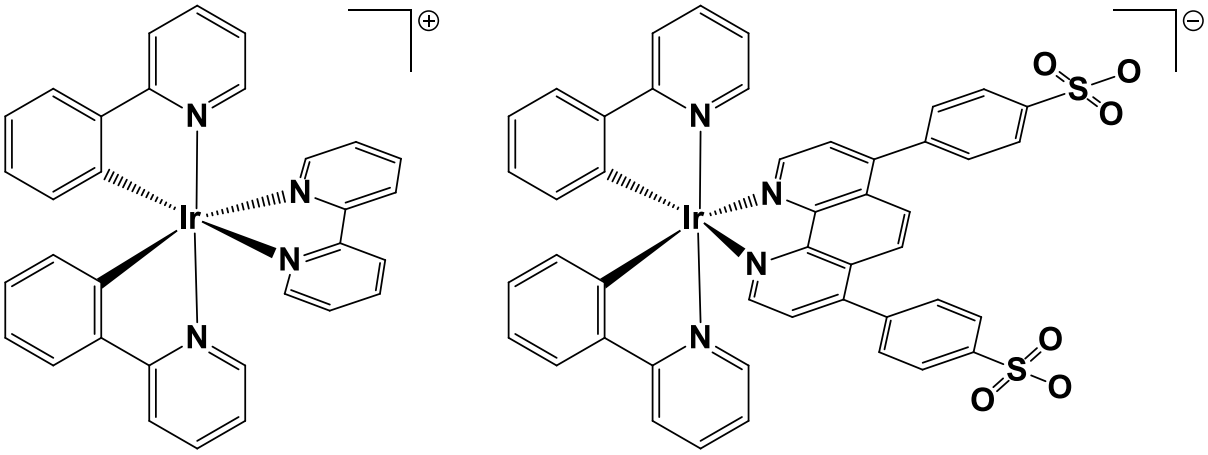

Scheme 8.1 A salt where iridium(III) complexes play the role of both cation and anion.

The discovery of the influence of chloride on the performance of LEC devices raises the question: are the short lifetimes of the blue emitting compounds in devices connected to the presence of fluorine atoms in the cyclometallating ligands? It has been reported, that in OLEDs, fluorine radicals can be released from the cyclometallating ligands (e.g. 2,4-difluorophenyl-2-pyridine) followed by a fast decrease of the device performance.[2] One of the current research targets in our group is the replacement of fluorine with other electron-withdrawing substituents, as the fluorine appears to have a detrimental influence upon the lifetime of the device.

Since the first report of an iridium-based light-emitting electrochemical cell, research efforts in this field have yielded many significant results. Starting from a yellow emission, the range of colours has been enlarged towards blue (452 nm)[3] and deep-red (687 nm)[4] with high colour purity. In addition, for LEC devices the lifetimes have been increased to many thousands of hours and the turn-on time has been shortened. There are still many goals to achieve in the near future before a product can become commercially viable. The combination of high efficiency, high brightness, long lifetime and short turn-on time in a LEC device is still a challenge. Complexes based on iridium are very useful models for investigating and improving the properties of iTMC based LEC devices. In future, the research should aim for more abundant elements, e.g. zinc or copper,[5] to replace the core iridium atom, to be able to produce commercial LEC products over a long period of time.

[1] H.-C. Su, H.-F. Chen, F.-C. Fang, C.-C. Liu, C.-C. Wu, K.-T. Wong, Y.-H. Liu, S.-M. Peng, *J. Am. Chem. Soc.,* 2008*,* **130**, 3413.
[2] S. Schmidbauer, A. Hohenleutner, B. König, *Adv. Mater.*, 2013, DOI: 10.1002/adma.201205022.
[3] M. Mydlak, C. Bizzarri, D. Hartmann, W. Sarfert, G. Schmid, L. De Cola, *Adv. Funct. Mater.*, 2010, **20**, 1812.
[4] J. L. Rodríguez-Redondo, R. D. Costa, E. Ortí, A. Sastre-Santos, H. J. Bolink, F. Fernández-Lázaro, *Dalton Trans.*, 2009, 9787.
[5] Q. Zhang, Q. Zhou, Y. Chen, L. Wang, D. Ma, X. Jing, F. Wang, *Adv. Funct. Mater.*, 2006, **16**, 1203.

Appendix

Compound Name	Lab-Journal	CIF-File	CCDC Code
$[Ir(ppy)_2(bpy)][PF_6]$ Batch 1	GES115	sg080-1_173k	
$[Ir(ppy)_2(bpy)][PF_6]$ Batch 2	GES161, GES162	GS161_123k	
$[Ir(ppy)_2(pbpy)][B(CN)_4]$	GES071, GES146	GS71_123k	
$[Ir(ppy)_2(bpy)][B(CN)_4]$	GES147	GS147_123k	
$[Ir(ppy)_2(pbpy)][BARF]$	GES150	GS150_123k	
$[Ir(ppy)_2(bpy)][BARF]$	GES151	GS151_123k	
$[Ir_2(dfppz)_4(\mu\text{-}Cl)_2]$	EB-229	GS52-2_173k	890 057
$[Ir(dfppz)_2(pbpy)][PF_6]$	GS050, GS061	GS50A-2_173k	890 056
$[Ir(dfppz)_2(\mathbf{1})][PF_6]$	GS051		
Ligand **2**	SG123	gs052_123k	890 060
$[Ir(dfppz)_2(\mathbf{2})][PF_6]$	GS052, GS060	GS52R_173k	890 058
$[Ir(dfppz)_2(\mathbf{3})][PF_6]$	GS053, GS062	GS53A_173k	089 059
$[Ir(ppy)_2(tpy)][PF_6]$	GS063, GES157	GS063_173k	
$[Ir(dmppz)_2(tpy)][PF_6]$	GS064	GS064_173k	
$[Ir(ppy)_2(\mathbf{4})][PF_6]$	GS065, GES159	GS065_173k	
$[Ir(dmppz)_2(\mathbf{4})][PF_6]$	GES092	GS92_123k	
$[Ir(dmppz)_2(\mathbf{5})][PF_6]_2$	GES100, GES101	GS101_173k	
$[Ir(ppy)_2(\mathbf{6})][PF_6]$	GS066, GES158	GS66_123k	
$[Ir(ppy)_2(\mathbf{7})][PF_6]$	GES089	GS089_173k	
$[Ir(ppy)_2(\mathbf{8})][PF_6]$	GES090	GS90_123k	
$[Ir(ppy)_2(\mathbf{9})][PF_6]$	GES091	GS91_123k	
$[Ir(ppy)_2(2,4'\text{-}bpy)Cl]$	GS032, GS033	GS032_173k	881 635
$[Ir(ppy)_2(2,4'\text{-}bpy)_2][PF_6]$	GES105	GS105_173k	881 636
$[\{Ir(ppy)_2Cl\}_2(\mu\text{-}4,4'\text{-}bpy)]$	GES098		
$[Ir(ppy)_2(tbpy)Cl]$	GES112, GES145	GS112_173k	